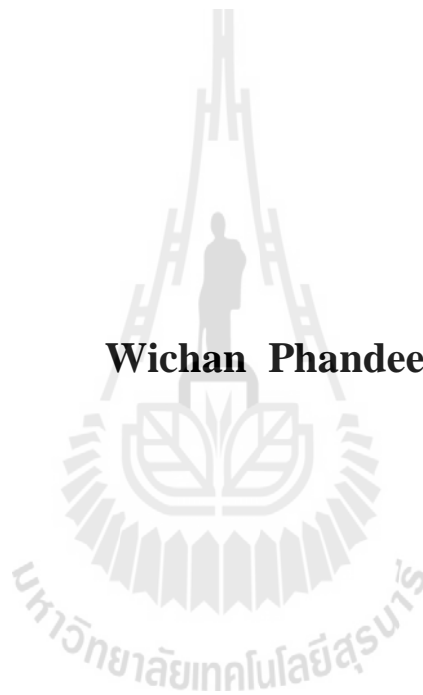


**DEVELOPMENT OF GRID-BASED HYDROLOGICAL
MODEL FOR IMPACT ASSESSMENT OF LAND USE
AND CLIMATE CHANGES ON FLOOD IN
CHIANG MAI MUNICIPALITY AREA**

Wichan Phandee



**A Thesis Submitted in Partial Fulfillment of the Requirements for the
Degree of Doctor of Philosophy in Geoinformatics
Suranaree University of Technology
Academic Year 2011**

การพัฒนาแบบจำลองอุทกวิทยาแบบกึ่งปริศนาเพื่อประเมินผลกระทบจากการ
เปลี่ยนแปลงการใช้ที่ดินและภูมิอากาศต่อการเกิดน้ำท่วม
ในพื้นที่เทศบาลนครเชียงใหม่



วิทยานิพนธ์นี้เป็นส่วนหนึ่งของการศึกษาตามหลักสูตรปริญญาวิทยาศาสตรดุษฎีบัณฑิต

สาขาวิชาภูมิสารสนเทศ
มหาวิทยาลัยเทคโนโลยีสุรนารี

ปีการศึกษา 2554

**DEVELOPMENT OF GRID-BASED HYDROLOGICAL MODEL
FOR IMPACT ASSESSMENT OF LAND USE AND CLIMATE
CHANGES ON FLOOD IN CHIANG MAI MUNICIPALITY
AREA**

Suranaree University of Technology has approved this thesis submitted in partial fulfillment of the requirements for the Degree of Doctor of Philosophy.

Thesis Examining Committee

(Asst. Prof. Dr. Sunya Sarapirome)

Chairperson

(Asst. Prof. Dr. Songkot Dasananda)

Member (Thesis Advisor)

(Asst. Prof. Dr. Chatchai Jothityangkoon)

Member

(Asst. Prof. Dr. Suwit Ongsomwang)

Member

(Assoc. Prof. Dr. Kampanad Bhaktikul)

Member

(Prof. Dr. Sukit Limpijumnong)

Vice Rector for Academic Affairs

(Assoc. Prof. Dr. Prapun Manyum)

Dean of Institute of Science

วิทยุ พันธุ์ดี : การพัฒนาแบบจำลองอุทกวิทยาแบบกริดเพื่อประเมินผลกระทบจากการเปลี่ยนแปลงการใช้ที่ดินและภูมิอากาศต่อการเกิดน้ำท่วมในพื้นที่เทศบาลนครเชียงใหม่ (DEVELOPMENT OF GRID-BASED HYDROLOGICAL MODEL FOR IMPACT ASSESSMENT OF LAND USE AND CLIMATE CHANGES ON FLOOD IN CHIANG MAI MUNICIPALITY AREA) อาจารย์ที่ปรึกษา : ผู้ช่วยศาสตราจารย์ ดร.ทรงกต ทศานนท์, 239 หน้า.

งานวิจัยนี้มีวัตถุประสงค์หลัก 3 ประการคือ (1) เพื่อพัฒนาแบบจำลองอุทกวิทยาแบบเชิงกริดที่สามารถจำลองผลของน้ำท่าได้อย่างสมจริง (ระดับรายเดือนและรายวัน) โดยการใช้ข้อมูล GIS (2) เพื่อสร้างแผนที่น้ำท่วมที่สัมพันธ์กันของเทศบาลนครเชียงใหม่ ระหว่างเดือนกันยายน 2548 อิงตามข้อมูลปริมาณน้ำท่าจำลองและกราฟความสัมพันธ์ระหว่างปริมาณน้ำท่าและระดับความสูงของน้ำ (3) เพื่อตรวจสอบผลกระทบของการเปลี่ยนแปลงรูปแบบการใช้ประโยชน์ที่ดินและสิ่งปกคลุมดิน (LULC) และการผันแปรของสภาพอากาศต่อปริมาณน้ำท่าจำลอง และแผนที่น้ำท่วมที่สัมพันธ์กัน อิงจากแผนที่ LULC ปี 2563 ที่ทำนายโดยแบบจำลอง CA-Markov และการเปลี่ยนแปลงภูมิอากาศในรูปของการเพิ่มขึ้นของปริมาณฝน พื้นที่ศึกษาที่เลือกคือส่วนหนึ่งของลุ่มน้ำปิงตอนบนซึ่งมีพื้นที่ประมาณ 1120 ตร.กม. ครอบคลุมพื้นที่เทศบาลนครเชียงใหม่ สำหรับวัตถุประสงค์แรก พบว่าผลการศึกษาของทั้งห้ากรณีศึกษาที่เลือกมาเพื่อการพัฒนาแบบจำลองรายเดือน แสดงให้เห็นว่าแบบจำลองดังกล่าวไม่อ่อนไหวต่อการผันแปรระดับความลึกของดินมากนัก แต่ขึ้นกับปริมาณและการผันแปรของความเข้มฝนเป็นอย่างสูง โดยพบว่าการไหลออกของน้ำได้ผิวดิน มีความจำเป็นอย่างยิ่งต่อการได้ผลการจำลองที่สมจริงมากกว่า สำหรับแบบจำลองรายวันซึ่งพัฒนามาจากแบบจำลองรายเดือนที่ดีที่สุด และผสานปัจจัยเกี่ยวกับการคายน้ำของพืชเข้าไปด้วย ส่งผลทำให้ได้ค่าความถูกต้องของการทำนายสูง โดยมีค่า R^2 ที่ 0.96 และค่าประสิทธิภาพ Nash-Sutcliffe (E) ที่ 0.94 สำหรับวัตถุประสงค์ที่สอง แผนที่น้ำท่วมได้ถูกสร้างขึ้นโดยอาศัยข้อมูลระดับน้ำในลำน้ำที่คำนวณจากปริมาณน้ำท่าจำลองในเดือนกันยายน 2548 ซึ่งพบว่าจากระดับน้ำท่าจำลองที่สถานี P1 ควรต้องมีน้ำท่วมจากแม่น้ำเกิดขึ้นสี่ครั้ง โดยค่าสูงสุดของระดับน้ำประจำเดือนที่สถานี P1 อยู่ที่ 305.23 เมตรเหนือระดับน้ำทะเลปานกลาง การเปรียบเทียบผลของแผนที่พื้นที่น้ำท่วมจากแบบจำลองและจากแผนที่พื้นที่อ้างอิงที่ทำนายไว้ แสดงให้เห็นว่าทั้งคู่มีระดับความสอดคล้องของผลที่เป็นพื้นที่ถูกน้ำท่วมตรงกันอยู่ในระดับปานกลางประมาณร้อยละ 58.9

สำหรับวัตถุประสงค์ที่สาม การศึกษาในเบื้องต้นพบว่า ทุกกรณีศึกษาที่เกี่ยวข้องกับการผันแปรของ LULC และความเข้มข้นน้ำฝนที่มีผลกระทบน้อยมากต่อ ข้อมูลน้ำท่าจำลองรายวันที่สถานี P1 แต่ปรากฏผลชัดเจนต่อปริมาณน้ำท่าจำลองที่สถานี P21 อย่างไรก็ตาม ผลกระทบดังกล่าวได้ปรากฏชัดเจนขึ้น หากการผันแปรดังกล่าวถูกกำหนดให้เกิदनอกเขตพื้นที่ศึกษาซึ่งยังคงอยู่ในพื้นที่ระบายน้ำเดียวกันของสถานี P1 ทั้งนี้แนวโน้มที่สังเกตได้คือปริมาณน้ำท่าจำลองจะมีค่าสูงขึ้นตามระดับของการสูญเสียป่าไม้และปริมาณฝนที่สูงขึ้น โดยผลกระทบจากการเปลี่ยนแปลงเหล่านี้เห็นได้ชัดเจนที่สถานี P1 แต่ยังไม่สามารถสรุปได้อย่างชัดเจนที่สถานี P21



สาขาวิชา การรับรู้จากระยะไกล

ลายมือชื่อนักศึกษา _____

ปีการศึกษา 2554

ลายมือชื่ออาจารย์ที่ปรึกษา _____

ลายมือชื่ออาจารย์ที่ศึกษาร่วม _____

WICHAN PHANDEE : DEVELOPMENT OF GRID-BASED
HYDROLOGICAL MODEL FOR IMPACT ASSESSMENT OF LAND USE
AND CLIMATE CHANGES ON FLOOD IN CHIANG MAI
MUNICIPALITY AREA. THESIS ADVISOR : ASST. PROF. SONGKOT
DASANANDA, Ph.D. 239 PP.

HYDROLOGICAL MODEL/FLOOD MODEL/GIS/CA-MARKOV MODEL/
IMPACT ASSESSMENT OF LAND USE CHANGE ON FLOOD

There are three main objectives of this research: (1) to develop grid-based hydrologic model capable of simulating realistic runoff scenarios (on monthly and daily basis) using GIS-based input data, (2) to generate associated flood maps of the Chiang Mai municipality during September 2005 based on the simulated runoff discharge data and the relevant rating curves, (3) to examine impact of the land use/land cover (LULC) and climate changes on runoff discharges and the associated flood maps based on the predicted LULC maps derived by CA-Markov model and probable increase of rainfall. The selected study area is part of the upper Ping Basin with the area about 1,120 km² and covering Chiang Mai Municipality area.

For the first objective, it was found from results of the five case studies chosen for the development of the monthly model that the preferred model was not sensitive much with the variation of soil depth but strongly dependent on amount and variation of rainfall intensity. The sub-surface runoff factor was also found very essential in the model's formulation in order to obtain the more realistic results. The daily model was adopted from the optimum monthly model in two case studies of model development

which the transpiration was alternative factor to include in the model. This model development made the model to have relatively high accuracy of the simulated runoff data with R^2 of 0.96 and Nash-Sutcliffe efficiency (E) of 0.94.

For the second objective, the flood maps were developed based on data of the water level in the stream channel calculated from the simulated daily stream discharge data in September 2005. It was found that, regarding to the simulated water level at the P1 station, there should be four river flood events seen in this month with the highest water level 305.23 m. above mean sea level (MSL). The comparison of predicted flood map and chosen reference flood map showed moderate level agreement of about 58.93% on the identified flooded area.

For the third part, it was preliminarily found that all the applied case studies of LULC and rainfall changes have little impact on the simulated discharge at the P1 station but they have obvious effect on the modeled discharges at P21 station. However, the impact was more obvious if those preferred changes were applied to zones outside the study area but still situated within the same drainage area of the P1 station. The observed trends were that amount of the simulated discharge increase with higher percentage of deforestation and the increase of rainfall. The impacts from these changes were highly pronounced at the P1 station but still inconclusive at the P21 station.

School of Remote Sensing

Academic Year 2011

Student's Signature_____

Advisor's Signature_____

Co-advisor's Signature_____

ACKNOWLEDGEMENTS

First of all, I wish to express my sincere gratitude to my major advisor, Asst. Prof. Dr. Songkot Dasananda, and co-advisor, Asst. Prof. Dr. Chatchai Jothityangkoon, for their support, guidance, and valuable suggestions throughout this study. I would also like to thank Asst. Prof. Dr. Sunya Sarapirome, a committee chairperson, for his several useful comments on my work. And I wish to extend my special thanks to the other committee members, Asst. Prof. Dr. Suwit Ongsomwang and Assoc. Prof. Dr. Kampanad Bhaktikul for their contributions to my study.

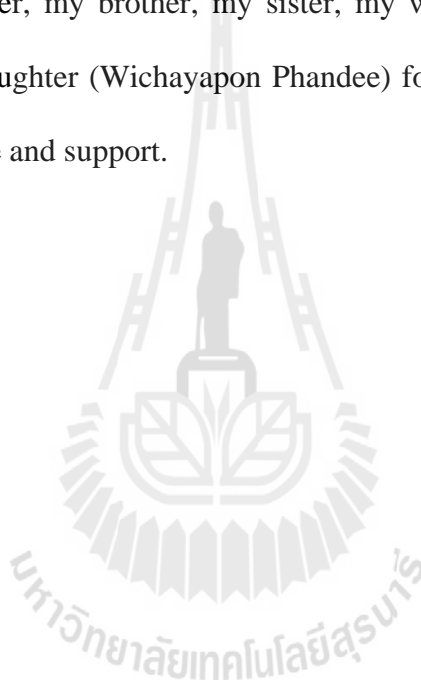
I would also like to thank the following organizations for providing essential data required in the research: Geo-Informatics and Space Technology Development Agency (GISTDA), Royal Thai Survey Department (RTSD), Department of Ground Water Resources (DGWR), Royal Irrigation Department (RID), Thai Meteorological Department (TMD), Royal Irrigation Department (RID), Department of Water Resources (DWR), Electricity Generating Authority of Thailand (EGAT), and Land Development Department (LDD).

Constant helps and advices given by Mr. Rawee Rattanakom, Miss. Siriwan Ruamkeaw, Mr. Nutthapol Junkaew, Mr. Tharapong Phetprayoon and Mr. Krairri Tenpuksee from the early stage of this research till the end are also very much appreciated. To complete the thesis, my great thanks are also due to Dr. Apiradee Saravisutra, Mrs. Sirilak Tanang, Ms. Ratchaneekorn ChatUthai and all friends at the School of Remote Sensing, for their help and being good friends for long time.

Thanks are also due to the School of Remote Sensing, Institute of Science, Suranaree University of Technology, for giving me the opportunity to pursue a Ph.D. program in geoinformatics and to learn more about geoinformatics techniques which are useful for my work and duty in the future. Also, I would like to thank the Nakhon Ratchasima Rajabhat University for its scholarship granted for my study.

Finally, I would like to express my deepest gratitude to my family including my mother, my father, my brother, my sister, my wife (Ms. Mattika Chaimeerang Phandee) and my daughter (Wichayapon Phandee) for giving me the inspiration and continuous love, care and support.

Wichan Phandee



CONTENTS

	Page
ABSTRACT IN THAI	I
ABSTRACT IN ENGLISH	III
ACKNOWLEDGEMENTS	V
CONTENTS	VII
LIST OF TABLES	XI
LIST OF FIGURES	XV
LIST OF ABBREVIATIONS	XX
CHAPTER	
I INTRODUCTION	1
1.1 Background problem	1
1.2 Research objectives	4
1.3 Scope and limitations of the study	4
1.4 Benefits of the study	5
1.5 Study area	5
II LITERATURE REVIEW	10
2.1 Definitions and types of flood	10
2.2 Great floods of Chiang Mai	12
2.2.1 Flood warning administration	13

CONTENTS (Continued)

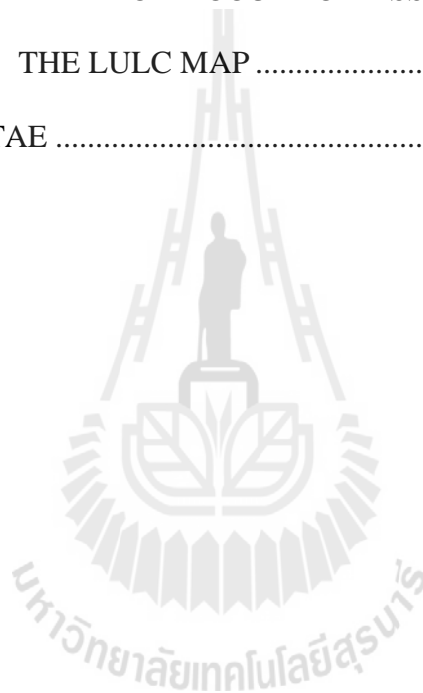
	Page
2.3 Hydrologic model	17
2.3.1 Types of the model.....	17
2.3.2 The local water balance model	22
2.3.3 Watershed runoff	24
2.3.4 Discharge determination and rating curve.....	28
2.3.5 Roles of remotely-sensed data in hydrologic modelling	32
2.3.6 Validation of hydrologic model.....	37
2.4 CA-Markov model.....	38
2.5 Review of the relevant research works.....	41
III METHODOLOGY	47
3.1 Conceptual framework of the study.....	47
3.2 Data preparation.....	50
3.3 Development of the hydrologic model	68
3.4 Construction of the flood maps.....	74
3.5 Impacts of the LULC and climate changes on flooding analysis	81
IV RESULTS AND DISCUSSION	83
4.1 LULC classification and application of the CA-Markov model	83
4.2 Development of grid-based hydrologic model	96
4.2.1 Monthly model formulation.....	100
4.2.2 Daily model formulation.....	112

CONTENTS (Continued)

	Page
4.2.3 Model comparison	117
4.3 Construction of the flood maps.....	120
4.4 Impacts of LULC and climate changes on the modeled runoff.....	128
4.4.1 Assessment on impact of LULC changes.....	128
4.4.2 Assessment on impact of climate changes.....	141
4.4.3 Applications of the original lumped model	144
V CONCLUSIONS AND RECOMMENDATIONS.....	155
5.1 LULC classification.....	155
5.2 Model's developing process and runoff simulation.....	156
5.3 Construction of the flood maps.....	158
5.4 Impacts of LULC and climate changes on the modeled runoff.....	158
5.5 Recommendations.....	160
REFERENCES	161
APPENDICES.....	170
APPENDIX A DATA OF DEPARTMENT OF GROUNDWATER RESOURCES SURVEYING HOLES	171
APPENDIX B EXAMPLE POROSITY AND SPECIFIC YIELD FOR THE SOIL	186
APPENDIX C LIST OF CROSS-SECTION	188

CONTENTS (Continued)

	Page
APPENDIX D DAILY HYDROLOGIC MODEL AND WATER LEVEL MODEL SCRIPT	199
APPENDIX E DATA FOR ACCURACY ASSESSMENT OF THE LULC MAP	210
CURRICULUM VITAE	239



LIST OF TABLES

Table	Page
2.1 List of main runoff measuring stations situated in the upper Ping Basin.....	15
3.1 Main required input data and their contributing sources.....	51
3.2 Monthly/daily (in September) discharge data at P1, P21, P67 stations in 2005.....	65
3.3 Parameters used in the original and developed hydrologic models	73
3.4 Stream-related data for the station P1, P21, and P67	75
3.5 Data of river stage and discharge at three stations, P1, P21, P67.....	78
4.1 Covering area for different LULC classes in year 2000, 2005, and 2010.....	85
4.2 Error matrix of the 2005 classified LULC map.....	89
4.3 Error matrix of the 2010 classified LULC map.....	89
4.4 LULC change matrix during period 2000 - 2010.....	90
4.5 LULC covering area of the predicted maps in 2010 and 2020.....	91
4.6a Transition probability matrix for the prediction of 2010 LULC map.	92
4.6b Transition probability matrix for the prediction of 2020 LULC map.	92
4.6c Transition area matrix for the prediction of 2010 LULC map.	93
4.6d Transition area matrix for the prediction of 2020 LULC map.	93
4.7 Error matrix of the predicted 2010 LULC map.....	96

LIST OF TABLES (Continued)

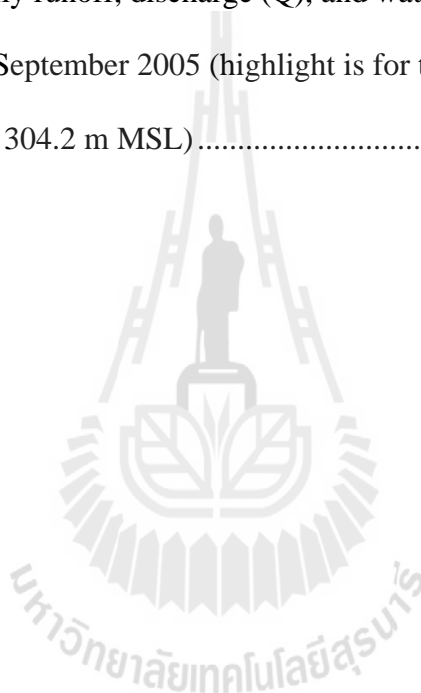
Table	Page
4.8a	Observed (OBS) and simulated (SIM) monthly runoff data at station P1 for all study cases (in unit of mm)..... 111
4.8b	Observed (OBS) and simulated (SIM) monthly runoff data at station P21 for all study cases (in unit of mm) 111
4.9	Correlation factor (R^2) and Nash-Sutcliffe efficiency (E) for the observed and simulated runoff data from all cases (monthly/daily)... 112
4.10	Observed (OBS) and simulated (SIM) daily runoff data at station P1 and P21 for Case 1 and Case 2 (in unit of mm)..... 114
4.11	Model comparison of the simulated runoff results..... 119
4.12a	Simulated daily runoff, discharge (Q), and water level (Z) data at station P1 in September 2005 (highlight is for the predicted flood date with $Z > 304.2$ m MSL)..... 121
4.12b	Simulated daily runoff, discharge (Q), and water level (Z) data at station P21 in September 2005 (highlight is for the predicted flood date by data at the P1 station)..... 122
4.12c	Simulated daily runoff, discharge (Q), water elevation (Z) data at station P67 in September 2005 (highlight is for the predicted flood date by data at the P1 station)..... 123

LIST OF TABLES (Continued)

Table	Page
4.13 Comparison between the simulated and reference flood areas at different water levels (Z) at the P1 station... ..	125
4.14 Simulated daily runoff discharge data (in mm) at the stations P1 and P21 in September 2005 (assumed difference LULC input data).....	130
4.15 LULC covering area of the predicted maps in 2020 (two cases of forest and orchard/perennial loss).....	134
4.16a Transition probability matrix for the 10% forest loss case.....	134
4.16b Transition area matrix for the 10% forest loss case....	134
4.17a Transition probability matrix for the 20% forest loss case.....	135
4.17b Transition area matrix for the for the 20% forest loss case.....	135
4.18 Simulated daily discharge data (in mm) at stations P1 and P21 for modified 2020 cases (assumed different rates of forest/orchard loss)....	139
4.19 Simulated daily runoff data (in mm) at stations P1, P21 in September 2005 (assumed different rates of rainfall intensity).....	142
4.20 Simulated daily runoff data (in mm) at P67 station using the original lumped model (assumed different rates of forest loss and rainfall)	145
4.21 Simulated daily runoff data (mm) at P1 station using the developed model (assumed different rates of forest loss and rainfall)	147

LIST OF TABLES (Continued)

Table	Page
4.22 Simulated daily runoff data (in mm) at P21 station using developed model (assumed different rates of forest loss and rainfall).	148
4.23 Simulated daily runoff, discharge (Q), and water level (Z) data at station P1 in September 2005 (highlight is for the predicted flood date with $Z > 304.2$ m MSL).....	151



LIST OF FIGURES

Figure	Page
1.1 Flooding scenario within Chiang Mai inner city during August-September 2005	2
1.2 Major basins in Chiang Mai Province associated to the great Ping Basin	7
1.3 Topographic map and stream network of the study area.....	8
1.4 False color composite map of the study area from the Landsat TM imagery 2005 (RGB = 453).....	9
2.1 The occurrences of severe flood in Chiang Mai city area in (a) 1987, (b) 1994, (c) 2001 and (d) 2005.....	13
2.2 Map of the network and runoff measuring stations of the upper Ping River 2005.....	14
2.3 The relationship between the observed peak water levels at the P67 and P1 stations for the flood warning administration (4.0 m for P67 and 3.7 m for P1 station)	15
2.4 Simulated flood maps of Chiang Mai city area at river stage of 3.7-4.6 m at the P1 station	16
2.5 Schematic of a watershed discretization and associated flow network in sub-watershed (left) and in grid-based artificial units (right).....	18
2.6 Diagram of the water cycle (at global scale).....	22

LIST OF FIGURES (Continued)

Figure	Page
2.7 Main components and flow directions in the water balance model	23
2.8 Example of a flood hydrograph.....	27
2.9 Relation of the river discharge and its stage in form of rating curve: (a) typical pattern and (b) for the P1 station during 2001-2009	31
3.1 Conceptual framework of the study	49
3.2 Components of the GIS dataset	52
3.3 Topographic data (DEM)	53
3.4 Distribution in location of the DGWR surveying holes	54
3.5 The interpolated effective soil depth map	55
3.6 The interpolated porosity of the effective soil layer.....	56
3.7 Locations of the rainfall and evaporation measuring stations	59
3.8 Distributing pattern of monthly rainfall data (in mm) in 2005.....	60
3.9 Distributing pattern of daily rainfall data (in mm) in September 2005.....	61
3.10 Stream network and locations of relevant discharge measuring stations	64
3.11 Variation of the observed discharges at P1, P21, P67 stations (a) monthly data in 2005 and (b) daily data in September 2005	67
3.12 Flow diagram of the hydrologic model development.....	68
3.13 Flow diagram of the flood map simulation process.	74
3.14 Associated flooding sub-region of three rating curves in Eqs. 3.12a-c....	76

LIST OF FIGURES (Continued)

Figure	Page
3.15 Relations of discharge and water level (rating curve) in 2005 at 3 stations (a) P1, (b) P21, (c) P67.....	77
4.1a Classified LULC map for year 2000 from the Landsat TM image	86
4.1b Classified LULC map for year 2005 from the Landsat TM image	87
4.1c Classified LULC map for year 2010 from the Landsat TM image	88
4.2 Predicted LULC map in 2010 by the CA-Markov model.	94
4.3 Predicted LULC maps in 2020 by the CA-Markov model.....	95
4.4 Pattern of flow direction in the study area.....	98
4.5 Flow accumulation map showing amount of the upward land grids that contribute runoff water to a specific grid of interest in the study area.....	99
4.6 Comparison of monthly runoff data in 2005 (simulated and observed) at (a) station P1 and (b) P21 for Case 1 (uniform rainfall and constant soil depth at 3m).	103
4.7 Comparison of monthly runoff data in 2005 (simulated and observed) at (a) station P1 and (b) P21 for Case 2 (non-uniform rainfall and constant soil depth).....	105
4.8 Comparison of monthly runoff data in 2005 (simulated and observed) at (a) station P1 and (b) P21 for Case 3 (uniform rainfall and nun-uniform soil depth).....	107

LIST OF FIGURES (Continued)

Figure	Page
4.9 Comparison of monthly runoff data in 2005 (simulated and observed) at (a) station P1 and (b) P21 for Case 4 [non-uniform rainfall and soil depth (without sub-surface runoff)].....	108
4.10 Comparison of monthly runoff data in 2005 (simulated and observed) at (a) stations P1 and (b) P21 for Case 5 [non-uniform rainfall and soil depth (with sub-surface runoff)]	110
4.11 Comparison of daily runoff data in September 2005 at station (a) P1 and (b) P21 for Case 6 [Non-uniform rainfall and soil depth (without transpiration rate)].....	115
4.12 Comparison of daily runoff data in September 2005 at station (a) P1 and (b) P21 for Case 7 [non-uniform rainfall and soil depth (with transpiration rate)].....	116
4.13 Comparison of the daily flow duration curve (observed and simulated) at the P1 station (for the present work)	119
4.14 Simulated flood depth maps on the 20th, 21st, 29th, 30th September 2005 when the water level (Z) exceeds the critical value of 304.2 m at the P1 station.	124
4.15 Comparison of flood maps under three condition of water levels at the P1 station (Z = 304.20 m, 304.60, 305.10 m).....	126

LIST OF FIGURES (Continued)

Figure	Page
4.16 Simulated discharge data of the 2005 and 2020 cases at stations P1, P21	131
4.17a Predicted 2020 LULC map with preferred rate of forest/orchard loss at about 10%	136
4.17b Predicted 2020 LULC map with preferred rate of forest/orchard loss at about 20%	137
4.18 Simulated discharge data at stations P1, P21 for the modified 2020 cases (assumed different rates of forest/orchard loss).....	140
4.19 Simulated daily runoff data at station P1 and P21 in September 2005 (assumed different rates of rainfall intensity).....	143
4.20 Simulated daily runoff data at P67 station using the original lumped model (assumed different rates of forest loss and rainfall).	146
4.21 Simulated daily runoff data (mm/day) at the P1 station using the developed model (assumed different rates of forest loss and rainfall).....	148
4.22 Simulated daily runoff data (mm/day) at stations P21 using the developed model (assumed different rates of forest loss and rainfall).....	149
4.23 Flood depth maps in case of the worst forest loss rate (20%)	153
4.24 Flood maps for case of most rainfall increase (15%)	154

LIST OF ABBREVIATIONS

ID	=	One-dimensional
AET	=	Actual Evapotranspiration
ANN	=	Artificial Neural Network
CA-Markov	=	Cellular Automata - Markov
CROP	=	Field Crop
CN	=	Curve Number
DDPM	=	Department of Disaster Prevention and Mitigation
DEM	=	Digital Elevation Model
DGWR	=	Department of Groundwater Resources
DTM	=	Digital Terrain Modeling
DUI	=	Disutility index
EGAT	=	Electricity Generating Authority of Thailand
ET	=	Evapotranspiration
FOR	=	Forest
GISTDA	=	Geo-informatics and Space Technology Development Agency (Public Organization)
GIS	=	Geographic Information System
HRU	=	Hydrologic Response Unit
IDW	=	Inverse Distance Weighted

LIST OF ABBREVIATIONS (Continued)

LDD	=	Land Development Department
LULC	=	Land Use and Land Cover
MIS	=	Miscellaneous
m. MSL.	=	meter above Mean Sea Level
ORC	=	Orchard
PAD	=	Paddy Field
RID	=	Royal Irrigation Department
RS	=	Remote Sensing
RTSD	=	Royal Thai Survey Department
SCS	=	Soil Conservation Service
SWAT	=	Soil and Water Assessment
TMD	=	Thai Meteorological Department
U/B	=	Urban and Built-up Land
WAT	=	Water

CHAPTER I

INTRODUCTION

1.1 Background problem

Floods are destructive natural phenomena which can lead to serious problems in lowland regions, resulting in significant loss of human life and affecting fertility of natural resources and man-made properties. In Thailand, news of the disastrous floods and their serious consequences has been reported by media and responsible agencies every year, notably during the local monsoon season (May-September). For example, the Department of Disaster Prevention and Mitigation had reported that there were six major floods occurred in 2006. These resulted in more than 500 losses of human life and nearly 10 billion bahts on property damages (Department of Disaster Prevention and Mitigation [DDPM], 2006).

Normal cause of these severe floods is pronounced heavy rainfall that may last for several days. Most vulnerable areas are typically situated close to the high hills or mountains (risk facing flash flood) and within vicinity of flood draining canals or rivers (risk to have river flood), especially ones located along several major rivers of the country, e.g. Chao Praya River (central region), Ping River (northern region), or Mun River (northeastern region). Floods are noticeably harmful to the economy and people activities of several major cities in Thailand that locate adjacent to the main rivers, like Chiang Mai in the north or Ubon Ratchatani in the northeast.

For example, during August and September 2005, the Chiang Mai Province had experienced at least 4 severe floods resulted from overbank flow from Ping River after having prolonged upstream intense rainfall. This event resulted in almost half of the municipal area was inundated for several days (Figure 1.1) and was regarded as being worst flooding scenario ever seen in the province for almost 50 years. The total damage was estimated about more than 5 billion baths. At the peak flood, the water level recorded from gauge station P.1 at the Navarat Bridge was as high as 4.93 meter while the critical value for having flood (or overbank flow) was approximately at 3.70 meter only (Somnuk Chatchawan, 2005).



Figure 1.1 Flooding within Chiang Mai inner city during August-September 2005 (Somnuk Chatchawan, 2005).

One of the effective approaches to analysis flood development and expansion can be achieved by using the hydrologic model. This model can describe relationship between rainfall distribution data and amount of the runoff discharge (that initiates river flood) based principally on knowledge of some factors such as soil properties,

topography, drainage system, and land use/land cover. Most hydrologic models had been developed using complicated mathematical formulation and mainly designed to utilize at basin scale. Some crucial deficiencies of these models are their lump-based segmentation of the study area in which fine details of the water balance process are still not realistically explained. They are also still lack of remote sensing and GIS applications integrated in the processing module. This can hinder ability of the model in predicting near-real time flood forecasting at fine scale.

To demonstrate advantages of using remote sensing (RS) and GIS technology in the prediction of runoff discharge and the associated flooding scenario, this thesis has developed a new grid-based hydrologic model using the Chiang Mai sub-basin (in the upper Ping watershed) as study area. The core processing algorithm of this model is based on the original lump-based model described in Jothityangkoon et al. (2001), Jothityangkoon and Sivapalan (2003), Jothityangkoon and Hirunteeyakul (2006; 2009). However, it has much better spatial resolution on the discharge analysis due to its grid-based nature on the contrary to the referred lumped model that can manage the analysis at basin/sub-basin scale only. The stated model is structured to realistically simulate observed runoff discharge data in the Ping River during year 2005 (monthly basis) and September 2005 (daily basis).

Knowledge of the simulated runoff discharge in the Ping River along with the relevant rating curves can be used to produce flood maps of the Chiang Mai municipal area that can be compared with the flood data records reported by general media and local/national authorities. In addition, impact of the land use/land cover (LULC) or climate changes (rainfall in particular) over runoff discharge data and their associated flooding characteristics can also be readily examined by the proposed model based on

the grid-based nature of its processing algorithm. It is hoped that, the results found in this thesis can provide better understanding on the runoff discharge formulation and its associated flooding characteristics in the Chiang Mai sub-basin, which is valuable for devising better flood forecasting, prevention and mitigation schemes in the future.

1.2 Research objectives

1.2.1 To develop grid-based hydrologic model capable of simulating realistic runoff scenarios (on monthly and daily basis) using GIS-based input data.

1.2.2 To generate flood maps of the Chiang Mai municipality during September 2005 based on the simulated runoff discharge data and the relevant rating curves.

1.2.3 To examine impact of LULC and climate changes on runoff discharges and the associated flood maps based on the predicted LULC maps derived by the CA-Markov model and the modified rainfall intensity.

1.3 Scope and limitations of the study

1.3.1 The proposed model is developed using Model Builder provided in Arc Toolbox of ArcGIS program as main platform.

1.3.2 Only DEM at scale of 1:50,000 is used in the analysis.

1.3.3 The targeted area of this study is a sub catchment of Upper Ping River Basin where Chiang Mai municipality is located. The upstream boundary of the area is gauge station P.67 and downstream boundary is gauge station P.66.

1.3.4 The credibility of the runoff data of the proposed model are evaluated based on the found relevant values of the coefficient of determination (R^2) and Nash-Sutcliffe efficiency (E).

1.3.5 As the assumption flooding scenario in this work is river flood.

1.4 Benefits of the study

1.4.1 Effective grid-based hydrologic model for realistic simulation of runoff scenarios (on monthly and daily basis).

1.4.2 Flood maps of the Chiang Mai municipality area during September 2005 based on the simulated daily runoff data generated by the established model.

1.4.3 Knowledge on impact of the used LULC and climate changing scenarios on the runoff discharge data and their associated flood characteristics.

1.5 Study area

The chosen study area is a part of the upper Ping Basin covering area of about 1,121.09 sq. km in the Chiang Mai Province. It is one of the 20 sub-basins associated to the great Ping Basin and is one of the four main tributaries of Chao Phraya River, the most essential river in the central Thailand. The basin locates in the upper-north of Thailand with most areas residing in Chiang Mai Province. It aligns itself along the north-south direction with Ping River as its core water drainage channel along with the other three main branch rivers: Mae Rim, Mae Taeng, and Mae Ngad (Figure 1.2).

Topography of the area has complex network of the high mountains dominates on the western side and flat plain terrain dominates on the eastern side with elevation ranging from about 278 m to 1,826 m (Figure 1.3). The satellite image classification (Landsat TM) (Figure 1.4) indicates that in 2010 about 60% of the total area was covered by forest while orchard and paddy plantation covers about 20% and

urban/built-up land covers about 14% of the area. Main types of orchard found in the area are, for examples, longan, lychee, mango, jackfruit.

Local climate is defined by large variations in annual rainfall and seasonality that is influenced by Pacific-born typhoon, superimposed on the south-west monsoon. Most of the rainfall occurs in the wet season from May to October (about 88%) while the rest (about 12%) occurs in dry season (November-April). Month with the highest amount of the average rainfall intensity (about 212 mm) is September and one with the lowest amount of the rainfall (about 7 mm) is February. Average temperatures at Chiang Mai station is about 25°C while the highest temperature can be at about 41°C (Faculty of Engineering, Chiang Mai University, 2007).





Figure 1.2 Major basins in Chiang Mai Province associated to the great Ping Basin
(Faculty of Engineering, Chiang Mai University, 2007).

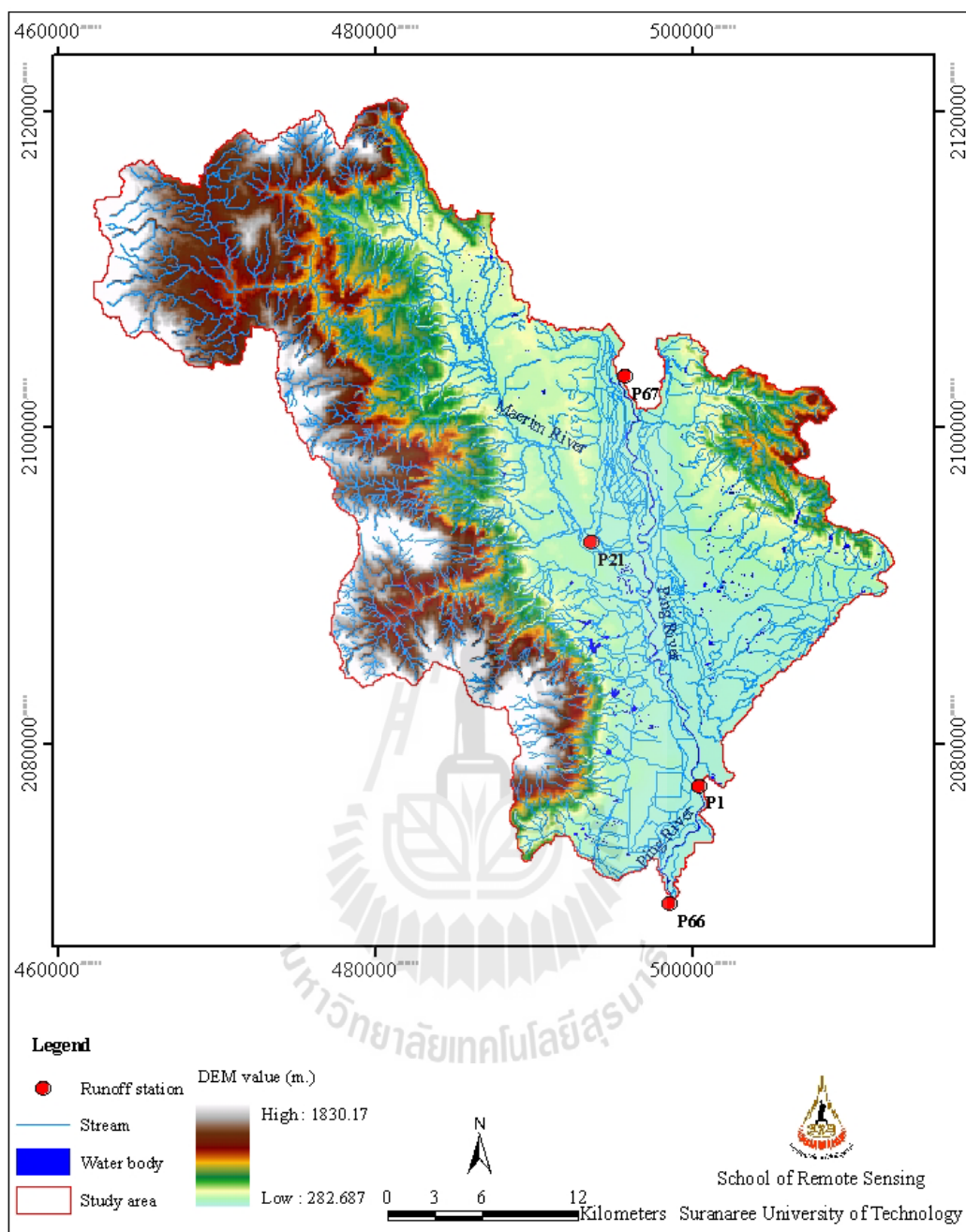


Figure 1.3 Topographic map and stream network of the study area.

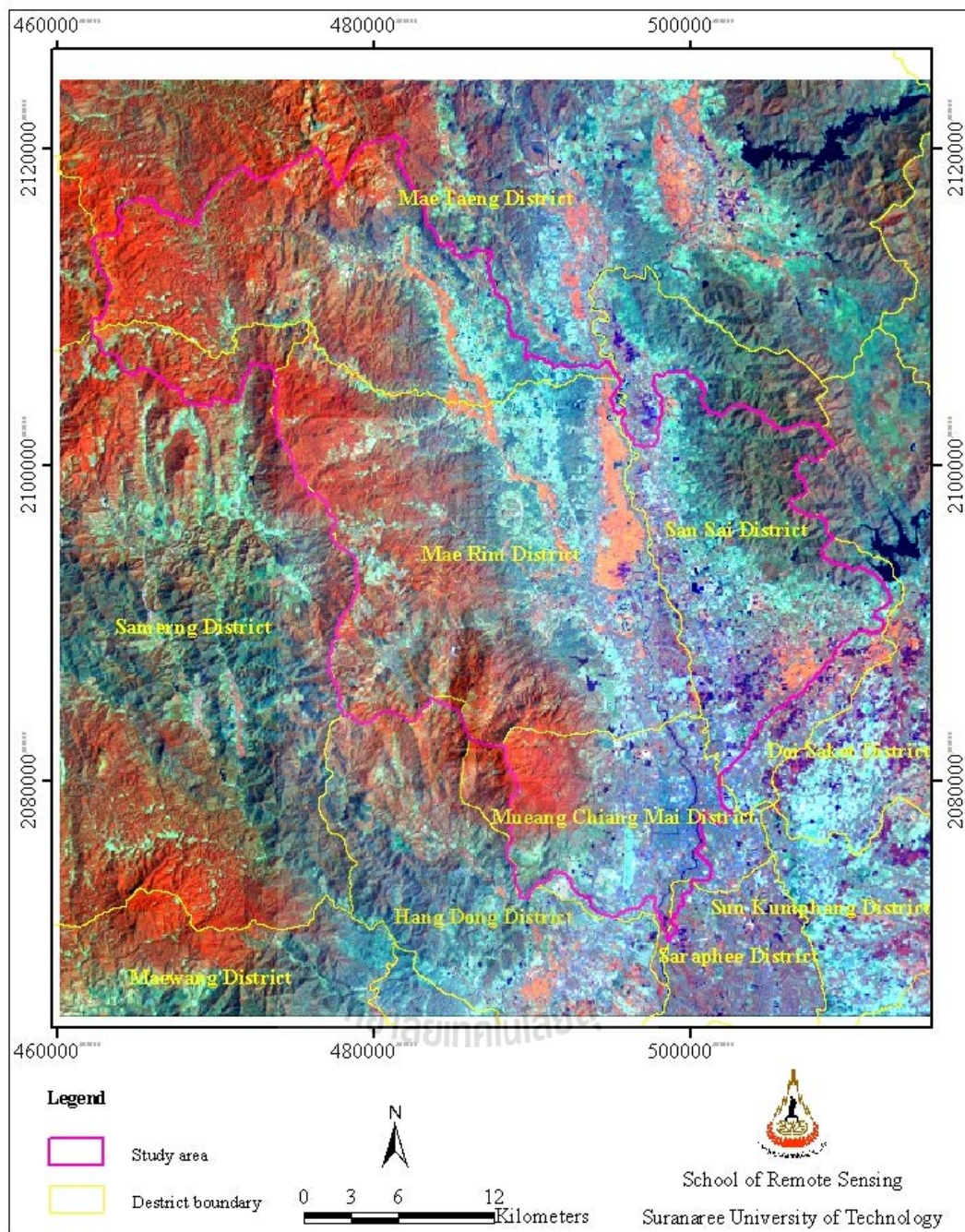


Figure 1.4 False color composite map of the study area from the Landsat TM imagery 2005 (RGB = 453).

CHAPTER II

LITERATURE REVIEW

This chapter provides fundamental knowledge of flood phenomenon, concepts of the water balance and hydrologic models, the CA-Markov model for LULC change prediction and the flood warning and management systems in Chiang Mai municipal area at present. Review of some works relevant to these topics is also presented.

2.1 Definitions and types of flood

Typically, flood can be defined as an overflow, or accumulation, of substantial water volume that inundates the land (which is not normally submerged) (Glossary of Meteorology, 2000). Floods are well-known natural hazard that sometimes can lead to devastated consequences like loss of human lives or costly damage to the properties. In general, floods can be divided into 5 main categories, which are (Floodsite, 2012)

1. River flood: It originates from the overflow of water from the overloaded canals or rivers and submerges low area situated close to river channel. This incidence is frequency seen in the lowland downstream where the rivers are most heavily loaded with drained water and it can last for weeks or months before disappearing.

2. Flash flood: It is a rapid local flooding of great water volume that is usually caused by prolonged heavy upstream rainfall over a small area. It can also occur after the sudden collapse of large dams and may last for short duration (e.g. < 1-2 hours). Massive landslides are frequently found to be induced by this kind of flood.

3. Pluvial flood: It is an infrequent incidence often occurred when the heavy rainfall induces excessive overland surface runoff that overwhelms drainage capacity of the lowland areas situated further away from main stream channels. In general, it is still rather difficult to predict occurring probability of this kind of flood and to assess its impacts conclusively due to limited knowledge on its formation and development.

4. Urban flood: It is mostly resulted from the heavy rainfall in urban area with inefficient draining system. It may last for few hours before disappearing.

5. Coastal flood: It is normally induced by large storm surge moving from sea into coastal lowland under the fueling of extra strong land-ward winds like hurricane or typhoon, or as a consequence of the tsunami phenomenon.

Primary effects of flooding are (1) physical damage to properties like houses, buildings, roads, and to natural resources like forest, topsoil, and (2) human/livestock casualties due to the drowning and subsequent epidemics or water-borne diseases. Its secondary effects include, for examples, water-supply contamination, spread of the water-borne diseases, diminishing of crop/food supply. Moreover, flooding can cause long-term effect by degrading natural resources and fertility of the ecosystem along with sustainable use of fertile land. High cost for recovering of the severely-damaged buildings, infrastructure and human illness is also a concerned issue.

In several countries across the world, rivers prone to floods are often carefully managed. Defenses such as levees, bunds, reservoirs, and weirs are normally used to prevent overbank flow. However, if these traditional defenses fail, other emergency measures such as sandbags or portable inflatable tubes might be introduced to handle the problem.

2.2 Great Floods of Chiang Mai

Chiang Mai Province has been long-time named capital of the north as it is a core city for economic activities and governmental service provision of the northern area. However, as its most urban area situates in low land close to the Ping River, it is greatly vulnerable to the river flood induced by the intense upland rainfall upstream. Officially, flooding shall be notified when the water volume of the Ping River at P1 station (Navarat Bridge) exceeds the critical level of 3.70 m (or 304.2 m MSL) on the measuring gauge. The province has been suffered from the occurrences of several devastated floods in the past, especially during two strong monsoon months: August and September. For examples, the severe floods were observed in 1987, 1994, 1995, 2001, 2005, and 2011 with peak water levels being measured at the P1 station of 4.53, 4.43, 4.27, 4.18, 4.93, and 4.94 m, respectively (Figure 2.1) (Faculty of Engineering, Chiang Mai University, 2007; Hydrology and Water Management Center for Upper Northern Region, 2012).

In 2005, the province had experienced at least 4 severe floods during August-September due to the overbank flow from Ping River after having prolonged upstream intense rainfall. This incidence resulted in almost half of the city area being inundated for several days. The devastated consequences of the 2005 floods, especially in the central economic and residential zones, had generated great public concern about the efficiency of flood protection and warning systems organized by local authorities and involved government's agencies. Some critical issues being raised by local people at that time were impacts of future LULC change, especially forest loss to agriculture. Their demand for more efficient flood warning and monitoring system (e.g. on the near-real-time) was also addressed (Somnuk Chatchawan, 2005).

2.2.1 Flood warning administration

At present, the Royal Irrigation Department (RID) has installed several stream discharge measuring stations along several main river channels of the upper Ping Basin area to collect and report river discharge data of the area in real-time basis (Figure 2.2 and Table 2.1). Prediction of flooding severity in Chiang Mai city area is now based primarily on the expected level of the water level at the P1 station that can be calculated (6-7 hours in advance) based on the approximated relationship between observed peak water levels at the P67 and P1 stations as seen in Figure 2.3.



(a) August 1987

(b) August 1994



(c) August 2001

(d) August 2005

Figure 2.1 The occurrences of severe flood in Chiang Mai city area in (a) 1987, (b) 1994, (c) 2001, and (d) 2005 (Faculty of Engineering, Chiang Mai University, 2007).

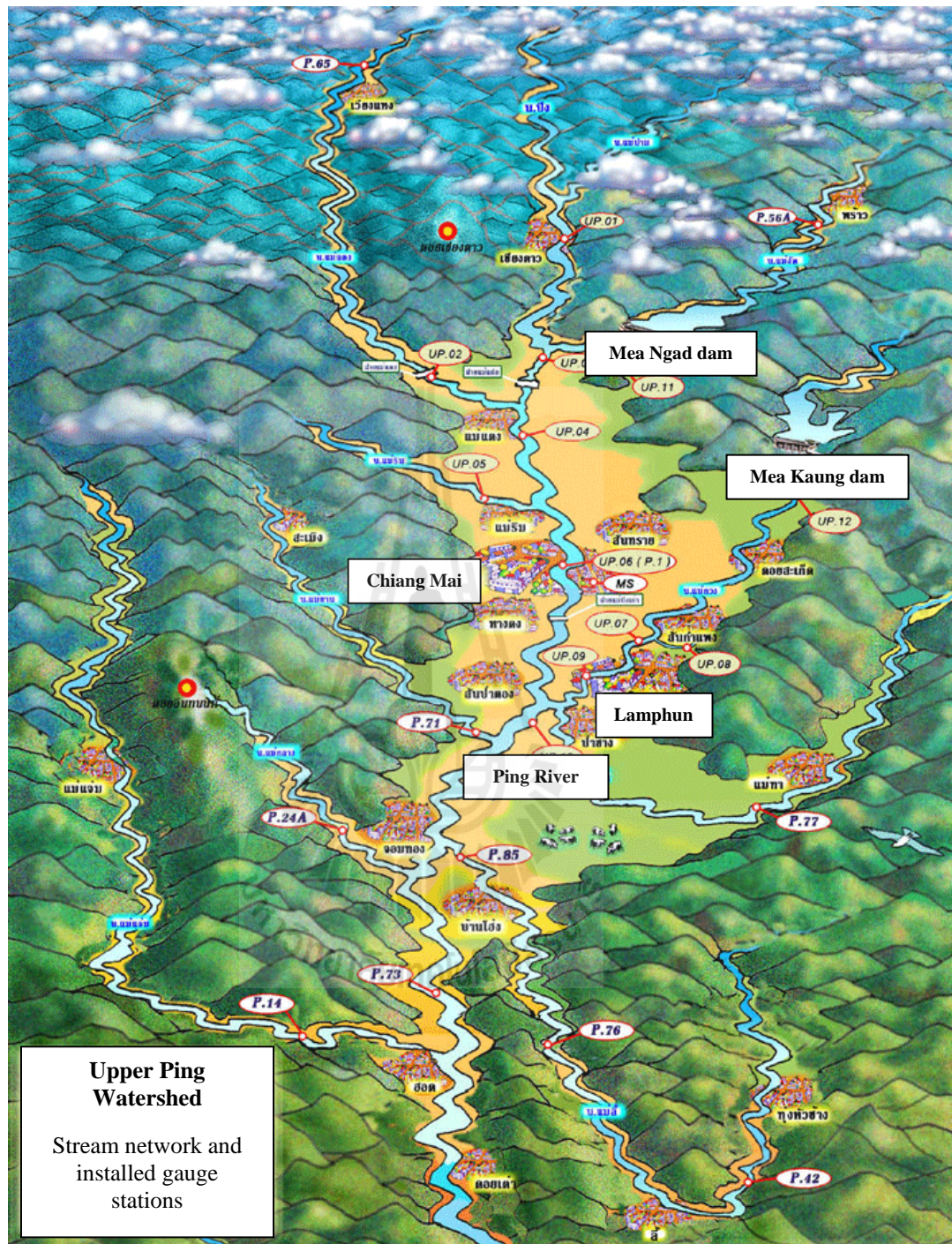


Figure 2.2 Map of the network and runoff measuring stations of the upper Ping River
(Hydrology and Water Management Center for Upper Northern Region,
2012).

Table 2.1 List of main runoff measuring stations situated in the upper Ping Basin (Hydrology and Water Management Center for Upper Northern Region, 2012).

River	Station	Location	Since
Ping	P1 (UP06)	Nawarat Bridge, Mueang District	1921
	P20 (UP01)	Tambon Chiang Dao, Chiang Dao District	1979
	P67 (UP04)	Tambon Mae Phag Kao, San Sai District	1996
	P73	Tambon Mae Soi, Chom Thong District	1998
	P75 (UP03)	Tambon Chor Lae, Mae Taeng District	1999
Mae Taeng	P4A	Mae Taeng Bridge, Mae Taeng District	1955
	P65	Tambon Piang Luang, Wiang Haeng District	1992
	UP02	Mae Taeng Check Dam, Mae Taeng District	1973
Mae Rim	P21 (UP05)	Tambon Rim Nuea, Mae Rim District	1954
Mae Ngad	P56A	Tambon Mae Wan, Phrao District	1999

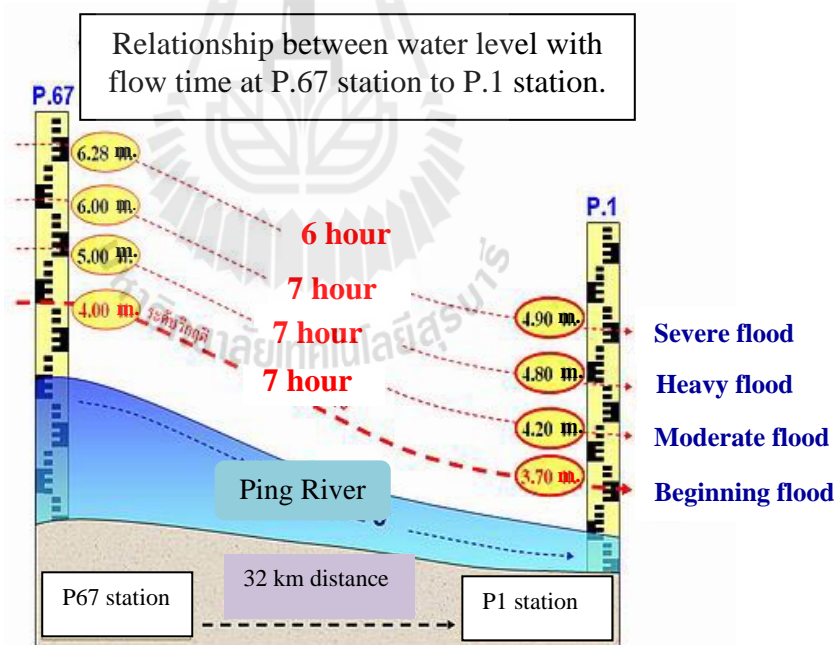


Figure 2.3 The relationship between the observed peak water levels at the P67 and P1 stations for the flood warning administration (4.0 m for P67 and 3.7 m for P1 station) (Hydrology and Water Management Center for Upper Northern Region, 2012).

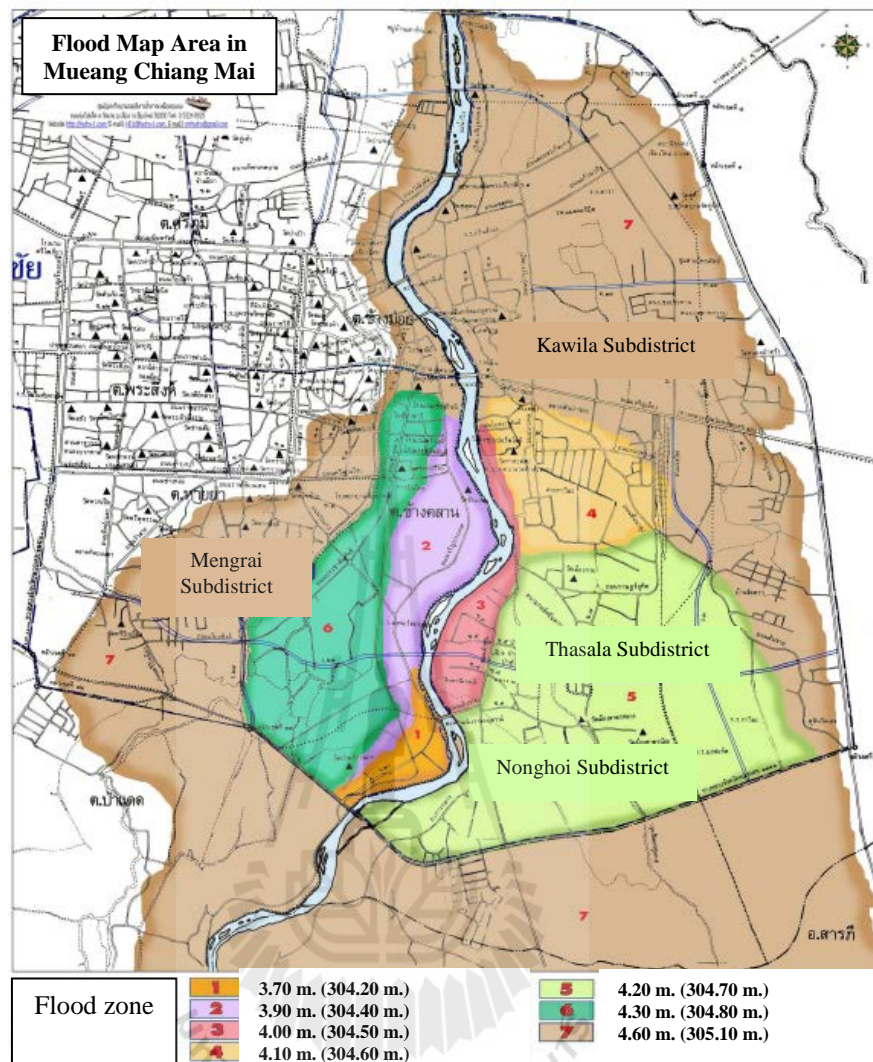


Figure 2.4 Simulated flood maps of Chiang Mai city area at river stage of 3.7-4.6 m at the P1 station (Faculty of Engineering, Chiang Mai University, 2007). This map (at a specific water height) was created based on modeled simulation of flat flood water distribution over the terrain (represented by DEM of 2 m interval) integrated with the surveyed field data to identify realistic flooded area in each particular case of water height. If the generated water level greater than the local elevation, the area shall be labeled as being flooded land unless the field surveyed data indicate otherwise.

2.3 Hydrologic model

2.3.1 Types of the model

Hydrologic models are simplified conceptual framework of the water balance at some particular area. Most models were developed using complicated mathematical formulation to utilize mainly at basin or catchment scale. They are primarily used for hydrologic prediction and for proper understanding of h processes and their consequences. The hydrologic models commonly used nowadays can be divided into two broad categories (Seth, 2006):

(1) Stochastic models. A stochastic model generates outputs that are at least partially random: produces the different output from a given input. In essence, they are black-box systems in nature as their main aim is to link certain input (for instance rainfall) to model output (for instance stream runoff) using some chosen mathematical and statistical concepts where the commonly used are regression, transfer functions, and system identification. The simplest form is the linear model, but it is common to employ non-linear components to represent some general aspects of the catchment's response without moving deeply into real physical processes that might be involved (no/little physical basis required). A well-known example is the ANN model (artificial neural network) which has the ability to model both linear and nonlinear relationships without the need to make any implicit assumptions at first.

(2) Deterministic models. This model does not consider randomness: a given input always produces the same output. The model's processes are developed based on definite physical laws and no uncertainties in prediction are admitted. The models are based on our understanding of physics of the hydrological processes which control catchment response and use physically-based equations to describe these

processes. They basically try to represent main physical processes observed in the real world, especially those of surface runoff, subsurface flow, evapotranspiration, and channel flow, but these can go far more complicated.

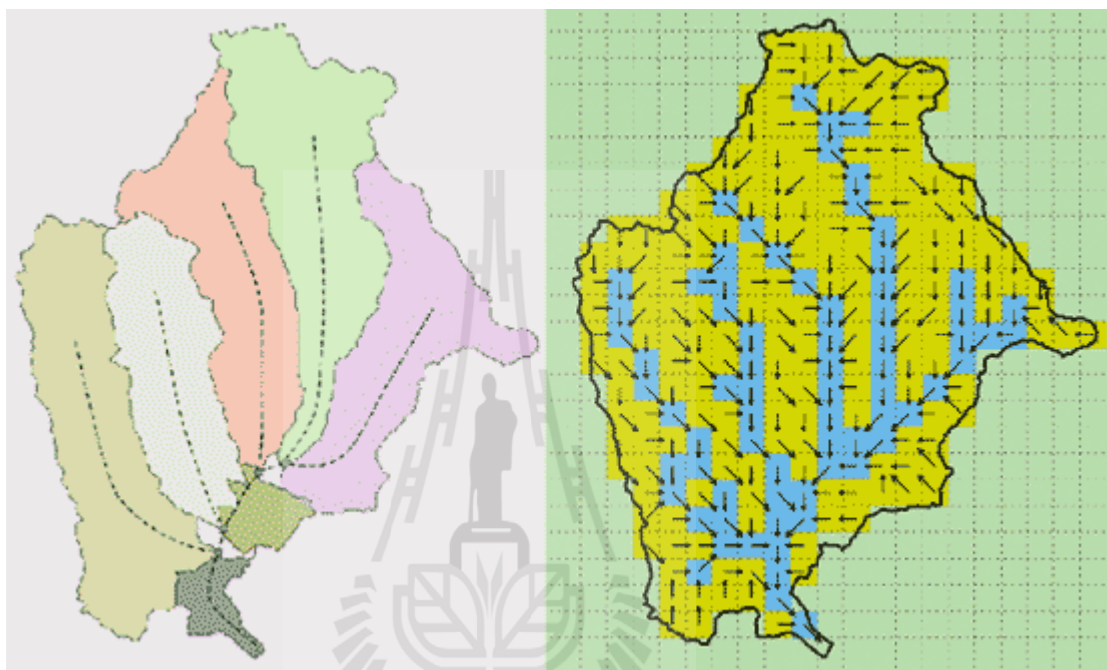


Figure 2.5 Schematic of a watershed discretization and associated flow network in sub-watershed (left) and in grid-based artificial units (right) (CRAHI, 2012).

Deterministic models can be further classified according to whether the model gives a spatially lumped or distributed description of the catchment area, and whether the description of hydrological processes is empirical, conceptual or fully physically based. Two groups of the models generally referred to in literature are (Figure 2.5) (CRAHI, 2012);

2.1 The lumped models. Such models conceptually assume that the transfer of water in the catchment taking place in only few well-defined storages (or lump), each of which has homogeneous property and represents a fundamental unit in the operating process (e.g. rainfall, soil characteristics, vegetation, land use practice). Though, this assumption is rarely fulfilled in reality, their concepts still provide some priory understanding in the water balance details of the examined area. These models can be regarded as in the intermediate position between the full grid-based approach and the empirical black box analysis. There are numerous lumped hydrologic models which are based on concept of a unit hydrograph, UH. This concept is valid within a framework which assumes that the watershed is a linear causative and time invariant system where only part of relevant excess rainfall that produce runoff.

2.2 The grid-based, or distributed, models. These models consider the hydrologic process that taking place within area divided into a large amount of small rectangular grids that enables them to describe the hydrologic processes with a fine resolution (e.g. 100-500 m). The equations of the processes are solved in each defined unit (grid) and combined with output from the neighbor. This structure leads to very complex models that require a great amount of information, and at least, up to present, the calibration of a tremendous amount of parameters, if not all the variables may be estimated from field data. This makes the use of the distributed models for realistic runoff forecasting is still rather difficult so far, particularly when performing in the large and heterogeneous area.

However, from their physical basis, such models can simulate complete runoff regime, providing multiple outputs (e.g. discharge, groundwater level, evaporation loss) while most black box models can offer just only one output. In these

models, transfers of mass, momentum and energy are calculated directly from the governing partial differential equations which are normally solved by using numerical methods, for examples, the St. Venant equations for the surface flow, the Richards equation for unsaturated zone flow and Boussinesq equation for ground water flow. As distributed models can incorporate spatial variability of the variables more accurately and they reproduce more faithfully the processes that occur in a watershed than lumped models do, they are expected to provide better results than a lumped one (CRAHI, 2012).

In general, the black-box model is appropriate for the preliminary study of the water balance process in the area due to its simple structure and no/little physical data of the area required. However, it gives little information about the actual process and several adjustments in the calculating algorithms might be needed just to fit the output data with the real observed ones. On the contrary, lumped model needs more physical data and knowledge of the hydrological process in the area to work properly. But its capacity is still limited to the analysis at basin/sub-basin scale only. To have model with better spatial resolution, the grid-based model is the most suitable alternative. However, the difficulties in developing such model lie in its need for huge amount of physical data and through knowledge of the hydrological process of the interested area. Therefore, it typically works well for the study in small area.

There are two strategic approaches to build the preferred hydrologic model, the downward (or top-down) and the upward (or bottom-up) approaches. As described by Klemes (1983), the downward (or top-down) approach was applied in the model's developing process. In essence, this kind of work tries to find a concept directly at the level or scale of interest (or higher) and then looks for steps that could

have led to it. This is in the contrary to the upward (or bottom-up) approach which tries to combine, by mathematical synthesis, the empirical facts and theoretical knowledge available at a lower level of scale into the theories capable of predicting the response at the higher scale. As a consequence, the simple form of the preferred model will be considered and test first at the preferred scale of interest, then more complexity will be added to the original model to gain higher accuracy in the obtained result until it reaches level of accuracy required.

Examples of the hydrologic model

There are several hydrologic models available at present. For example the soil and water assessment tool (SWAT) model. SWAT is a GIS-based hydrological model that has a modular structure and consists of the hydrological, sedimentological, and chemical subroutines applicable to the watershed-scales. It was developed to predict impacts of land management practices on water, sediment, and agricultural chemical yields in relatively large complex watersheds. A central part of SWAT is the general water balance equation in which surface runoff will be determined by the SCS Curve Number (CN) approach. For the modeling purposes, SWAT divides a watershed into several sub-basins and portion them that possesses unique land use/management/soil attributes will be grouped together to define a single hydrologic response unit (HRU). By using a water balance equation, runoff is predicted separately for each HRU and routed to obtain total runoff (Wang et al., 2006; Schulz and Matthies, 2007).

Similar to SWAT, MIKE SHE has a modular structure, sub-surface and stream flow involving distributed grid points. MIKE BASIN is another product within MIKE family and functions as an extension of ArcView. The water resources

management tool is raster-based and works mainly on a basin scale. In a case study, the main flaw of MIKE BASIN was its failure to simulate high water flow but otherwise satisfactory results were achieved (Schulz and Matthies, 2007).

2.3.2 The local water balance model

Essential concept of the hydrologic model is to realistically simulate details of the water cycle that produce surface runoff over some particular area, mostly at the basin scale. The water cycle describes the continuous movement of water on the Earth (in different forms). This cycle (at global scale) can be outlined as seen in Figure 2.6. Main parts of the cycle are precipitation (e.g. rain, snow), surface runoff, subsurface runoff, and water vapor (from the transpiration and evaporation processes).

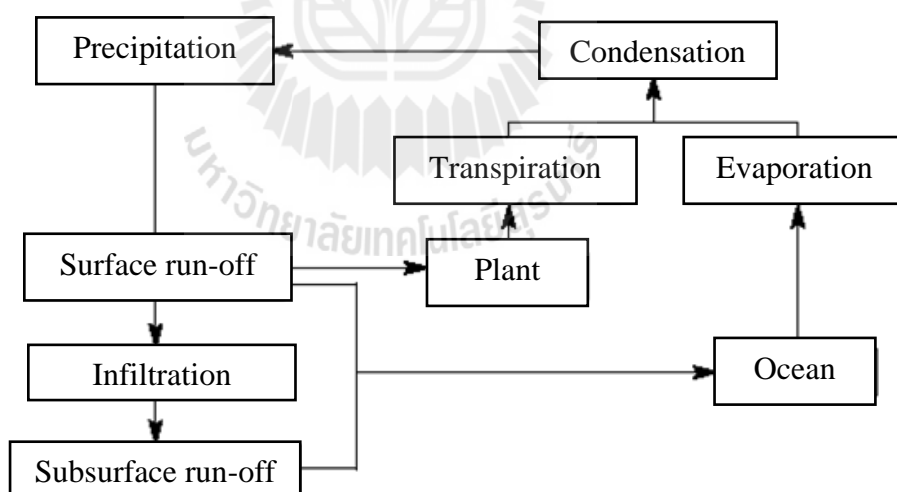


Figure 2.6 Diagram of the water cycle (at global scale).

Knowledge of water cycle in nature can be used to construct the framework of the water balance situation over some specific area, e.g. at basin or sub-basin scales. The water balance model is used to describe the conservation in volume of water over some particular area in according to the local water cycle characteristics of the area (Figure 2.7). The fundamental water balance equation can be written as follows (over a specified period of time):

$$\Delta S = P - Q_{SF} - Q_{SSF} - AET \quad (2.1)$$

Where ΔS is change in soil water storage of the area, P is the precipitation (e.g. rainfall or snow), AET is actual evapotranspiration from land and vegetation (ET), Q_{SF} is total overland surface runoff, Q_{SSF} is total sub-surface runoff.

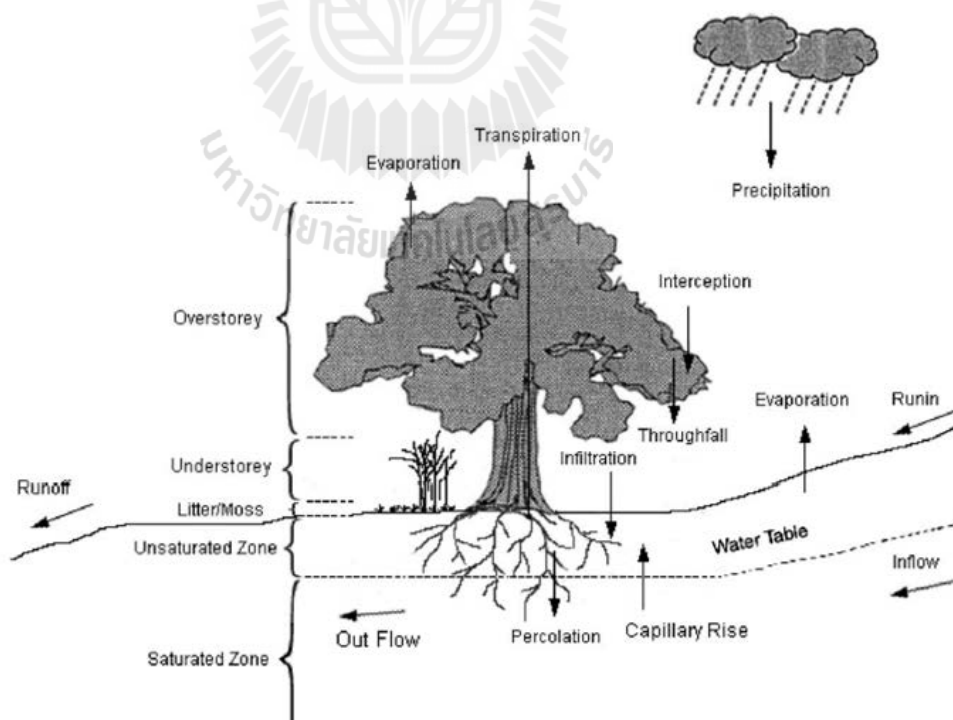


Figure 2.7 Main components and flow directions in the water balance model (from Chen, 2005).

In the hydrologic model, the local water balance model in Eq. 2.1 is applied to determine amount of the total overland surface runoff over each considered unit area under the prior input data. It then simulates the runoff movement to the neighboring land units before finding its way to the stream channel situated nearby. Flow pattern of the existing surface runoff usually determined by the topographic elements of the area, especially surface slope and aspect. Primary output from the hydrologic model is hydrographs at varying locations along the waterways to describe quantity, rate and timing of stream flow that results from the associated rain events. These hydrographs then become a key input into the hydraulic model. The hydraulic model simulates the movement of flood waters through waterway reaches, storage elements, and hydraulic structures. It calculates flood levels and flow patterns and also complex effects of backwater, overtopping of embankments, waterway confluences, bridge constructions and other hydraulic structure behavior.

2.3.3 Watershed runoff

Typically, the watershed can be defined as an enclosed region where the direct precipitation occurs within the confines of its drainage basin and collects into a stream channel, flowing downhill to a common basin outlet. A drainage basin is the physical boundary between watersheds where slope of the watershed diverts all surface runoff to the same drainage outlet. The boundary between watersheds is called a drainage divide. Watershed hydrology deals with the rainfall-runoff relationships found across a drainage basin (Singh 1992).

Conceptually, watershed runoff is composed of three components: (1) surface runoff, (2) interflow, (3) groundwater runoff (i.e. base flow). Surface runoff flows over the surface of the watershed and downstream in stream channels to the

watershed basin outlet. Interflow is the portion of runoff that infiltrates into the upper soil layers of the watershed and moves laterally until it reaches the stream channel. Interflow moves slower than surface runoff, reaching the stream channel later in time. Base flow percolates through soil until it reaches the water table and then moves laterally until reaching the stream. Base flow is much slower than both surface runoff and interflow and has little to no impact on flood peaks resulting from a storm (Shultz, 2007).

The surface runoff is composed of two main components: (1) overland flow and (2) channel flow. Overland flow is the portion of runoff which flows over the land surface to the stream channel. Overland flow occurs when the precipitation rate from a storm exceeds the interception capacity of the vegetative canopy, the infiltration capacity of soil on the watershed, and surface storage. Channel flow is the translation of a flood wave as it moves downstream in a stream channel. As runoff moves across a watershed and then downstream to the outlet, it undergoes changes across both the overland flow plane and within the stream channel (Shultz, 2007).

Regarding to general concept of the hydrologic model stated earlier, there are five main factors that contribute the most to variation of the observed channel runoff:

1. Precipitation (e.g. duration, distribution, intensity): To be used as the input water resource in the water balance model;
2. Topography (e.g. slope, geologic structure, drainage system): To determine general flow direction of the surface runoff;

3. AET: To determine rate of water loss due to the evapotranspiration process (depends mostly on the climatic and soil conditions and vegetation cover pattern);
4. Soil infiltration capacity: To determine the water loss due to the infiltration process (depends mostly on soil type);
5. Land use/land cover (LULC) pattern: To assist the determination of flow movement, infiltration rate and AET rate the most.

Hydrograph characteristics

The relation of rainfall and resulted stream discharge at a particular basin, or sub-basin, is often described in form of a “hydrograph” (Figure 2.8). The stream flow hydrograph is the time distribution of the water discharge at a specific point on a stream channel. A hydrograph is affected by both characteristics of basin and storm system causing the rainfall. Shape of the hydrograph is influenced by the transmission rates of overland flow and channel flow along stream way to the basin outlet. Major factors that determine shape of a hydrograph (and variation of runoff) are the drainage characteristics, soil type, vegetation type, land use, and rainfall distribution (Shultz, 2007).

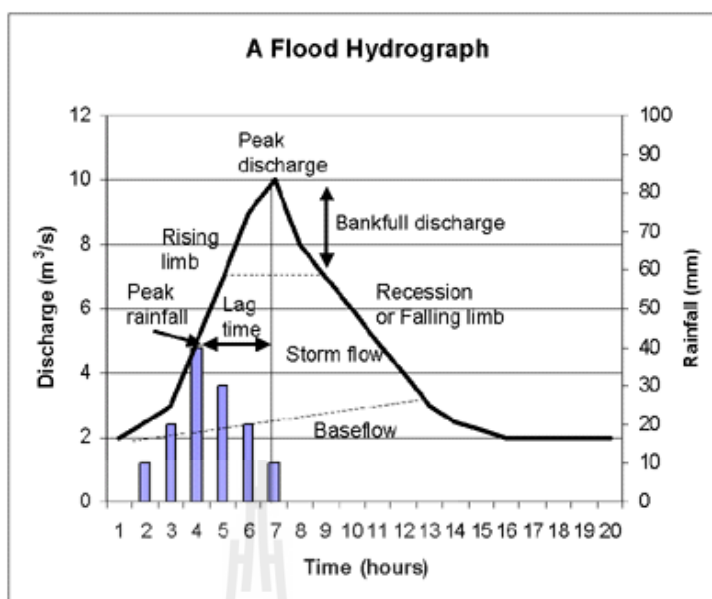


Figure 2.8 Example of a flood hydrograph (Odblog, 2008).

In general, a deeper soil structure retards runoff, lowers the magnitude of flood peaks, and results in a longer sustained period of minimum flows. Also, steeper slopes cause the runoff to be more rapid, resulting in greater maximum peak flows with a shorter time of concentration and hydrograph decay time. The clay soils are highly impervious causing higher runoff and higher river discharge compared to sand which is very pervious, resulting in the lower runoff and lower stream flow discharges. Silt produces runoff which lies between these two soil types.

Vegetation also affects shape of the hydrograph. A densely forested canopy increases amount of rainfall which is intercepted and evaporated directly back into the atmosphere, resulting in the lower runoff and lower stream flow at the basin outlet. In contrast, a sparsely covered grassland decreases amount of rainfall being intercepted, resulting in higher runoff and higher stream flow at the basin outlet. Land use changes typically increase amount of runoff resulting in higher water flow

discharges. Several practices like urbanization, farming, and timber harvesting normally increase runoff while other practices such as building dams and diversions usually decrease runoff.

Rainfall distribution across a watershed varies both spatially and temporally. Spatial properties include both location and amount of precipitation across watershed. Temporal properties include the time distribution of rainfall at a particular location in the basin. Rainfall intensity has direct impact on the rate of peak flow and amount of produced runoff. Increasing of rainfall intensity will increase both the peak discharge and volume of runoff providing it is greater than the soil infiltration rate. Variations in rainfall intensity will have an impact on the hydrograph shape for small basins but this will be minimal for large basin (Shultz, 2007).

2.3.4 Discharge determination and rating curve

In theory, the discharge volume of the channel flow (in 1D analysis) at some specific location along the river can be computed by the following relationship:

Discharge = Cross-sectional area x Average flow velocity,

$$\text{or} \quad Q = A \times \bar{V} \quad (2.2)$$

For uniform flow, the average velocity (\bar{V}) can be determined using the Manning Equation as follows (Chow, Maidment and Mays, 1988):

$$\bar{V} = \frac{kR^{2/3}S^{1/2}}{n} \quad (2.3)$$

where

\bar{V} \equiv Average velocity of the flow (in m/s for the SI unit or ft/s for the US customary unit);

k \equiv 1.0 for SI unit or 1.486 for US customary unit (dimensionless);

R \equiv Hydraulic radius = cross-sectional area/wetted perimeter (in m for the SI unit or ft for the US customary unit);

S \equiv Hydraulic gradient (slope of the channel) (dimensionless);

n \equiv Manning's roughness coefficient of the channel
(in $\text{m}^{-1/3}\text{s}$ for the SI unit or $\text{ft}^{-1/3}\text{s}$ for the US).

Rating curve

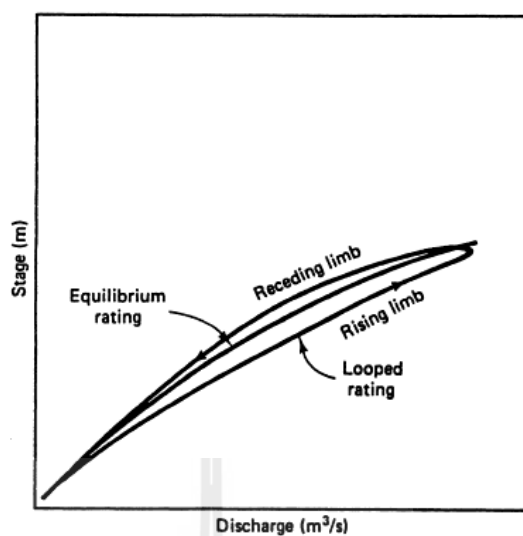
For river flood, the flood warning is typically announced when the water level in the river channel reaches a defined critical level, mostly bank level, which depends directly on the amount of runoff discharge in the river. Though it is known that river stage (the elevation of the water surface) varies with discharge, but the exact nature of this specific relationship is usually not readily apparent. However, given a long and essentially prismatic channel reach, a single-valued relationship between the stage and discharge at a cross-section defines equilibrium rating curve. Rating curve is a very useful and practical tool in hydrologic analysis, allowing direct conversion of stage to discharge and vice versa.

There are several ways to find an equation for the rating. Invariably, they are based on curve-fitting stage discharge data and widely used equation is the following:

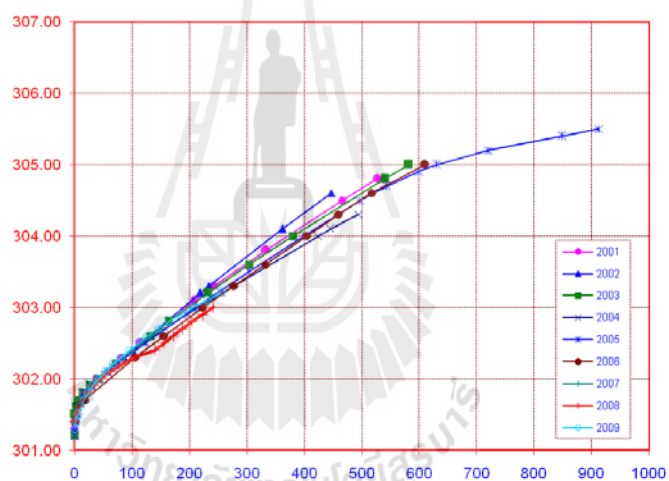
$$Q = a(z - z_o)^b \quad (2.4)$$

where Q is discharge (m^3/s), z is the gauge height (m), z_o is the reference height (m), and a , b are constants. Several values of reference height may be attempted. The proper value is that makes the stage discharge data plot as close as possible to a straight line on logarithmic paper, which values of a and b determined by regression.

In reality, other flow conditions, specifically non uniform and unsteady, can cause deviations from the equilibrium rating. In particular, flood wave theory justifies the presence of a loop in the rating curve. Intuitively, the rising limb of the flood wave hydrograph has steeper water surface slope than that of equilibrium flow, leading to greater flows at the lower stages. Conversely, the receding limb has a milder water surface slope, resulting in smaller flows at higher stage; however, the stated loop effect is likely to be small (Figure 2.9a). The stream basically stops flowing when it gets so shallow and being reduced to the isolated pools of water. This will occur when $z = z_o$. Example of the observed rating curve (Q - z relationship) for P1 station during years 2001-2009 is illustrated in Figure 2.9b (American Society of Civil Engineer, 1996).



(a) Typical rating curves (American Society of Civil Engineer, 1996).



(b) Measured rating curves in 2001-2009 at P1 station (mainly equilibrium rating).

Figure 2.9 Relation of the river discharge and its stage in form of rating curve: (a) typical pattern and (b) for the P1 station during 2001-2009 (Hydrology and Water Management Center for Upper Northern Region, 2012).

2.3.5 Roles of remotely-sensed data in hydrologic modeling

Due to the intensive need of land's physical data in most hydrologic models, remotely-sensed images acquired by satellite sensors or aerial cameras can be used to extract some crucial input parameters of the models like the LULC characteristics, topography, vegetation types, evapotranspiration (ET) rate, temperature, water bodies, rainfall/snow cover, soil moisture, or water drainage system (Schmugge et al., 2002).

Major focus of remote sensing applications in hydrology at present is for the estimation of hydro-meteorological states and flux (Su and Troch, 2003). The primary set of state variables include, for examples, land surface temperature, near-surface soil moisture, landscape roughness, water quality, snow cover/water equivalent, land use and vegetation cover. The hydro-meteorological fluxes are primarily soil evaporation and plant evapotranspiration (ET), and snowmelt runoff. The hydrologic models are usually constructed using water and energy balance equations and input data provided by the remote observations. The water balance is commonly expressed as described in Eq. 2.2. Notable applications of remote sensing in hydrology are as follows:

1. Evapotranspiration (ET) mapping

Chen et al. (2005) had developed a distributed hydrology-vegetation model for the complex terrain to simulate details of the spatial and temporal variation patterns of ET around a flux tower site. The model utilizes Landsat TM data (at 30 m resolution) to characterize the distributions of vegetation types and leaf area index (LAI). The LAI data were used to determine major hydrological processes by the established model including transpiration, precipitation interception and evaporation

from vegetation and soil. In McCabe and Wood (2006), role of landscape heterogeneity and its influence on the scaling behavior of surface flux as observed by satellite sensors with different spatial resolutions were used to independently estimate ET. These data include Landsat-ETM (60 m), ASTER (90 m), and MODIS (1020 m). As a result, a high degree of the consistency was found between retrievals from higher-resolution data (Landsat-ETM and ASTER). The MODIS-based estimates, while unable to discriminate influence of land surface heterogeneity at field scale, effectively reproduced the watershed average response, illustrating the utility of this sensor for regional-scale ET estimation. And in Hoedjes et al. (2008), the daily ET data were extracted from satellite-based ASTER images over an olive orchard in a semi-arid region of Moroccan. It has been shown that evaporative fraction (EF) is almost constant under dry conditions, but it depicts a pronounced concave up shape under wet conditions.

2. Soil moisture estimation

Merlin et al. (2006), a downscaling method of the surface soil moisture was applied to the aircraft-based L-band PushBroom Microwave Radiometer (PBMR) data. The obtained results show good agreement between the downscaled and ground-based soil moisture as long as the intensity of solar radiation is sufficiently high to use soil temperature as a tracer of the spatial variability of surface soil moisture. Also in Vivoni et al. (2008), the spatio-temporal variability of soil moisture in a mountainous basin in northwestern Mexico was retrieved from the Polarimetric Scanning Radiometer. Their results indicate that the derived soil moisture show similar variability with mean water content. Statistical analysis,

however, reveals clear differences in soil moisture in the basin, in particular for wet periods and high elevations.

3. Water management

Kongo and Jewitt (2006), the hydrological impacts of water use innovations on a catchment and river basin (in the Thukela river basin, South Africa) were assessed. The approach includes a catchment monitoring network, hydrological modelling and application of a remote sensing technique, the Surface Energy Balance Algorithm for Land (SEBAL) model, for spatially estimating of total evaporation in the targeted region. Preliminary results indicated that the water use innovations in the area have influenced the partitioning of rainfall by greatly reducing surface runoff over agricultural lands under conservation tillage practices, with a reduction of above 100%, while encouraging infiltration and deeper percolation into the soil. This knowledge shall contribute to formulation of sustainable adaptation of water use innovations and up-scaling strategies to enhance food production and hydro-ecological balance in semi-arid savannahs of Africa, at which stage hydrological modelling will form an important part of the study. And in Khan et al. (2008), they applied a holistic systematic approach of water accounting using remote sensing and GIS coupled with groundwater modeling to evaluate water saving options in the Liuyankou Irrigation System (LIS) of China. The lumped water balance analysis showed high fallow evaporation losses which needed to be reduced for improving water productivity. Application of the SEBAL algorithm for 18 NOAA AVHRR-12 images confirmed that a fair amount of water can be saved by reducing evaporation from fallow land which will result in improved water productivity at the irrigation system.

4. Snow observation

Andreadis and Lettenmaier (2006) reports the use of ensemble Kalman filter (EnKF) to assimilate remotely sensed snow observations into variable infiltration capacity (VIC) macroscale hydrologic model over the Snake River basin. The snow cover extent (SCE) product from the MODIS data was used to update VIC snow water equivalent (SWE) during four consecutive winters (1999-2003). A simple snow depletion curve model was also applied for the necessary SWE-SCE inversion. The results showed that the EnKF is an effective and operationally feasible solution; the filter successfully updated model SCE predictions to better agree with the MODIS observations and ground surface measurements.

5. Hydrologic modeling

McCabe et al. (2008), a multi-sensor/multi-platform approach to the water and energy cycle prediction was reported in an effort to understand the variability and feedback of land surface and atmospheric processes over large space/time scales. Remote sensing-based variables; soil moisture (from AMSR-E), surface heat fluxes (from MODIS) and precipitation rates (from TRMM); were combined with THE North American Regional Reanalysis derived atmospheric components to examine the degree of hydrological consistency throughout these diverse and independent hydrologic data sets. Results indicate that this multi-sensor approach, in combination with available atmospheric observations, is able to find a comprehensive and hydrometeorologically consistent characterization of the land surface water cycle, leading to an improved understanding of water and energy cycles within the NAME region and providing a novel framework for future remote observation and analysis of the coupled land surface-atmosphere system.

Mello et al. (2008), a semi-physically based hydrologic model in semi-distributed to sub-basins approach was created based on the GIS and Remote Sensing tools and then used to simulate hydrologic responses of the Grande River Basin. The model is based on the SCS Curve Number (SCS-CN) and MGB/IPH models, In order to estimate actual evapotranspiration (AET), the crop coefficient, soil moisture and satellite-based land-use data were applied. The long-term hydrologic data series were structured for period between 1990 and 2003. The calibration and validation process was carried out by evaluating the behavior of the Nash-Sutcliffe Coefficient (CNS). The statistical precision showed that the model was able to simulate the hydrologic impacts, including years of El Nino and La Nina events, with CNS scores greater than 0.70 in both situations. In addition, the model was also able to simulate the hydrologic impacts of land-use change in the Grande River Basin, based on the CNS scores of 0.80 for different combinations of validation periods.

Also, Pellarin et al. (2009) tried to find accurate soil moisture mapping over a 120x100 km² area in West Africa using considerable amount of data recorded during the African monsoon multidisciplinary analysis (AMMA) experiment. The modelling strategy was based on the use of a land surface model (LSM) to provide high-resolution soil moisture mapping over the study area. A microwave emission model was then introduced to simulate associated microwave brightness temperatures (TB) to compare with the Advanced microwave scanning radiometer (AMSR) at the same spatial (25x20 km²) and temporal resolution (daily). Discrepancies between observed and simulated TB were analyzed and used to calibrate the LSM and the microwave emission models to match the specific hydrology and soil microwave behavior of the studied area. A secondary surface soil

layer was later added to match with in situ soil moisture measurements as well as satellite microwave measurements. Finally, a soil moisture retrieval algorithm based on AMSR and Meteosat second generation (MSG) measurements was proposed to improve the quality of the soil moisture estimates over the studied area (the root mean square error decreases from 5.4% vol. to 2.8% vol).

2.3.6 Validation of hydrologic model

In statistics, the coefficient of determination R^2 is used in the context of statistical models whose main purpose is the prediction of future outcomes on the basis of other related information. It is the proportion of variability in a data set that is accounted for by the statistical model. It provides a measure of how well future outcomes are likely to be predicted by the model. There are several different definitions of R^2 which are only sometimes equivalent. One class of such cases includes that of linear regression. In this case, if an intercept is included then R^2 is simply the square of the sample correlation coefficient between the outcomes and their predicted values, or in the case of simple linear regression, between the outcomes and the values of the single regressor being used for prediction. In such cases, the coefficient of determination ranges from 0 to 1. Important cases where the computational definition of R^2 can yield negative values, depending on the definition used, arise where the predictions which are being compared to the corresponding outcomes have not been derived from a model-fitting procedure using those data, and where linear regression is conducted without including an intercept. Additionally, negative values of R^2 may occur when fitting non-linear trends to data. In these instances, the mean of the data provides a fit to the data that is superior to that of the trend under this goodness of fit analysis.

In essence, the Nash-Sutcliffe efficiency has been generally used to assess the predictive power of the specified hydrological models whose definition is:

$$E = 1 - \frac{\sum_{T=1}^N [Q_{OT} - Q_{MT}]^2}{\sum_{T=1}^N [Q_{OT} - \bar{Q}_O]^2} \quad (2.5)$$

where Q_{OT} is the observed discharge at each time step (from 1 to N), Q_{MT} is the modeled discharge at the same time step and \bar{Q}_O is the mean value of the observed data. Nash-Sutcliffe efficiencies can range from $-\infty$ to 1. An efficiency of 1 ($E = 1$) corresponds to a perfect match of modeled data and the observed data while $E = 0$ indicates that the model predictions are as accurate as the mean of the observed data. An efficiency less than zero ($E < 0$) occurs when the observed mean becomes a better predictor than the modeled one or, in other words, when residual variance (described by the numerator in the expression above), is larger than the data variance (described by the denominator). Essentially, the closer the model efficiency is to 1, the more accurate the model is.

2.4 CA-Markov model

To perform LULC prediction in the near future, the CA-Markov model will be utilized and the obtained results will be used as input data to quantify the consequent flood scenarios for that particular state of new LULC maps. The model is the result of integration between two individual modules, the Markov chain model and CA model.

Concept of the Markov chain (MC) model was firstly developed by a Russian mathematician, Andrey Markov in 1907 (Markov, 1907). It describes an evolution of a system that has Markov property, which means its next future state (along evolution line) could be identified based solely on knowledge of its present state (and priori states). These state-to-state changes are called transitions and at each step the system may change its state from current state to another possible state, or still remain in the same state, according to a certain probability distribution.

According to these assumptions, this state-to-state of LULC changes could be described using the so-called “transition probability matrix”, or “Markov matrix”, which is accounted for the probability of changing from one state to every other state in a single time-step and normally written as:

$$P = \begin{bmatrix} P_{11} & P_{12} & \cdots & P_{1n} \\ P_{21} & P_{22} & \cdots & P_{2n} \\ \vdots & \vdots & \ddots & \vdots \\ P_{n1} & P_{n2} & \cdots & P_{nn} \end{bmatrix} \quad (2.6)$$

where P_{ij} stands for probability of transition from state i to state j and n is number of all states available. From this perspective, Eq. 2.6 must satisfy these two conditions: (1) $0 \leq P_{ij} \leq 1$ and (2) $\sum_{j=1}^n P_{ij} = 1$ (the sum of all elements in each row is 1).

Note that, the diagonal components (e.g. P_{11} , P_{22} , P_{33}) represent the probability of remaining in the same state after the transition (no-change situation).

Though, the MC model could forecast total amount of LULC changing area per category (or classes) given an initial transition probability matrix, it still lacks

spatial knowledge of where future LULC should occur geographically. This need can be fulfilled by using the CA module of the program.

The Cellular Automata (CA) was first proposed by John Von Neumann, the Hungarian-born mathematician in the 1950s (Von Neumann, 1966) and later has been applied to several research fields including the LULC study. Similar to the Markov chain model, the CA is a discrete, spatial model normally used to describe evolution process of the systems that consist of a regular grid of cells, one of which can be in a finite number of possible states. Each cell could independently varies its state over time (in discrete time-step manner) based solely on its present state and that of its immediate neighbors under some given specific rules called the “transition rules”. The crucial advantage of the CA over MC is that they are capable of simulate evolution of the systems in two dimensions which significantly benefits for the LULC prediction.

The CA-Markov module is available in the IDRISI software and can be used to generate such a transition probability matrix in which it takes two LULC maps as input data and then produces the following output: (1) transition probability matrix, (2) transition areas matrix, and (3) set of conditional probability maps. A transition areas matrix is produced by multiplying each column in transition probability matrix by the number of cells of corresponding LULC in the later image. In both of these files, the rows represent the older LULC categories and the columns represent the newer categories (Eastman, 2003a, 2003b).

2.5 Review of the relevant research works

Several hydrologic models have been developed and applied to the study of surface runoff characteristics and the associated flooding analysis for the interested areas. Examples of these works are reviewed here as follows.

Werner (2000) indicates that the flood hazard in areas adjacent to rivers may be estimated by applying hydrological/hydraulic models to calculate parameters such as flood extent, depth and duration. However, by using a two-dimensional flow model based on the topography has the drawback that computational requirements are high, making this approach unattractive when applying in, e.g., a decision support system.

Sinnakaudan et al. (2002) found that the Geographic Information Systems (GIS) are an efficient and interactive spatial decision support tool for flood risk analysis. They had developed the ArcView GIS extension namely AVHEC-6.avx to integrate the HEC-6 hydraulic model within GIS environment. It has the capability of analyzing the computed water surface profiles generated from HEC-6 model and producing a related flood map for the Pari River in the ArcView GIS. The flood risk model was tested using the hydraulic and hydrological data from the Pari River catchment area. The results of this study clearly show that GIS provides an effective environment for flood risk analysis and mapping.

Jothityangkoon and Sivapalam (2003) developed the distributed rainfall-runoff model to predict extreme flood. It was found from this work that when increase of normal flood condition to the extreme flood condition, the model's results showed that process of the runoff occurrence has changed by increasing of saturation excess overland flood from the increase of the saturated area with water. The overflowing process of the river bank had the role more than the flowing in the waterway.

Jothityangkoon et al. (2006) applied the distributed rainfall-runoff model developed in Australia to analyze daily water balance in Lum Pang Chu Watershed, which is sub-catchment of Mun River in the northeast of Thailand. Result of the daily model being developed by using long term water balance concept found that, it was necessary to add more complexity to runoff generation processes from soil-water storage to increase loss flow in the stream and receive a better fit to the observed flow duration curve.

Liu et al. (2003) studied a diffusive transport approach for flow routing in GIS-based flood modeling. This research proposes a GIS-based diffusive transport approach for the determination of rainfall runoff response and flood routing through a catchment. The watershed is represented as a grid cell mesh and routing of runoff from each cell to the basin outlet is accomplished using first passage time response function based on the mean and variance of the flow time distribution derived from the advection–dispersion transport equation. The flow velocity is location dependent and calculated in each cell by using the Manning equation based on the local slope, roughness coefficient and hydraulic radius. The total direct runoff at the basin outlet is obtained by superimposing all contributions from every grid cell.

The model was tested on the Attert catchment in Luxembourg with 30 months of observed hourly rainfall and discharge data. The results are in excellent agreement with the measured hydrograph at the basin outlet. A sensitivity analysis shows that the parameter of flood frequency and the channel roughness coefficient have a large influence on the outflow hydrograph and the calculated watershed unit hydrograph, while threshold of minimum slope and the threshold of drainage area in delineating channel networks have a marginal effect. Since the method accounts for spatially

distributed hydrologic and geophysical characteristics of the catchment, it has great potential for studying the influence of changes in land use or soil cover on hydrologic behavior of a river basin.

Smith and Banting (2004) examined pressures of land use change resulting from urban development on the runoff contribution. To achieve this purpose, a modeling methodology was developed to integrate the GIS and a hydrologic model (e.g. storm- water management model) in a water balance analysis on a watershed basis. Results showed that, discretization of a watershed was found to affect the differences between measured and simulated runoff volume. However, this can be refined with calibration. It was found that a strong correlation between measured and predicted rainfall values did not always guarantee strong relationship between measured and generated runoff. Recommendations include the use of a longer time series of rainfall, stream flow and predicted rainfall to observe temporal variations.

Sahoo et al. (2006) modified a physically distributed hydrological model, MIKE SHE, to predict stream flow at high frequency in a flashy mountainous Hawaii stream. It was found that as Hawaii streams are short and steep, they often produce dangerous flash floods as a result of rainfall events that can be short but intense. The study of watershed response to storm events at the Manoa–Palolo stream system on the island of Oahu, Hawaii, found that the rainfall distribution along the watershed is the main driving factor for the estimation of streamflow. The reciprocal of Manning's roughness coefficient for the watershed and the hydraulic conductivities (vertical and horizontal) of the saturated zone had the most pronounced effects in determining the shape of flood peaks.

Wolski et al. (2006) studied the Okavango Delta, which is dominated by annual flood events from the Okavango River, based on the developed model that introduces realistic physical knowledge of the Okavango Delta system into the model. The major improvements of the model are a better representation of surface water–groundwater interactions and the application of measurement-based rather than model calibrated parameterisation of topographic controls of floodplain water storage. These enabled a successful representation of 34 years of observed outflows and 15 years of observed inundation area in a conceptually sound way. Additionally, a GIS model had been developed for determination of spatial distribution of the simulated floods.

Borah et al. (2007) applied the SWAT and DWSM models to simulate the channel runoff during 1995-2002 of the Little Wabash River watershed. They found that the visual comparisons of the hydrographs indicated the SWAT's weakness in predicting monthly peak flows (mostly underpredictions). Therefore, SWAT needs enhancements in the storm event simulations for improving of its high and peak flow predictions. Comparisons of DWSM's 15-min flow hydrographs with SWAT's daily flow hydrographs along with the 15-min and daily observed flow hydrographs during three considered storms showed that DWSM predicted more accurate high and peak flows and precise arrival times than SWAT.

Liang et al. (2007) coupled surface/subsurface flows in a depth averaged flood wave model. In this study, vertically averaged free-surface and subsurface flows were linked and solved simultaneously in a 2D numerical model for predicting flood flows. A TVD-MacCormack scheme was used to solve the shallow water equations for free surface flows while the standard MacCormack scheme was employed to solve the transient Boussinesq equations for unconfined groundwater flows. The dynamic

linking of the surface/subsurface models enables the interactions between the surface water flow and neighbouring groundwater flow in the horizontal plane to be studied. The developed model was verified against the analytical solutions and experimental measurements and then used to investigate the influence of buildings on flood flows, where the buildings were modeled as being porous media. This approach of modeling buildings is compared with two other common methods: the first is to represent the buildings by solid blocks, and the second is to include the buildings by increasing the local roughness. It was found that the combined surface/subsurface model provides a high degree of flexibility in representing the buildings in a flood flow simulation.

Ramlal and Baban (2007) developed a GIS-based hydrologic model to flood management in Trinidad, West Indies. This work uses GIS to map the extent of the flooding, estimate soil loss due to erosion and estimate sediment loading in the rivers in the Caparo River Basin. The results indicate that flooding was caused by several factors including clear cutting of vegetative cover, especially in areas of steep slopes that lead to sediment filled rivers and narrow waterways. Other factors include poor agricultural practices and uncontrolled development in floodplains.

Chen et al. (2009) developed a GIS-based urban flood inundation model called GUFIM which consists of two components: a storm-runoff model and an inundation model. Cumulative surface runoff, output of the storm-runoff model, serves as input to the inundation model. The storm-runoff model adapts the Green-Ampt model to compute infiltration based on rainfall characteristics, soil properties, and drainage infrastructure conveyance. The basis of the inundation model is a flat-water model. This effort uses publicly available elevation data, storm data, and insurance claim data to develop, implement and verify the model approach.

In Thailand, GIS and remotely-sensed data (e.g. satellite images) have been applied in the analysis of flooding scenarios and flood risk area in several works. For examples, Sombat Umuang (2006) has developed the flood risk model for the management of flood risk areas in central Thailand. The flood maps were produced from the radar images and LULC data were derived from the Landsat TM images. Chuchok Ayupong (2007) developed the effective flood forecasting and warning system in Chiang Mai city. Results of the project consist of the 3-D digital map from scanning lidar system, flood forecasting, flood warning by communications system, flood preparation handbook and flood level warning columns. The neural network model with a support vector machine algorithm was used for flood forecasting.

Sansena and Bhaktikul (2008) created flood risk mapping in Mae Klong River by the application of hydraulic model with GIS. The objectives of this research were to integrate hydraulic model and GIS for studying Mae Klong River runoff and to create the flood risk map based on hydrology and hydraulic approach. The process involved runoff frequency analysis for designing runoff return period, developing GIS data for generating Digital Terrain Modeling (DTM), integration of HEC-RAS model with the DTM to develop regional model for flood plain determination, and designing flood return periods as a model for simulation of the prevention, warning, forecasting and estimating flood risk area. The result from the simulation model of flood in 1996 was presented together with GIS and DTM data. Accuracy of the model, comparing to the flooded data interpreted by the Royal Irrigation Department, was 60.52%.

CHAPTER III

METHODOLOGY

3.1 Conceptual framework of the study

This work comprises of 3 main parts in according with the proposed objectives described in Section 1.2. The first part contributes to the development of a grid-based hydrologic model that is capable of simulating realistic runoff scenarios using GIS-based input data. The proper water balance equation to represent water-flow scenario of the area is determined first by comparing the predicted runoff output with the observed ones (real data). Two hydrologic models based on the water balance concept are developed: (1) monthly model and (2) daily model. The actual runoff data at the P1 and P21 are used to validate model's efficiency. In addition, results gained by this newly-created model are also compared with those gained from the original lump-based models by Jothityangkoon and Sivapalan (2003) and Jothityangkoon et al. (2001; 2006) to determine their similarities or differences. The second part of the study focuses on the generating of the flood maps for the Chiang Mai municipality during September 2005 based on the simulated river discharge data obtained from the developed model stated earlier. The resulted maps are then compared with available and reliable data of flooded areas during that time prepared by the referred agencies.

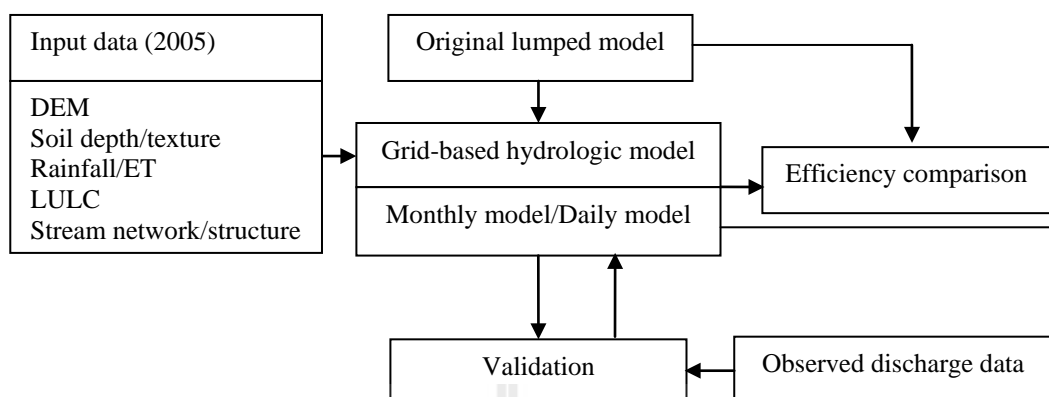
The third part describes applications of the derived model to examine impacts of the LULC and climate changes on runoff discharges and flood developing process in the area. Three specific cases were considered: (1) impact of LULC changes in year

2020 predicted by the CA-Markov model, (2) impact of forest loss at 10 and 20%, and (3) impact of rainfall increase by 5, 10 and 15% (under the same distributing pattern).

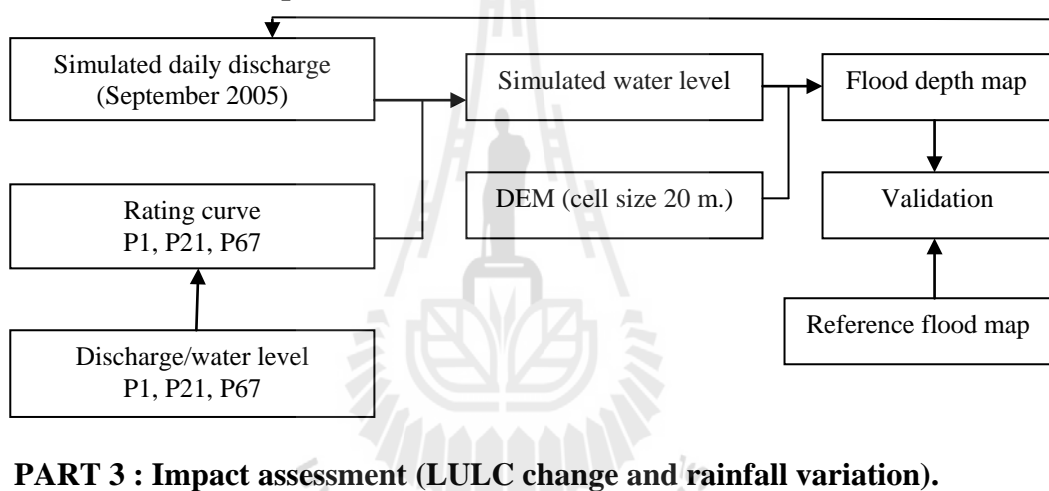
The entire working process can be separated into 3 main steps as follows (see overall work flowchart in Figure 3.1):



PART 1 : Grid-based hydrologic model development.



PART 2 : Flood map construction.



PART 3 : Impact assessment (LULC change and rainfall variation).

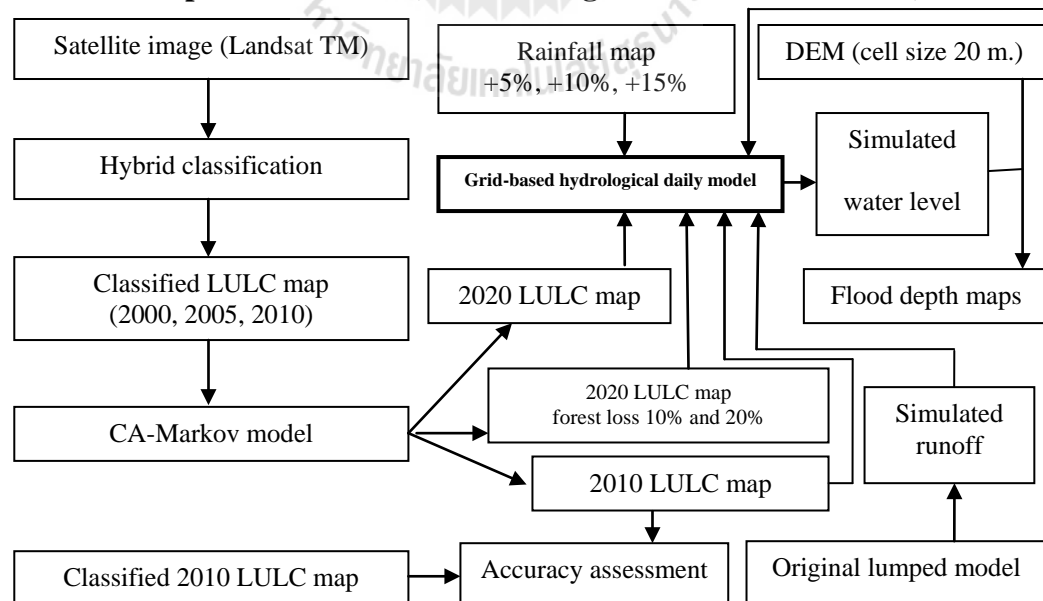


Figure 3.1 Conceptual framework of the study.

3.2 Data preparation

All necessary data for the study, e.g. rainfall, temperature, stream channels, satellite imagery, are acquired from the responsible sources (Table 3.1). They are then kept and displayed as separated GIS-based maps on the GIS dataset (Figure 3.2). Figures 3.3-3.6 present maps of some data relevant to the formulation of the preferred hydrologic model, which are,

(1) Topographic data (DEM). This was generated based on the data of the 20m contour, spot height, stream network from topographic map 1:50,000 (Table 3.1) and cross-section (Appendix C) of the Ping River (Figure 3.3). This knowledge is very crucial for the determination of runoff flow direction (routing path) and eventual flow accumulation in the model.

(2) Soil data. There are two main properties to be considered here: (1) depth of the effective soil layer and soil texture (in term of the soil porosity). These data were mapped based on original data extracted from 321 surveying wells of the Department of Groundwater Resources (DGWR) existing within and around the area (Figure 3.4). The Inverse Distance Weighted (IDW) interpolation method was applied to generate the associated raster-based soil data maps from their original point-based data maps of the DGWR (Figures 3.5 and 3.6). The effective soil depth for each well is defined as distance from ground to the bedrock level of the well and data are presented in Appendix A. The porosity is calculated from the average porosity value of the mixed soil textures found at each well based on the known porosity of each relevant soil texture shown in Appendix B. Knowledge of effective soil depth and soil porosity data can lead to the calculation of soil stored bucket capacity (= soil depth x porosity) needed in the formulation of water balance model (Eq. 3.3).

Table 3.1 Main required input data and their contributing sources.

	Description	Scale	Sources
1	Topographic map	1:50,000	1. Royal Thai Survey Department (RTSD) 2. Royal Irrigation Department (RID)
2	Effective soil depth map Soil texture (porosity)	1:50,000	1. Department of Ground Water Resources (DGWR)
3	Rainfall/potential evaporation 2005 data	-	1. Thai Meteorological Department (TMD) 2. Royal Irrigation Department (RID) 3. Electricity Generating Authority of Thailand (EGAT)
4	Runoff data (monthly and daily records)	-	1. RID 2. Department of Water Resources
5	Landsat data 2000, 2005, and 2010 for LULC extraction	30 m.	1. GISTDA 2. Land Development Department (LDD) 3. Field surveys
6	River structure/floodplain data	-	1. RTSD

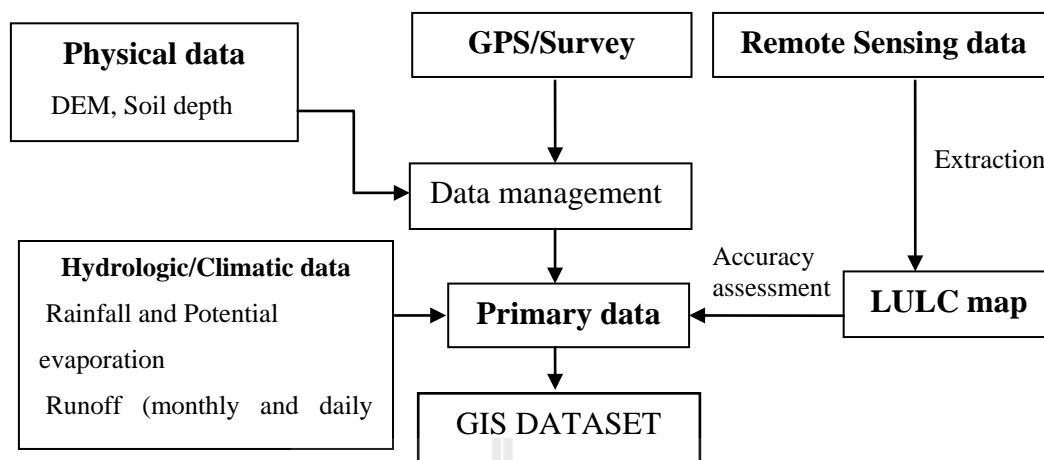


Figure 3.2 Components of the GIS dataset.



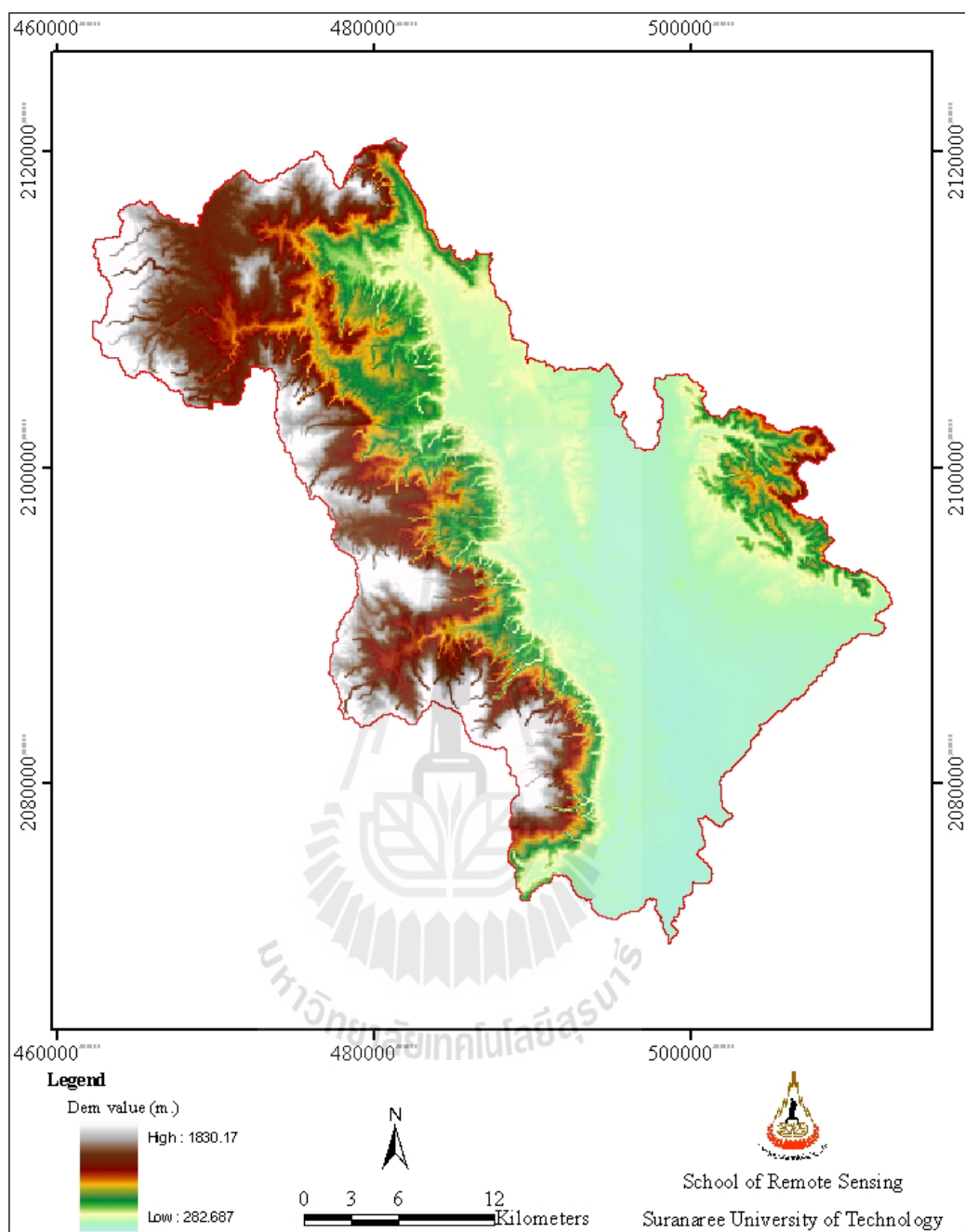


Figure 3.3 Topographic data (DEM).

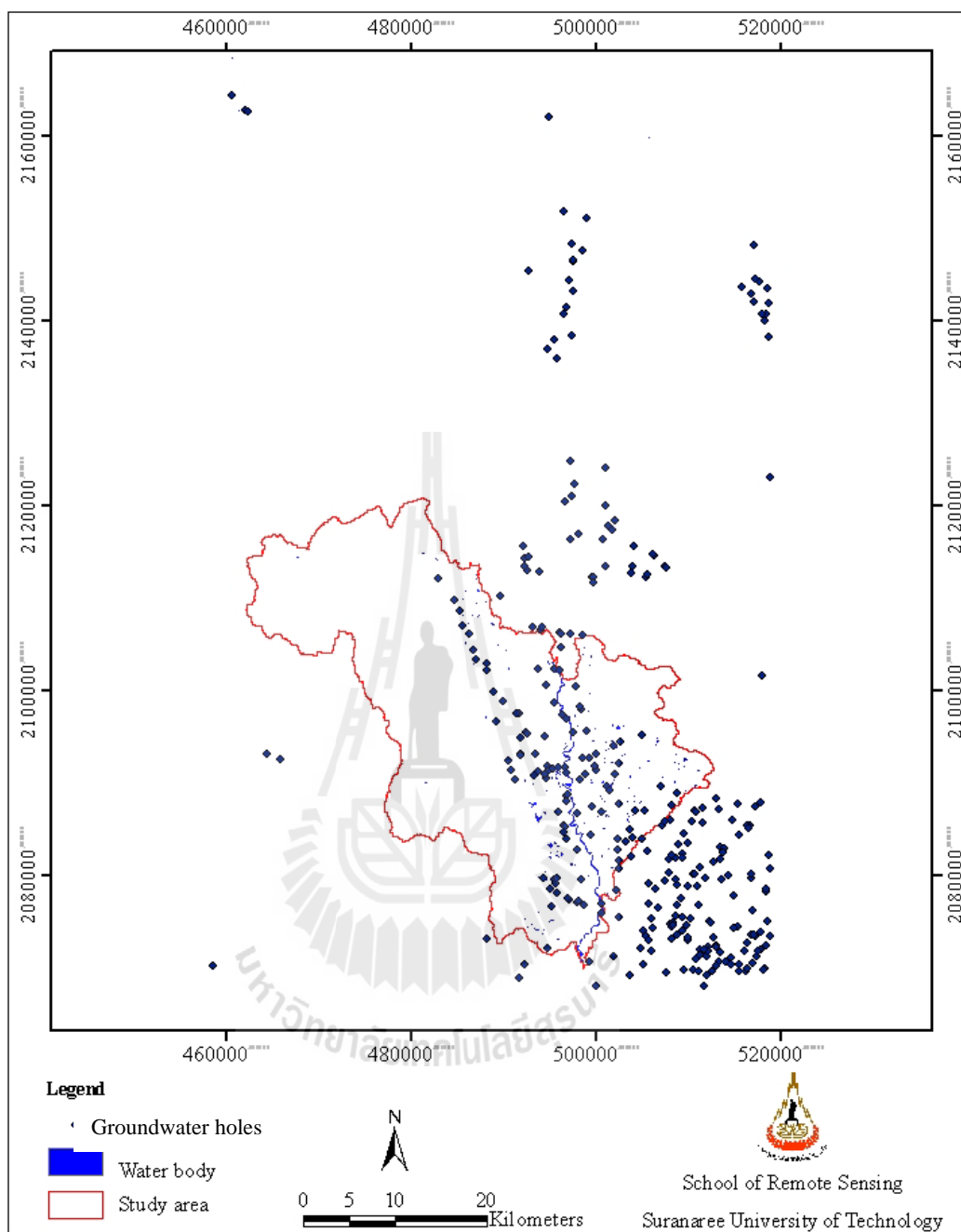


Figure 3.4 Distribution in location of the DGWR surveying holes.

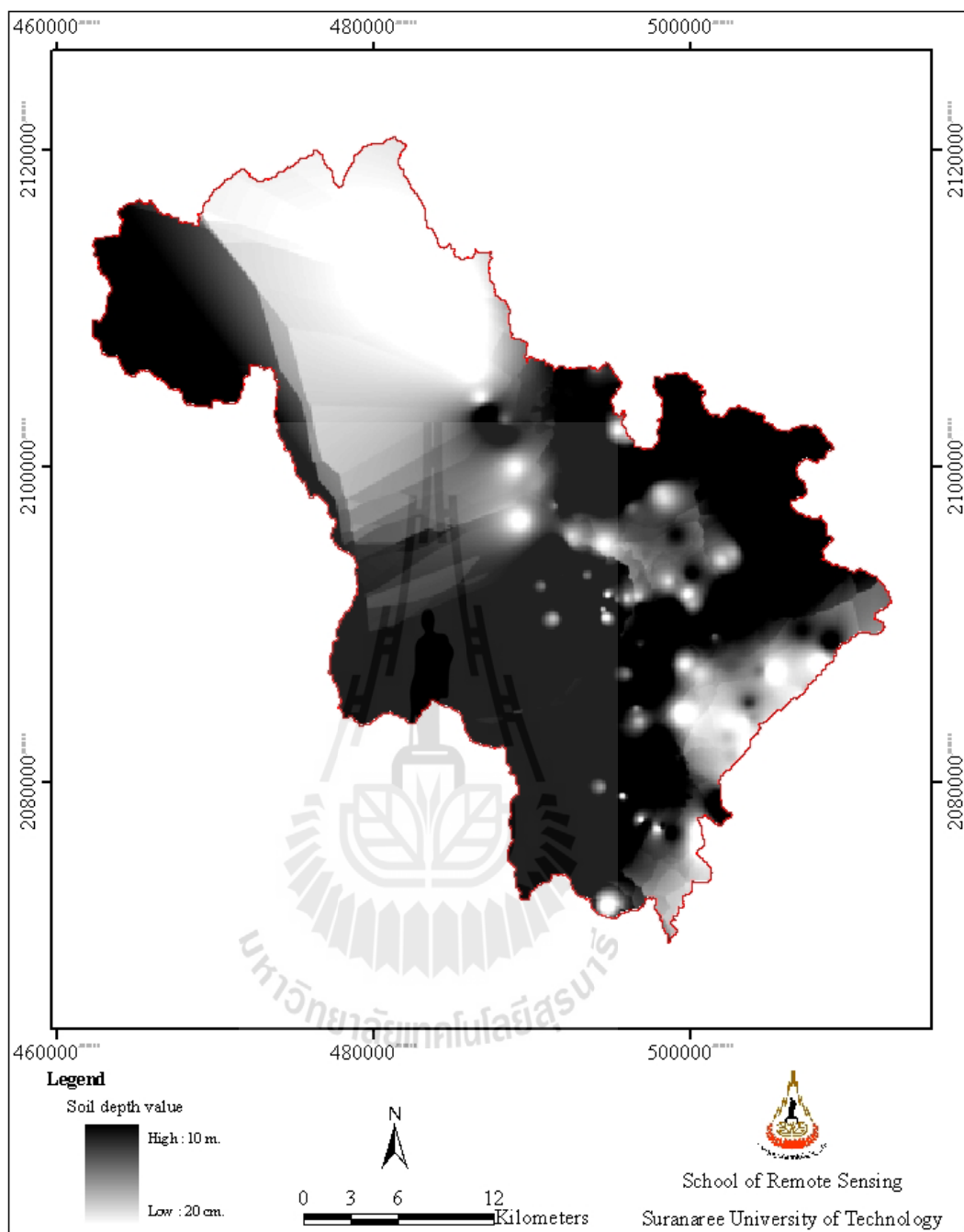


Figure 3.5 The interpolated effective soil depth map.

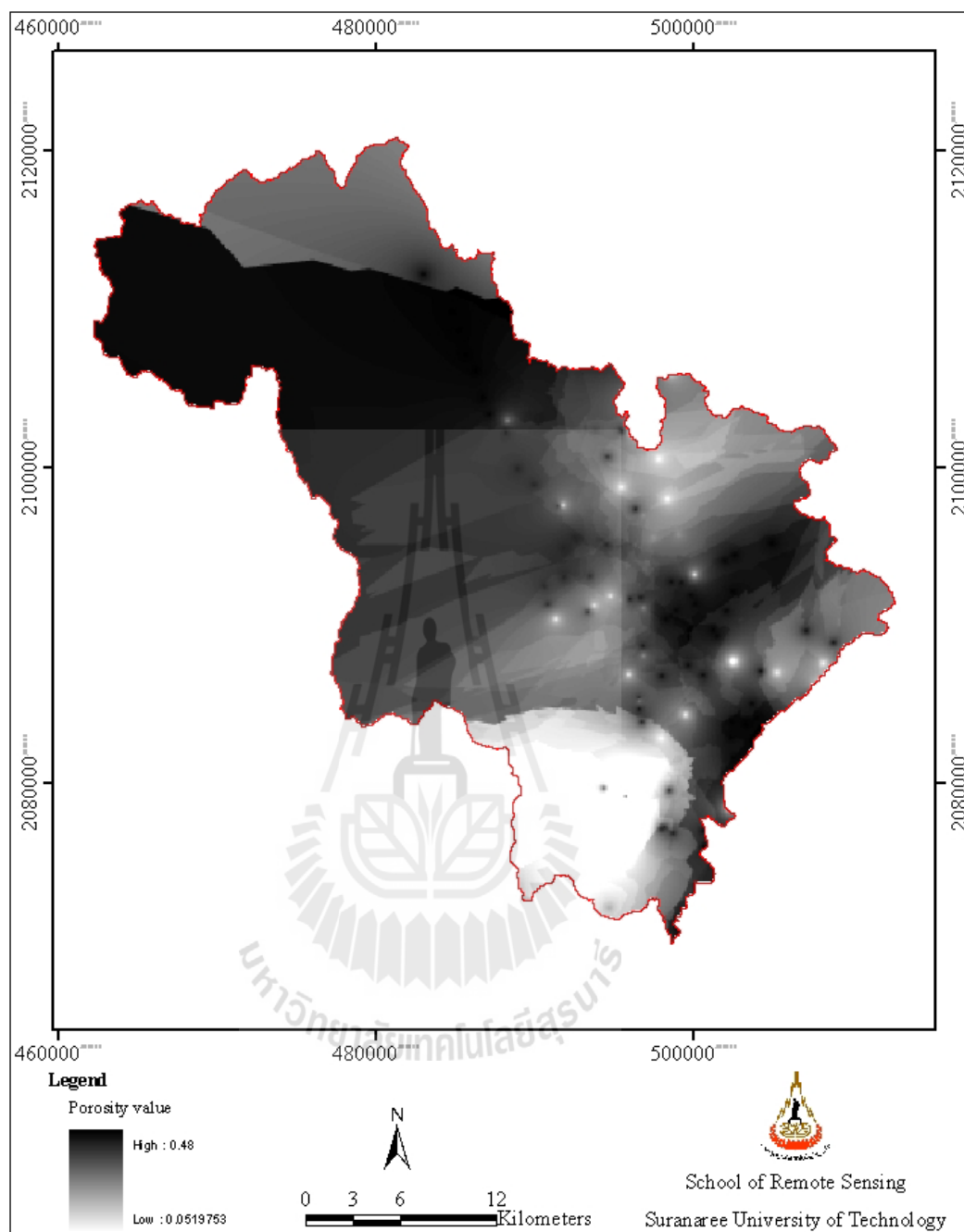


Figure 3.6 The interpolated porosity of the effective soil layer.

(3) LULC data. The used LULC data are classified from Landsat TM imagery (30 m resolution) of the entire study area on three specific dates: (1) 13th March 2000, (2) 11th March 2005, and (3) 25th March 2010. The original images are geometrically corrected using a set of ground control points (GCP) (and image to map registration) and false color composite images (RGB=453) are then prepared (e.g. Figure 1.4). They are classified using hybrid classification method which starts by using the unsupervised method (ISODATA) then followed by the supervised method (Maximum Likelihood) where the visual interpretation is also partly implemented. The seven main LULC types are classified: forest land (evergreen forest, deciduous forest, forest plantation, agro-forestry), orchard/perennial (mixed orchard, orange, litchi, mango, longan, sub-tropical fruit, mixed perennial, teak, acacia, pterocarpus sp., coffee, tea, bamboo), field crop (abandoned field crop, mixed field crop, corn, soybeen, upland rice, cabbage), paddy field (abandoned paddy field, rice paddy field), urban/built-up land (city, town, commercial, village, institutional land, transportation, communication and utility, industrial land, golf course, cemetery, gasoline station), water body (natural water body, reservoir(built-up)), and miscellaneous (rangeland, marsh and swamp, mine, pit, rock out crop, landfill). Examples of these maps are presented in Figure 4.1 (Section 4.1).

(4) Rainfall and potential evaporation data. Maps of rainfall are interpolated (using IDW technique) from the original point-based data measured at 15 measuring stations of the TMD situating within and around the study area (Figure 3.7). And results are displayed in Figures 3.8-3.9. However, there were only three evaporation stations existing within the study area (Figure 3.7) which are not enough for valid interpolation work. Therefore, only observed data at the Maejo University

Station are chosen to be a representative of the whole study area. The actual evapotranspiration (AET) data of each land unit (or grid) are then quantified based on the knowledge of potential evapotranspiration (PE) data (from the reference evaporation data) and soil capacity. This is performed by dividing LULC into two broad groups: (1) vegetation (forest and orchard/perennial), (2) bare land (crop, paddy field, urban/built-up, water body, and miscellaneous). Then the AET data were determined as follows:

$$\text{Vegetation group: } AET = (s/s_f) \times PE, \quad (3.1a)$$

$$\text{Bare land group : } AET = (s/S_b) \times PE, \quad (3.1b)$$

where s is the actual volume of soil-moisture storage, s_f is the soil-moisture storage at field capacity and S_b is the bucket's soil-moisture storage capacity (see more detail of these parameters in Section 3.2).

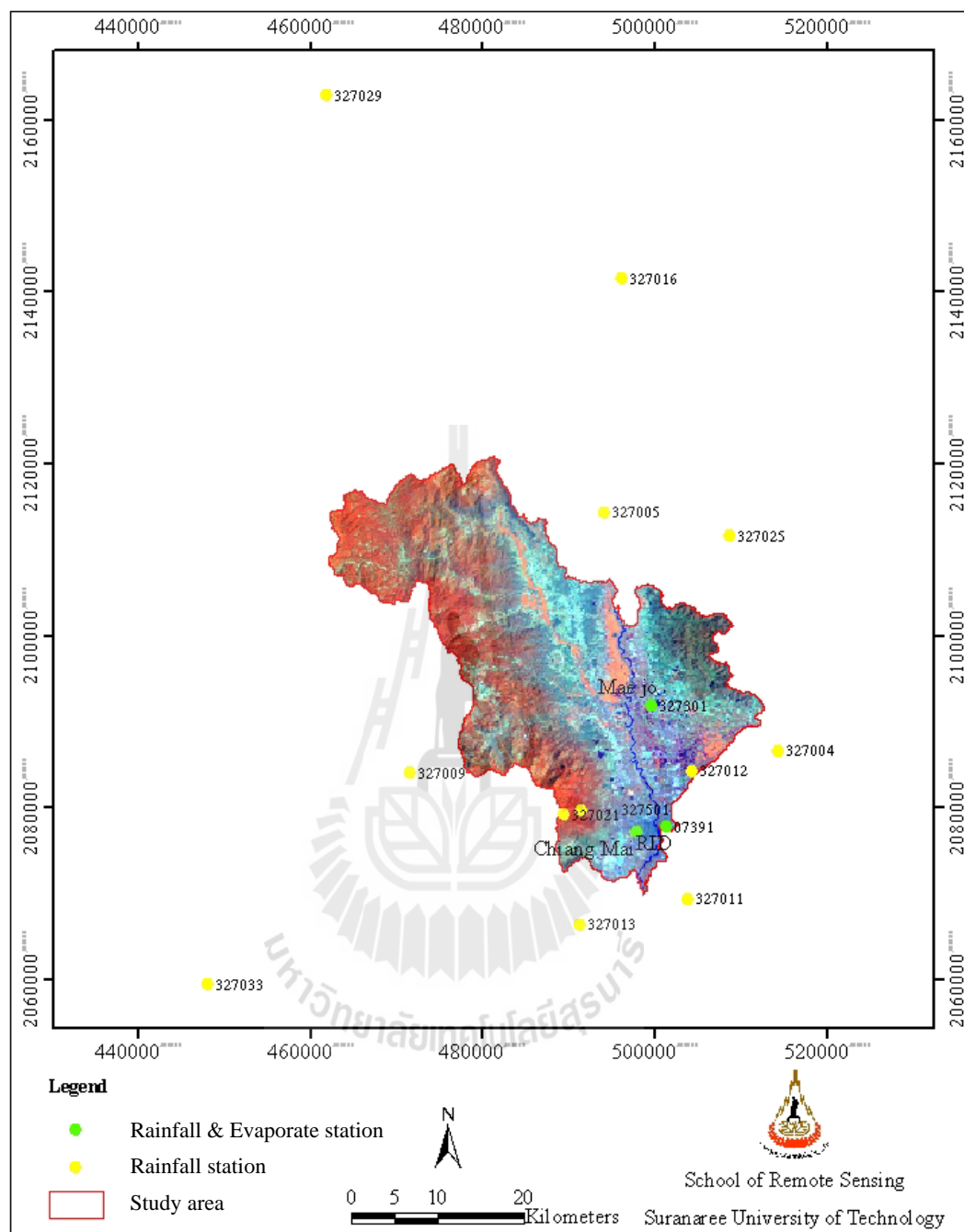


Figure 3.7 Locations of the rainfall and evaporation measuring stations.

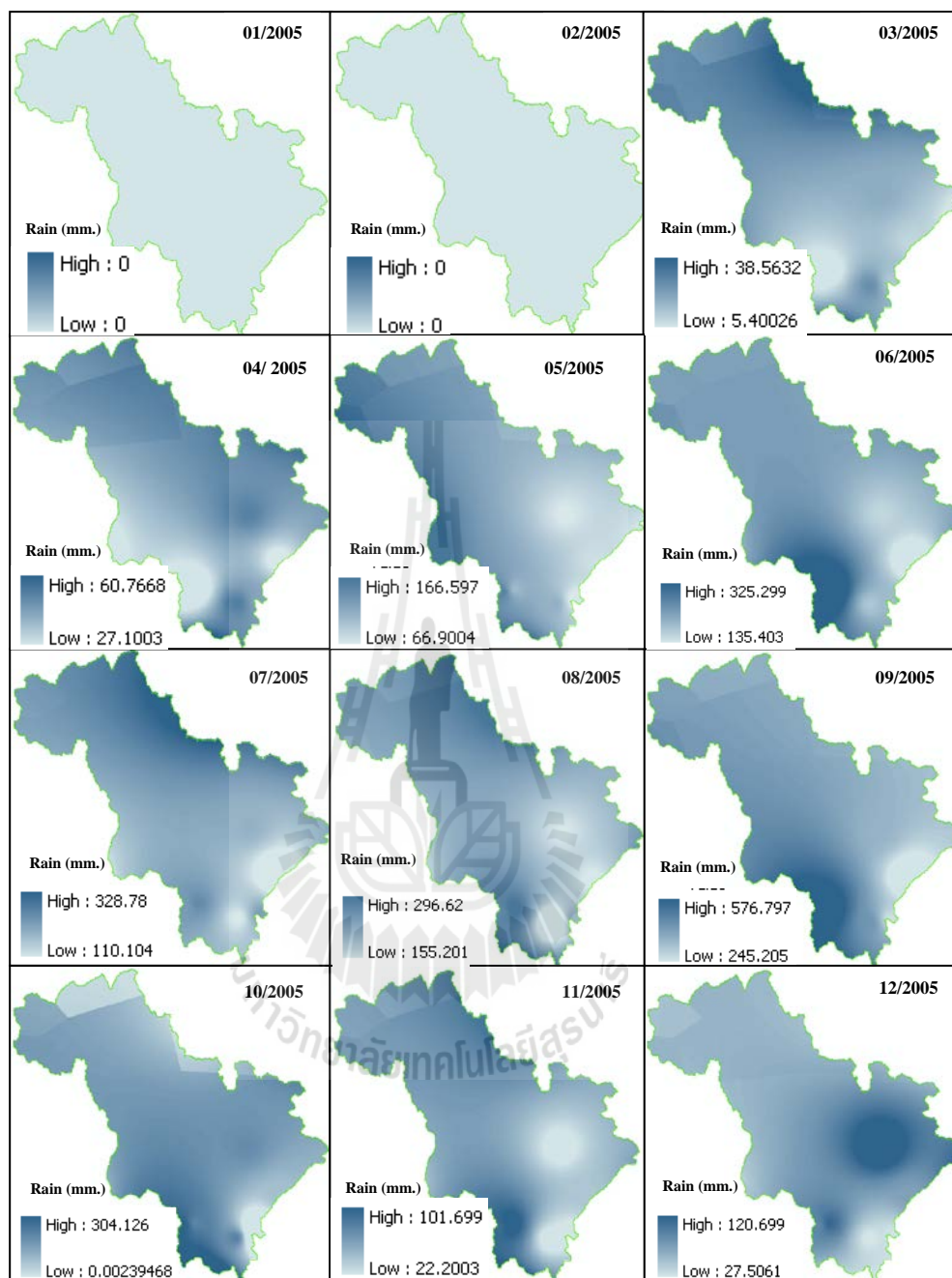


Figure 3.8 Distributing patterns of monthly rainfall data in 2005.

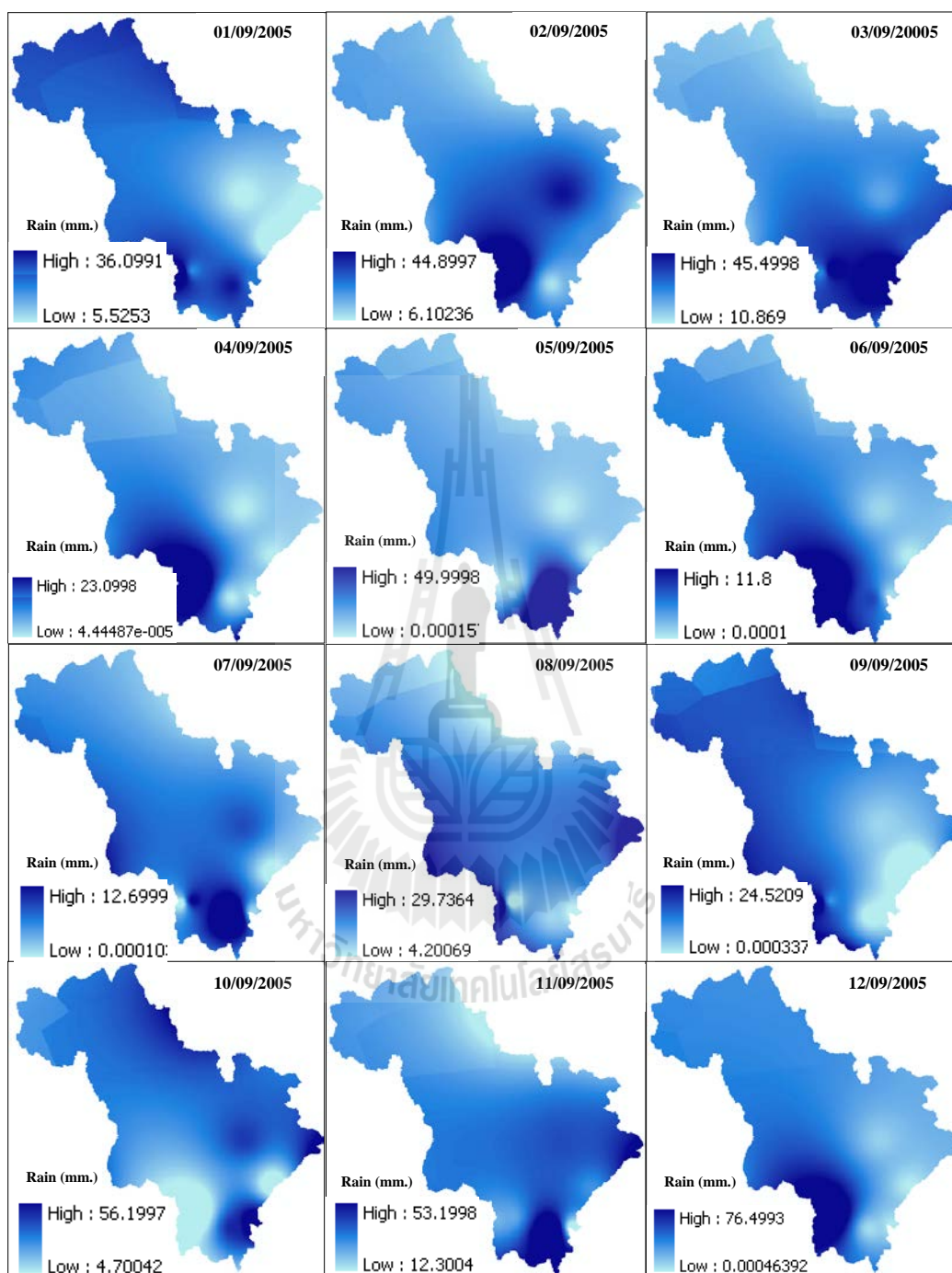


Figure 3.9 Distributing pattern of daily rainfall data in 2005 (September).

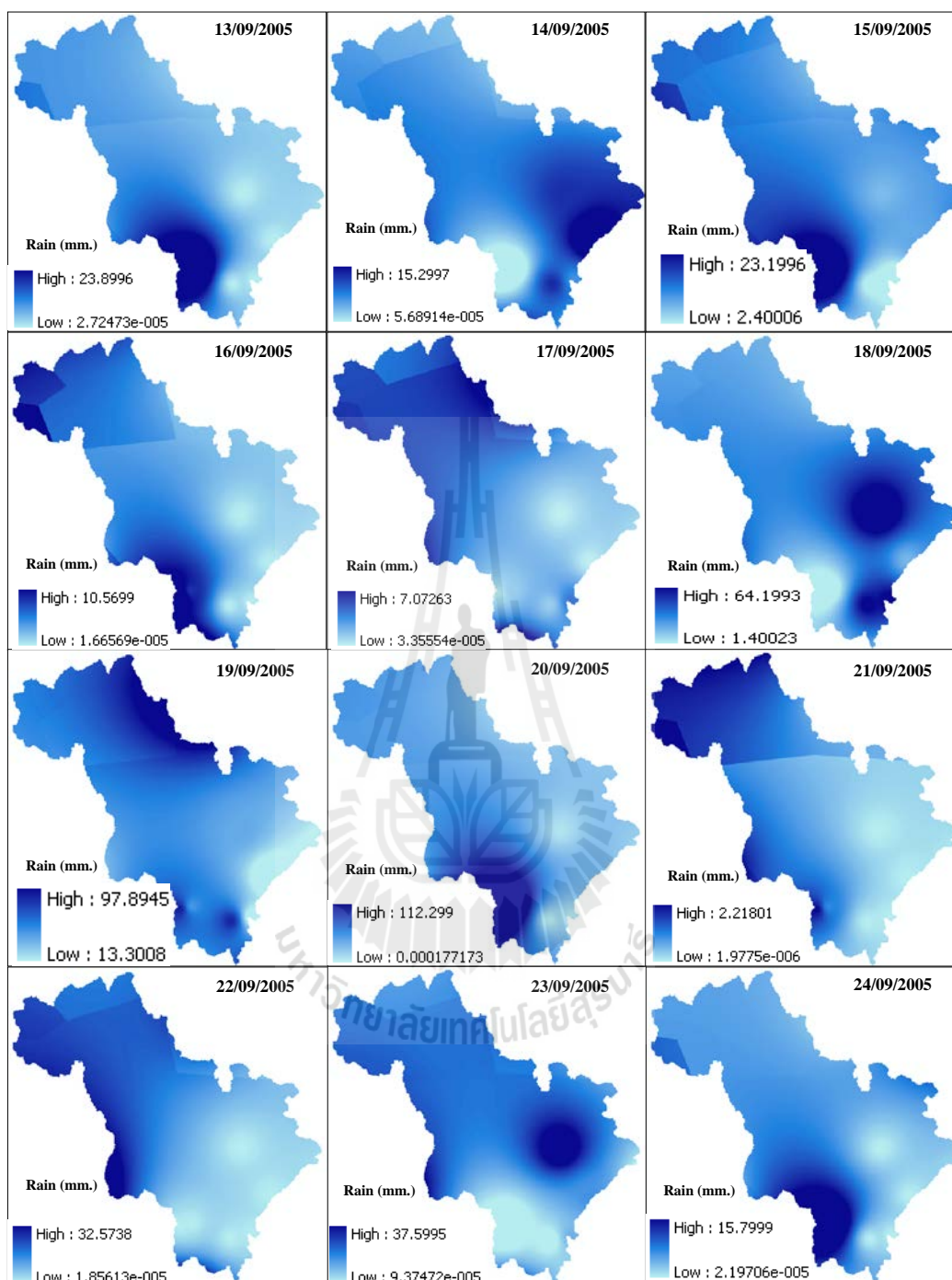


Figure 3.9 (Continued).

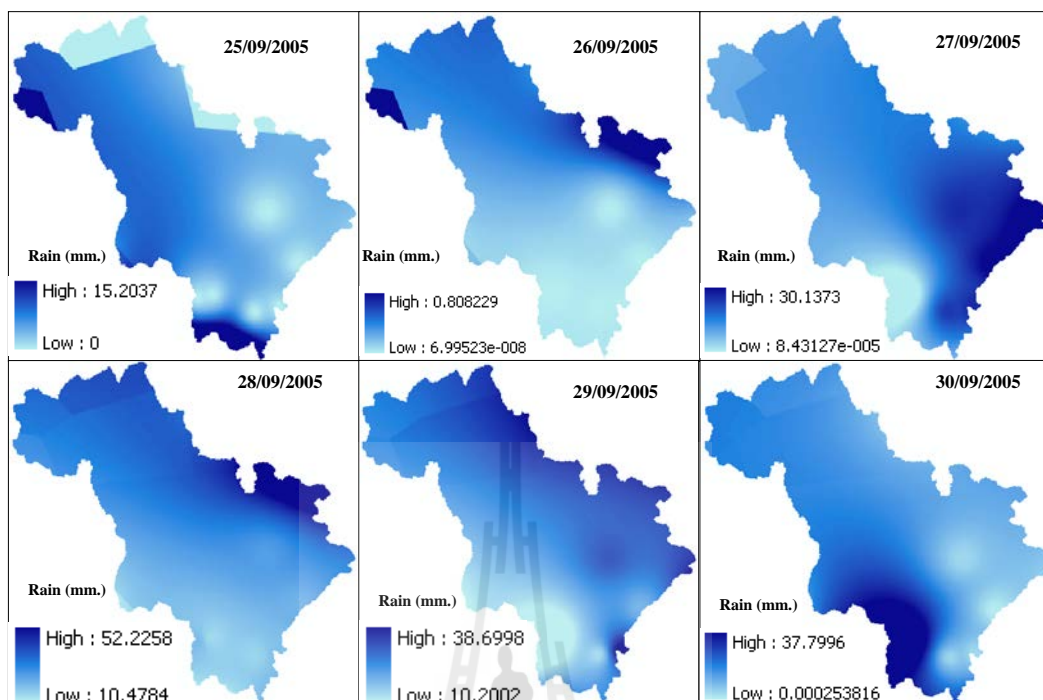


Figure 3.9 (Continued).

(5) Runoff data. The runoff data at three measuring stations: P1, P21, P67 (Figure 3.10) are acquired from the RID (Figure 3.11 and Table 3.2). These data are used for model's calibration and validation process while the P66 station is used to identify the outlet spot of the watershed. Unit of the discharge Q is mm/day which is converted from the actual observed data (in unit of m^3/s), using following relation:

$$Q(\text{mm/day}) = \frac{\text{Actual discharge (m}^3/\text{s)} \times 84,000 \text{ s} \times 1000}{\text{Associated drainage area (m}^2\text{)}} \quad (3.2)$$

The associated drainage areas for the three stations stated earlier are $6,213 \text{ km}^2$ (P1), 510 km^2 (P21), and $5,229 \text{ km}^2$ (P67). This conversion is done to enable the gained data to be directly comparable with other data sources, such as precipitation in

the area. From Figure 3.11b and Table 3.2, there are three apparent peaks of the observed discharge amount in September 2005 on dates 12th-13th, 20th-21th, 29th-30th.

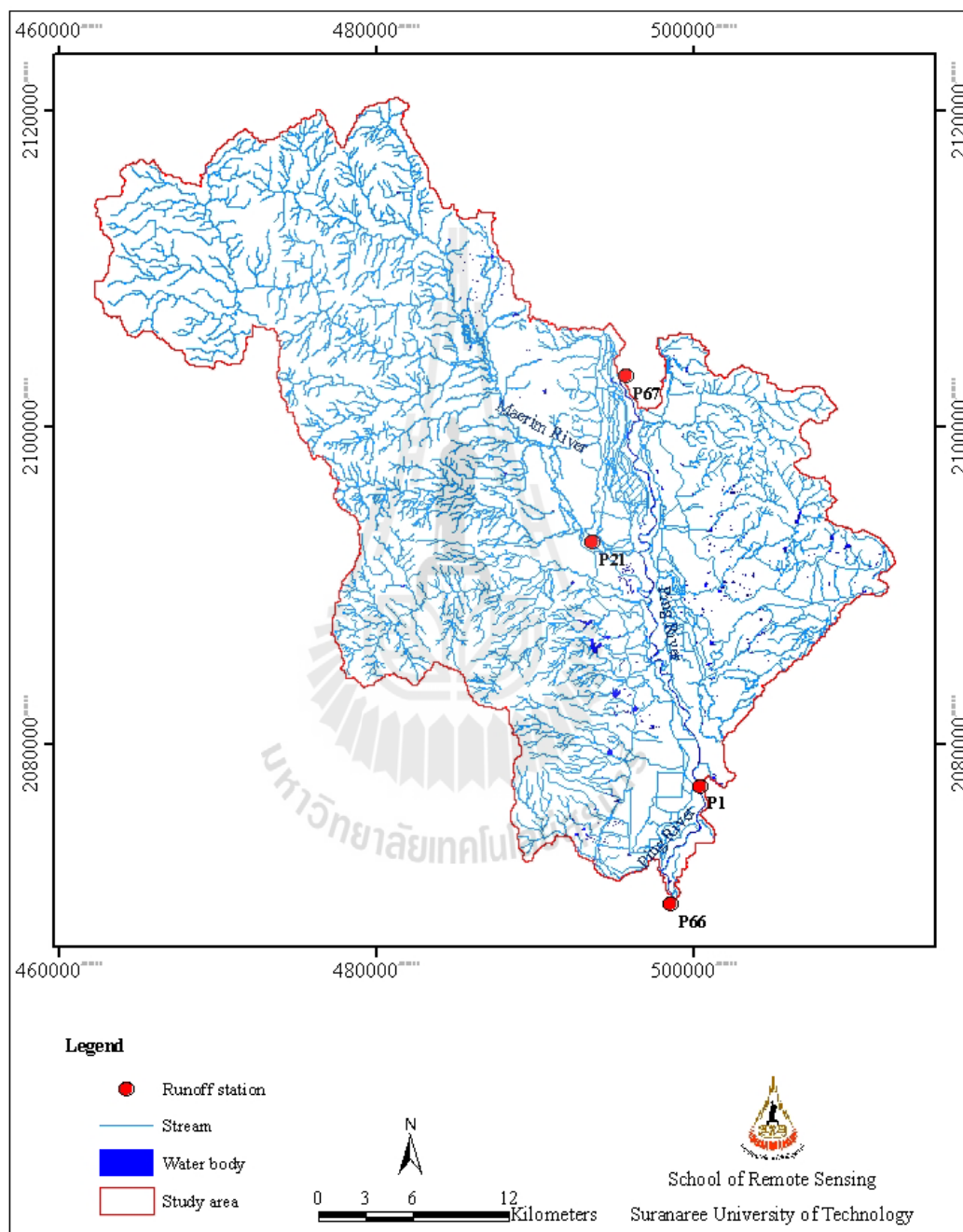


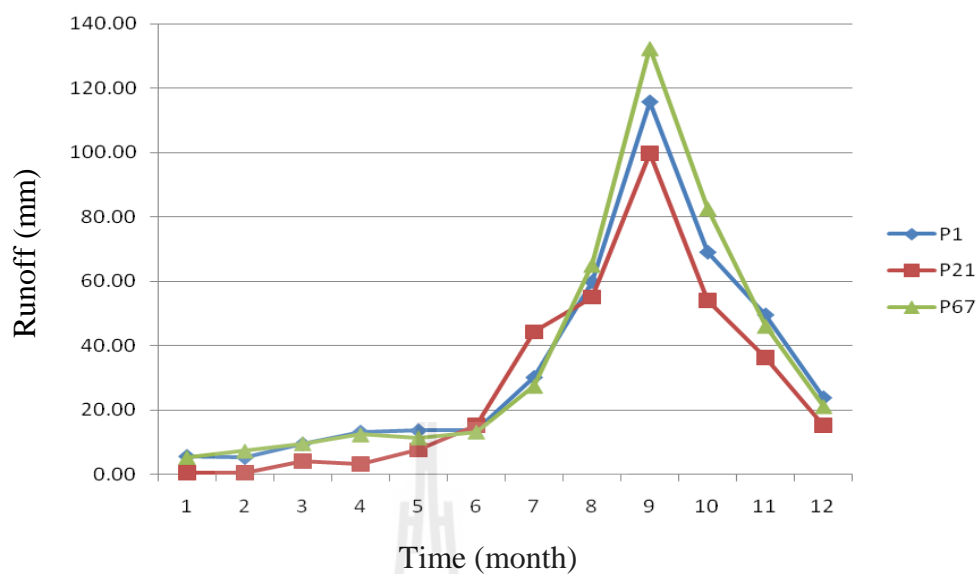
Figure 3.10 Stream network and locations of relevant discharge measuring stations.

Table 3.2 Monthly/daily (in September) discharge data at P1(A = 6,213 km²), P21 (A = 510 km²), P67(A = 5,229 km²) stations in 2005.

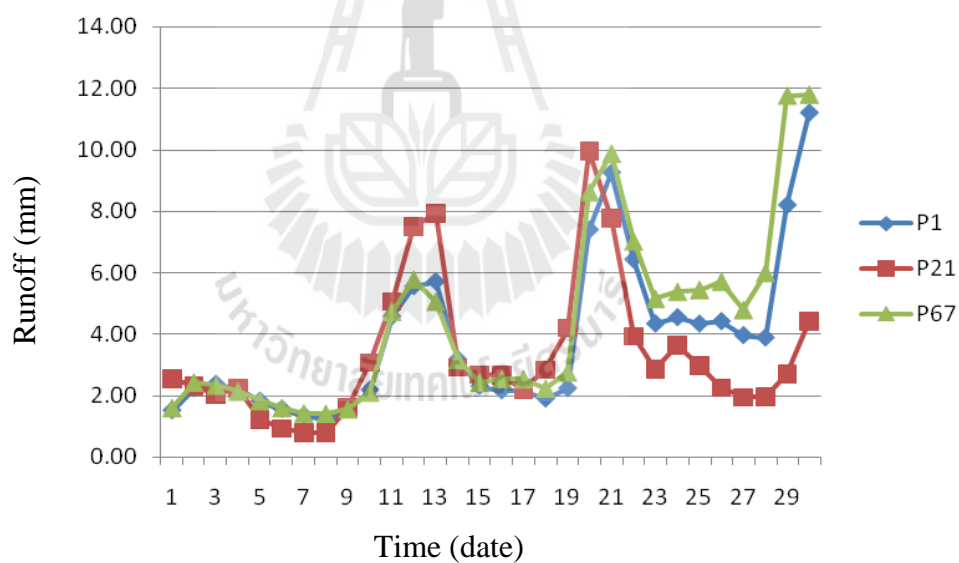
Month	Discharge (mm) at station			Day	Discharge (mm) at station		
	P1	P21	P67		P1	P21	P67
1	5.67	0.40	5.19	1	1.51	2.54	1.60
2	5.32	0.46	7.17	2	2.23	2.31	2.44
3	9.50	4.00	9.50	3	2.37	2.03	2.33
4	13.22	3.19	12.26	4	2.23	2.23	2.14
5	13.62	7.60	11.33	5	1.82	1.22	1.83
6	13.79	15.30	13.14	6	1.56	0.93	1.60
7	30.17	44.29	27.35	7	1.35	0.78	1.42
8	59.83	55.05	64.97	8	1.23	0.80	1.41
9	115.67	99.87	132.37	9	1.56	1.60	1.57
10	69.02	54.07	82.54	10	2.18	3.07	2.11
11	49.57	36.35	46.01	11	4.56	5.06	4.74
12	23.85	15.19	21.04	12	5.54	7.50	5.78
-	-	-	-	13	5.70	7.92	5.06
-	-	-	-	14	3.18	2.92	3.17
-	-	-	-	15	2.30	2.68	2.44
-	-	-	-	16	2.16	2.66	2.54
-	-	-	-	17	2.18	2.17	2.54
-	-	-	-	18	1.89	2.83	2.24
-	-	-	-	19	2.23	4.20	2.76

Table 3.2 (Continue)

Month	Discharge (mm) at station			Day	Discharge (mm) at station		
	P1	P21	P67		P1	P21	P67
-	-	-	-	20	7.39	9.96	8.62
-	-	-	-	21	9.25	7.77	9.88
-	-	-	-	22	6.42	3.93	7.02
-	-	-	-	23	4.33	2.86	5.15
-	-	-	-	24	4.54	3.65	5.39
-	-	-	-	25	4.33	2.97	5.45
-	-	-	-	26	4.41	2.26	5.72
-	-	-	-	27	3.95	1.94	4.79
-	-	-	-	28	3.88	1.96	6.00
-	-	-	-	29	8.19	2.70	11.77
-	-	-	-	30	11.19	4.41	11.80
-	-	-	-	Total	115.660	99.860	132.074
-	-	-	-	Average	3.855	3.329	4.402



(a) Monthly data



(b) Daily data

Figure 3.11 Variation of the observed discharges at P1, P21, P67 stations (a) monthly data in 2005 and (b) daily data in September 2005.

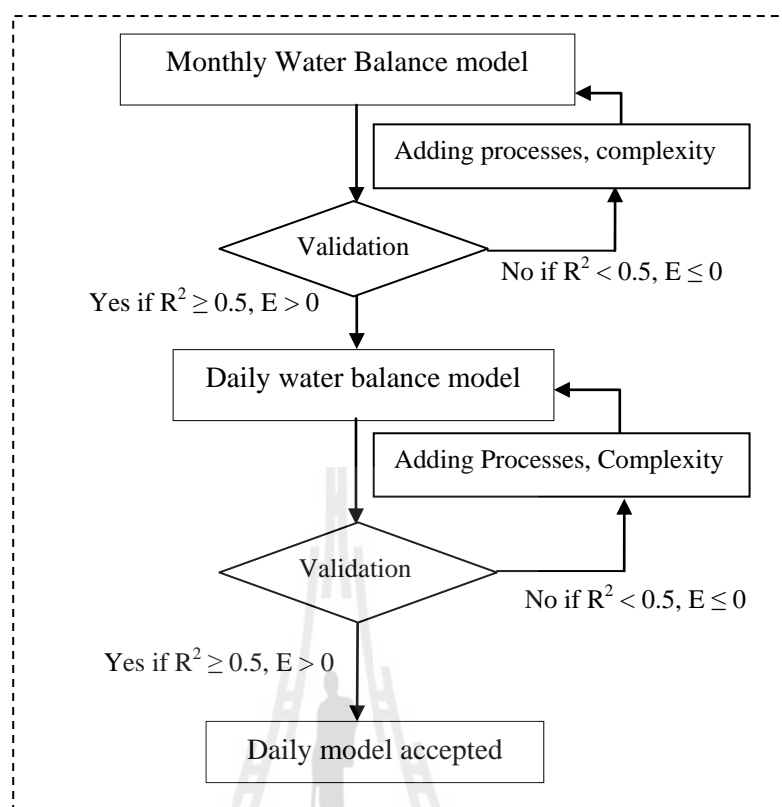


Figure 3.12 Flow diagram of the hydrologic model development.

3.3 Development of the hydrologic model

This process begins with the formulating of catchment water balance model (on monthly and daily basis) using the prepared (grid-based) input data and channel network routing model. Flow diagram of the proposed hydrologic model is described in Figure 3.12. The model is developed with ArcToolbox model of ArcGIS software based on the original lumped model detailed in Jothityangkoon and Sivapalan (2003) and Jothityangkoon et al. (2001; 2006). The water balance equation is as follows:

$$\frac{ds(t)}{dt} = p(t) - q_{ss}(t) - q_{se}(t) - e_b(t) - e_v(t), \quad (3.3)$$

where $s(t)$ is the volume of soil moisture storage, $p(t)$ is the rainfall input rate, q_{ss} is subsurface runoff, q_{se} is saturation excess runoff rate, e_b is bare soil evaporation rate and e_v is the transpiration rate. Note that the interception rate of 10% was applied to the vegetation group (forest/orchard/perennial) which reduces the initial rainfall input data by the same amount over land unit in that group. Details of the four outflow rates (ones with a negative sign on the right hand side of Eq. 3.3) can be described as follows:

(1) Subsurface runoff

The subsurface runoff term, q_{ss} , was determined using the relation:

$$q_{ss} = \frac{s - s_f}{t_c} \quad \text{if } s > s_f ; \quad (3.4a)$$

$$q_{ss} = 0 \quad \text{if } s < s_f ; \quad (3.4b)$$

where s_f is the soil-moisture storage at field capacity, and t_c is a catchment response time with respect to the subsurface flow. The threshold storage, s_f , is assumed to be equal to $s_f = f_c D$, where f_c is soil's field capacity, and D is average effective soil depth (Figure 3.5). The reason for the use of field capacity is that often when the moisture content is less than the field capacity, capillary forces are larger than those of gravity and drainage is prevented. In the study, maximum value of D that is found to have strong impact on the water balance outcome was about 10m depth. As a result, only data of $D = 0.2-10$ m are applied in the model's building and application (as an effective soil depth) and D greater than 10 are represented by $D = 10$ m.

In theory, the catchment response time, t_c , defines average traveling time of the induced runoff (e.g by a storm) within the catchment to reach catchment's outlet. For the subsurface flow, this value can be estimated by the Darcy's law for idealized triangular representation of the unconfined aquifer within a hill slope, assuming that the hydraulic gradient can be approximated by slope of ground surface. This gives:

$$t_c = \frac{L\phi}{2K_s \tan \beta}, \quad (3.5)$$

where ϕ is the average soil porosity, L is the average hill slope length, $\tan \beta$ is the average ground surface slope, K_s is the average saturated hydraulic conductivity. However, due to the lack of necessary data, especially the hydraulic conductivity, for performing direct calculation of t_c from Eq. 3.5, its proper value was calibrated to provide the best fit of the simulated discharge to the observed one.

(2) Saturation excess runoff rate

Similarly, the surface runoff term, q_{se} , was determined using the relation:

$$q_{se} = (s - S_b) / \Delta t \quad \text{if} \quad s > S_b ; \quad (3.6a)$$

$$q_{se} = 0 \quad \text{if} \quad s \leq S_b ; \quad (3.6b)$$

where S_b is the bucket's soil-moisture storage capacity, given by $S_b = D\phi$ where ϕ is the average soil porosity, and Δt is the time interval. Eq. 3.6 indicates that the excess surface runoff exists if amount of soil moisture storage is higher than bucket's soil-moisture storage capacity only, otherwise this term will be zero.

(3) Bare soil evaporation rate

The evaporation term, e_b , was estimated through the relation:

$$e_b = \frac{s}{t_e}, \quad (3.7)$$

$$t_e = \frac{S_b}{(1-M)e_p}, \quad (3.8)$$

where t_e is a characteristic time scale associated with bare soil evaporation, estimated using Eq. 3.8, e_p is potential evaporation rate, and M is fraction of forest vegetation cover. In the original lumped model, M can vary between 0 and 1 as the forest cover can vary significantly basin to basin. But in the grid-based concept proposed here, as the fundamental land unit is small ($30 \times 30 \text{ m}^2$), M was then assumed to be 0 for the bare land LULC group (e.g. crop, paddy field) and to be 1 for the vegetation LULC group (forest and orchard/perennial). This gives $e_b = (s/S_b) e_p$ (as seen in Eq. 3.1b).

(4) Transpiration rate

The transpiration term, e_v , was estimated through the relation:

$$e_v = Mk_v e_p \quad \text{if} \quad s > s_f ; \quad (3.9a)$$

$$e_v = \frac{s}{t_g} \quad \text{if} \quad s < s_f ; \quad (3.9b)$$

$$t_g = \frac{s_f}{Mk_v e_p} \quad (3.10)$$

where t_g is a characteristic time scale associated with the transpiration and k_v is a plant transpiration efficiency (here set equal to 1). As stated above, M was also set to be 1 (for the vegetation LULC group) which gives $e_v = e_p$ if $s > s_f$ and $e_v = (s/s_f) e_p$ if $s < s_f$ (as seen in Eq. 3.1a).

Table 3.3 provides list of the parameters relevant to the model's development. The formulated hydrologic model receives values of all physical parameters from GIS model and generates simulated runoff for each grid cell. Then, the flow path and flow accumulation are formulated using DEM and converted to parameters for the routing model. Simulated runoff discharges from the invented model (at P1 and P21 stations) were compared to the observed one at the same stations. And model's modification is accepted if it can produce moderate to good agreement between both set of data in term of the coefficient of determination (R^2), e.g., with $R^2 \geq 0.5$, and also satisfies the acceptable Nash-Sutcliffe efficiency criterion of $E \geq 0$ (Moriassi et al., 2007).

Table 3.3 Parameters used in the original and developed hydrologic models.

Order	Symbol	Term	Unit
1	P	Rainfall input rate	Length/Time
2	q_{ss}	Subsurface runoff	Length/Time
3	q_{se}	Saturation excess runoff rate	Length/Time
4	e_b	Bare soil evaporation rate	Length/Time
5	e_v	Transpiration rate	Length/Time
6	s_f	Soil-moisture storage at field capacity	Length/Time
7	t_c	Catchment's response time with respect to subsurface flow	Length/Time
8	fc	Soil's field capacity	Length/Time
9	D	Average effective soil depth	Length/Time
10	ϕ	Average soil porosity	-
11*	L	Average hill slope length	Length/Time
12*	$\tan \beta$	Average ground surface slope	-
13*	K_s	Average saturated hydraulic conductivity	Length/Time
14	S_b	Bucket's soil-moisture storage capacity	Length/Time
15	Δt	Time period	Length/Time
16	t_e	Characteristic time scale associated with bare soil evaporation	Length/Time
17*	M	Fraction of forest vegetation cover	%
18	t_g	Characteristic time scale associated with transpiration	Length/Time
19	k_v	Plant transpiration efficiency	-

Note: * is parameter unused in the developed model (but used in the original one)

(Jothityangkoon and Hirunteeyakul, 2009).

3.4 Construction of the flood maps

This part contributes to the generating of preferred flood maps for the Chiang Mai municipality during September 2005 based on the simulated runoff data gained from the derived model described earlier (see work flowchart in Figure 3.13). The obtained maps are then compared with the reference flood map (of the same event) prepared by the Faculty of Engineering, Chiang Mai University (Figure 2.4).

3.4.1 Simulation of flooding scenarios

As the assumed flooding scenario in this work is river flood, therefore, the occurrence of flood will be recognized if the overbank flow was found.

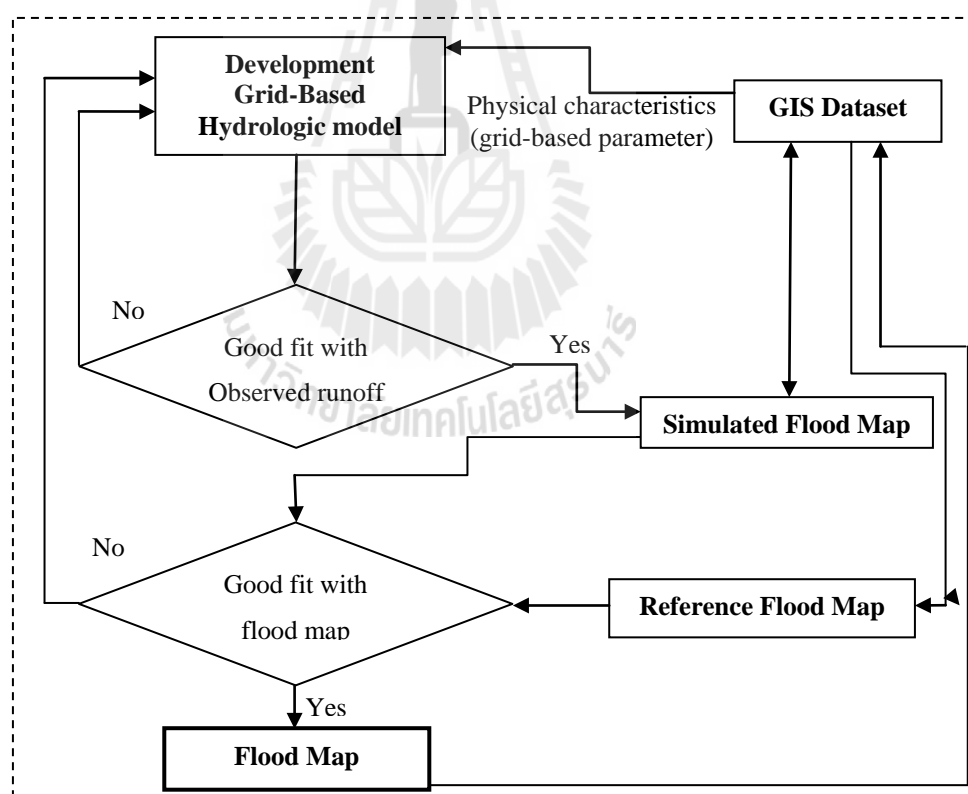


Figure 3.13 Flow diagram of the flood map simulation process.

Table 3.4 Stream-related data for the station P1, P21, and P67 (Hydrology and Water Management Center for Upper Northern Region, 2012).

Station	Height from mean sea level (m) (2005 data)				Associated drainage area (km ²)
	Left bank	Right bank	River bed	Pole base	
P1	305.116	304.288	299.077	300.500	6,213
P21	325.150	325.15	319.720	319.700	510
P67	326.303	326.206	313.749	315.926	5,229

However, as the developed hydrologic model describe earlier can provide only data of the stream discharge at a particular location along the river network, therefore, the associated water level at that point was assessed individually based on the proper rating curve chosen for that location. To fulfill this task, the study area was divided into three sub-regions (assuming based on similar characteristics) as seen in Figure 3.14 and main rivers in each region were assumed to have similar rating curve to one found at the reference station of that region (P1, P21, and P67 station), which are:

$$\text{Station P1: } Z = -0.000004(Q)^2 + 0.008Q + Z_0; (R^2 = 0.99) \quad (3.12a)$$

$$\text{Station P21: } Z = -0.00(Q)^2 + 0.087(Q) + Z_0; (R^2 = 0.99) \quad (3.12b)$$

$$\text{Station P67: } Z = -0.000005(Q)^2 + 0.01(Q) + Z_0; (R^2 = 0.98) \quad (3.12c)$$

where Z is the water level (in meter above MSL) at the considered location along the stream network, Q is the discharge (in m³/s) and Z_0 is constant of the equation (water level when $Q = 0$ equivalent to the assumed height of the river bed above MSL of the considered stream location). For the P1, P21, and P67, these values of Z_0 are 301.5, 320.1 and 316.5 m, respectively. Structural data of the ping River at these stations are given in Table 3.4. To obtain more realistic values of Z_0 along Ping River, structures

of the river cross-section at 10 different locations were prepared and used as described in Appendix C. To generate the preferred flood map, over flown water (from stream channel) is assumed to spread laterally into lowland area situating nearby until reaching the high land/place that it cannot flow over.

The flooding incidence shall occur (over a specific area) if the water level Z (from Eq. 3.12) greater than the local elevation (above MSL) of the considered area. Or, if $Z > DEM$, the area shall be labeled as being flooded land. As a result, the flood maps can be produced based on knowledge of water level at each location along the associated stream network and local elevation of considered area (in each sub-region).

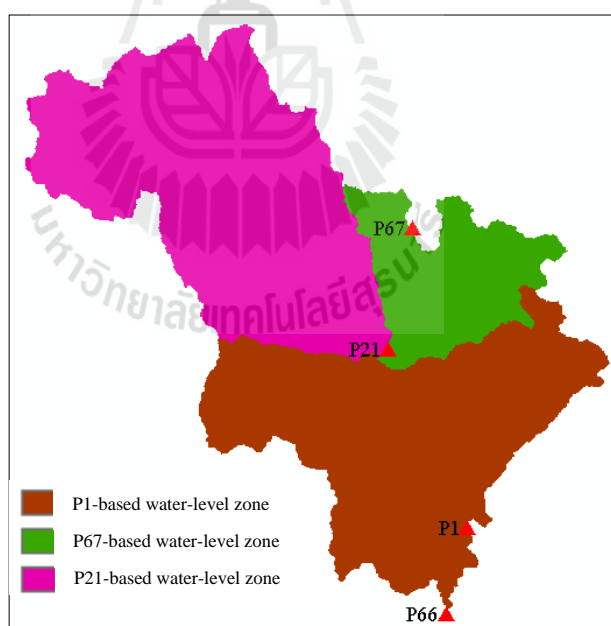


Figure 3.14 Associated flooding sub-region of three rating curves in Eqs. 3.12a-3.12c.

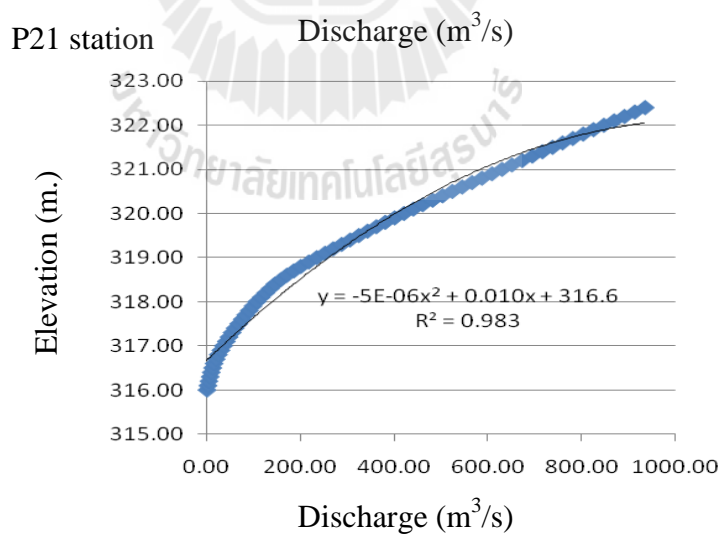
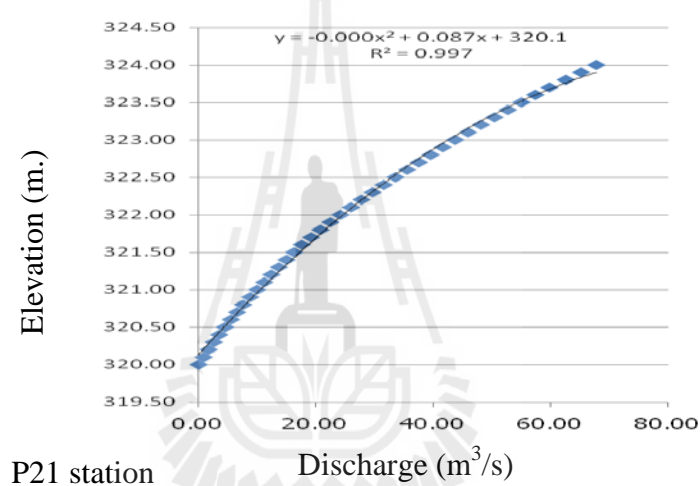
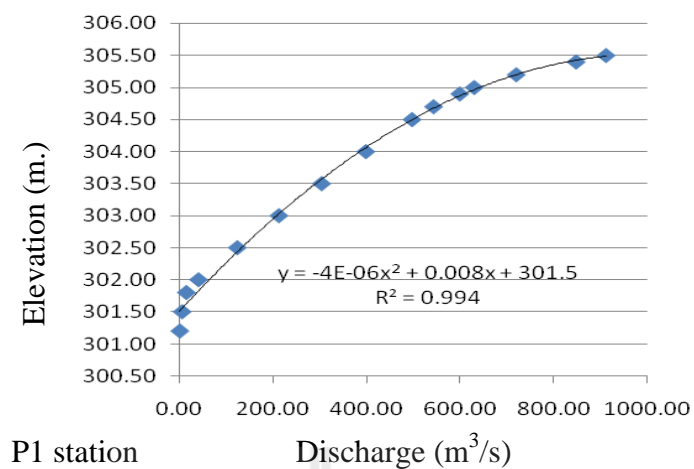


Figure 3.15 Relations of discharge and water level (rating curve) in 2005 at 3 stations (a) P1, (b) P21, (c) P67.

Table 3.5 Data of river stage and relevant discharge at three stations, P1, P21, P67
(Hydrology and Water Management Center for Upper Northern Region, 2012).

Station P1		Station P21		Station P67	
Discharge (m ³ /s)	Water level (m)	Discharge (m ³ /s)	Water level (m)	Discharge (m ³ /s)	Water level (m)
0.00	301.20	0.00	320.00	0.00	316.00
5.00	301.50	0.85	320.10	2.00	316.10
14.00	301.80	1.70	320.20	4.00	316.20
40.00	302.00	2.60	320.30	6.50	316.30
123.00	302.50	3.50	320.40	9.00	316.40
212.00	303.00	4.50	320.50	12.00	316.50
303.50	303.50	5.50	320.60	15.00	316.60
398.00	304.00	6.55	320.70	19.50	316.70
497.00	304.50	7.60	320.80	24.00	316.80
543.00	304.70	8.80	320.90	29.50	316.90
599.00	304.90	10.00	321.00	35.00	317.00
630.00	305.00	11.20	321.10	41.00	317.10
720.00	305.20	12.40	321.20	47.00	317.20
848.00	305.40	13.70	321.30	53.50	317.30
912.00	305.50	15.00	321.40	60.00	317.40
-	-	16.30	321.50	67.50	317.50
-	-	17.60	321.60	75.00	317.60
-	-	19.20	321.70	82.50	317.70
-	-	20.80	321.80	90.00	317.80
-	-	22.50	321.90	98.00	317.90
-	-	24.20	322.00	106.00	318.00
-	-	26.00	322.10	115.50	318.10

Table 3.5 (Continued).

Station P1		Station P21		Station P67	
Discharge (m ³ /s)	Water level (m)	Discharge (m ³ /s)	Water level (m)	Discharge (m ³ /s)	Water level (m)
-	-	27.80	322.20	125.00	318.20
-	-	29.70	322.30	135.00	318.30
-	-	31.60	322.40	145.00	318.40
-	-	33.60	322.50	157.50	318.50
-	-	35.60	322.60	170.00	318.60
-	-	37.60	322.70	185.00	318.70
-	-	39.60	322.80	200.00	318.80
-	-	41.70	322.90	217.00	318.90
-	-	43.80	323.00	234.00	319.00
-	-	46.00	323.10	251.50	319.10
-	-	48.20	323.20	269.00	319.20
-	-	50.50	323.30	287.00	319.30
-	-	52.80	323.40	305.00	319.40
-	-	55.10	323.50	323.50	319.50
-	-	57.50	323.60	342.00	319.60
-	-	59.90	323.70	361.00	319.70
-	-	62.70	323.80	380.00	319.80
-	-	65.30	323.90	400.00	319.90
-	-	67.90	324.00	420.00	320.00
-	-	-	-	440.00	320.10
-	-	-	-	460.00	320.20
-	-	-	-	481.00	320.30
-	-	-	-	502.00	320.40
-	-	-	-	523.00	320.50

Table 3.5 (Continued).

Station P1		Station P21		Station P67	
Discharge (m ³ /s)	Water level (m)	Discharge (m ³ /s)	Water level (m)	Discharge (m ³ /s)	Water level (m)
-	-	-	-	544.00	320.60
-	-	-	-	565.00	320.70
-	-	-	-	586.00	320.80
-	-	-	-	607.50	320.90
-	-	-	-	629.00	321.00
-	-	-	-	650.00	321.10
-	-	-	-	672.00	321.20
-	-	-	-	693.50	321.30
-	-	-	-	715.00	321.40
-	-	-	-	736.50	321.50
-	-	-	-	758.00	321.60
-	-	-	-	780.00	321.70
-	-	-	-	802.00	321.80
-	-	-	-	824.00	321.90
-	-	-	-	846.00	322.00
-	-	-	-	868.00	322.10
-	-	-	-	890.00	322.20
-	-	-	-	912.00	322.30
-	-	-	-	934.00	322.40

3.5 Impacts of the LULC and climate changes on flooding analysis

The part deals with applications of the derived model to examine impacts of the LULC and climate changes on the observed flood occurrence of the study area.

Three specific cases were considered at this stage:

(1) Impact of the predicted LULC changes in 2020 given by the CA-Markov model while other factors in the water balance model are unchanged.

(2) Impact of the specifically-modified LULC maps based on some preferred scenarios (forest/orchard loss at rates of 10 and 20%). These values are chosen to resemble work of Jothityangkoon (2009) that assumes forest loss of 10 and 20% and assesses the impacts on amount of maximum runoff data of the Ping Basin area above the Bhumipol Dam (which includes the target area in this study).

(3) Impact of the variation in amount of the rainfall intensity (increase by 5, 10, 15%) in the area (under the same distributing pattern).

In the first case, future LULC map for year 2020 is generated by using the CA-Markov model in which the classified LULC maps of years 2000 and 2010 are used as prior references to predict the 2020 LULC map. Accuracy assessment of the classified 2005 LULC map and 2010 predicted map (constructed based on the 2000 and 2005 LULC maps through the CA-Markov model) are assessed and results are reported in form of standard error matrix. The gained 2020 LULC maps are then used as an input data to calculate runoff data in the study area (under assumption that all other parameters used in the daily water balance model are the same as prescribed in the year 2005 case). Knowledge of the simulated runoff data can be further used to compute discharge and to create the associated flood depth map later on.

In the second case, specific rates of forest and orchard/perennial loss over the entire study area were proposed first, and then the CA-Markov model was applied to identify areas of that preferred loss (10 and 20% of the original forest/orchard area in 2005). To fulfill this task, the model's transition area matrix had been modified to suit such an assumption of forest/orchard loss scenario (10 and 20%) and the predicted LULC maps are generated based on these modified matrices. The obtained maps are then used as an input data in the developed hydrologic model to simulate discharge data at the P1 and P21 stations and their associated flood maps subsequently.

In the third case, rainfall intensity are adjusted to increase by 5, 10, and 15% of the original values in 2005 while its distributing pattern (as seen in Figure 3.8 and 3.9) and other factors in the water balance model are assumed to be unchanged. These adjustments was inspired by work of Kripalani and Kulkarni (1997) which found that the intense La Nina phenomenon is able to increase total rainfall amount in Thailand by about 5%. The obtained discharge volumes at P1 station for each assigned rainfall amount were then applied to the flood mapping process described in Section 3.4 to produce the associated flood depth maps. By comparing results arisen from all three values of the rainfall intensity, its sole impact can then be examined. These values (of 5, 10, 15%) are also resemble to work of Jothityangkoon (2009) done for the Ping Basin area above the Bhumipol Dam as stated earlier.

CHAPTER IV

RESULTS AND DISCUSSION

This chapter reports results of works detailed in Chapter 3. These include LULC classification and application of CA-Markov model, grid-based hydrologic model's development and runoff simulation, flood depth mapping from simulated discharge and impact assessment of the variation in LULC pattern, forest/orchard cover and rainfall intensity on the simulated discharge and associated flood map, respectively.

4.1 LULC classification and application of the CA-Markov model

The first task in this part is to produce classified LULC maps of the study area for years 2000, 2005, 2010 from the Landsat TM images using hybrid classification method which starts by the unsupervised method (ISODATA) then followed by the supervised method (Maximum Likelihood). The results are illustrated in Figure 4.1 with the associated covering area shown in Table 4.1. Accuracy assessment was also performed for the 2005 and 2010 classified map used in the model's developing process (Section 4.2) using 540 reference points from high resolution satellite imagery in 2nd February 2005, 1st March 2010 on Google Earth Program and field survey during 13th-15th October 2010 (as detailed in APPENDIX E) [based on the multinomial distribution theory described in Jensen (2005) with desired precision 5%, level of confidence 15%, 7 LULC classes], and results are displayed in Table 4.2 and

Table 4.3. Here, the overall accuracy of 90.56% and 87.22%, and the kappa coefficient of 0.84 and 0.78 are achieved for the LULC classified maps of years 2005 and 2010, respectively. These values indicate high accuracy and reliability of the LULC maps in use.

Figures 4.1a-c indicates that the forest class dominates in the western side and urban dominates in the far south of the study area (the Chiang Mai city area) while orchard/perennial mostly situates close to the forest boundary and the paddy field is usually found mixed up with the urban/built-up class in the southeastern part of the area. Table 4.1 suggests that pattern of the LULC does not change much during period 2000-2010 with forest occupies about 62-64% of the entire study area followed by urban/built-up about 13-14%, orchard/perennial about 10-12% and the paddy fields about 9%. If consider in term of the loss/gain area during 2000-2010, forest and paddy field have lost about 3.16 and 1.57% of their original area in 2010 (total of 22.78 and 1.63 km², respectively). Over same period, orchard/perennial, crop and urban/built-up have gained about 10.56, 22.46 and 6.76% of their original areas (total of 12.59, 4.18, 9.82 km², respectively).

The LULC change matrix during 2000-2010 reveals that the original forest in 2000 are turned into orchard/perennial the most followed by crop and urban/built-up, respectively. Over the same period, urban/built-up area is grown about 6.76% of the original area in 2000 in expense of the paddy field the most followed by forest and miscellaneous class, respectively. In the mean time, the orchard/perennial class has grown about 10.56% of the original area in 2000 in the expense of forest mostly and paddy field was reduced by 1.57% which was turned to be urban/built-up the most. It should be noted that the forest zone on the western side of the study area is under

strong threat from the invasion of agricultural activities (e.g. crop and paddy field) and less severity from the urban/built-up expansion.

Table 4.1 Covering area for different LULC classes in year 2000, 2005, and 2010 based on Figure 4.1.

LULC type	2000		2005		2010	
	km ²	%	km ²	%	km ²	%
Forest (FOR)	718.11	64.05	700.31	62.47	695.33	62.02
Orchard/Perennial (ORC)	119.13	10.63	128.33	11.45	131.72	11.75
Crop (CROP)	18.61	1.66	22.23	1.98	22.79	2.03
Paddy field (PAD)	104.13	9.29	102.92	9.18	102.50	9.14
Urban/built-up (U/B)	145.19	12.95	152.69	13.62	155.01	13.83
Water body (WAT)	7.91	0.71	8.10	0.72	7.86	0.70
Miscellaneous (MIS)	8.00	0.71	6.52	0.58	5.88	0.52
Total	1,121.09	100.00	1,121.09	100.00	1,121.09	100.00

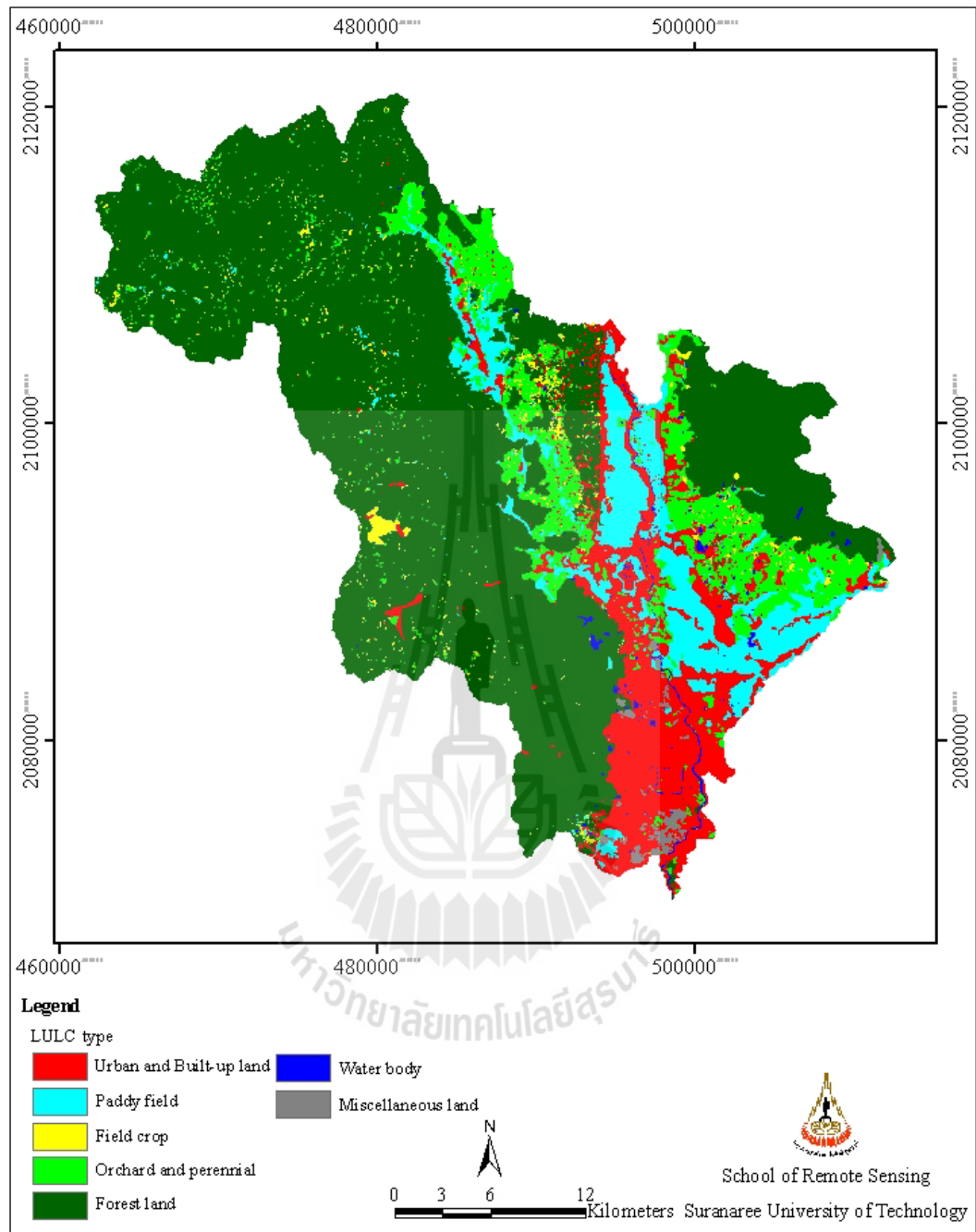


Figure 4.1a Classified LULC map for year 2000 from the Landsat TM image.

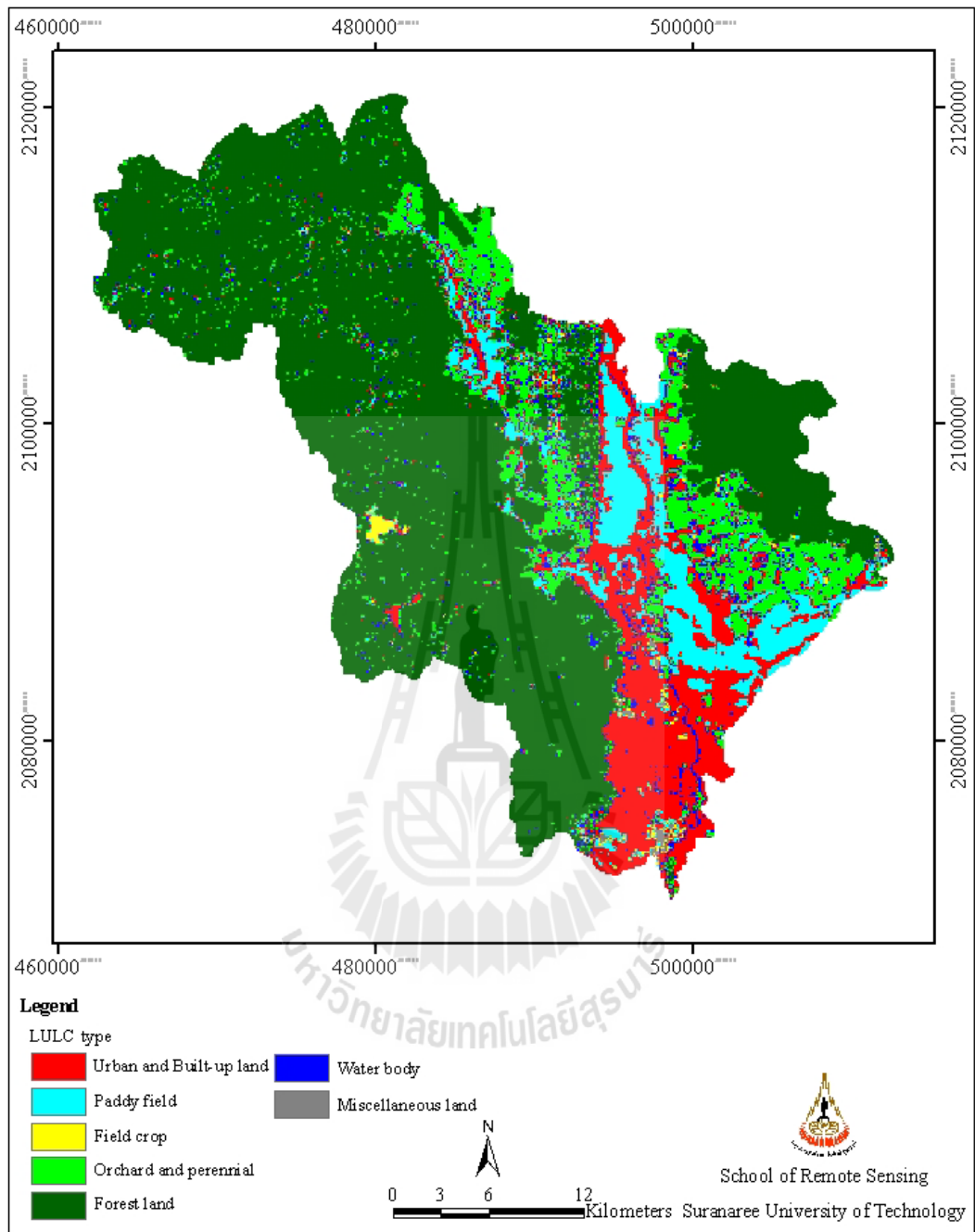


Figure 4.1b Classified LULC map for year 2005 from the Landsat TM image.

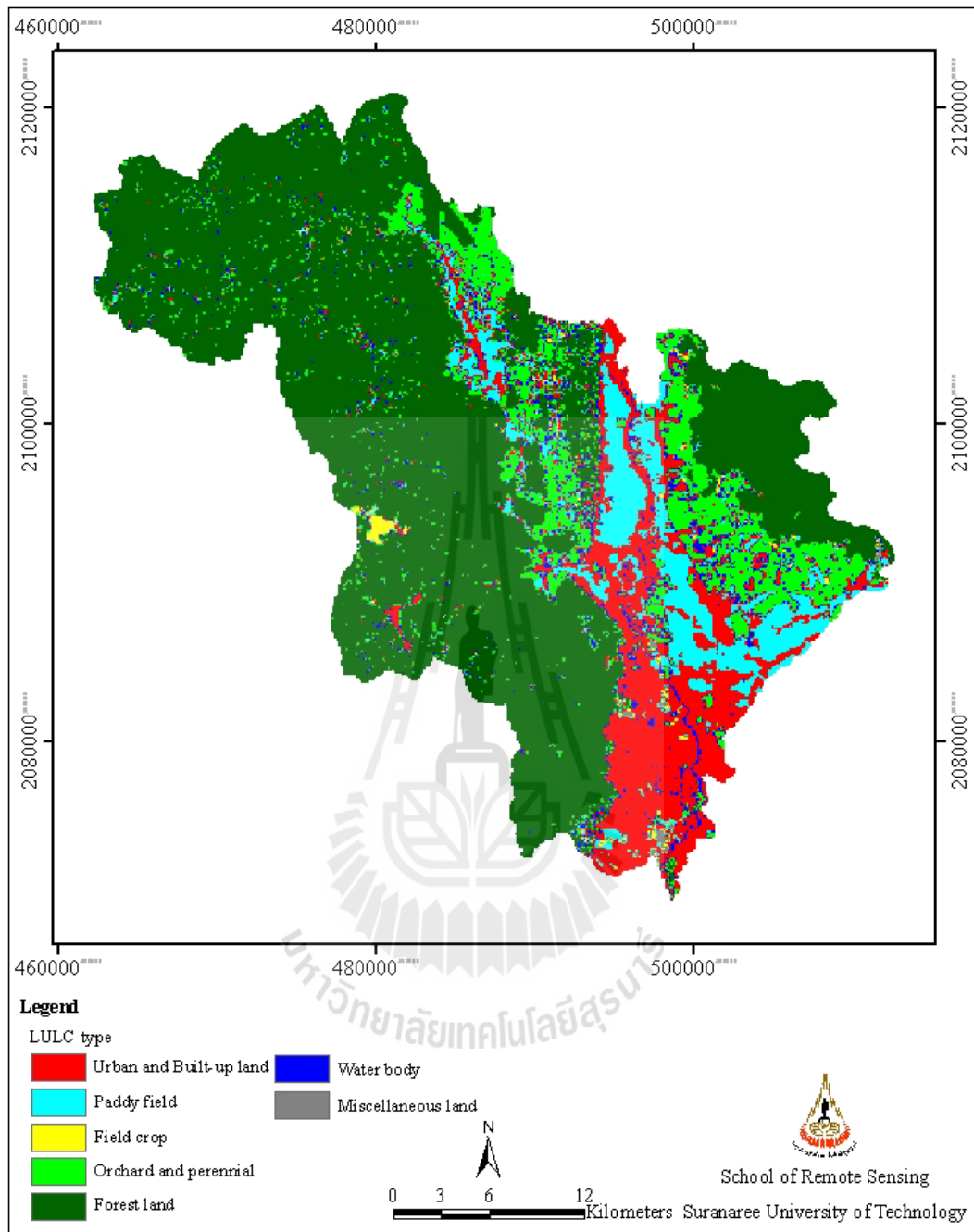


Figure 4.1c Classified LULC map for year 2010 from the Landsat TM image.

Table 4.2 Error matrix of the 2005 classified LULC map (Figure 4.1b).

	LULC class	Reference Data							Total (pixel)	Accuracy	
		MIS	CROP	PAD	U/B	WAT	ORC	FOR		EC	UA
Classified data	MIS	2	-	-	-	-	1	-	3	33.33	66.67
	CROP	-	10	-	-	-	-	1	11	9.09	90.91
	PAD	1	1	41	2	-	5	-	50	18.00	82.00
	U/B	2	1		66		2	2	73	9.59	90.41
	WAT	-	-	-	-	4	-	-	4	0.00	100.00
	ORC		1	6	1	2	46	6	62	25.81	74.19
	FOR	-	6	1	-	-	10	320	337	5.04	94.96
Total (pixel)		5	19	48	69	6	64	329	540	-	-
Accuracy	EO	60.00	47.37	14.58	4.35	33.33	28.12	2.74	-	-	-
	PA	40.00	52.63	85.42	95.65	66.67	71.88	97.26	-	-	-

Note: Overall accuracy = 90.56%; Kappa coefficient = 0.84

Table 4.3 Error matrix of the 2010 classified LULC map (Figure 4.1c).

	LULC class	Reference Data							Total (pixel)	Accuracy	
		MIS	CROP	PAD	U/B	WAT	ORC	FOR		EC	UA
Classified data	MIS	2	-	-	1	-	-	-	3	33.33	66.67
	CROP	1	6	-	-	-	2	2	11	45.45	54.55
	PAD	1		35	8		5	-	49	28.57	71.43
	U/B	3	3	1	63	2	2	1	75	16.00	84.00
	WAT	-	-	-	-	4	-	-	4	0.00	100.00
	ORC	-	5	5	3	1	44	5	63	30.16	69.84
	FOR	-	4	1	4	-	9	317	335	5.37	94.63
Total (pixel)		7	18	42	79	7	62	325	540	-	-
Accuracy	EO	71.43	66.67	16.67	20.25	42.86	29.03	2.46	-	-	-
	PA	28.57	33.33	83.33	79.75	57.14	70.97	97.54	-	-	-

Note: Overall accuracy = 87.22%; Kappa coefficient = 0.78

Table 4.4 LULC change matrix during period 2000 - 2010 (from Figure 4.1).

	LULC class	2010 data							Total (km ²)
		MIS	CROP	PAD	U/B	WAT	ORC	FOR	
2000 data	MIS	5.42	0.00	0.16	2.30	0.01	0.09	0.01	8.00
	CROP	0.06	18.02	0.00	0.18	0.00	0.36	0.00	18.61
	PAD	0.07	0.09	100.72	2.91	0.12	0.21	0.00	104.13
	U/B	0.00	0.00	0.00	145.19	0.00	0.00	0.00	145.19
	WAT	0.02	0.00	0.00	0.07	7.51	0.00	0.31	7.91
	ORC	0.10	0.00	0.63	1.67	0.15	116.58	0.00	119.13
	FOR	0.21	4.67	0.99	2.69	0.06	14.48	695.01	718.11
Total (km ²)		5.88	22.79	102.50	155.01	7.86	131.72	695.33	1121.09

The second task achieved in this part is to synthesize the expected LULC maps in year 2010 and 2020 using the CA-Markov model and based on the classified LULC maps of years 2000 and 2005 (for the prediction of year 2010) and years 2000-2010 (for the prediction of year 2020). Results of the analysis (predicted map in 2010 and 2020) are given in Figure 4.2 and Figure 4.3, respectively, and Table 4.5. The relevant transition probability matrices (probability of state change from class to class) and transitional area matrices (amount of predicted changing area from class to class) for 2010 and 2020 LULC prediction are shown in Tables 4.6a-d, respectively.

To determine efficiency of the CA-Markov model in use, accuracy assessment of the 2010 predicted map is assessed (when compared to the classified one in the same year) and results are reported in form of standard error matrix (Table 4.7). The overall accuracy of 97.60% and kappa coefficient of 0.96 are achieved here which indicate high capability of the CA-Markov model in use.

Results in Table 4.5 suggest that, in 2020, forest should still dominate the study area (about 60.35%) followed by urban/built-up (14.46%), orchard/perennial

(12.83%) and paddy field (8.94%), while crop area covers just 2.38% of the total area. If compared to the original classified area in 2010, forest and paddy field losses of 2.69 and 2.23% were found during 2010-2020 while the orchard/perennial, crop, and urban/built-up areas increase by 9.19, 16.94, and 4.57%, respectively. However, if compared to the original area in year 2000 (Table 4.1), forest and paddy losses would be about 5.78 and 3.76% while orchard/perennial, crop, and urban/built-up areas would increase by 20.73, 43.20, and 11.64%, respectively.

Table 4.5 LULC covering area of the predicted maps in 2010 and 2020.

LULC type	2010 classified		2010 predicted		2020 predicted	
	km ²	%	km ²	%	km ²	%
Forest	695.33	62.02	685.81	61.17	676.62	60.35
Orchard/Perennial	131.72	11.75	137.22	12.24	143.82	12.83
Crop	22.79	2.03	25.58	2.28	26.65	2.38
Paddy field	102.50	9.14	101.18	9.03	100.21	8.94
Urban/built-up	155.01	13.83	158.00	14.09	162.09	14.46
Water body	7.86	0.70	8.04	0.72	7.53	0.67
Miscellaneous	5.88	0.52	5.26	0.47	4.18	0.37
Total	1121.09	100.00	1121.09	100.00	1121.09	100.00

Table 4.6a Transition probability matrix for the prediction of 2010 LULC map.

2000 data	2005 data						
	MIS	CROP	PAD	U/B	WAT	ORC	FOR
Miscellaneous	0.7936	0.0008	0.0012	0.1907	0.0011	0.0117	0.0009
Crop	0.0013	0.9718	0.0000	0.0086	0.0002	0.0180	0.0000
Paddy field	0.0002	0.0009	0.9741	0.0217	0.0010	0.0020	0.0000
Urban/built-up	0.0000	0.0000	0.0000	1.0000	0.0000	0.0000	0.0000
Water body	0.0016	0.0003	0.0000	0.0068	0.9816	0.0000	0.0097
Orchard/Perennial	0.0002	0.0000	0.0052	0.0123	0.0012	0.9811	0.0000
Forest	0.0001	0.0056	0.0012	0.0028	0.0001	0.0150	0.9751

Table 4.6b Transition probability matrix for the prediction of 2020 LULC map.

2000 data	2010 data						
	MIS	CROP	PAD	U/B	WAT	ORC	FOR
Miscellaneous	0.6769	0.0006	0.0204	0.2881	0.0018	0.0114	0.0009
Crop	0.0030	0.9681	0.0000	0.0095	0.0002	0.0191	0.0000
Paddy field	0.0007	0.0009	0.9673	0.0279	0.0012	0.0020	0.0000
Urban/built-up	0.0000	0.0000	0.0000	1.0000	0.0000	0.0000	0.0000
Water body	0.0026	0.0003	0.0001	0.0088	0.9487	0.0000	0.0395
Orchard/Perennial	0.0009	0.0000	0.0053	0.0140	0.0012	0.9786	0.0000
Forest	0.0003	0.0065	0.0014	0.0037	0.0001	0.0202	0.9678

Table 4.6c Transition area matrix for the prediction of 2010 LULC map.

2000 data	2005 data							Total (pixels)
	MIS	CROP	PAD	U/B	WAT	ORC	FOR	
Miscellaneous	5,747	6	9	1,381	8	85	7	7,243
Crop	32	24,009	0	213	6	446	0	24,706
Paddy field	21	104	111,392	2,486	115	233	0	114,351
Urban/built-up	0	0	0	169,650	0	0	0	169,650
Water body	14	3	0	61	8,833	0	87	8,998
Orchard/Perennial	29	0	740	1,750	169	139,904	0	142,592
Forest	96	4,379	923	2,197	77	11,708	758,741	778,121
Total (pixels)	5,939	28,501	113,064	177,738	9,208	152,376	758,835	1,245,661

Note: Number of pixels along diagonal line indicates the no-change area of that class. These values indicate that only small portion of the area for each class that was turned into other classes.

Table 4.6d Transition area matrix for the prediction of 2020 LULC map.

2000 data	2010 data							Total (pixels)
	MIS	CROP	PAD	U/B	WAT	ORC	FOR	
Miscellaneous	4,424	4	133	1,883	12	74	6	6,536
Crop	77	24,512	0	240	6	485	0	25,320
Paddy field	82	101	110,166	3,181	132	232	0	113,894
Urban/built-up	0	0	4	172,227	0	0	0	172,231
Water body	23	3	1	76	8,285	0	345	8,733
Orchard/Perennial	126	0	775	2,053	180	143,226	0	146,360
Forest	228	5,021	1,060	2,890	70	15,582	747,736	772,587
Total (pixels)	4,960	34,601	112,139	182,548	8,685	159,599	748,087	1,245,661

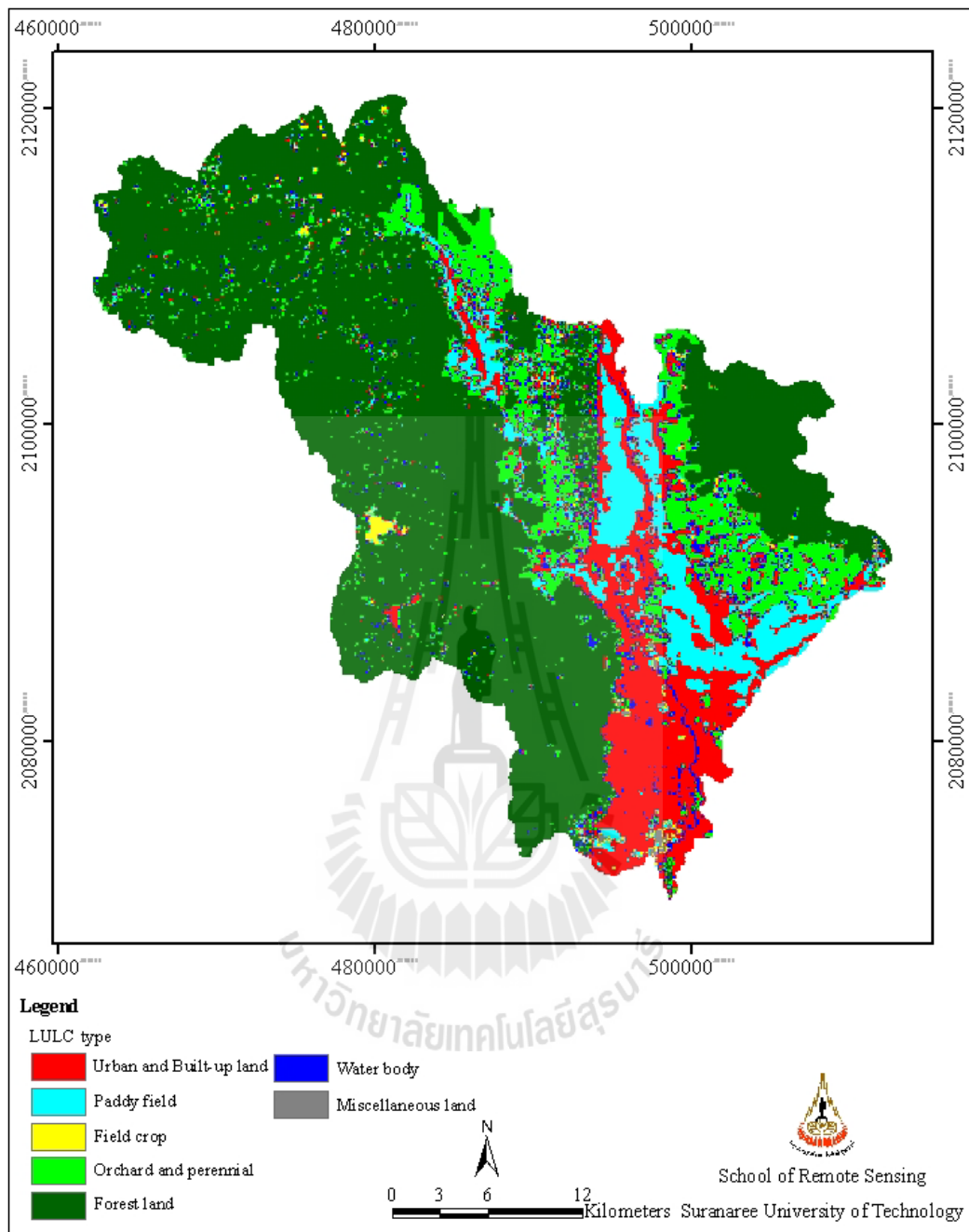


Figure 4.2 Predicted LULC map in 2010 by the CA-Markov model.

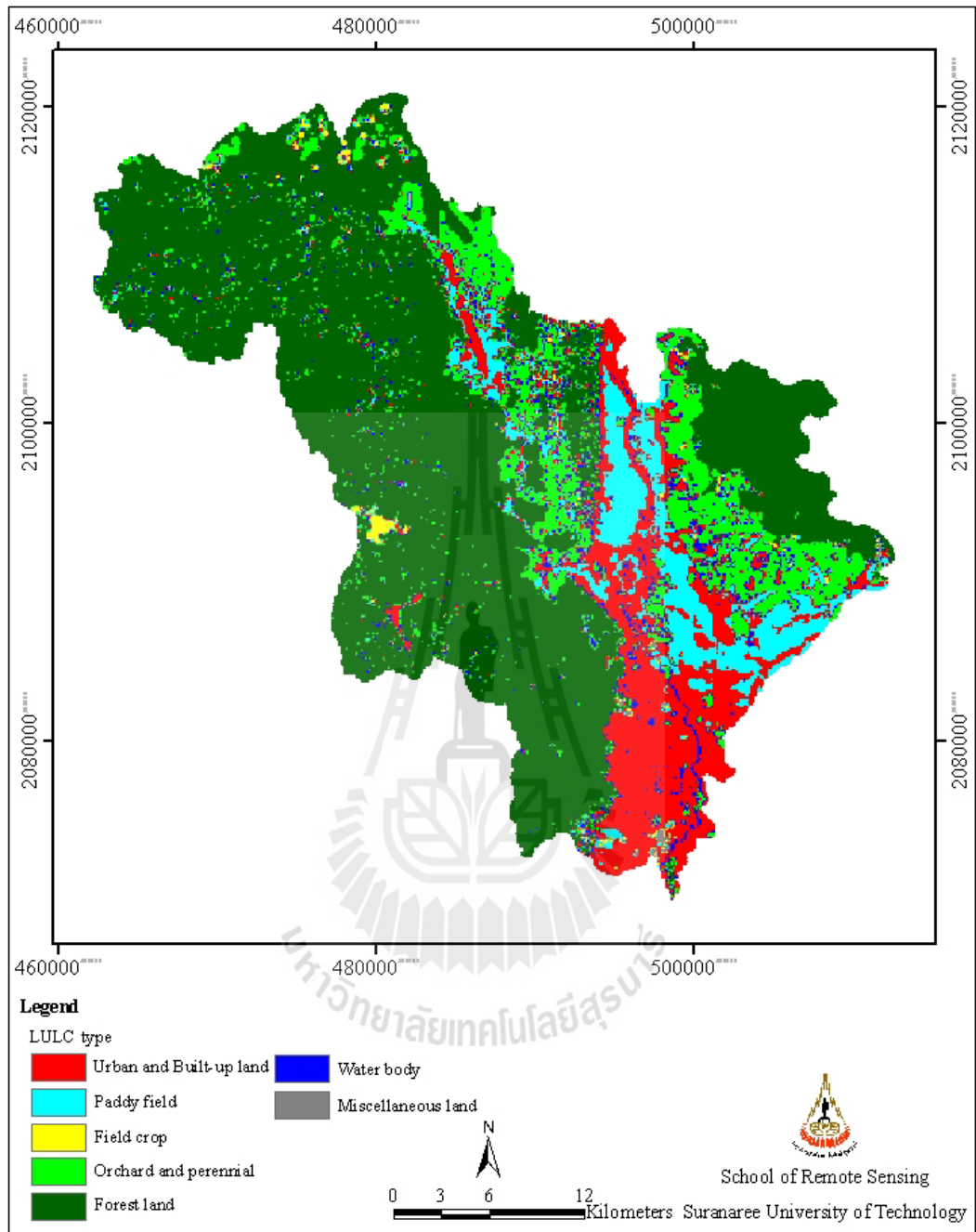


Figure 4.3 Predicted LULC maps in 2020 by the CA-Markov model.

Table 4.7 Error matrix of the predicted 2010 LULC map (Figure 4.2).

	LULC class	LULC 2010 (Classified data)							Total (pixel)	Accuracy	
		MIS	CROP	PAD	U/B	WAT	ORC	FOR		EC	UA
LULC 2010 (Predicted data)	MIS	4,972	-	170	700	2	-	-	5,844	14.92	85.08
	CROP	36	23,953	-	23	-	34	4,379	28,425	15.73	84.27
	PAD	60	1	111,076	710	19	556	1	112,423	1.20	98.80
	U/B	1,223	217	2,477	169,820	53	1,735	36	175,561	3.27	96.73
	WAT	16	-	1	11	8,633	-	268	8,957	3.32	96.68
	ORC	97	499	19	238	6	140,475	11,130	152,464	7.86	92.14
	FOR	132	650	151	727	20	3,561	756,774	762,015	0.69	99.31
Total (pixel)		6,536	25,320	113,894	172,229	8,733	146,361	772,588	1,245,661	-	-
Accuracy	EO	23.93	5.40	2.47	1.40	1.15	4.02	2.05	-	-	-
	PA	76.07	94.60	97.53	98.60	98.85	95.98	97.95	-	-	-

Note: 1. Overall accuracy = 97.60% ; Kappa coefficient = 0.96
2. See Table 4.1 for full name of each referred class.

4.2 Development of grid-based hydrologic model

The first objective of this study is to develop grid-based hydrologic model that is capable of simulating realistic runoff scenarios (on monthly and daily basis) using GIS-based input data. This development was carried out based on the water balance equation as described in Section 3.3 (Eq. 3.3). This relation was executed over every defined grid of the study area (treated as being single bucket with 30x30 m² covering area) at every time step of interest (e.g. 1 day or 1 month). The generated surface and sub-surface runoff from each defined grid will move downward due to gravity force in a specific direction (depended on topographic properties like slope and aspect) into the neighboring grid (Figure 4.4). The surplus amount of water is then accumulated downward until it reaches the lowland flowing channel, like stream or river, and becomes channel runoff flow. Rate of its flow along the channel can be measured as

the runoff discharge (mostly in unit of m^3/s). Figure 4.5 shows amount of the upward land grids that contribute runoff to a specific location of interest (flow accumulation). This value can range from very low (e.g. < 10 grids) to very high (e.g. $> 10^6$ grids), the lower in location indicates the higher in amount of the contributing grids upward.



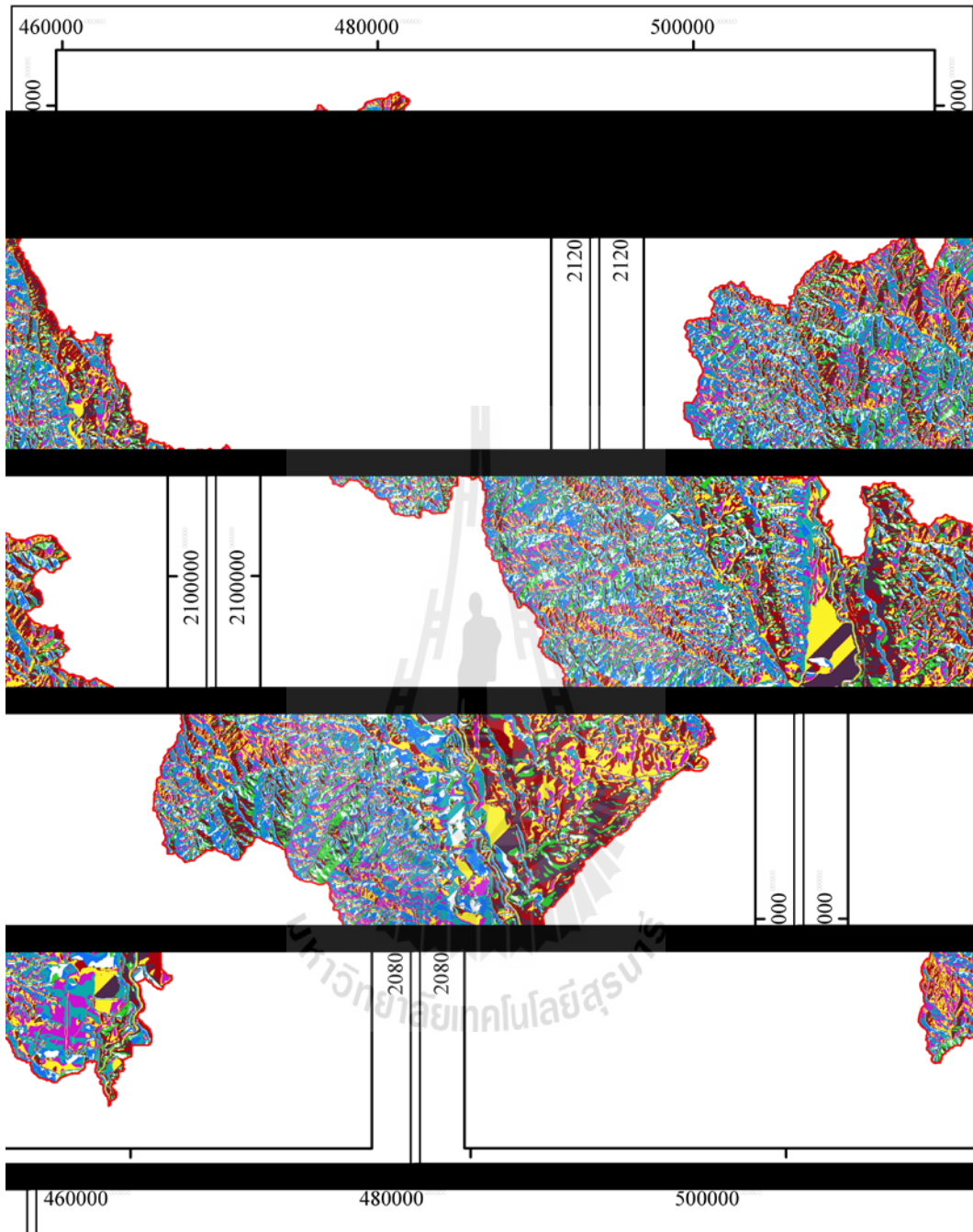


Figure 4.4 Pattern of flow direction in the study area.

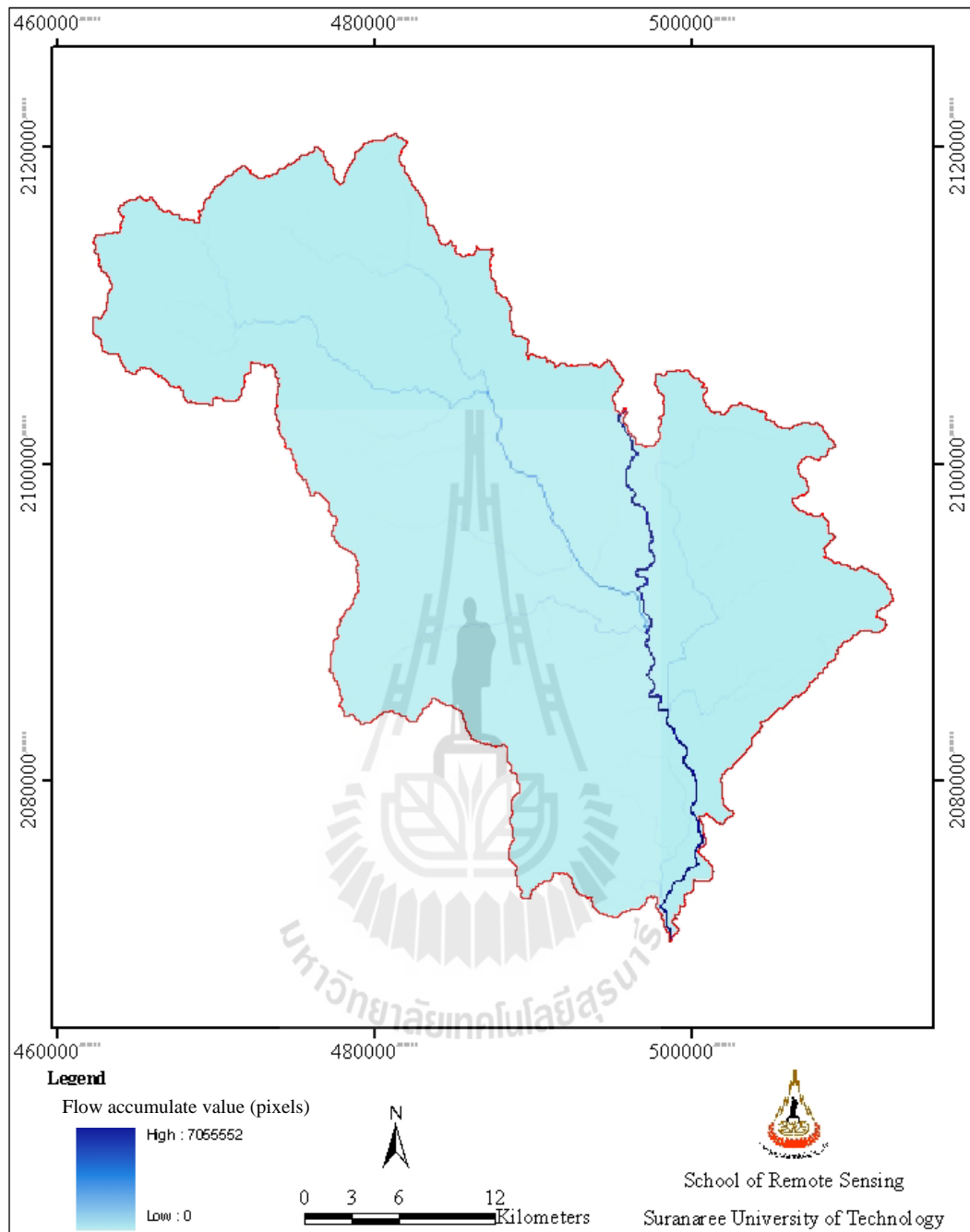


Figure 4.5 Flow accumulation map showing amount of the upward land grids that contribute runoff water to a specific grid of interest in the study area.

4.2.1 Monthly model formulation

The model's developing process of interest here was divided into 2 types: the monthly model and the daily model. The first type tries to realistically predict the stream discharge on the monthly basis (month by month) and the second type tries to achieve this task on the daily basis. Working on different time scale suggests that their needed parameters in the preferred water balance model (Eq. 4.1) might be different also. In the working process, the monthly model is formulated first under several assumptions, or criteria, on the parameters in use. The accepted monthly model is then used as a prototype for the development of the preferred daily model later on. The developments of both models (monthly and daily) are based on the knowledge of precipitation (pattern and intensity) and all other model's parameters in 2005, e.g. soil, LULC and ET. For daily model, daily data in September 2005 were employed. This year is chosen due to the occurrence of great floods in Chiang Mai city due to the overbank flow of water from the Ping River in August and September (see more details in Section 2.2). As a consequence, it is hoped that the developed models might be satisfactorily used to explain nature of this kind of severe flood in the area based on the simulated discharges along the stream channel.

For the monthly model, five cases of preferred water balance model are considered and tested:

Case 1: Uniform rainfall and constant soil depth (3 m);

Case 2: Non-uniform rainfall and constant soil depth (3 m);

Case 3: Uniform rainfall and non-uniform soil depth;

Case 4: Non-uniform rainfall and soil depth (without sub-surface runoff);

Case 5: Non-uniform rainfall and soil depth (with sub-surface runoff).

At this stage, the preferred water balance equation for all aforementioned scenarios is as follows:

$$\frac{ds(t)}{dt} = p(t) - q_{ss}(t) - q_{se}(t) - e_b(t) \quad (4.1)$$

where meaning of all seen parameters are detailed in Table 3.3. Note that, the sub-surface runoff term (q_{ss}) was included in the analysis of the monthly runoff for case 5 only to gain more realistic results of the predicted discharges. Details and results of the study in each case are as follows.

Case 1: Uniform rainfall and constant soil depth (3 m)

In this case, the simple form of water balance equation, Eq. 4.1, was examined in which the precipitation term (rainfall), $p(t)$, is assumed to be constant all over the area (being represented by data measured at the Maejo University station), as well as the evaporation term (e_b), and the effective soil depth was fixed at 3 m (a trial data). The used water balance equation in this case is as follows:

$$\frac{ds(t)}{dt} = p(t) - q_{se}(t) - e_b(t) \quad (4.2)$$

Results of the study are presented in Figure 4.6.

It is found that results of the simulated runoff discharges at the P1 and P21 stations are very similar in which they are often underestimated by the model except in August and September when the simulated data are very overestimated (especially in September that are strongly overestimation). It should be noticed that the simulated discharges at both stations are extremely low in most months except September and October (the strong monsoon months) that this value increases dramatically. This is because, without sub-surface runoff in the model, the simulated runoff will occur only when the soil is fully saturated. This requirement is often met during the strong monsoon months only (September and October here) which results in the sharp increase and rapid decline in the modeled runoff data during this period while during dry months the modeled runoff data is extremely low by the same reason as seen in Figures 4.6-4.9. Though the found R^2 is rather satisfies at both stations (P1: $R^2 = 0.74$, P21: $R^2 = 0.66$) but the Nash-Sutcliffe efficiency index (E) is still rather unacceptable (P1: $E = -0.12$, P21: $E = -0.49$). These results indicate that further improvement of Eq. 4.2 is needed to gain more realistic runoff output from the model.

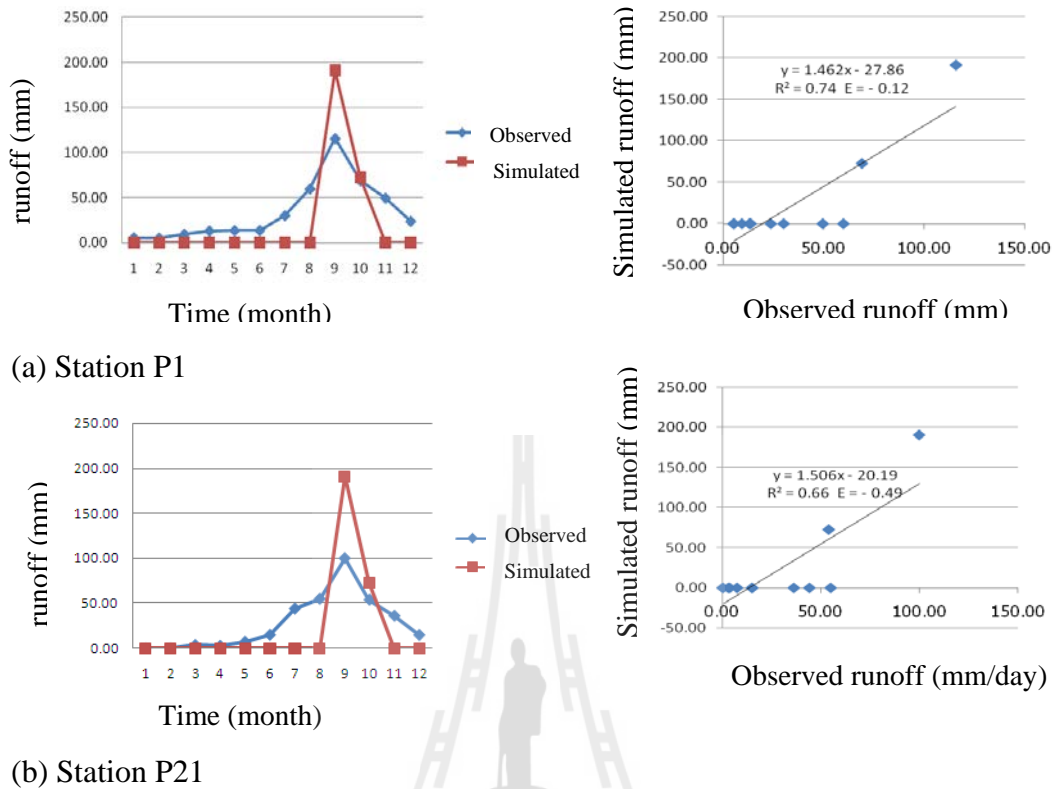


Figure 4.6 Comparison of monthly runoff data in 2005 (simulated and observed) at (a) station P1 ($A = 6,213 \text{ km}^2$) and (b) P21 ($A = 510 \text{ km}^2$) for Case 1 (uniform rainfall and constant soil depth at 3m).

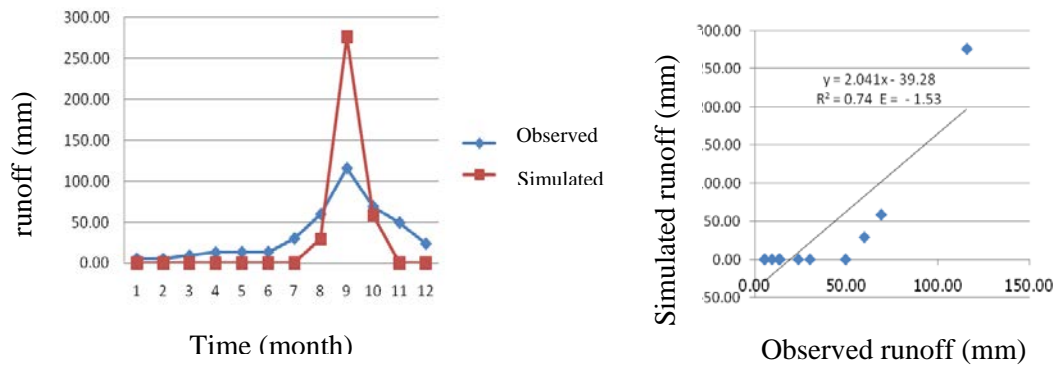
Case 2: Non-uniform rainfall and constant soil depth (3 m)

In this case, the simple form of water balance equation, Eq. 4.2, is applied to each grid with non-uniform rainfall, in which the spatial pattern of the rainfall term, $p(t)$, was interpolated from the observed values of 15 weather stations situating within the study area (Figure 3.5) but the effective soil depth is still used the averaged depth of 3 m. Results of the study are presented in Figure 4.7.

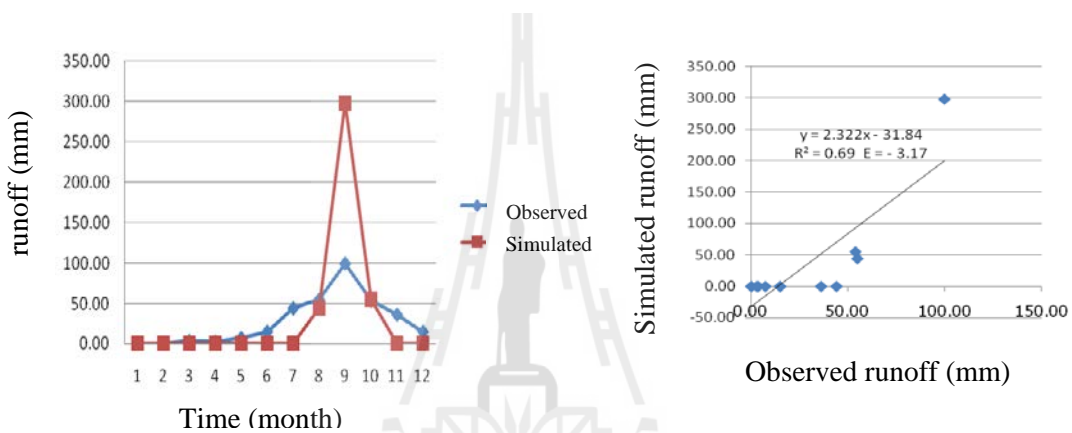
It is found that results of the simulated runoff discharges at the P1 and P21 stations are still very similar in which they are underestimated in most months except in September when the modeled value is highly overestimated. However,

graphs of the simulated data for both stations now look more resemble to the observed one as August does pick up a noticeable value of discharge (not extremely low as in Case 1). This might be due to the use of more realistic rainfall data in the processing which gives higher variation of rainfall to the headwater forest area that subsequently result in higher temporal variability of the discharge in the strong monsoon months of August, September and October. Note that peak value of the discharge in September increases greatly from 191.22 mm in Case 1 to be 276.13 mm in Case 2 (P1 station) and from 190.14 mm in Case 1 to be 298.09 mm in Case 2 (P21 station) (Table 4.7a).

Similar to Case 1, most months (apart from August, November and October) still have extremely low discharges which is rather unrealistic as there should be some runoff seen during these months as suggesting by the observed data at both stations. Also, though the R^2 is rather satisfies for both stations (P1: $R^2 = 0.74$, P21: $R^2 = 0.69$) but the Nash-Sutcliffe efficiency index (E) is still highly unacceptable regarding to the preferred standard of $E > 0$ (P1: $E = -1.53$, P21: $E = -3.17$).



(a) Station P1



(b) Station P21

Figure 4.7 Comparison of monthly runoff data in 2005 (simulated and observed) at (a) station P1 and (b) P21 for Case 2 (non-uniform rainfall and constant soil depth)

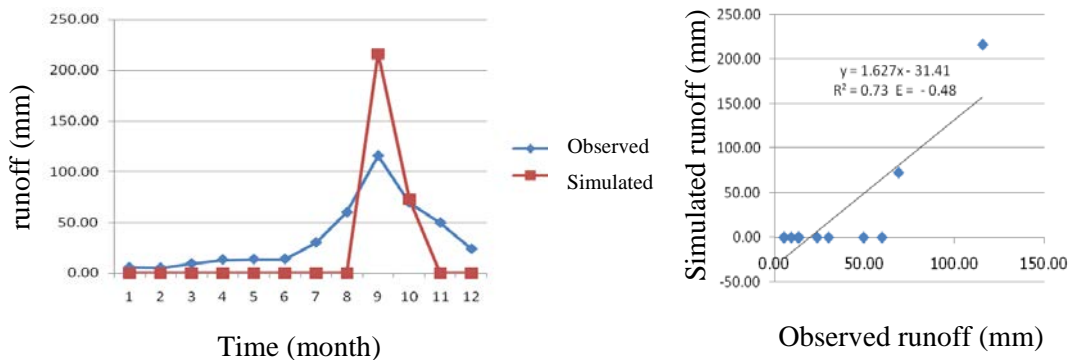
Case 3: Uniform rainfall and non-uniform soil depth

In this case, the rainfall intensity is assumed to be uniform (like in Case 1) but the effective soil depth can vary grid-by-grid (in range of 0.2-10 m). It is found that, in this case, values of the simulated discharges are mostly identical to the Case 1 (Table 4.7 and Figure 4.8), except in September that peak discharge value rises from 191.22 mm in Case 1 to be 216.42 mm in Case 3 (at the P1 station) and from 190.14 mm in Case 1 to be 216.36 mm in Case 3 (at the P21 station). These results indicate

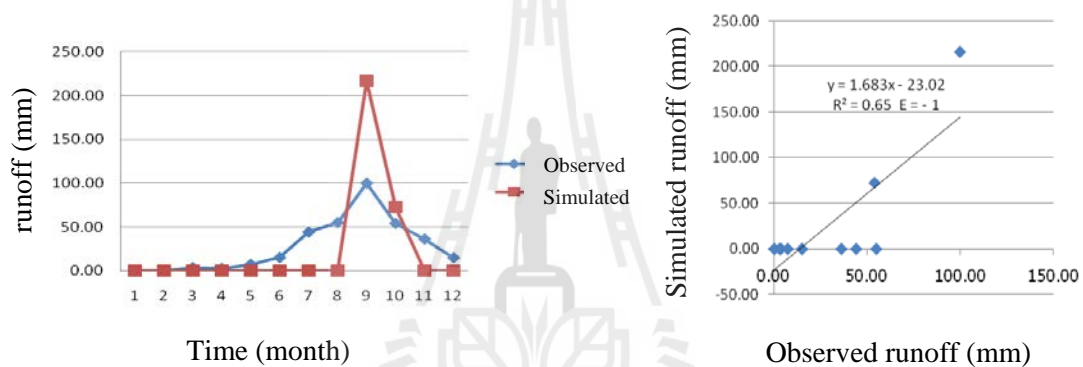
that the variation of soil depth does not affect the discharge outcome from the model much, especially if compared to effect of the variation in rainfall distributing pattern seen in Case 2. However, this variation of soil depth still provides some noticeable change in the peak value of discharge in September but it has no observed impact on the simulated values of other months. This means, to reduce the process of data collection and interpolation, the fixed soil depth value of 3m should be sufficient for the use in the developed model here without much error to be concerned of.

Case 4: Non-uniform rainfall and soil depth (without sub-surface runoff)

In this case, both rainfall and effective soil depth map are interpolated from point data acquired from the responsible agencies (Figures 3.8 and 3.5). It was found that the obtained results in this case are very similar to those of Case 2 at both stations (Table 4.7 and Figure 4.9). This fact emphasizes the conclusion stated in Case 3 that varying soil depth does not affect outcome of the simulated discharge by the model much (when compared to case of constant soil depth at 3 m). This makes the modeled discharge data (at both stations) being controlled mostly by the rainfall distributing pattern of the study area. However, the gained results at this stage are still not realistic much with values of R^2 and E values similar to those of Case 2 (Table 4.8).

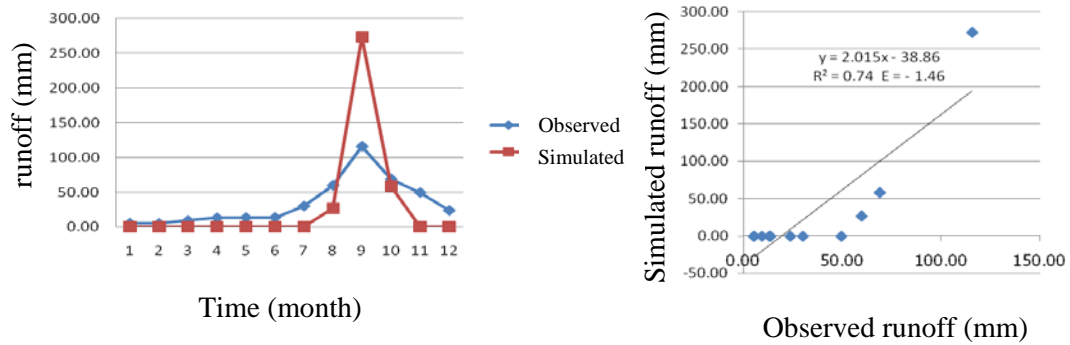


(a) Station P1

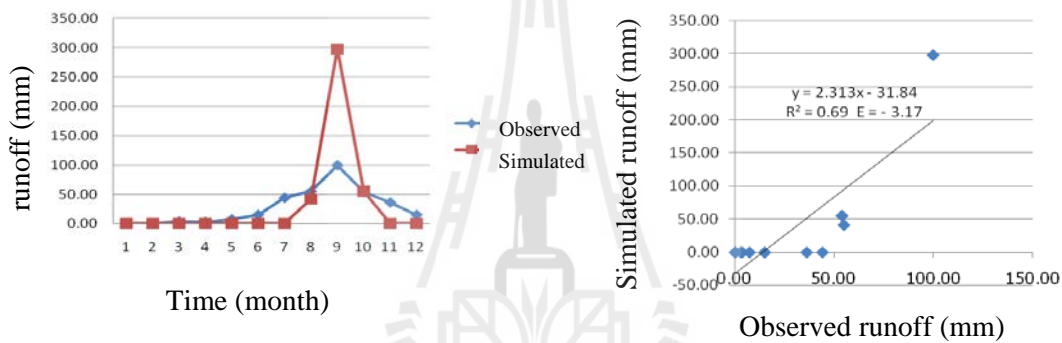


(b) Station P21

Figure 4.8 Comparison of monthly runoff data in 2005 (simulated and observed) at (a) station P1 and (b) P21 for Case 3 (uniform rainfall and non-uniform (b) soil depth).



(a) Station P1



(b) Station P21

Figure 4.9 Comparison of monthly runoff data in 2005 (simulated and observed) at (a) station P1 and (b) P21 for Case 4 [non-uniform rainfall and soil depth (b) (without sub-surface runoff)].

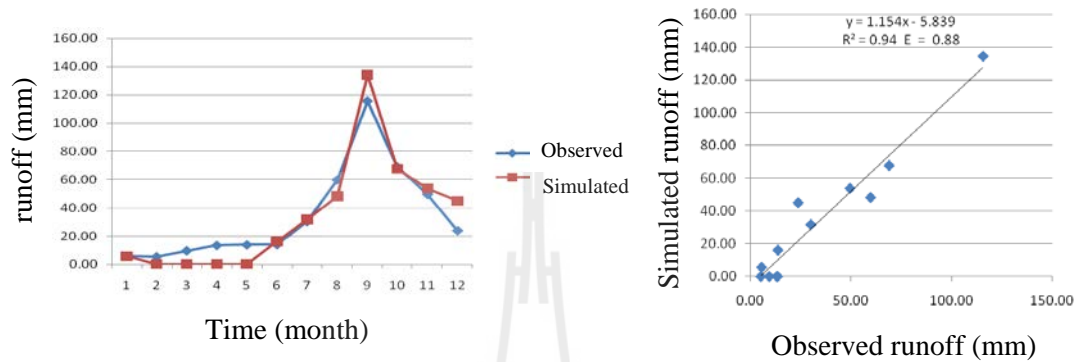
Case 5: Non-uniform rainfall and soil depth (with sub-surface runoff)

This case is similar to the analysis in Case 4, but the sub-surface runoff term (q_{ss}) was now included in the study also as seen in Eq. 4.1. This modification seems to be very critical in the simulation of realistic discharge data by the developed model as illustrated in Table 4.8 and Figure 4.7. This is obviously evidenced from the improved value of R^2 and Nash-Sutcliffe efficiency (E). As seen in Table 4.8, for P1

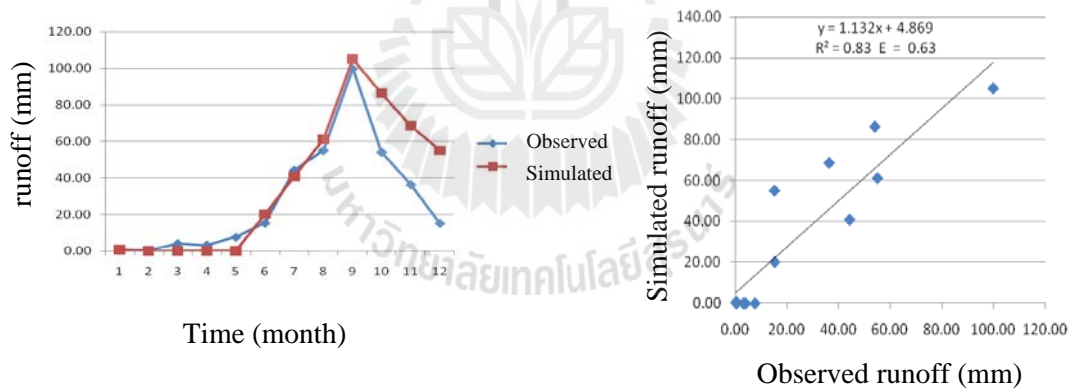
station, the R^2 is increased from 0.74 (Case 4) to 0.94 (Case5) and E is risen from -1.46 (Case 4) to 0.88 (Case 5). And, for P21 station, the R^2 is increased from 0.69 (Case 4) to 0.83 (Case5) and E is risen from -3.17 (Case 4) to 0.63 (Case 5). No obvious deviation is noticed in data of P1 station but the obvious error was seen at P21 station in October, November and December where its modeled data are notably overestimated when compared to the observed data at the same period. This might affect effective use of the modeled data on these months (from this station) in the relevant applications, e.g. the flooding analysis or water resource management.

In conclusion, it is found that the derived monthly model achieved at this stage can predict the amount of discharged runoff at both the stations P1 and P21 relatively well throughout the year 2005 (especially during monsoon season: June-September) in term of R^2 and Nash-Sutcliffe efficiency (E) values. This might be because, with the inclusion of the sub-surface runoff, the simulated runoff can occur even though the soil is still not fully saturated. This shall result in the more gradual increase and recede of the modeled runoff data during the monsoon season. However, the underestimations of the observed discharges at both stations during dry season (February-May) and the strong overestimations during October-December at the P21 station indicate the still are still needed to be examined more in details in the future (e.g. the inclusion of the transpiration rate in the model).

Table 4.7 presents the observed and simulated monthly discharge data at both stations (P1 and P21) while Table 4.8 gives values of R^2 and Nash-Sutcliffe efficiency (E) for each case study at each station.



(a) Station P1



(b) Station P21

Figure 4.10 Comparison of monthly runoff data in 2005 (simulated and observed) at (a) stations P1 and (b) P21 for Case 5 [non-uniform rainfall and soil depth (with sub-surface runoff)].

Table 4.8a Observed (OBS) and simulated (SIM) monthly runoff data at station P1 for all study cases (in unit of mm).

Station P1	Case 1		Case 2		Case 3		Case 4		Case 5	
	SIM	OBS								
JAN	0.00	5.67	0.00	5.67	0.00	5.67	0.00	5.67	5.62	5.67
FEB	0.00	5.32	0.00	5.32	0.00	5.32	0.00	5.32	0.00	5.32
MAR	0.00	9.50	0.00	9.50	0.00	9.50	0.00	9.50	0.00	9.50
APR	0.00	13.22	0.00	13.22	0.00	13.22	0.00	13.22	0.00	13.22
MAY	0.00	13.62	0.00	13.62	0.00	13.62	0.00	13.62	0.03	13.62
JUN	0.00	13.79	0.00	13.79	0.00	13.79	0.00	13.79	16.07	13.79
JUL	0.00	30.17	0.00	30.17	0.00	30.17	0.00	30.17	31.67	30.17
AUG	0.00	59.83	29.18	59.83	0.00	59.83	27.03	59.83	48.16	59.83
SEP	191.22	115.67	276.13	115.67	216.42	115.67	272.95	115.67	134.33	115.67
OCT	72.71	69.02	58.69	69.02	72.71	69.02	58.54	69.02	67.67	69.02
NOV	0.00	49.57	0.00	49.57	0.00	49.57	0.00	49.57	53.76	49.57
DEC	0.00	23.85	0.00	23.85	0.00	23.85	0.00	23.85	44.97	23.85

Table 4.8b Observed (OBS) and simulated (SIM) monthly runoff data at station P21 for all study cases (in unit of mm).

Station P21	Case 1		Case 2		Case 3		Case 4		Case 5	
	SIM	OBS								
JAN	0.00	0.40	0.00	0.40	0.00	0.40	0.00	0.40	0.70	0.40
FEB	0.00	0.46	0.00	0.46	0.00	0.46	0.00	0.46	0.00	0.46
MAR	0.00	4.00	0.00	4.00	0.00	4.00	0.00	4.00	0.00	4.00
APR	0.00	3.19	0.00	3.19	0.00	3.19	0.00	3.19	0.00	3.19
MAY	0.00	7.60	0.00	7.60	0.00	7.60	0.00	7.60	0.02	7.60
JUN	0.00	15.30	0.00	15.30	0.00	15.30	0.00	15.30	20.24	15.30
JUL	0.00	44.29	0.00	44.29	0.00	44.29	0.00	44.29	40.92	44.29
AUG	0.00	55.05	44.36	55.05	0.00	55.05	41.37	55.05	61.24	55.05
SEP	190.84	99.87	298.09	99.87	216.36	99.87	297.88	99.87	105.15	99.87
OCT	72.71	54.07	55.22	54.07	72.71	54.07	55.22	54.07	86.45	54.07
NOV	0.00	36.35	0.00	36.35	0.00	36.35	0.00	36.35	68.70	36.35
DEC	0.00	15.19	0.00	15.19	0.00	15.19	0.00	15.19	55.11	15.19

Table 4.9 Correlation factor (R^2) and Nash-Sutcliffe efficiency (E) for the observed and simulated runoff data from all cases (monthly/daily).

Station P1 (monthly)	Expressed relationship	Accuracy		Station P21 (monthly)	Expressed relationship	Accuracy	
		R^2	E			R^2	E
Case 1	$Y = 1.462(x) - 27.86$	0.74	- 0.12	Case 1	$Y = 1.506(x) - 20.19$	0.66	- 0.49
Case 2	$Y = 2.041(x) - 39.28$	0.74	- 1.53	Case 2	$Y = 2.322(x) - 31.84$	0.69	- 3.17
Case 3	$Y = 1.627(x) - 31.41$	0.73	- 0.48	Case 3	$Y = 1.683(x) - 23.02$	0.65	- 1.00
Case 4	$Y = 2.015(x) - 38.86$	0.74	- 1.46	Case 4	$Y = 2.313(x) - 31.84$	0.69	- 3.17
Case 5	$Y = 1.154(x) - 5.839$	0.94	0.88	Case 5	$Y = 1.132(x) + 4.869$	0.83	0.63

Station P1 (daily)	Expressed relationship	Accuracy		Station P21 (daily)	Expressed relationship	Accuracy	
		R^2	E			R^2	E
Case 1	$Y = 1.262(x) - 0.427$	0.63	- 0.06	Case 1	$Y = 1.116(x) + 1.916$	0.45	- 1.64
Case 2	$Y = 1.050(x) - 0.065$	0.96	0.94	Case 2	$Y = -0.058(x)^2 + 1.658(x) - 1.162$	0.71	0.47

Note: $Y \equiv$ simulated runoff , $x \equiv$ observed runoff

4.2.2 Daily model formulation

In this part, the daily discharge simulation model is described in details. This model is modified from the developed Case 5 of the monthly model described earlier and using only daily rainfall data in September 2005 as an input precipitation term. There are two cases of interest here, which are:

Case 1: Non-uniform rainfall/soil depth (without transpiration rate);

Case 2: Non-uniform rainfall/soil depth (with transpiration rate).

The proposed water balance equation in use for these two scenarios is followed from Eq. 3.3 directly except that the first case (Case 1) does not take into account effect of the transpiration term (e_v) in the analysis.

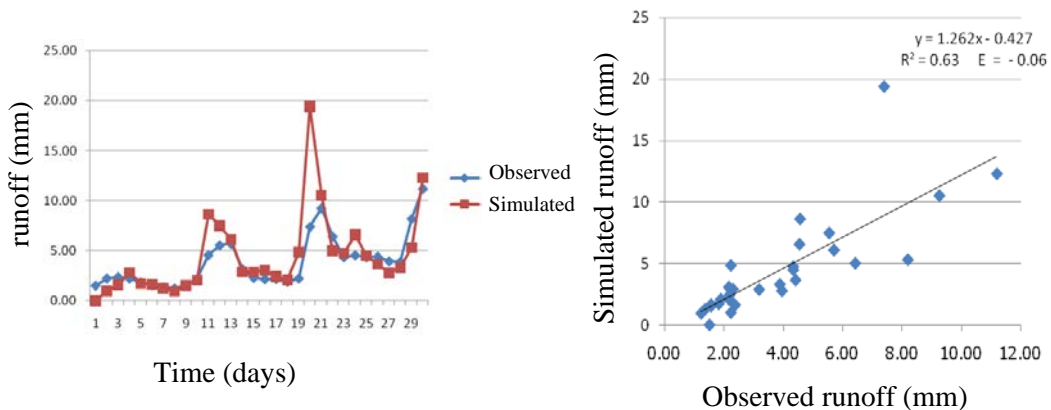
Case 1: Non-uniform rainfall/soil depth (without transpiration rate)

The exclusion of the transpiration term (e_v) in the model's analysis indicates that the R^2 is still acceptable for the P1 station but it fails to meet the acceptable level of 0.5 at the P21 station (P1: $R^2 = 0.63$, P21: $R^2 = 0.45$) (Table 4.8). The Nash-Sutcliffe efficiency (E) is also considered unacceptable at both stations ($E < 0$). This means the model in this case must be further improved to attain the accepting level of $E > 0$. Similar to the monthly model, the model's prediction at P21 has lower rate of accuracy than those at P1 station, and it produced strong overestimated data at the later dates of the month (from the 21st date onward) (Table 4.9 and Figure 4.11).

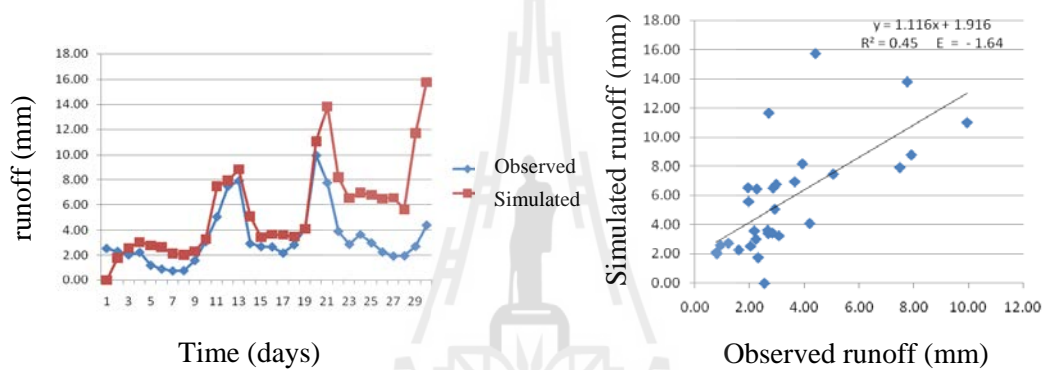
There are three apparent peaks of the discharge data (for both observed and modeled data), one is around 11th-13th September and the other two are around 20th -21st and 30th September. As a consequence, these dates are most prone to the flooding occurrence. However, as the model tends to overestimate the peak discharge data, the flood risk probability should be overestimated also.

Table 4.10 Observed (OBS) and simulated (SIM) daily runoff data at station P1 and P21 for Case 1 and Case 2 (in unit of mm).

Station P1 (September)	Case 1		Case 2		Station P21 (September)	Case 1		Case 2	
	SIM	OBS	SIM	OBS		SIM	OBS	SIM	OBS
1	0.00	1.51	1.35	1.51	1	0.00	2.54	0.00	2.54
2	1.00	2.23	2.11	2.23	2	1.76	2.31	0.61	2.31
3	1.62	2.37	2.06	2.37	3	2.54	2.03	0.99	2.03
4	2.83	2.23	1.96	2.23	4	3.02	2.23	1.57	2.23
5	1.72	1.82	1.64	1.82	5	2.74	1.22	1.00	1.22
6	1.65	1.56	1.44	1.56	6	2.60	0.93	0.91	0.93
7	1.25	1.35	1.24	1.35	7	2.10	0.78	0.46	0.78
8	0.95	1.23	1.21	1.23	8	2.02	0.80	0.15	0.80
9	1.54	1.56	1.4	1.56	9	2.28	1.60	0.66	1.60
10	2.05	2.18	1.92	2.18	10	3.25	3.07	1.55	3.07
11	8.64	4.56	4.42	4.56	11	7.48	5.06	4.63	5.06
12	7.49	5.54	5.38	5.54	12	7.93	7.50	5.27	7.50
13	6.10	5.70	4.78	5.70	13	8.79	7.92	5.56	7.92
14	2.88	3.18	3.00	3.18	14	5.07	2.92	3.53	2.92
15	2.90	2.30	2.35	2.30	15	3.41	2.68	2.97	2.68
16	3.08	2.16	2.43	2.16	16	3.63	2.66	2.98	2.66
17	2.42	2.18	2.33	2.18	17	3.59	2.17	1.93	2.17
18	2.09	1.89	2.04	1.89	18	3.45	2.83	1.55	2.83
19	4.85	2.23	2.69	2.23	19	4.10	4.20	3.51	4.20
20	19.42	7.39	8.30	7.39	20	11.01	9.96	10.98	9.96
21	10.54	9.25	9.33	9.25	21	13.80	7.77	10.55	7.77
22	5.02	6.42	6.56	6.42	22	8.18	3.93	6.73	3.93
23	4.75	4.33	4.87	4.33	23	6.53	2.86	5.7	2.86
24	6.58	4.54	5.16	4.54	24	6.96	3.65	6.32	3.65
25	4.49	4.33	4.99	4.33	25	6.78	2.97	4.03	2.97
26	3.66	4.41	5.1	4.41	26	6.46	2.26	2.78	2.26
27	2.78	3.95	4.2	3.95	27	6.55	1.94	1.56	1.94
28	3.30	3.88	5.3	3.88	28	5.59	1.96	1.96	1.96
29	5.32	8.19	10.43	8.19	29	11.66	2.70	4.62	2.70
30	12.31	11.19	10.8	11.19	30	15.74	4.41	7.91	4.41

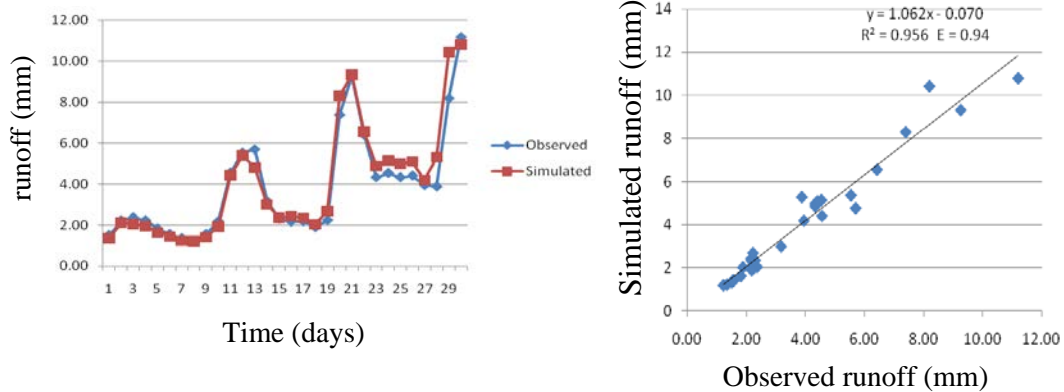


(a) Station P1

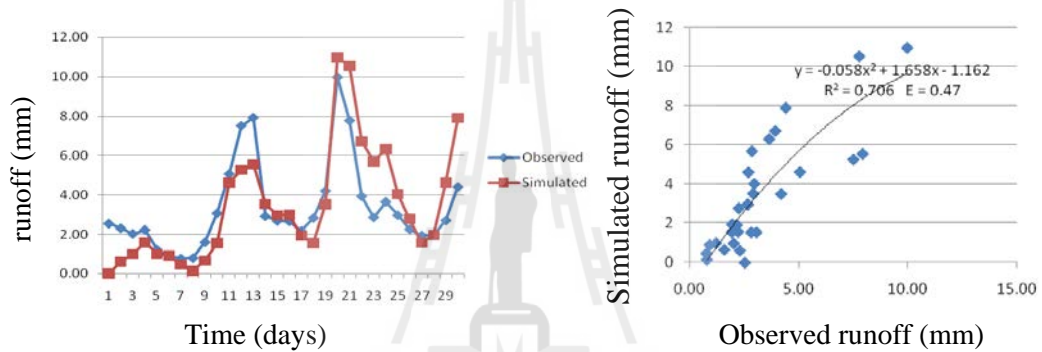


(b) Station P21

Figure 4.11 Comparison of daily runoff data in September 2005 at station (a) P1 and (b) P21 for Case 1 [Non-uniform rainfall and soil depth (without transpiration rate)].



(a) Station P1



(b) Station P21

Figure 4.12 Comparison of daily runoff data in September 2005 at station (a) P1 and (b) P21 for Case 2 [non-uniform rainfall and soil depth (with transpiration rate)].

Case 2: Non-uniform rainfall/soil depth (with transpiration rate)

If the transpiration term (e_v) is included in the model's analysis, it is found that both R^2 and E values are improved significantly from Case 1 (Table 4.2, Figure 4.9). For P1 station, values of R^2 and E are now 0.96 and 0.94 respectively (rising from 0.63 and -0.06 in Case 1) and for P21 station, values of R^2 and E are now 0.71 and 0.47 respectively (rising from 0.45 and -1.64 in Case 1). And similar to case 1, the model's prediction at P21 has lower rate of accuracy than those at P1 station, and it still produces some strong overestimated data at the latter dates of the month.

From the results obtained in Case 1 and Case 2, it can be concluded that the transpiration term (e_v) is very crucial in the building of highly effective daily model as it can greatly reduce the differences between the observed and modeled discharge data at both stations (especially at P1 station). The high values of R^2 and E found for the model indicates its high predictive power for stream discharge in the study area despite several assumptions of input parameters are applied.

And, similar to monthly model in Case 5, as the model in this case can predict the monthly discharge data in most months quite well in general (especially in August and September which are most prone to flooding incidence), this makes it valuable for the use in the assessment about impact of some concerning scenarios, e.g. forest loss and increased rainfall intensity on flooding severity in the study area as detailed in Section 4.4. It should be noted that the notable deficiency of the model's prediction at P21 station might not affect the flooding forecast in the Chiang Mai city much as the model can still work relatively well at the P1 station. And, as the total catchment area of the P21 station is relatively small compared to that of the P1 station (Table 3.4), its contribution to the observed discharges at P1 station should be relatively small also. This makes errors in the modeled runoff at the P21 station be not very crucial to the determination of observed values at P 1 station, and as a result, the subsequent flood analysis for the Chiang Mai city area as a whole.

4.2.3 Model comparison

To learn about improved efficiency of the developed grid-based model from the original one that it is based upon, best results achieved by this newly-built model are compared to those from the original lumped models described in Jothityangkoon and Sivapalan (2003) and Jothityangkoon et al. (2001; 2006) under

the same scenario (monthly/daily basis) and the compared results are given in Table 4.10.

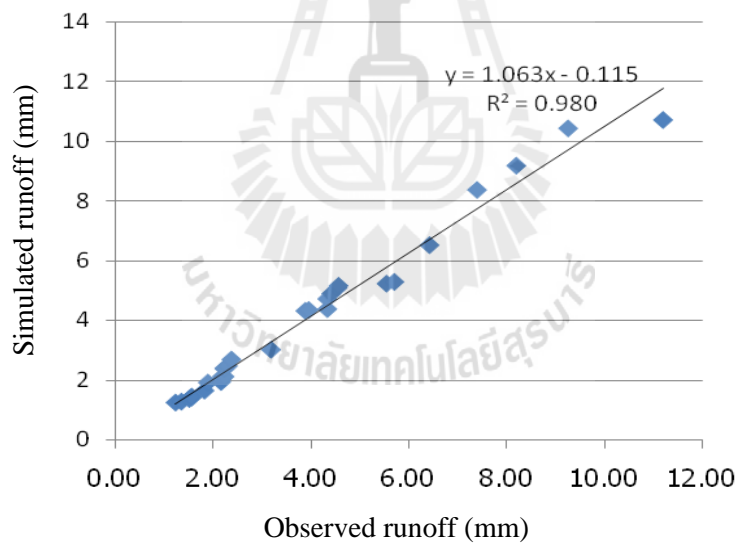
Note that, as the original model has generated only flow duration curve at the P1 station, therefore, the comparison is carried out based on this referred parameter only. Figure 4.10 illustrates the strong correlation ($R^2 = 0.98$) between the observed and modeled flow discharge data in the duration curve at P1 station for the present work. The comparison is done at P1 station only as the original model did not perform at P21 station, therefore, no data existed to be compared with the new model.

In conclusion, it is found that both models perform comparably well in terms of both R^2 and E values (on monthly and daily basis) but the newly-developed model is superior as it can capture the spatial pattern of used water balance models (monthly and daily) in finer scales based on its GIS-based platform and the model's structure in use. Moreover the new model is thoroughly GIS-based in nature for the input data and most operating algorithms inside. Therefore, it is capable of supporting the change in input data that have GIS-based structure, like the LULC, soil map, stream network, and rainfall map. This advantage is still not found in the original model that was used. However, the original lumped model is superior in its more simple structure which results in less time consuming for the construction and processing of the runoff simulation.

Table 4.11 Model comparison of the simulated runoff results.

Station P1	Monthly averaged		Flow duration curve		Hydrograph monthly		Hydrograph daily	
	R ²	E	R ²	E	R ²	E	R ²	E
Original model	0.95	0.92	0.99	0.99	*no	*no	*no	*no
Developed model	0.96	0.91	0.98	0.97	0.94	0.88	0.96	0.95
Station P21	Monthly averaged		Flow duration curve		Hydrograph monthly		Hydrograph daily	
	R ²	E	R ²	E	R ²	E	R ²	E
Original model	*no	*no	*no	*no	*no	*no	*no	*no
Developed model	0.92	0.75	0.91	0.85	0.83	0.63	0.71	0.47

Note: *no ≡ no available data for the comparison.

**Figure 4.13** Comparison of the daily flow duration curve (observed and simulated) at the P1 station (for the present work).

4.3 Construction of the flood maps

This part focuses on the derivation of flood maps associated to the simulated discharge along the main river network (especially Ping River and Mae Rim River) during September 2005. The predicted flood map of the Chiang Mai municipality is then compared with the reference flood map (of the same event) prepared by the Faculty of Engineering, Chiang Mai University (Figure 2.4) to assess the reliability of the method and resulted map in use.

As described in Section 3.4, the assumed flooding scenario in this work is the river flood, therefore, the occurrence of flood will be recognized if the overbank flow of stream discharge from the rivers appears (when water level exceeds bank level on either side). To generate the preferred flood map, over flown water (from the stream channel) is assumed to spread laterally into the lowland area situating nearby until reaching the high land/place that it cannot flow over. The flooding incidence shall occur (over a specific area) if the water level Z (derived from Eq. 3.12) greater than the local elevation (above MSL) of the considered area. Or, if $Z > DEM$, the area shall be labeled as being flooded land and the value of $Z-DEM$ becomes the flood depth. As a result, the flood depth maps can be produced based on knowledge of the water level at each location along the associated stream network and local elevation of considered area from DEM (in each sub-region seen in Figure 3.14).

From this stated concept, the daily flood depth maps are derived based on the known water level Z (in meter above MSL) along the main stream network for each day. And, as mentioned in Chapter II, the flood warning in the Chiang Mai city will be issued if Z reaches a critical value of 304.2m at the P1 station (or 3.7 m on the

gauging pole), therefore, only dates with flood incidence in the city area identified (with $Z > 304.2\text{m}$) are presented here as seen in Table 4.11 and Figure 4.14.

Table 4.12a Simulated daily runoff, discharge (Q), and water level (Z) data at station P1 in September 2005 (highlight is for the predicted flood date with $Z > 304.2$ m MSL).

Date	Parameter			Date	Parameter		
	Runoff (mm/d)	Q (m^3/s)	Z (m)		Runoff (mm/d)	Q (m^3/s)	Z (m)
1	1.35	97.23	302.37	16	2.43	174.73	302.74
2	2.11	151.86	302.63	17	2.33	167.44	302.70
3	2.06	147.81	302.61	18	2.04	146.36	302.60
4	1.96	140.55	302.57	19	2.69	193.75	302.82
5	1.64	117.89	302.47	20	8.30	596.90	304.55
6	1.44	103.31	302.40	21	9.33	671.13	304.84
7	1.24	89.46	302.33	22	6.56	471.66	304.05
8	1.21	86.90	302.32	23	4.87	349.85	303.53
9	1.40	100.39	302.38	24	5.16	370.93	303.62
10	1.92	138.22	302.56	25	4.99	358.91	303.57
11	4.42	317.80	303.39	26	5.10	366.53	303.60
12	5.38	386.78	303.69	27	4.20	301.83	303.32
13	4.78	343.77	303.50	28	5.30	381.00	303.66
14	3.00	215.68	302.93	29	10.43	750.02	305.13
15	2.35	168.68	302.71	30	10.80	776.65	305.23

Note: Unit of Q in m^3/s is calculated from Eq. 3.2 based on the drainage area of the associated basin stated above $6,213 \text{ km}^2$.

Table 4.12b Simulated daily runoff, discharge (Q), and water level (Z) data at station P21 in September 2005 (highlight is for the predicted flood date by data at the P1 station).

Date	Parameter			Date	Parameter		
	Runoff (mm/d)	Q (m ³ /s)	Z (m)		Runoff (mm/d)	Q (m ³ /s)	Z (m)
1	0.00	0.00	305.85	16	2.98	17.56	306.02
2	0.61	3.60	305.88	17	1.93	11.36	305.96
3	0.99	5.81	305.91	18	1.55	9.13	305.94
4	1.57	9.26	305.94	19	3.51	20.73	306.05
5	1.00	5.87	305.91	20	10.98	64.78	306.48
6	0.91	5.34	305.90	21	10.55	62.20	306.45
7	0.46	2.68	305.88	22	6.73	39.67	306.24
8	0.15	0.88	305.86	23	5.70	33.64	306.18
9	0.66	3.89	305.89	24	6.32	37.29	306.21
10	1.55	9.13	305.94	25	4.03	23.79	306.08
11	4.63	27.32	306.12	26	2.78	16.39	306.01
12	5.27	31.09	306.15	27	1.56	9.22	305.94
13	5.56	32.77	306.17	28	1.96	11.58	305.96
14	3.53	20.82	306.05	29	4.62	27.27	306.12
15	2.97	17.54	306.02	30	7.91	46.67	306.30

Note: Unit of Q in m³/s is calculated from Eq. 3.2 based on the drainage area of the associated basin stated above 510 km².

From data of water level Z at P1 station shown in Table 4.11a in September 2005, it is found that there should be floods in the Chiang Mai municipal area only on four dates: 20th, 21st, 29th, 30th with Z = 304.55, 304.84, 305.13, and 305.23 m above MSL respectively, while on the other dates no floods should occur (as Z < 304.2). The flooding zone concentrates mostly along the lowland area of the river bank as should be expected. However, only flooding in the municipal area that usually attracts most

attention from the state and the public as it can affect the economy, public services, and daily life of people the most.

Table 4.12c Simulated daily runoff, discharge (Q), water elevation (Z) data at station P67 in September 2005 (highlight is for the predicted flood date by data at the P1 station).

Date	Parameter			Date	Parameter		
	Runoff (mm/d)	Q (m ³ /s)	Z (m)		Runoff (mm/d)	Q (m ³ /s)	Z (m)
1	1.60	96.83	323.93	16	2.54	153.72	324.42
2	2.44	147.67	324.37	17	2.54	153.72	324.42
3	2.33	141.01	324.31	18	2.24	135.57	324.27
4	2.14	129.51	324.22	19	2.76	167.04	324.54
5	1.83	110.75	324.05	20	8.62	521.69	326.86
6	1.60	96.83	323.93	21	9.88	597.94	327.20
7	1.42	85.94	323.83	22	7.02	424.85	326.35
8	1.41	85.33	323.82	23	5.15	311.68	325.64
9	1.57	95.02	323.91	24	5.39	326.21	325.74
10	2.11	127.70	324.20	25	5.45	329.84	325.76
11	4.74	286.87	325.46	26	5.72	346.18	325.87
12	5.78	349.81	325.89	27	4.79	289.89	325.48
13	5.06	306.23	325.60	28	6.00	363.12	325.98
14	3.17	191.85	324.74	29	11.77	712.33	327.59
15	2.44	147.67	324.37	30	11.80	714.14	327.60

Note: Unit of Q in m³/s is calculated from Eq. 3.2 based on the drainage area of the associated basin stated above 5,229 km².

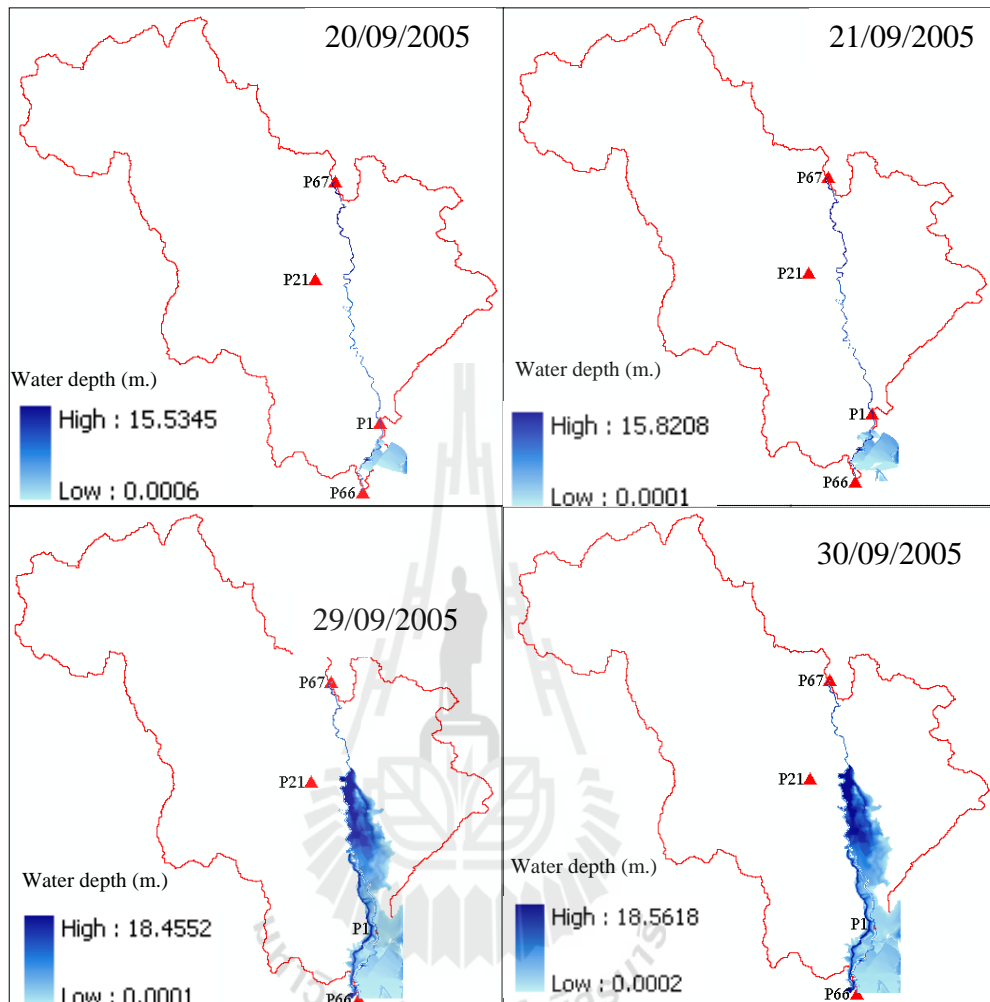


Figure 4.14 Simulated flood depth maps on the 20th, 21st, 29th, 30th September 2005 when the water level (Z) exceeds the critical value of 304.2 m at the P1 station.

Flood map validation

To assess credibility of the generated flood maps, the specifically-generated flood map was compared with the one reported by the Civil Engineering Department of the Chiang Mai University as seen in Figure 2.4 (Chuchoke Aryupong, 2007). This map informs the classified flooded area in the Chiang Mai municipal area at different

level of water level above MSL, or on the gauging pole at the P1 station based on data from the great floods in the past. The comparison is performed at three water levels, 304.20 m, 304.60, 305.10 m on the gauging pole at P1 station and results are reported in Table 4.13 and Figure 4.15.

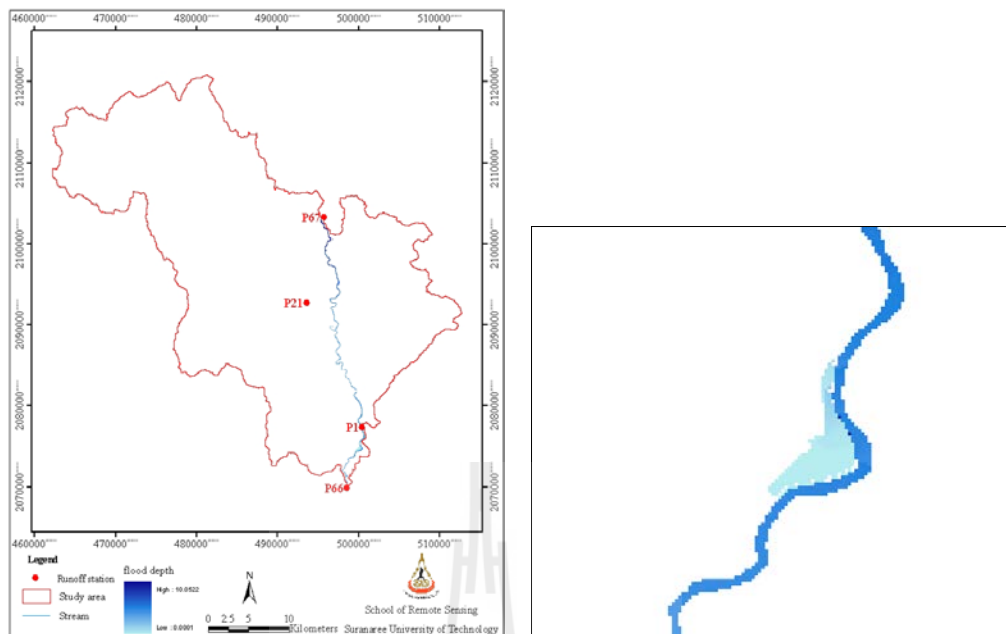
It was found that these two maps have rather moderate correlation in average regarding to the identified flooded area in all three cases (about 58.93% agreement and 41.07% discrepancy). Highest level of the agreement is at water level of 304.2 m (about 87.10% agreement/12.90% discrepancy) and lowest is at water level 304.6 m (about 12.42% agreement/87.58% discrepancy). Main source of the difference should be the scales of DEM being used in each work (20 m contour interval for present work and 2 m for reference work).

Table 4.13 Comparison between the simulated and reference flood areas at different water levels (Z) at the P1 station.

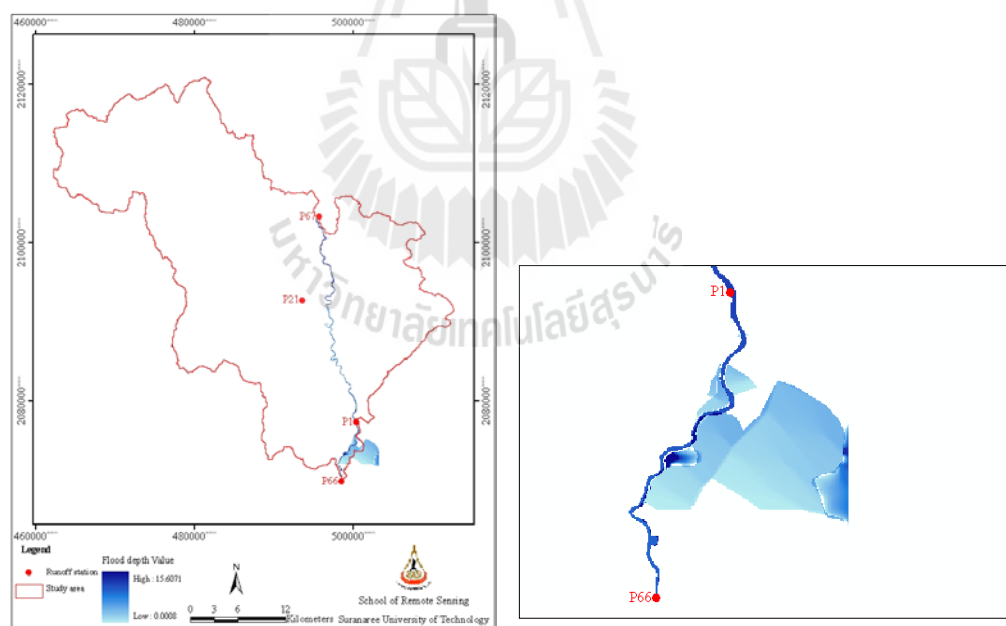
Category	Z = 304.20 m		Z = 304.60 m		Z = 305.10 m		Average (%)
	km ²	%	km ²	%	km ²	%	
Agreement	0.27	87.10	1.03	12.42	22.54	77.28	58.93
Discrepancy1	0.04	12.90	1.73	20.87	1.42	4.86	12.88
Discrepancy 2	0.00	0.00	5.53	66.71	5.21	17.86	28.19
Total	0.31	100.00	8.29	100.00	29.16	100.00	100.00

Note: Discrepancy1 = non-flooded in simulated but flooded in the reference

Discrepancy2 = flooded in simulated but non-flooded in the reference

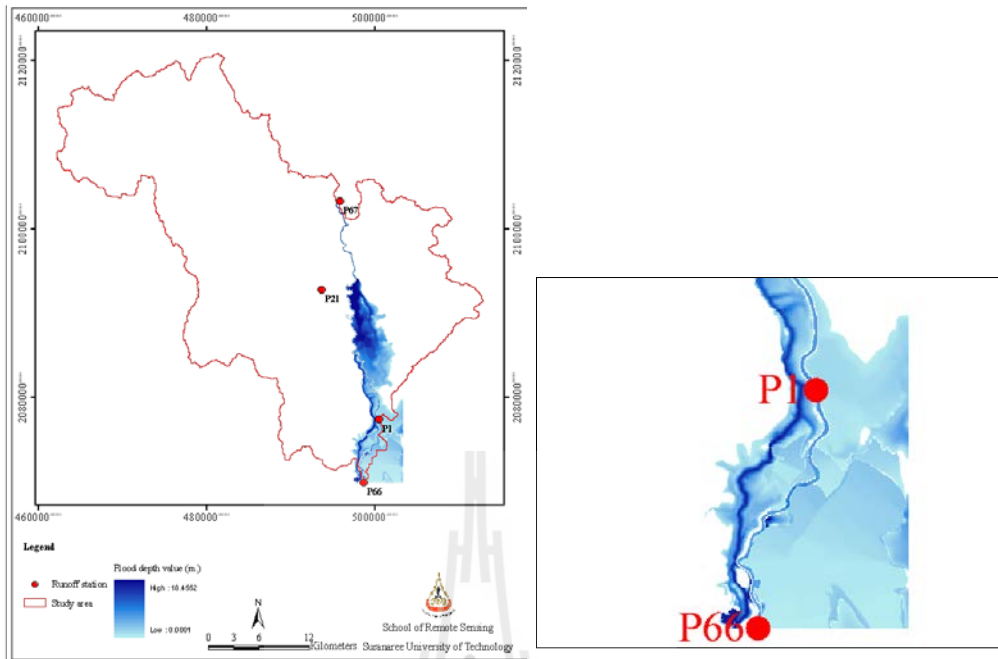


(a) Simulated flood map zone 1 (Z = 304.20 m)

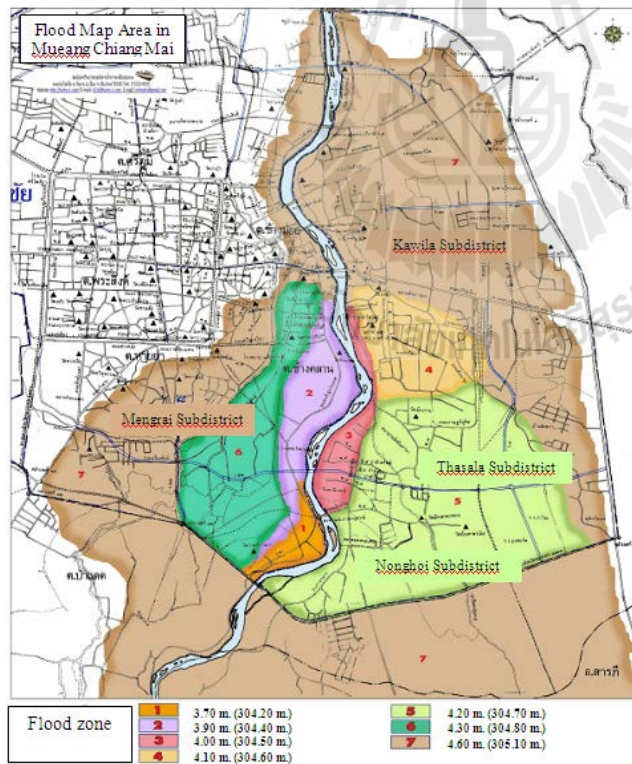


(b) Simulated flood map zone 4 (Z = 304.60m)

Figure 4.15 Comparison of flood maps under three condition of water levels at the P1 station (Z = 304.20, 304.60, 305.10 m).

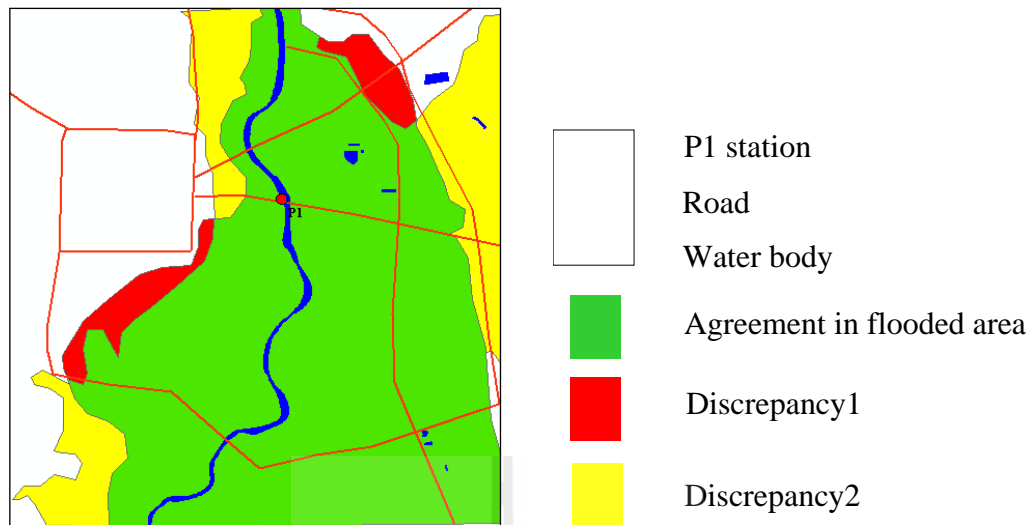


(c) Simulated flood map zone 7 ($Z = 305.10$ m)



(d) Reference map

Figure 4.15 (Continued)



(e) Compared result

Note: Discrepancy1 \equiv non-flooded in simulated but flooded in the reference

Discrepancy2 \equiv flooded in simulated but non-flooded in the reference

Figure 4.15 (Continued)

4.4 Impacts of LULC and climate changes on the modeled runoff

The part deals with applications of the derived model to examine impacts of the LULC and climate changes on the resulted discharge and associated flood map of the area. Three specific cases were considered at this stage: (1) impact of the LULC changes in the future (year 2020) given by the CA-Markov model, (2) impact of the specifically modified LULC maps (forest/orchard loss at rate of about 10 and 20%), and (3) impact of the change in amount of rainfall intensity (increase by 5, 10, 15%).

4.4.1 Assessment on impact of LULC changes

In this part, impact of the LULC changes on amount of the modeled discharge is quantified. This objective is divided into two parts based on different kinds of the proposed LULC changing patterns: (1) the predicted LULC map in 2020

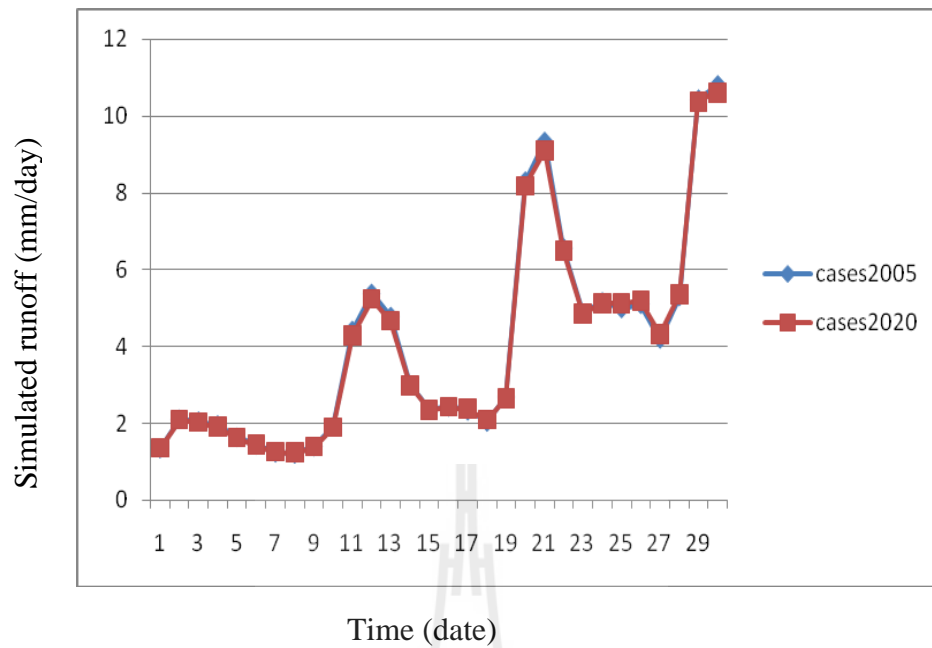
by the CA-Markov model (Figure 4.3) and (2) the predicted LULC map by the CA-Markov model with attached criteria of the possible rate of vegetation group loss.

In the first part, the derived 2020 LULC map (Figure 4.3) was applied as an input to the formerly developed hydrologic model while all other parameters in the used water balance model are assumed to be of those in 2005, e.g. rainfall, soil data, topography, stream network. This means only impact of the predicted 2020 LULC change is assessed while those of the other parameters left intact. Result of the study in this first part (daily simulated discharge) is presented in Table 4.13 and Figure 4.16 (along with data of the original 2005 case).

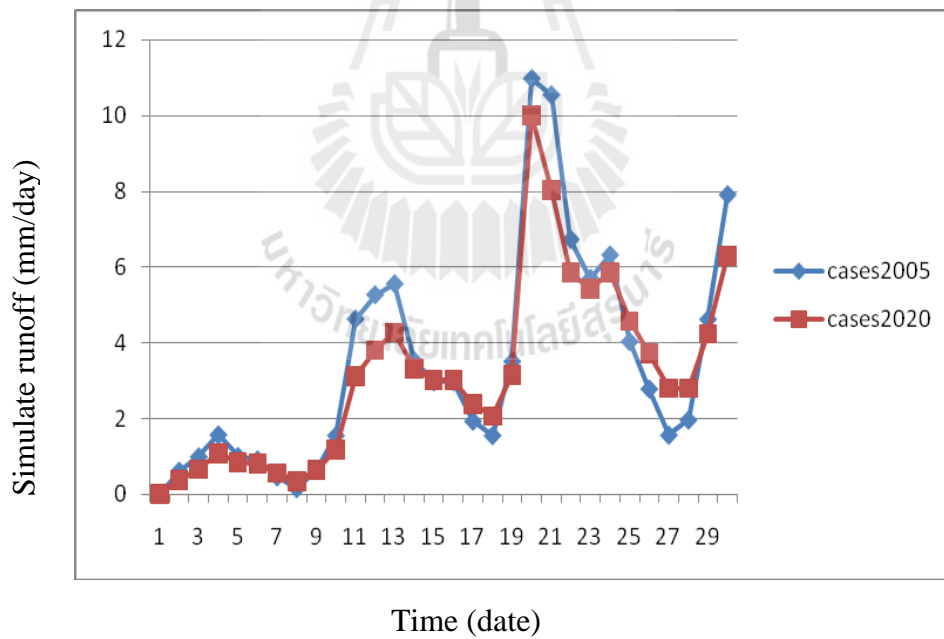
The preliminary results indicated that the introducing of the 2020 LULC map to the developed model does not have much impact on amount of simulated discharge at the P1 station but the effect is more pronounced at P21 station with both the notable reduced value (at peak locations) and increased values (at bottom locations).

Table 4.14 Simulated daily runoff discharge data (in mm) at the stations P1 and P21 in September 2005 (assumed different LULC input data).

Date	2005 LULC input		2020 LULC input	
	P1	P21	P1	P21
1	1.35	0.00	1.35	0.00
2	2.11	0.61	2.09	0.37
3	2.06	0.99	2.03	0.65
4	1.96	1.57	1.91	1.08
5	1.64	1.00	1.62	0.83
6	1.44	0.91	1.43	0.81
7	1.24	0.46	1.25	0.56
8	1.21	0.15	1.23	0.35
9	1.40	0.66	1.39	0.63
10	1.92	1.55	1.89	1.18
11	4.42	4.63	4.28	3.11
12	5.38	5.27	5.24	3.80
13	4.78	5.56	4.66	4.27
14	3.00	3.53	2.98	3.31
15	2.35	2.97	2.34	3.02
16	2.43	2.98	2.43	3.02
17	2.33	1.93	2.37	2.38
18	2.04	1.55	2.08	2.06
19	2.69	3.51	2.64	3.14
20	8.30	10.98	8.19	10.00
21	9.33	10.55	9.10	8.02
22	6.56	6.73	6.48	5.86
23	4.87	5.70	4.85	5.42
24	5.16	6.32	5.11	5.85
25	4.99	4.03	5.11	4.57
26	5.10	2.78	5.18	3.71
27	4.20	1.56	4.31	2.79
28	5.30	1.96	5.36	2.79
29	10.43	4.62	10.38	4.23
30	10.80	7.91	10.62	6.28
Total	120.790	102.970	119.924	94.114
Average	4.026	3.432	3.997	3.137



(a) Station P1



(b) Station P21

Figure 4.16 Simulated discharge data of the 2005 and 2020 cases at stations P1, P21.

On the average, the discharge at the P1 station is reduced by about 0.72% in 2020 compared to that of 2005, while at the P21 station, the loss is at about 8.60%. These results indicate that the simulation of discharge data at the P21 station is considerably more sensitive to the LULC changes in 2020 (e.g. forest loss about 3.39%, or 23.69 km² of the original area in 2005) than at the P1 station. This finding might originate from several possible reasons, for examples,

(1) Forest area might be transformed to be other LULC class that has similar hydrologic characteristics, like the orchard and perennial (they are put in the same vegetation group for purpose of the ET calculation as described by Eq. 3.1a). This assumption is found convincing based on the obtained LULC change matrix during 2000-2010 in Table 4.3 as an example (which found that forest was changed into the orchard and perennial class the most);

(2) Forest loss might appear at some particular areas that do not have much influence on the observed discharge within the study area, for example, along border with orchard/perennial or with urban/built-up area;

(3) Area of interest (1,121 km²) is still relatively small if compare to the total associated drainage area of the observed runoff at P1 station which is about 6,300 km² (nearly six times larger than the current study area) (Table 3.4). As a result, the relatively small changes of the LULC components within the study area should prove difficult to show noticeable change in the modeled discharges at P1 station as most of their drainage areas upstream are still left intact. While the drainage area of the P21 station is about 500 km² only, relatively smaller when compared to the present study area. This makes it might be more vulnerable to the forest loss at this scale (3-4%) than the P1 station and the obvious changes in modeled runoff might be easier to be exhibited.

To obtain more knowledge on the relationship of deforestation and modeled discharge, the CA-Markov model was applied again to derive the potential LULC map of year 2020 but, at this time, the preferred rates of forest and orchard/perennial loss during period 2005-2020 of about 10 and 20% were also used in the process of LULC map producing. This has been done by adjusting values related to forest and orchard/perennial loss (into other classes) in the relevant transition area matrix until the preferred amount of the total loss fulfilled (or nearly fulfilled) on the derived 2020 LULC map. The orchard/perennial class was included here due to its role in the modeled simulation of the runoff data is similar to that of the forest class. Therefore, the area loss (or gain) of this LULC class is very crucial for the determination of modeled runoff data as the forest class does. The corresponding 2020 classified LULC maps in case of the preferred 10 and 20% forest and orchard/perennial loss are displayed in Figure 4.17a-b while Table 4.15 presents LULC covering area for both cases under consideration. Tables 4.16a-b and 4.17a-b show the relevant transition probability and transitional area matrices for the case of 10% loss and 20% loss, respectively. Note that, for the case of preferred 10% loss, about 8.58% is achieved, and for the case of 20% loss, about 19.32% is achieved and processed.

Table 4.15 LULC covering area of the predicted maps in 2020 (two cases of forest and orchard/perennial loss).

LULC type	2005 (normal)		2020 (10% loss)		2020 (20% loss)	
	km ²	%	km ²	%	km ²	%
Forest	700.31	62.47	625.94	55.83	607.55	54.19
Orchard/Perennial	128.33	11.45	131.72	11.75	61.11	5.45
Crop	22.23	1.98	91.73	8.18	109.16	9.74
Paddy field	102.92	9.18	102.22	9.12	113.90	10.16
Urban/built-up	152.69	13.62	157.45	14.04	217.34	19.39
Water body	8.10	0.72	7.85	0.70	7.84	0.70
Miscellaneous	6.52	0.58	4.19	0.37	4.19	0.37
Total	1121.09	100.00	1121.09	100.00	1121.09	100.00

Table 4.16a Transition probability matrix for the 10% forest loss case.

2000 data	2010 data						
	MIS	CROP	PAD	U/B	WAT	ORC	FOR
Miscellaneous	0.6769	0.0006	0.0204	0.2881	0.0018	0.0114	0.0009
Crop	0.0030	0.9681	0.0000	0.0095	0.0002	0.01919	0.0000
Paddy field	0.0007	0.0009	0.9673	0.0279	0.0012	0.0020	0.0000
Urban/built-up	0.0000	0.0000	0.0000	1.0000	0.0000	0.0000	0.0000
Water body	0.0026	0.0003	0.0001	0.0088	0.9487	0.0000	0.0395
Orchard/Perennial	0.0009	0.0000	0.0053	0.0140	0.0012	0.9786	0.0000
Forest	0.0003	0.0065	0.0014	0.0037	0.0001	0.0202	0.9678

Table 4.16b Transition area matrix for the 10% forest loss case.

2000 data	2010 data						
	MIS	CROP	PAD	U/B	WAT	ORC	FOR
Miscellaneous	4,479	4	135	1,906	12	0	0
Crop	77	24,980	0	245	5	0	0
Paddy field	80	103	110,390	3,184	137	0	0
Urban/built-up	0	0	4	172,225	0	0	0
Water body	24	3	1	80	8,612	0	0
Orchard/Perennial	0	0	0	0	0	146,360	0
Forest	3,940	85,371	18,388	48,596	1,313	0	614,979

Table 4.17a Transition probability matrix for the 20% forest loss case.

2000 data	2010 data						
	MIS	CROP	PAD	U/B	WAT	ORC	FOR
Miscellaneous	0.6769	0.0006	0.0204	0.2881	0.0018	0.0114	0.0009
Crop	0.0030	0.9681	0.0000	0.0095	0.0002	0.01919	0.0000
Paddy field	0.0007	0.0009	0.9673	0.0279	0.0012	0.0020	0.0000
Urban/built-up	0.0000	0.0000	0.0000	1.0000	0.0000	0.0000	0.0000
Water body	0.0026	0.0003	0.0001	0.0088	0.9487	0.0000	0.0395
Orchard/Perennial	0.0009	0.0000	0.0053	0.0140	0.0012	0.9786	0.0000
Forest	0.0003	0.0065	0.0014	0.0037	0.0001	0.0202	0.9678

Table 4.17b Transition area matrix for the for the 20% forest loss case.

2000 data	2010 data							Total (pixels)
	MIS	CROP	PAD	U/B	WAT	ORC	FOR	
Miscellaneous	4,479	4	135	1,906	12	0	0	6,536
Crop	77	24,980	0	245	5	0	0	25,307
Paddy field	80	103	110,390	3,184	137	0	0	113,894
Urban/built-up	0	0	4	172,235	0	0	0	172,239
Water body	24	3	1	80	8,612	0	0	8,720
Orchard/Perennial	4,231	0	24,809	65,534	5,617	46,187	0	146,378
Forest	19,315	418,485	90,135	238,214	6,438	0	0	772,587
Total (pixels)	28,206	443,575	225,474	481,398	20,821	46,187	0	1,245,661

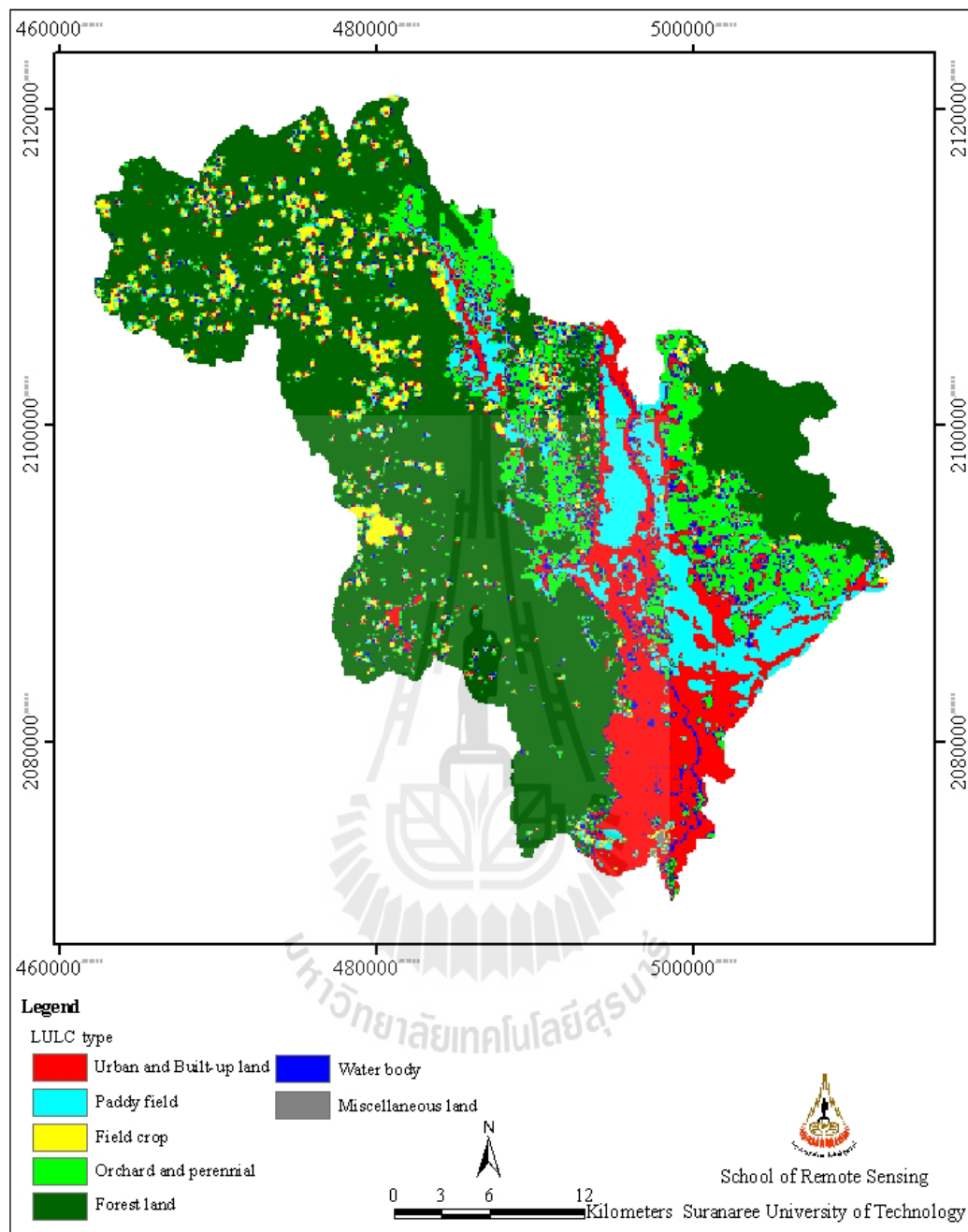


Figure 4.17a Predicted 2020 LULC map with preferred rate of forest/orchard loss at about 10%.

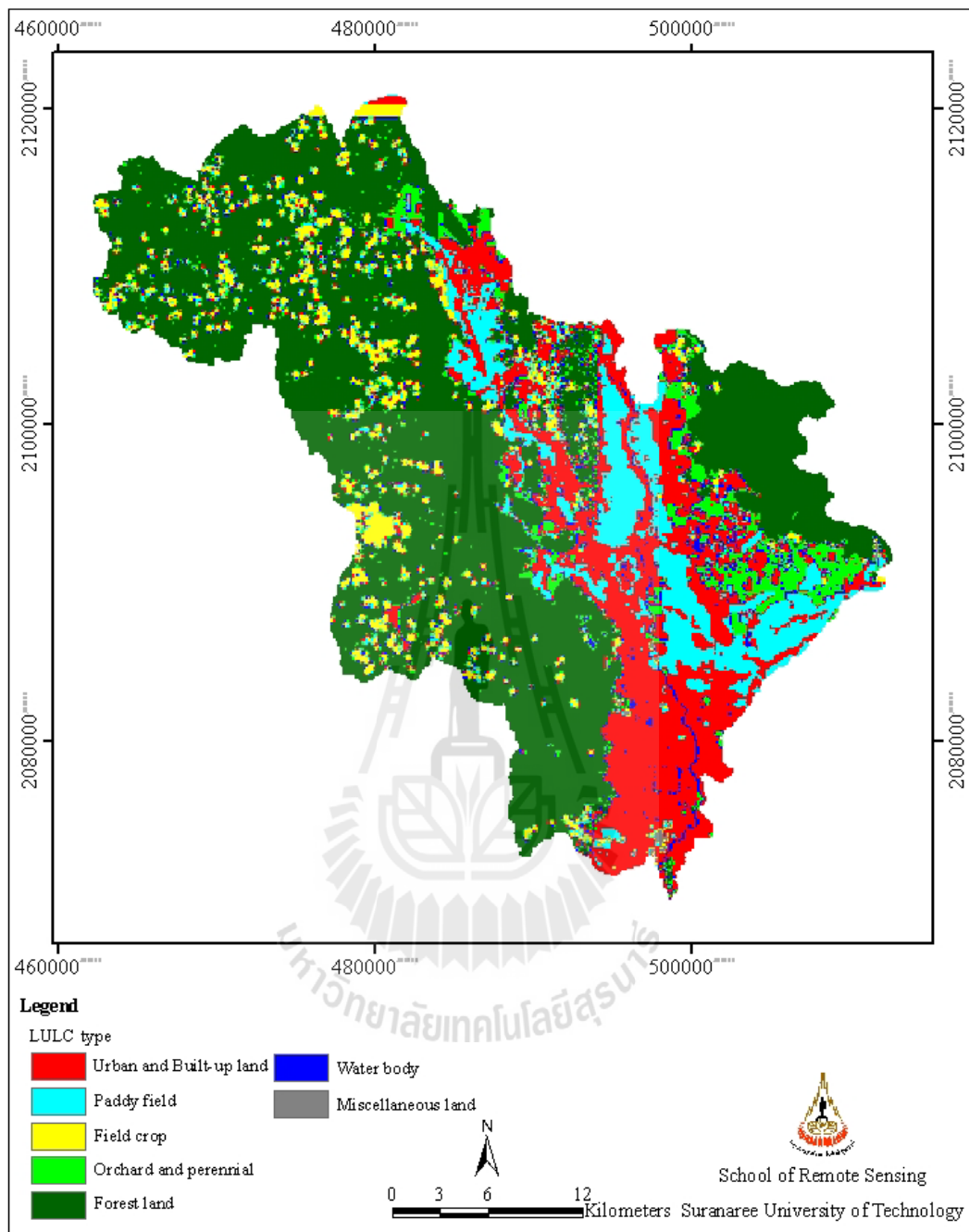


Figure 4.17b Predicted 2020 LULC map with preferred rate of forest/orchard loss at about 20%.

The next step was to produce the simulated discharges data along the river network by the developed model using each modified 2020 LULC map in Figure 4.17 as LULC input into the model while other parameter kept constant as of 2005 and results are reported in Table 4.18 and Figure 4.18. It was found that the obtained modeled discharges at P1 are still rather identical to those obtained in 2005 but the averaged values slightly increase about 0.27% (for the 10% loss case) and 1.27% (for the 20% loss case) of the value in 2005. On the contrary, the simulated discharges at station P21 have dropped significantly about 8.13% (10% loss case) from 2005 case and 7.95% (20% loss case), respectively. In addition, both notable decreased values (at peak flow) and increased values (at bottom locations) are found at the station P21 but not at the P1 station.

Similar to case of the 2020 LULC change, the modeled discharges at the P21 station display much higher sensitivity to the forest/orchard loss than those at the P1 station and potential trends of change are also different: slightly increase at the P1, considerably decrease at the P21. The main reason for this finding should be as stated earlier that because the associated drainage area of the P21 station is much smaller than that of the P1 station (about 12 times smaller), this makes it more sensitive to the same LULC changing scenarios than that of the P1 station in average.

Table 4.18 Simulated daily discharge data (mm) at stations P1 and P21 for modified 2020 cases (assumed different rates of forest/orchard loss).

Date	Normal (2005)		10% loss rate		20% loss rate	
	P1	P21	P1	P21	P1	P21
1	1.350	0	1.366	0	1.379	0
2	2.110	0.610	2.113	0.375	2.134	0.375
3	2.060	0.990	2.046	0.656	2.066	0.658
4	1.960	1.570	1.927	1.082	1.946	1.084
5	1.640	1.000	1.640	0.838	1.656	0.840
6	1.440	0.910	1.442	0.818	1.456	0.820
7	1.240	0.460	1.265	0.567	1.278	0.568
8	1.210	0.150	1.238	0.351	1.250	0.351
9	1.400	0.660	1.404	0.635	1.418	0.636
10	1.920	1.550	1.909	1.183	1.928	1.186
11	4.420	4.630	4.327	3.126	4.370	3.132
12	5.380	5.270	5.292	3.821	5.345	3.828
13	4.780	5.560	4.711	4.293	4.758	4.301
14	3.000	3.530	3.010	3.328	3.040	3.335
15	2.350	2.970	2.368	3.037	2.392	3.043
16	2.430	2.980	2.454	3.031	2.478	3.037
17	2.330	1.930	2.392	2.388	2.416	2.393
18	2.040	1.550	2.104	2.070	2.125	2.074
19	2.690	3.510	2.671	3.157	2.698	3.163
20	8.300	10.980	8.268	10.049	8.350	10.069
21	9.330	10.550	9.191	8.062	9.282	8.078
22	6.560	6.730	6.549	5.890	6.614	5.902
23	4.870	5.700	4.899	5.449	4.948	5.459
24	5.160	6.320	5.162	5.880	5.213	5.892
25	4.990	4.030	5.162	4.593	5.213	4.602
26	5.100	2.780	5.237	3.729	5.289	3.737
27	4.200	1.560	4.356	2.808	4.399	2.814
28	5.300	1.960	5.413	2.804	5.467	2.809
29	10.430	4.620	10.481	4.247	10.585	4.255
30	10.800	7.910	10.727	6.316	10.833	6.328
Total	120.790	102.970	121.124	94.585	122.323	94.773
Average	4.026	3.432	4.037	3.153	4.077	3.159

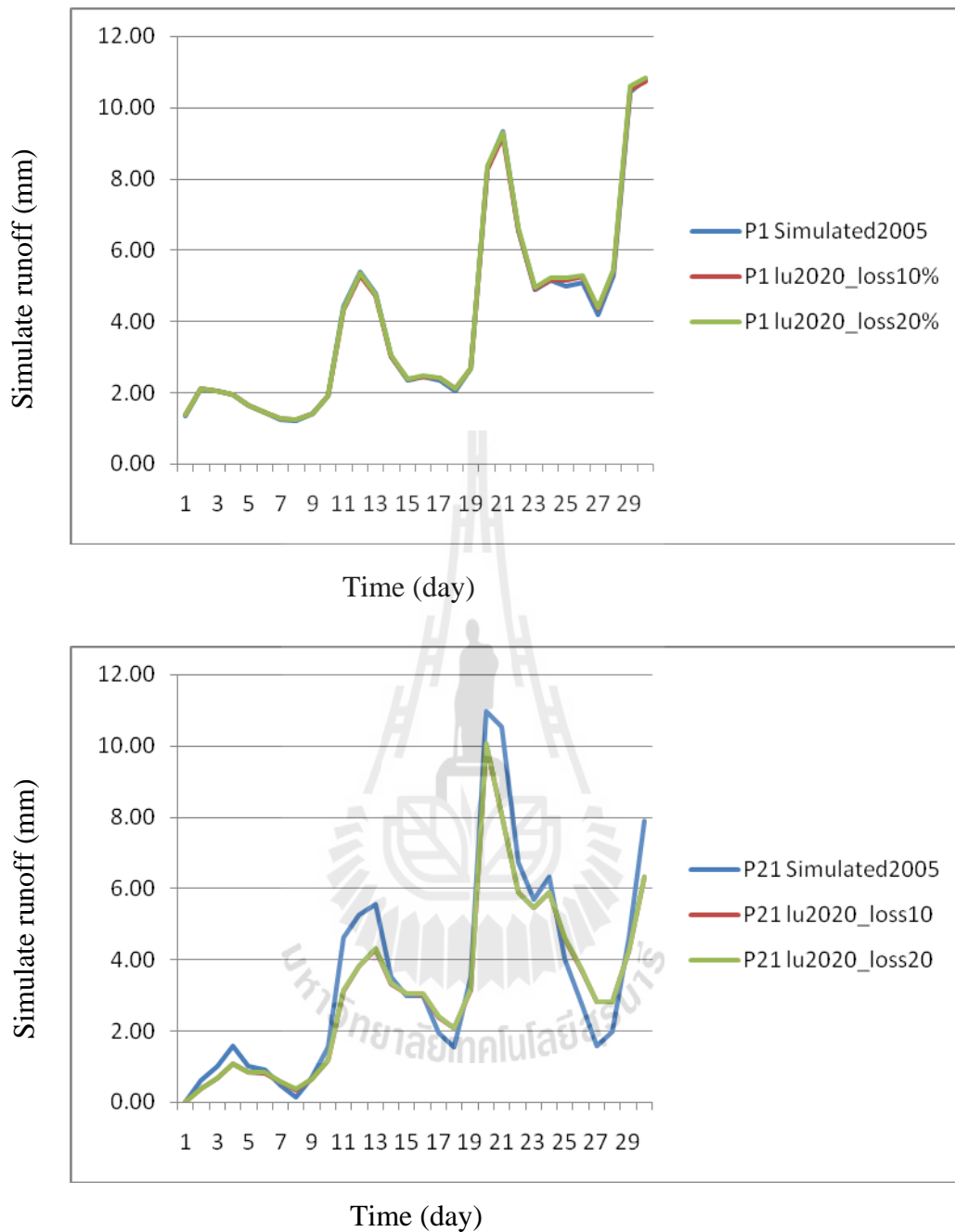


Figure 4.18 Simulated discharge data at stations P1, P21 for the modified 2020 cases (assumed different rates of forest/orchard loss).

4.4.2 Assessment on impact of climate changes

The sole element of climate which is responsible the most to the variation of runoff discharge along stream network of a particular basin is rainfall (Eq. 3.3) but exact relation of the rainfall intensity/distributing pattern to the observed discharge is rather difficult to foresee. In this study, impact of the rainfall variation (in intensity) on amount of the modeled discharge is quantified to gain prior knowledge on their relation in this chosen sub-basin. To fulfill the task, intensity of rainfall at every grid on the rainfall map is assumed to increase by 5, 10, and 15%, respectively, while the distributing pattern of those rainfall data are still the same (as of 2005). The modeled discharge data are described in Table 4.19 and Figure 4.19.

It is found that the increase in amount of rainfall has resulted in higher value of the associated discharge (compared to the 2005 normal case) at the P1 station, but scale of the increase is still relatively small. For example, in case of the 15% up in rainfall intensity, the discharge data were raised just about only 1.49% in average. However, changes in modeled discharge are clearly visible at the P21 station (about 18% up at 15% increase case). These results are similar to those found earlier where the much stronger sensitivity to the changes is found at the P 21 station compared to that of the P1 station. And the responsible answer is possibly the same as stated earlier about the much smaller size of the P21 catchment when compared to that of the P1 station, and only about 1/6 of the P1 catchment is considered at this stage.

Table 4.19 Simulated daily runoff data (in mm) at stations P1, P21 in September 2005
(assumed different rates of rainfall intensity).

Date	Normal (2005)		5% up		10% up		15% up	
	P1	P21	P1	P21	P1	P21	P1	P21
1	1.35	0.00	1.35	0.00	1.35	0.00	1.35	0.00
2	2.11	0.61	2.10	0.41	2.13	0.78	2.10	0.51
3	2.06	0.99	2.03	0.71	2.08	1.23	2.04	0.87
4	1.96	1.57	1.92	1.17	1.99	1.91	1.94	1.40
5	1.64	1.00	1.63	0.91	1.66	1.25	1.65	1.12
6	1.44	0.91	1.43	0.89	1.46	1.14	1.45	1.09
7	1.24	0.46	1.26	0.63	1.26	0.63	1.27	0.80
8	1.21	0.15	1.23	0.40	1.22	0.26	1.24	0.54
9	1.40	0.66	1.40	0.71	1.42	0.89	1.42	0.92
10	1.92	1.55	1.90	1.30	1.96	1.95	1.93	1.62
11	4.42	4.63	4.31	3.38	4.50	5.49	4.37	3.99
12	5.38	5.27	5.27	4.13	5.47	6.23	5.35	4.88
13	4.78	5.56	4.70	4.64	4.88	6.56	4.78	5.50
14	3.00	3.53	3.01	3.61	3.07	4.24	3.07	4.26
15	2.35	2.97	2.37	3.29	2.40	3.54	2.43	3.87
16	2.43	2.98	2.45	3.28	2.48	3.54	2.51	3.86
17	2.33	1.93	2.39	2.59	2.37	2.34	2.44	3.08
18	2.04	1.55	2.10	2.25	2.07	1.90	2.14	2.69
19	2.69	3.51	2.68	3.43	2.77	4.22	2.74	4.07
20	8.30	10.98	8.31	11.31	8.50	13.01	8.57	14.18
21	9.33	10.55	9.16	8.64	9.51	12.25	9.31	10.02
22	6.56	6.73	6.53	6.24	6.67	7.86	6.62	7.09
23	4.87	5.70	4.89	5.81	4.97	6.74	4.98	6.65
24	5.16	6.32	5.16	6.30	5.28	7.48	5.26	7.27
25	4.99	4.03	5.08	4.94	5.08	4.86	5.17	5.75
26	5.10	2.78	5.22	4.02	5.16	3.37	5.29	4.70
27	4.20	1.56	4.34	3.04	4.24	1.94	4.40	3.57
28	5.30	1.96	5.39	3.04	5.36	2.45	5.46	3.63
29	10.43	4.62	10.42	4.59	10.54	5.56	10.52	5.46
30	10.80	7.91	10.69	6.85	10.98	9.46	10.84	8.18
Total	120.79	102.97	120.70	102.51	122.81	123.07	122.64	121.56
Average	4.03	3.43	4.02	3.42	4.09	4.10	4.09	4.05

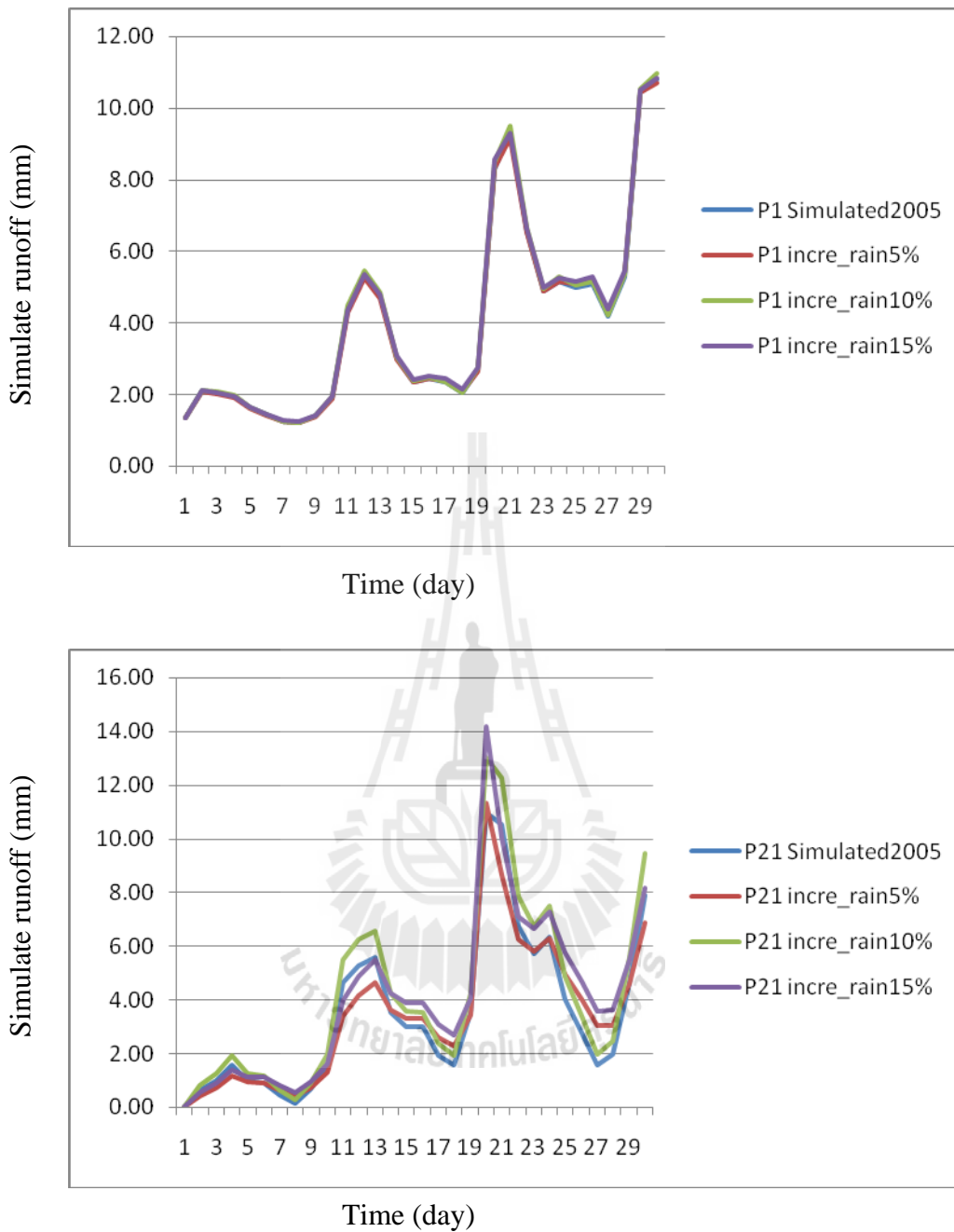


Figure 4.19 Simulated daily runoff data at station P1 and P21 in September 2005 (assumed different rates of rainfall intensity).

4.4.3 Applications of the original lumped model

As a preliminary study has indicated that the loss of forest/orchard at the preferred rates (10 and 20%) within the study area still does not affect the modeled discharge at P1 station much, therefore, impact of forest loss in the headwater basin (of the river) further north of the study area is also addressed here by integrating the original lumped model with the newly-developed grid-based model described in this research. The expansion of the study area into the headwater forest upstream should proved significant in the assessment of forest loss impact on the discharge volume along the Ping River and the subsequent flooding map of the municipal area. This might be because total drainage area associated to the discharge observed at P1 station is about 6,200 km² (Table 3.4) out of which only about 1,000 km² was included in the study area proposed in this thesis (the rest is located upstream outside the current study area).

To achieve this task, the original lumped model was applied throughout the drainage area of P1 based on same prior assumption of the forest loss (about 10, 20%) and rainfall increase (5, 10, 15%). This integration of the original model in this study is primarily intended to simulate the inlet discharge data at P67 station which is used as an input parameter for the newly-developed model. Results of the simulation at P67 station are shown in Table 4.17 and Figure 4.20 and the associated modeled discharge data at the P1 station (for all considered scenarios) are reported in Table 4.20 and Figure 4.21, and data for the P21 station are reported in Table 4.21 and Figure 4.22. It was found that the integration of the original model into this study was very useful as the modeled discharge are now more sensitive to the changes in LULC

and rainfall amount where the higher forest loss is related to higher amount of the discharge data as well as the increase in rainfall intensity.

Table 4.20 Simulated daily runoff data (in mm) at P67 station using the original lumped model (assumed different rates of forest loss and rainfall).

Date (September)	Observed	Forest loss		Rainfall increase		
		10%	20%	5% up	10% up	15% up
1	1.604	1.670	1.734	1.831	2.058	2.289
2	2.435	2.536	2.633	2.780	3.124	3.475
3	2.354	2.451	2.545	2.687	3.020	3.360
4	2.159	2.248	2.335	2.465	2.770	3.082
5	1.844	1.920	1.994	2.105	2.366	2.632
6	1.604	1.670	1.734	1.831	2.058	2.289
7	1.424	1.483	1.540	1.626	1.827	2.033
8	1.412	1.471	1.527	1.612	1.812	2.016
9	1.578	1.643	1.706	1.801	2.024	2.252
10	2.126	2.214	2.300	2.428	2.728	3.035
11	4.746	4.943	5.133	5.419	6.089	6.775
12	5.829	6.070	6.304	6.655	7.478	8.320
13	5.071	5.281	5.484	5.789	6.506	7.238
14	3.198	3.330	3.458	3.651	4.103	4.564
15	2.455	2.557	2.655	2.803	3.150	3.504
16	2.556	2.662	2.765	2.919	3.280	3.649
17	2.536	2.641	2.743	2.896	3.254	3.620
18	2.256	2.350	2.440	2.576	2.895	3.221
19	2.759	2.874	2.984	3.150	3.540	3.939
20	8.694	9.054	9.402	9.926	11.154	12.410
21	9.930	10.342	10.740	11.338	12.741	14.175
22	7.077	7.370	7.654	8.080	9.080	10.102
23	5.191	5.406	5.614	5.926	6.660	7.410
24	5.431	5.656	5.874	6.201	6.968	7.753
25	5.491	5.719	5.939	6.269	7.045	7.838
26	5.767	6.006	6.237	6.584	7.399	8.232
27	4.805	5.004	5.196	5.485	6.164	6.858
28	6.045	6.295	6.537	6.901	7.755	8.628

Table 4.20 (Continued).

Date (September)	Observed	Forest loss		Rainfall increase		
		10%	20%	5% up	10% up	15% up
29	11.815	12.304	12.778	13.489	15.159	16.865
30	11.885	12.377	12.853	13.569	15.249	16.965
Total	132.074	137.547	142.840	150.793	169.457	188.530
Average	4.402	4.585	4.761	5.026	5.649	6.284

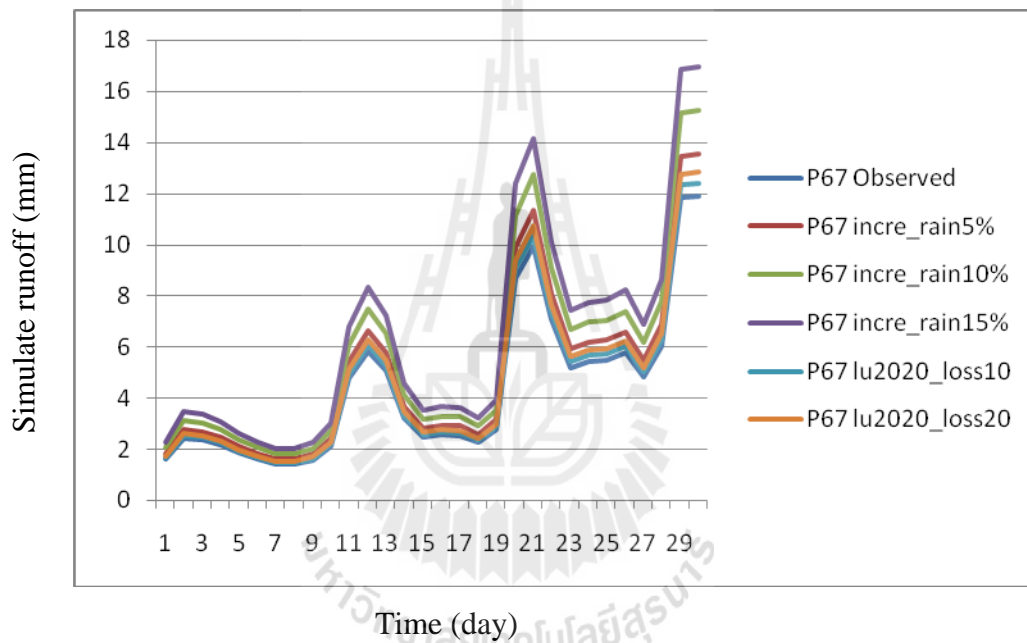


Figure 4.20 Simulated daily runoff data at P67 station using the original lumped model (assumed different rates of forest loss and rainfall).

Table 4.21 Simulated daily runoff data (mm) at P1 station using the developed model (assumed different rates of forest loss and rainfall).

Date (September)	Normal (2005)	Forest loss		Rainfall increase		
		10%	20%	5% up	10% up	15% up
1	1.35	1.41	1.46	1.55	1.74	1.94
2	2.11	2.18	2.25	2.38	2.68	2.98
3	2.06	2.13	2.21	2.34	2.62	2.92
4	1.96	2.00	2.08	2.20	2.46	2.73
5	1.64	1.70	1.76	1.87	2.10	2.33
6	1.44	1.49	1.54	1.63	1.83	2.04
7	1.24	1.30	1.35	1.44	1.61	1.79
8	1.21	1.28	1.33	1.40	1.57	1.76
9	1.40	1.45	1.51	1.59	1.79	1.99
10	1.92	1.97	2.05	2.17	2.44	2.72
11	4.42	4.45	4.61	4.88	5.48	6.09
12	5.38	5.48	5.68	6.02	6.75	7.49
13	4.78	4.85	5.02	5.32	5.96	6.62
14	3.00	3.12	3.23	3.41	3.82	4.24
15	2.35	2.45	2.53	2.68	3.00	3.32
16	2.43	2.53	2.62	2.78	3.11	3.45
17	2.33	2.45	2.54	2.69	3.01	3.35
18	2.04	2.18	2.25	2.39	2.68	2.97
19	2.69	2.74	2.83	3.01	3.37	3.74
20	8.30	8.55	8.85	9.41	10.57	11.77
21	9.33	9.49	9.83	10.40	11.65	12.94
22	6.56	6.78	7.02	7.42	8.31	9.22
23	4.87	5.07	5.24	5.55	6.21	6.89
24	5.16	5.34	5.52	5.84	6.54	7.26
25	4.99	5.27	5.45	5.77	6.47	7.19
26	5.10	5.43	5.62	5.94	6.67	7.41
27	4.20	4.49	4.66	4.93	5.51	6.14
28	5.30	5.61	5.82	6.15	6.91	7.68
29	10.43	10.83	11.23	11.87	13.33	14.83
30	10.8	11.11	11.51	12.18	13.67	15.21
Total	120.79	125.12	129.59	137.20	153.88	171.01
Average	4.03	4.17	4.32	4.57	5.13	5.70

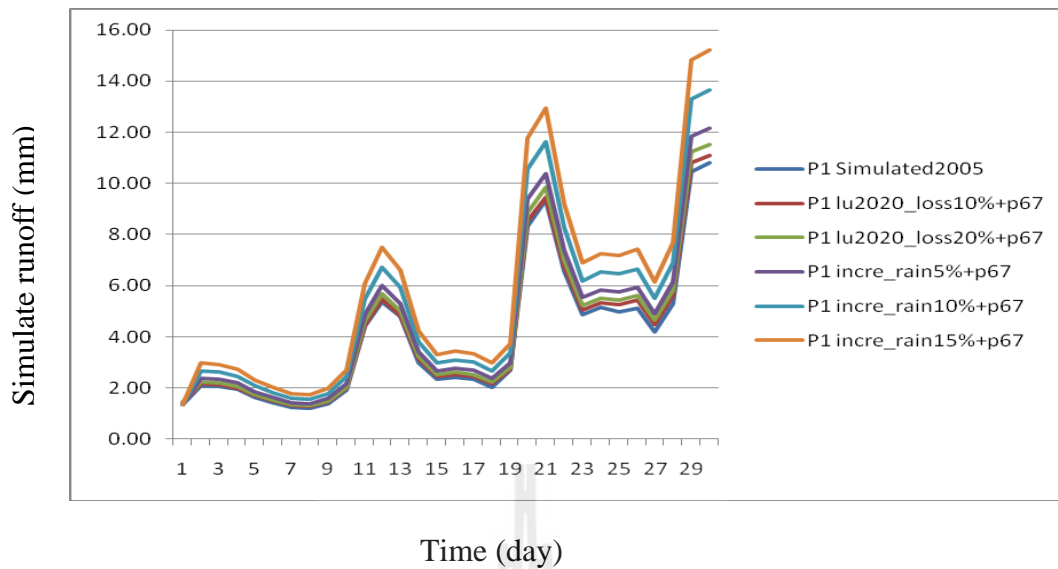


Figure 4.21 Simulated daily runoff data (mm/day) at the P1 station using the developed model (assumed different rates of forest loss and rainfall).

Table 4.22 Simulated daily runoff data (in mm) at P21 station using developed model (assumed different rates of forest loss and rainfall).

Date (September)	Normal (2005)	Forest loss		Rainfall increase		
		10%	20%	5% up	10% up	15% up
1	0.00	0.000	0.000	0.000	0.000	0.000
2	0.61	0.375	0.375	0.414	0.782	0.514
3	0.99	0.656	0.658	0.715	1.228	0.871
4	1.57	1.082	1.084	1.171	1.907	1.400
5	1.00	0.838	0.840	0.914	1.252	1.118
6	0.91	0.818	0.820	0.893	1.136	1.094
7	0.46	0.567	0.568	0.629	0.627	0.802
8	0.15	0.351	0.351	0.399	0.259	0.544
9	0.66	0.635	0.636	0.708	0.892	0.916
10	1.55	1.183	1.186	1.304	1.953	1.622
11	4.63	3.126	3.132	3.377	5.492	3.987
12	5.27	3.821	3.828	4.126	6.227	4.876
13	5.56	4.293	4.301	4.637	6.556	5.498

Table 4.22 (Continued).

Date (September)	Normal (2005)	Forest loss		Rainfall increase		
		10%	20%	5% up	10% up	15% up
14	3.53	3.328	3.335	3.612	4.238	4.256
15	2.97	3.037	3.043	3.290	3.543	3.870
16	2.98	3.031	3.037	3.277	3.537	3.857
17	1.93	2.388	2.393	2.594	2.340	3.084
18	1.55	2.070	2.074	2.252	1.896	2.689
19	3.51	3.157	3.163	3.430	4.223	4.067
20	10.98	10.049	10.069	11.311	13.005	14.176
21	10.55	8.062	8.078	8.637	12.250	10.023
22	6.73	5.890	5.902	6.238	7.859	7.086
23	5.70	5.449	5.459	5.808	6.742	6.652
24	6.32	5.880	5.892	6.298	7.481	7.272
25	4.03	4.593	4.602	4.941	4.857	5.754
26	2.78	3.729	3.737	4.018	3.367	4.697
27	1.56	2.808	2.814	3.036	1.943	3.567
28	1.96	2.804	2.809	3.044	2.450	3.632
29	4.62	4.247	4.255	4.590	5.565	5.465
30	7.91	6.316	6.328	6.845	9.457	8.178
Total	102.97	94.585	94.773	102.511	123.065	121.565
Average	3.43	3.153	3.159	3.417	4.102	4.052

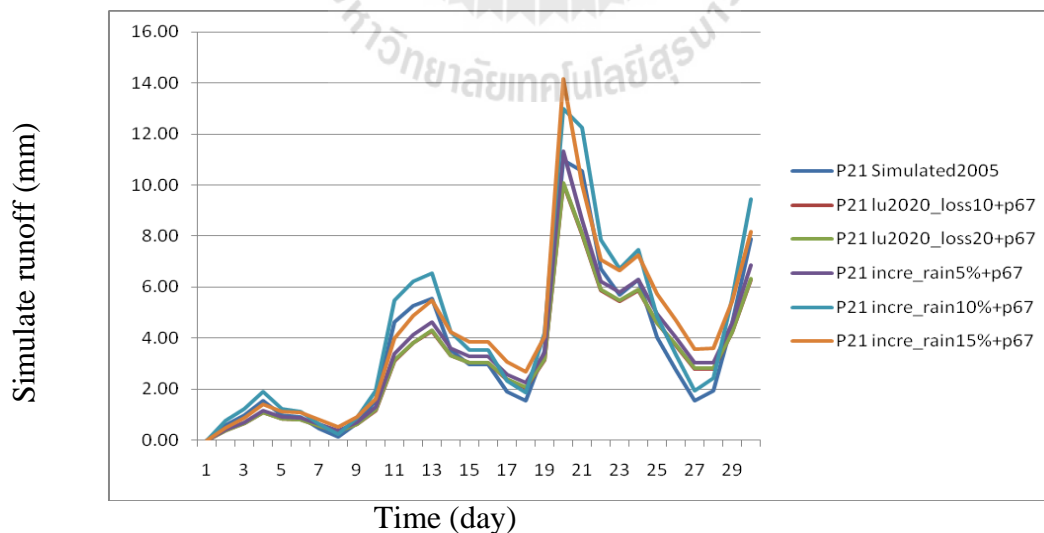


Figure 4.22 Simulated daily runoff data (mm/day) at stations P21 using the developed model (assumed different rates of forest loss and rainfall).

Results of the study indicate that, by considering its whole drainage area, the forest loss of 10 and 20% would result in the notable rise of modeled runoff discharge (from the normal 2005 case) by about 3.5% and 7.2%, respectively, at the P1 station. Similarly, the rise of rainfall amount by 5%, 10%, 15%, would result in the substantial increase of the modeled runoff at about 13.4%, 27.3%, and 41.4%, respectively. This means the assumed forest loss and rainfall intensity changes at the referred rates over the entire drainage area of the P1 station have strong effect on the amount of modeled discharge observed at the P1 station (and also on the associated flooding intensity in the Chiang Mai city area). But this conclusion still cannot be applied to the modeled runoff found at the P21 station as no obvious trends of change were seen under the proposed rates of forest loss and rainfall increase.

Simulate flood maps

Figures 4.23 and 4.24 depict flood maps for worst case of forest loss (20%) and most rainfall increase (15%). The flooding dates are ones with $Z > 304.2\text{m}$ MSL at the P1 station (Table 4.22). It is found that in case of the 20% forest loss, there are still only four flood dates like in normal case (2005): 20th, 21th, 29th, 30th but the water area is expanded due to higher water level (Figure 4.23). But in case of the 15% increased rainfall, there are 10 flood dates found: 12th, 20th, 21th, 22th, 24th, 25th, 26th, 28th, 29th, 30th (Figure 4.24).

This difference in the number of dates here is understandable as the 20% forest loss would result in the increase of modeled discharge just about 7% only, while the increase of rainfall intensity by 15% shall result in the rise of modeled discharge of about 41% in average. As a result, number of flooded date in this case is much higher also. This indicates that forest loss might not be as vulnerable as the

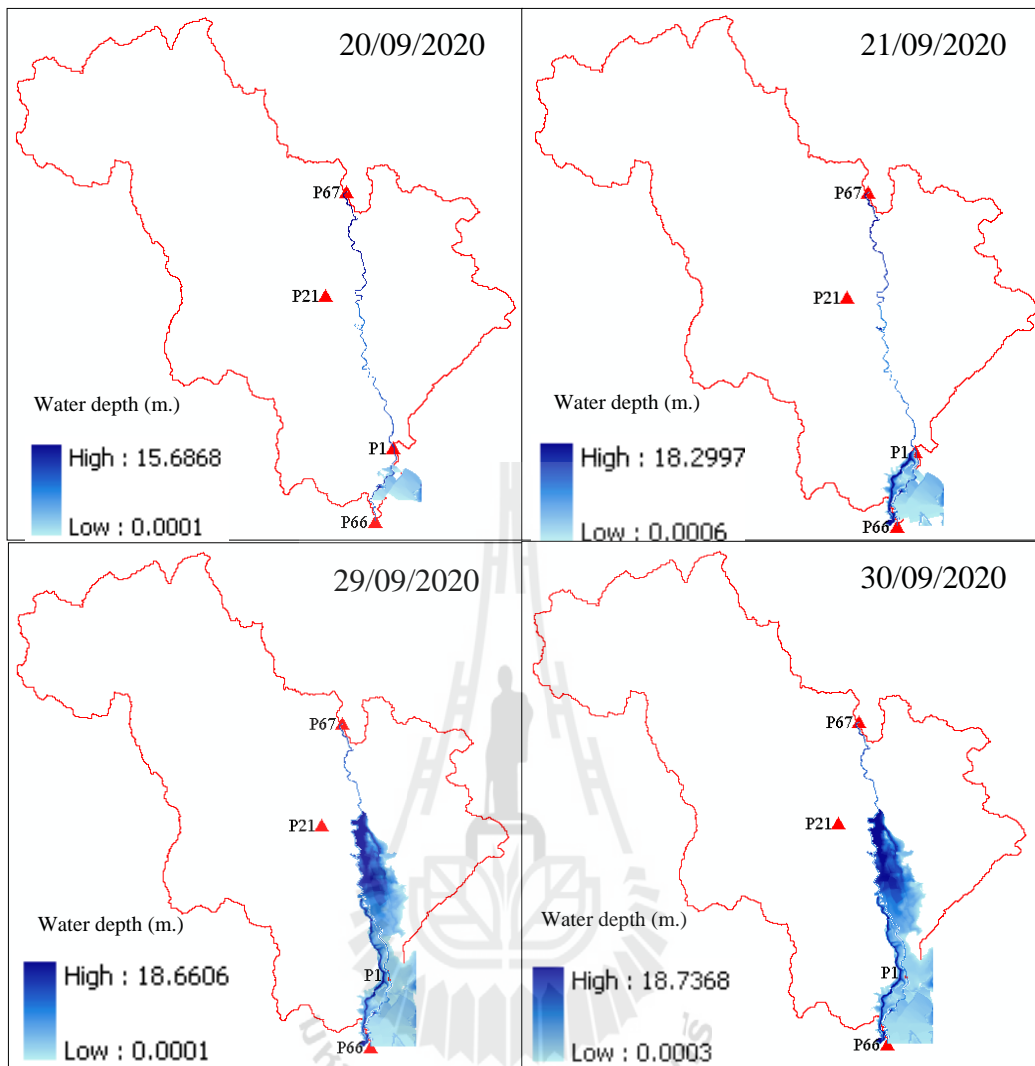
rising trend of rainfall intensity in the area, regarding to the flood severity concern in the Chiang Mai city.

Table 4.23 Simulated daily runoff, discharge (Q), and water level (Z) data at station P1 in September 2005 (highlight is for the predicted flood date with $Z > 304.2$ m MSL).

Date (September)	Case 1 (20% forest loss)			Date	Case 2 (15% rainfall increase)		
	Runoff (mm/d)	Q (m ³ /s)	Z (m)		Runoff (mm/d)	Q (m ³ /s)	Z (m)
1	1.46	105.13	302.40	1	1.94	139.16	302.57
2	2.25	162.01	302.68	2	2.98	214.50	302.92
3	2.21	159.05	302.66	3	2.92	209.62	302.90
4	2.08	149.32	302.62	4	2.73	196.44	302.84
5	1.76	126.46	302.51	5	2.33	167.22	302.70
6	1.54	110.54	302.43	6	2.04	146.42	302.60
7	1.35	97.38	302.37	7	1.79	128.73	302.52
8	1.33	95.41	302.36	8	1.76	126.48	302.51
9	1.51	108.46	302.42	9	1.99	143.25	302.59
10	2.05	147.45	302.61	10	2.72	195.33	302.83
11	4.61	331.78	303.45	11	6.09	437.92	303.91
12	5.68	408.39	303.78	12	7.49	538.89	304.32
13	5.02	360.95	303.58	13	6.62	476.14	304.07
14	3.23	231.91	303.00	14	4.24	305.13	303.33
15	2.53	181.99	302.77	15	3.32	238.94	303.03
16	2.62	188.67	302.80	16	3.45	248.03	303.07
17	2.54	182.46	302.77	17	3.35	240.84	303.04
18	2.25	161.94	302.68	18	2.97	213.64	302.92
19	2.83	203.56	302.87	19	3.74	269.06	303.17
20	8.85	636.05	304.71	20	11.77	846.30	305.48
21	9.83	706.66	304.97	21	12.94	930.51	305.76

Table 4.23 (Continued).

Date (September)	Case 1 (20% forest loss)			Date	Case 2 (15% rainfall increase)		
	Runoff (mm)	Q (m ³ /s)	Z (m)		Runoff (mm)	Q (m ³ /s)	Z (m)
22	7.02	504.56	304.18	22	9.22	663.00	304.81
23	5.24	376.75	303.65	23	6.89	495.25	304.14
24	5.52	396.66	303.73	24	7.26	521.99	304.25
25	5.45	392.18	303.71	25	7.19	516.81	304.23
26	5.62	404.44	303.76	26	7.41	532.95	304.30
27	4.66	335.05	303.46	27	6.14	441.86	303.92
28	5.82	418.21	303.82	28	7.68	552.24	304.38
29	11.23	807.58	305.34	29	14.83	1066.24	306.20
30	11.51	827.52	305.41	30	15.21	1093.89	306.28



Figures 4.23 Flood depth maps in case of the worst forest loss rate (20%).

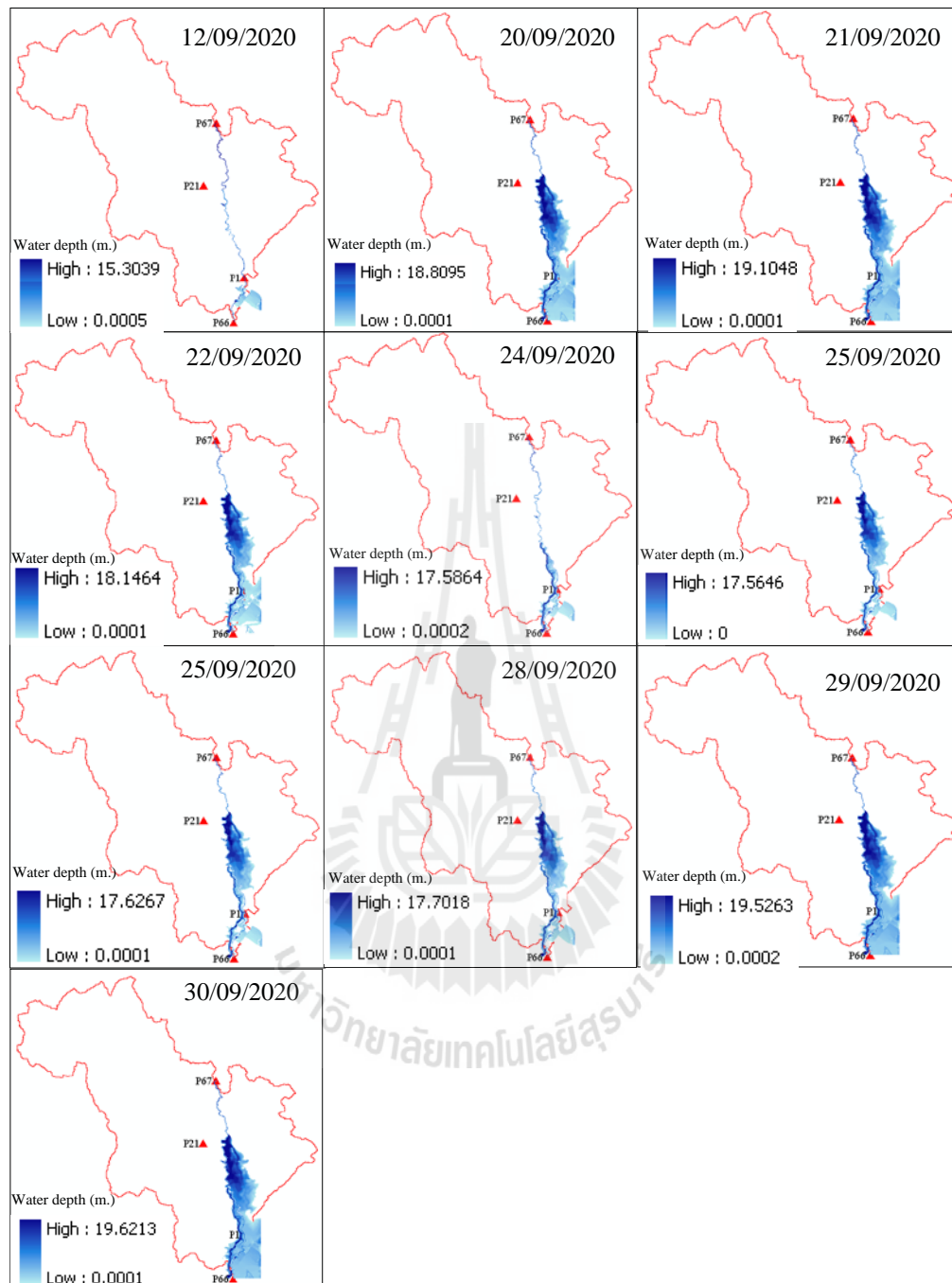


Figure 4.24 Flood maps for case of most rainfall increase (15%).

CHAPTER V

CONCLUSIONS AND RECOMMENDATIONS

5.1 LULC classification

The preferred LULC maps for years 2000, 2005, 2010 are generated from the chosen Landsat TM data of each stated year using the hybrid classification method. The results indicate that the forest class dominates in the western side and urban/built-up dominates in the far south of the area (location of the Chiang Mai city area) while orchard/perennial mostly situates close to the forest boundary and the paddy field is usually found mixed up with the urban/built-up class in the southeastern part of the area. In general, pattern of the LULC distribution does not change much during period 2000-2010 where most dominant class is forest (62-64%), followed by urban/built-up (13-14%), orchard/perennial (10-12%) and paddy fields (9%). During this period, forest and paddy field losses about 3.16 and 1.57% of their original area in 2010 while orchard/perennial, crop and urban/built-up had gained about 10.56, 22.46, and 6.76% of their original areas. The LULC change matrix during 2000-2010 indicates that the original forest in 2000 was turned into orchard/perennial the most followed by crop and urban/built-up, respectively. Over the same period, urban/built-up area was grown about 6.76% of the original area in 2000 in expense of paddy field the most followed by forest and miscellaneous class, respectively.

5.2 Model's developing process and runoff simulation

In this part, the monthly model (for monthly runoff simulation) is produced first based on five cases of preferred water balance model:

Case 1: Uniform rainfall and constant soil depth (3 m);

Case 2: Non-uniform rainfall but constant soil depth (3 m);

Case 3: Uniform rainfall but Non-uniform soil depth;

Case 4: Non-uniform rainfall and soil depth (without sub-surface runoff);

Case 5: Non-uniform rainfall and soil depth (with sub-surface runoff).

Efficiency of the model developed in each mentioned case is determined based on the comparison of its simulated runoff discharges to the observed discharges at P1 and P21 stations. Results from Case 1 and Case 3 indicate that the variation of soil depth data does not affect the discharge outcome from the model (with fixed 3m soil depth) much. Therefore, for convenience in the data preparing process, this 3m fixed value of the soil depth might be applied instead of the genuine data-varying soil depth map. Similarly, resulted runoff data from Case 2 and Case 4 are also rather identical which imply that variation of soil depth is not an important aspect in this developed model. The rainfall intensity should be a main contributing factor to both observed and simulated runoff data as amount of the runoff discharge is found to be noticeably high in the strong monsoon season (August-October) the most. However, it is found that if the sub-surface runoff is very crucial factor to make the runoff output appear more realistic (as in Case 5 with $R^2 = 0.94$ and Nash-Sutcliffe efficiency (E) = 0.88 at P1 station and $R^2 = 0.83$ and E = 0.63 at P21 station).

The developed model in Case 5 is then used as a prototype for the construction of the daily model (for daily runoff simulation) in which two cases were considered:

Case 1: Non-uniform rainfall/soil depth (without transpiration rate).

Case 2: Non-uniform rainfall/soil depth (with transpiration rate).

Results obtained from these cases indicate that the transpiration term is very essential in the building of effective daily model as it can notably reduce existing differences between the observed and modeled discharge data at both P1 and P21 stations. Here in Case 2 mentioned above (with best yielded results), the $R^2 = 0.96$ and $E = 0.94$, and $R^2 = 0.61$ and $E = 0.47$ were gained at the P1 and P21 station, respectively.

The grid-based hydrological model can simulate run-off in accordance with water balance process and to known water level Z (in meter above MSL) along the main stream network for each interested day. The gained water level data (along the stream network) from the model can be further used to produce realistic flood map by using the proper GIS technique as described in Section 5.3.

In view of model comparison, the original lumped model and the grid-based hydrological model can generate similar outcome on simulated runoff data. However, the original model had a good long-term simulation but the grid-based model is only a short time simulated. In addition, original model considers specified runoff data only the outlet point but the new model can generate its detail at every grid of the area. Also, the newly-developed model is superior in term of the GIS-based structure that can support the GIS dataset input/output very efficiently. This property is useful for the runoff data simulating under different scenarios, e.g. changes in the LULC pattern, or the climate data.

5.3 Construction of the flood maps

The assumed flooding scenario here is river flood that occurs from overbank flow of stream discharge into the lowland areas situating nearby. As a result, the water level Z (above MSL) at each location along stream channel is determined first from the known simulated channel discharge and the derived rating curve (for the P1, P21, P67 stations). It was assumed the over flown water shall move overland until it reaches the area/place it cannot pass which marks boundary of the flooded area. As a consequence, the flood depth map can be generated based on the difference between the known water level (Z) and elevation (above MSL) of the area.

From data of simulated water level Z at the P1 station in September 2005, it was found that there should be floods in the Chiang Mai municipal area only on four dates: 20th-21st, 29th- 30th with $Z = 304.57, 304.79, 305.13,$ and 305.20 m respectively while on the other dates no floods should occur (as Z is less than the critical level of 304.2 m). The strongest flood appears on the 30th September as it has the highest level of water at the P1 station. By the comparison of simulated flooded area for $Z = 304.2, 304.6,$ and 305.1 m with the reference flood map made at the same level, it was found that these two maps have moderate level of the agreement in average (about 58.93% agreement and 41.07% discrepancy). Highest level of the agreement is at water level of 304.2 m (about 87.10% agreement and 12.90% discrepancy)

5.4 Impacts of LULC and climate changes on the modeled runoff

In this part, impact assessment on the modeled runoff was performed in three specific cases: (1) impact from the LULC changes in the future (year 2020) given by the CA-Markov model, (2) impact from the forest/orchard loss at the preferred rates

of about 10 and 20% and (3) impact from the increase of the rainfall intensity by 5, 10, and 15% under the same distributing pattern.

Primary results gained in these cases indicated that the modeled discharges at the P1 station are not sensitive much with the proposed variations in LULC pattern and the rainfall increase. In the contrary, modeled discharges at the P21 stations show strong response to the assumed changes in LULC (forest/orchard loss) and the rise in rainfall intensity. Theoretically, the difference in response level between these two stations may be originated from the great difference in size of the associated drainage area of each station of which that of the P21 station is about 12 times smaller that of the P1 station (about 500 to 6,000 km²) (Jothityangkoon and Hirunteeyakul, 2009).

This problem is further explored by applying the original lumped model into the study. The stated model was used to generate the inlet runoff at the P67 station under assumptions suggested in all three cases referred to above (forest loss of 10 and 20% and rainfall increase by 5, 10, 15%) but these assumptions are applied to the whole associated drainage area of the P1 station, not only in the study area as usual. These inlet runoff data were then used as a new input data into the developed model and the simulation process was carried out for this model under these assumptions.

Results of the study indicate that, under the aforementioned circumstance, the forest loss of 10 and 20% resulted in the average increase of modeled runoff by about 3.5% and 7.2% respectively, at the P1 station (if compared to the 2005 case). And the increase of rainfall intensity by 5%, 10%, 15%, resulted in the increase of modeled runoff about 13.4%, 27.3%, and 41.4%, respectively. This means the assumed forest loss and rainfall intensity changes at the stated rates over the whole drainage area of the P1 station have strong impact on the amount of modeled discharge observed at the

station (and also on the associated flooding intensity in the Chiang Mai city area). But this conclusion still cannot be applied to the modeled runoff found at the P21 station as no obvious trends of change under the same assumptions. For the worst case of forest loss (20% loss), number and detail of flood dates is still similar to that in 2005 (4 dates at 20th, 21th, 29th, 30th) but the flood area is higher due to higher level of flood depth. But for case of 15% rainfall increase, number of flood dates rises to 10.

5.5 Recommendations

5.5.1 DEM with high precision (e.g. with 2m contour interval) should be tried to generate flood depth maps (regarding to the simulated water level from the model) to gain more realistic outcome than ones obtained in this research.

5.5.2 To assess relationships of the LULC or rainfall intensity changes to the modeled discharge data at the P1 station more realistically, the study area should be expanded to cover the entire drainage area of the station (about 6,000 km²).

5.5.3 The model should be improved to be able to explain other kind of floods, e.g. flash flood, urban flood, or pluvial flood.

5.5.4 The model should be introduced to explain severe river floods elsewhere in Thailand to find its general applicability to this task.

5.5.5 The model should be implemented in the flood prevention planning (design structure for protection of flood) and warning administration as appropriate.



REFERENCES

REFERENCES

- American Society of Civil Engineer. (1996). **Hydrology Handbook**. 2nd sub edition. Amer Society of Civil Engineers.
- Andreadis, K.M. and Lettenmaier, D.P. (2006). Assimilating remotely sensed snow observations into a macroscale hydrology model. **Advances in Water Resources**. 29(6): 872-886.
- Chuchok aryooiphong. (2007). **Chiang Mai Flood Forecasting and Warning System** (in Thai). Survey Engineering Department, Faculty of Engineering, Chiang Mai University.
- Borah, D.K., Arnold, J.G., Bera, M., Krug, E.C. and Liang, X.Z. (2007) Storm Event and Continuous Hydrologic Modeling for Comprehensive and Efficient Watershed Simulations. **Journal of Hydrologic Engineering**. 12(6): 604-616
- Chatchawan, S. (2005). **Report of flood situation and management in Chiang Mai municipal area 2005** (in Thai). [Online]. Available: <http://www.thaienvimonitor.net/News/CHANGMAI.pdf>.
- Chen, J., Hill, A.A. and Urbano, L.D. (2009). A GIS-based model for urban flood inundation. **Journal of Hydrology**. 373: 184-192.
- Chen, J. M., Chen, X., Ju, W. and Geng, X. (2005). Distributed hydrological model for mapping evapotranspiration using remote sensing inputs. **Journal of Hydrology**. 305(1-4): 15-39.

- Chen, J.M. (2005). **A distributed hydrological model: TerrainLab**. [Online]. Available:http://faculty.geog.utoronto.ca/Chen/Chen%27s%20homepage/res_terrainlab.htm.
- Chow, V.T. Maidment, D.R. and Mays, L.W. (1988). **Applied Hydrology**. McGraw-Hill Book Company, Singapore.
- CRAHI. (2012). **Type of hydrological models**. [Online]. Available: <http://www.crahi.upc.edu/en/projects/areas-of-expertise/78-tipus-de-models-hidrologics>.
- Department of Disaster Prevention and Mitigation [DDPM]. (2006). **Annual Disaster Report 2006**. [Online]. Available:http://61.19.54.137/public/news01/06_50/k2549.pdf.
- Eastman, J.R. (2003a). **Idrisi Kilimajaro tutorial**. USA: Clark Laboratories, Clark University.
- Eastman, J.R. (2003b). **IDRISI Kilimanjaro: Guide to GIS and Image Processing**. USA: Clark Laboratories, Clark University.
- Faculty of Engineering, Chiang Mai University. (2007). **Flood prevention and warning system for Chiang Mai municipal area** (in Thai). [Online]. Available: <http://cendru.net/>.
- Floodsite. (2012). **Flood types**. [Online]. Available: <http://www.floodsite.net/juniorfloodsite/html/en/student/thingstoknow/hydrology/floodtypes.html>.
- Glossary of Meteorology. (2000). **American Meteorological Society** [Online]. Available: <http://amsglossary.allenpress.com/glossary/search?id=flood1>.

- Hoedjes, J.C.B., Chehbouni, A., Jacob, F., Ezzahar, J. and Boulet, G. (2008). Deriving daily evapotranspiration from remotely sensed instantaneous evaporative fraction over olive orchard in semi-arid Morocco. **Journal of Hydrology**. 354(1-4): 53-64.
- Hydrology and Water Management Center for Upper Northern Region. (2012). **Runoff monitoring and report** (in Thai). [Online]. Available: <http://hydro-1.net/>.
- Jensen, J.R. (2005). **Introduction digital image processing: A remote sensing perspective**. USA: Prentice Hall.
- Jothityangkoon, C., Sivapalan, M., and Farmer, D.L. (2001). Process controls of water balance variability in a large semiarid catchment: Downward approach to hydrological model development. **Journal of Hydrology**. 254: 174-198.
- Jothityangkoon, C. and Sivapalan, M. (2003). Towards estimation of extreme flood: Examination of the roles of runoff process changes and floodplain flows. **Journal of Hydrology**. 281: 206-229.
- Jothityangkoon, C. and Hirunteeyakul, C. (2006). **Hydrological model development for water balance study in subcatchment of Mun River**. School of survey engineering, Suranaree University of Technology.
- Jothityangkoon, C. and Hirunteeyakul, C. (2009). **The prediction Probable Maximum Flood (PMF) Case study; Bhumibol Dam**. Bangkok: EGAT.

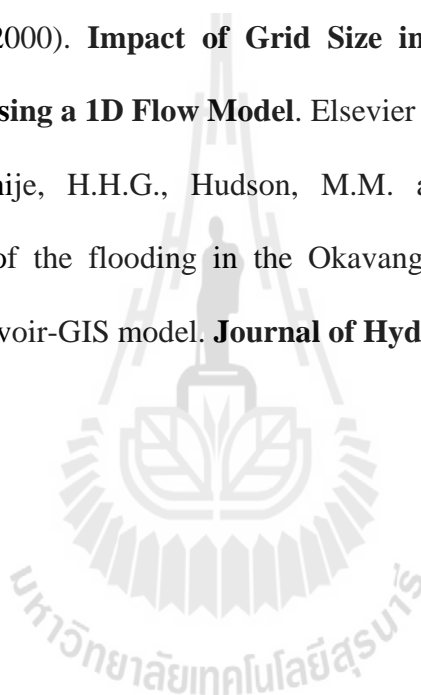
- Khan, S., Hafeez, M.M., Rana, T. and Mushtaq, S. (2008). Enhancing water productivity at the irrigation system level: A geospatial hydrology application in the Yellow River Basin. **Journal of Arid Environments**. 72(6): 1046-1063.
- Klemes, V. (1983). Conceptualisation and scale in hydrology. **J. Hydrol.** 65: 1-23.
- Kongo, V.M. and Jewitt, G.P.W. (2006). Preliminary investigation of catchment hydrology in response to agricultural water use innovations: A case study of the Potshini catchment-South Africa. **Physics and Chemistry of the Earth, Parts A/B/C**. 31(15-16): 976-987.
- Kripalani, R.H. and Kulkarni, A. (1997). Rainfall variability over south-east Asia connections with Indian monsoon and ENSO extremes: new perspectives. **International Journal of climatology**. 17: 1155-1168.
- Liang, D., Falconer, R.A. and Lin, B. (2007). Coupling surface and subsurface flows in a depth averaged flood wave model. **Journal of Hydrology**. 337: 147-158.
- Liu, Y.B., Gebremeskel, S., Smedt, F.D., Hoffmann, L. and Pfister, L. (2003). A diffusive transport approach for flow routing in GIS-based flood modeling. **Journal of Hydrology**. 283: 91-106.
- Markov, A. (1907). Extension of the limit theorems of probability theory to a sum of variables connected in a chain. The Notes of the Imperial Academy of Sciences of St. Petersburg, VIII Series. **Physio-Mathematical College**. 1(9): 9.

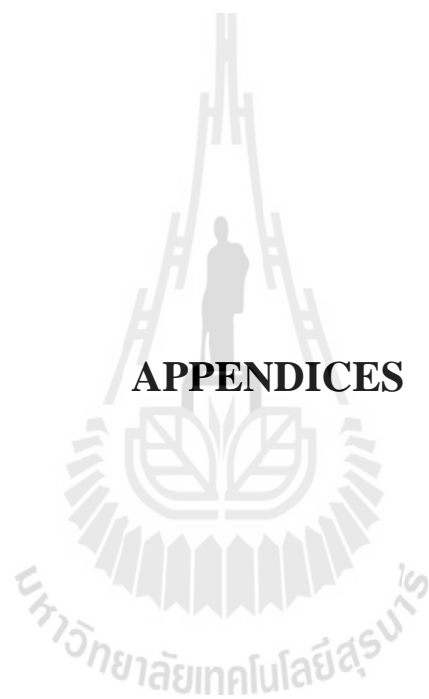
- McCabe, M.F. and Wood, E.F. (2006). Scale influences on the remote estimation of evapotranspiration using multiple satellite sensors. **Remote Sensing of Environment**. 105(4): 271-285.
- McCabe, M.F., Wood, E.F., Pan, W.M., Sheffield, J., Gao, H. and Su, H. (2008). Hydrological consistency using multi-sensor remote sensing data for water and energy cycle studies. **Remote Sensing of Environment**. 112(2): 430-444.
- Mello, C.R., Viola, M.R., Norton, L.D., Silva, A.M. and Weimar, F.A. (2008). Development and application of a simple hydrologic model simulation for a Brazilian headwater basin. **CATENA**. 75(3): 235-247.
- Merlin, O., Chehbouni, A., Kerr, Y.H. and Goodrich, D.C. (2006). A downscaling method for distributing surface soil moisture within a microwave pixel: Application to the Monsoon '90 data. **Remote Sensing of Environment**. 101(3): 379-389.
- Moriasi, D.N., Arnold, J.G., Van Liew M.W., Bingner, R.L., Harmel, R.D. and Veith, T.L. (2007). Model Evaluation Guidelines for Systematic Quantification of Accuracy in Watershed Simulations. **American Society of Agricultural and Biological Engineers**. 50(3): 885-900.
- Odblog, (2008). **A flood hydrograph**. [Online]. Available: http://geodonn.blogspot.com/2008_10_01_archive.html.
- Pellarin, T., Laurent, J.P., Cappelaere, B., Decharme, B., Descroix, L. and Ramier, D. (2009). Hydrological modelling and associated microwave emission of a semi-arid region in South-western Niger. **Journal of Hydrology**. 375(1-2): 262-272.

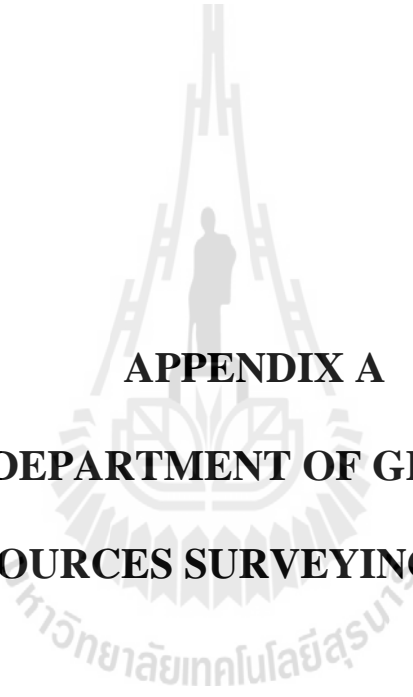
- Ramlal, B. and Baban, S.M.J. (2007). Developing a GIS based integrated approach to flood management in Trinidad, West Indies. **Journal of Environmental Management**. 88: 1131-1140.
- Sahoo, G.B., Ray, C. and Carlo, E.H.D. (2006). Calibration and validation of a physically distributed hydrological model, MIKE SHE, to predict streamflow at high frequency in a flashy mountainous Hawaii stream. **Journal of Hydrology**. 327: 94-109.
- Sansena T. and Bhaktikul K. (2008). **The Application of Hydraulic Model with Geographic Information System to Flood Risk Mapping Creation in Mae Klong River**. Thailand: Geo-Informatic Scientist, Geo-Informatics and Space Technology Department Agency (Public Organization).
- Schmugge, T.J., Kustas, W.P., Ritchie, J.C., Jackson, T.J., and Rango, A. (2002). Remote Sensing of Hydrology. **Advances in Water Resources**. 25: 1367-1385.
- Schulz, M. and Matthies, M. (2007). **Runoff of Pesticides: Achievements and Limitations of Modelling agrochemical Dislocation from Non-Point Sources at Various Landscape Related Scales** [Online]. Available: [http:// www.livingreviews.org/lrl-2007-1](http://www.livingreviews.org/lrl-2007-1).
- Seth, S.M. (2006). **Role of Remote Sensing and GIS inputs in physically based Hydrological Modeling** [Online]. Available: <http://www.gisdevelopment.net/application/nrm/water/overview/wato0006pf.htm>.

- Shultz, M.J. (2007). **Comparison of Distributed Versus Lumped Hydrologic Simulation Models Using Stationary and Moving Storm Events Applied to Small Synthetic Rectangular Basins and an Actual Watershed Basin**. Ph.D. THESIS, The University of Texas at Arlington.
- Singh, V.P. (1992). **Elementary Hydrology**. New Jersey: Prentice Hall, Englewood Cliffs.
- Sinnakaudan, S.K., Ghani, A.A., Ahmad, M.S.S. and Zakaria, N.A. (2002). Flood risk mapping for Pari River incorporating sediment transport. **Environmental Modelling & Software**. 18: 119-130.
- Smith, D., Li, J. and Banting, D. (2004). A PCSWMM/GIS-based water balance model for the Reesor Creek watershed. **Atmospheric Research**. 77: 388-406.
- Sombut Umuang. (2006). **Application of Geographic Information Systems (GIS) and remotely sensed data** to the management of disasters for landslides – debris flow and inundation in northern in 2006 (in Thai). GISTHA, Department of Geology Faculty of Science, Chulalongkorn University.
- Su, Z.B. and Troch, P.A. (2003). Applications of quantitative remote sensing to hydrology. **Physics and Chemistry of the Earth, Parts A/B/C**. 28(1-3): 1-2.
- Vivoni, E.R., Gebremichael, M., Watts, C.J., Bindlish, R. and Jackson, T.J. (2008). Comparison of ground-based and remotely-sensed surface soil moisture estimates over complex terrain during SMEX04. **Remote Sensing of Environment**. 12(2): 314-325.

- Von Neumann, J. (1966). **Theory of Self-reproducing Automata**. Illinois: University of Illinois Press.
- Wang, X., Melesse, A.M. and Yang, W. (2006). Influences of potential evapotranspiration estimation methods on SWAT's hydrologic simulation in a northwestern Minnesota watershed. **Journal: Transactions of the ASABE**. 49(6): 1755-1771.
- Werner, M.G.F. (2000). **Impact of Grid Size in GIS Based Flood Extent Mapping Using a 1D Flow Model**. Elsevier Science Ltd.
- Wolski, P., Savenije, H.H.G., Hudson, M.M. and Gumbricht, T. (2006). Modelling of the flooding in the Okavango Delta, Botswana, using a hybrid reservoir-GIS model. **Journal of Hydrology**. 331: 58-72.







APPENDIX A

DATA OF DEPARTMENT OF GROUNDWATER

RESOURCES SURVEYING HOLES

A.1 Data of DGWR surveying holes.

Name holes	Easting	Northing	shell1	type	shell2	type1	shell3	type2	shell4	type3	shell5	type4
DG122	517100	2148100	30.49	clay+sand	4.57	rock	0.00		0.00			
DG123	512243	2072208	10.67	clay	7.62	rock	0.00		0.00			
DG125	517454	2071142	35.06	clay+sand laterite brown,	12.20	rock clay brownish	0.00		0.00			
DG14	497700	2122300	3.05	clayey	24.39	orange, sandy	1.52	gravel	4.58	clay		
DG19	517900	2071890	9.15	clay	3.05	sand/gravel	15.24	clay	10.67	grevel	4.57	gravel
DG2	513400	2087100	10.67	clay	9.15	gravel	4.57	gravel	0.00			
DG222	518842	2123066	9.00	clay/laterite	7.50	clay	7.50	top soil	0.00			
DG228	462161	2162653	4.50	clay/sand	6.00	sand	4.50	clay	1.50	sand	33	clay
DG229	462384	2162645	7.50	clay/gravel	28.50	clay	3.00	sand	9.00	clay	3	sand
DG23	518818	2138189	6.10	clay	3.05	clay	6.09	gravel	7.63	grevel	4.57	clay
DG230	460600	2164329	4.50	clay	6.00	sand	7.50	clay	4.50	sand	3	clay
DG238	497525	2143212	19.50	sand+gravel	28.50	clay/sand	4.50	clay/sand	15.00	clay	3	sand
DG239	495479	2102226	4.50	clay	6.00	sand	19.50	gravel	0.00			
DG240	502016	2093976	6.00	clay	4.50	laterite	35.00	sand	40.00	gravel		
DG241	505304	2086902	1.50	sand	33.00	clay/laterite	1.50	sand	6.00	clay	3	sand
DG244	492561	2112900	1.83	clay	1.83	gravel	1.83	clay	5.03	gravel	4.57	clay
DG26	516790	2142861	1.52	silt	10.68	clay	19.81	clay	6.10	clay	7.62	sandstone
DG31	518900	2080600	1.52	rock	32.02	limestone	0.00		0.00			
DG4	513000	2088300	6.10	sand	4.57	gravel	10.67	gravel	0.00			
DG47	517800	2144200	27.44	clay/sand	1.52	rock	0.00		0.00			
DG48	499600	2112250	18.29	clay/sand	6.10	rock	0.00		0.00			
DG49	505500	2112200	7.62	clay	4.58	rock	0.00		0.00			
DG50	518300	2139950	0.00		0.00		0.00		0.00			
DG82	517875	2087800	13.72	clay/sand	10.67	rock	0.00		0.00			

A.1 (Continued).

Name holes	Easting	Northing	shell1	type	shell2	type1	shell3	type2	shell4	type3	shell5	type4
DG85	516650	2085250	35.06	clay	1.53	rock	0.00		0.00			
DG97	515886	2143523	30.49	clay	4.57	clay	8.67	sandstone	0.00			
DMR3 9	504040	2084050	9.15	clay	1.52	sand	1.53	sand	1.52	clay	12.19	clay
DMR4 1	514400	2079940	6.10	clay	1.52	filled deposit	4.58	clay	1.52	laterite	15.24	clay
G1000	498390	2097890	6.10	sand	16.77	gravel	0.00		0.00			
G1004	496600	2085300	22.87	clay	6.09	sand	13.72	gravel	0.00			
G1005	496700	2091640	6.10	clay	6.10	gravel	18.29	gravel sand/sand	0.00			
G1006	491850	2094800	24.39	clay	4.57	clay	16.77	stone	0.00			
G1007	491790	2097500	22.87	clay/gravel	1.52	sandstone	0.00		0.00			
G1019	498000	2077000	1.52	clay	1.53	sand	6.10	clay	1.52	sand	4.57	clay
G1027	494800	2091738	1.52	sand	4.58	gravel	4.57	gravel	12.20	clay	7.62	gravel
G1029	502600	2075390	4.57	clay	9.15	gravel	7.62	clay	21.34	gravel		
G1041	517250	2087300	7.62	clay	10.67	clay	3.05	tuff	0.00			
G1042	516400	2085390	13.72	clay	3.05	gravel	6.10	clay	4.57	gravel	6.1	clay
G1043	516790	2079690	12.20	clay	1.52	laterite	12.19	clay	3.05	gravel	1.53	clay
G1044	510600	2080100	3.05	sand	0.00		0.00		0.00			
G1053	518500	2140600	1.52	clay	32.02	gravel	0.00		0.00			
G1054	500100	2093100	16.77	sand	19.82	gravel	0.00		0.00			
G1056	499540	2084250	1.52	sand	19.82	gravel	9.15	sand	0.00			
G1059	518700	2082100	6.10	sand	6.10	sandstone	0.00		0.00			
G1062	510700	2087000	4.57	clay	6.10	gravel/sand	19.82	gravel	0.00			
G1063	489700	2110190	10.67	clay	13.72	gravel	3.05	gravel	1.52	clay	32.02	sand
G1064	484790	2109690	1.52	clay	9.15	sand	19.82	granite	0.00			

A.1 (Continued).

Name holes	Easting	Northing	shell1	type	shell2	type1	shell3	type2	shell4	type3	shell5	type4
G1065	483000	2112100	1.52	clay	10.68	sand	18.29	sandstone	0.00			
G1066	501100	2124000	24.39	clay/sand	0.00		0.00		0.00			
G1067	501140	2119940	10.67	clay	7.62	sandstone	0.00		0.00			
G1068	507500	2113390	6.10	clay	9.14	sandstone	0.00		0.00			
G1091	517340	2144440	13.72	clay	19.82	sandstone	0.00		0.00			
G1107	495600	2079500	16.77	sandy clay	9.14	clay/gravel	19.82	clay	33.54	sand/gravel		
G1109	518900	2073300	7.62	clay	10.67	shale	16.77	sand	0.00			
G1117	498600	2105890	13.72	clay/laterite	9.15	rock	0.00		0.00			
G1118	500750	2116300	7.62	sandy clay	15.25	gravel	0.00		0.00			
G1119	498200	2116890	4.57	clay	19.82	granite	0.00		0.00			
G1122	517150	2142000	3.05	clay	12.19	slate	3.05	sandstone	0.00			
G126	495750	2079100	1.52	clay	6.10	clay	13.72	boulder	10.67	gravel	6.1	gravel
G132	512000	2071100	1.52	sand	1.53	clay	7.62	sand	4.57	clay	1.53	gravel
G133	495890	2079600	54.88	gniess	1.52	clay	7.62	gniess	3.05	clay	21.43	gniess sand/grav
G134	513040	2072350	1.52	clay	1.53	sand	3.05	clay	6.10	sand	18.29	el
G137	500692	2075901	1.52	clay	1.53	sand	3.05	clay	3.05	sand	3.05	clay
G139	498000	2082750	19.82	sand	44.20	gravel	0.00		0.00			
G154	495140	2078500	24.39	sand	0.00		0.00		0.00			
G155	495890	2078050	16.77	sand	7.62	gravel	9.15	clay	3.05	sand/gravel	3.04	clay
G156	495950	2086800	10.00	sand	10.00	clay	10.00	sand	5.00	clay	10	sand
G193	506100	2071690	99.09	clay	18.29	sand/gravel	1.52	clay	1.53	sand/gravel	1.52	clay
G194	510540	2069640	25.91	sand	13.72	sand/clay	0.00		0.00			
G195	511250	2071890	3.05	sand	21.34	sand/clay	6.10	clay	42.68	sand/clay	12.2	sand
G196	508950	2083350	4.57	clay	3.05	sand	53.36	gravel	9.14	sand		
G198	501290	2089600	28.96	clay	50.31	clay/sand	54.88	gravel	15.24	clay		

A.1 (Continued).

Name holes	Easting	Northing	shell1	type	shell2	type1	shell3	type2	shell4	type3	shell5	type4
G226	494700	2090390	1.52	top soil	6.10	clay	1.53	gravel	4.57	gravel/clay	1.52	clay
G227	494500	2090890	6.10	top soil	7.62	clay	13.72	gravel	50.30	clay	13.72	gravel
G260	498500	2079440	19.82	clay	10.67	gravel	0.00		0.00			
G261	508250	2087500	1.52	sand	22.87	gravel	0.00		0.00			
G262	517000	2076050	12.20	clay	24.39	sand/gravel	9.14	gravel	0.00			
G278	496525	2140675	15.24	clay	9.15	limestone	0.00		0.00			
G279	496550	2151700	18.29	clay	16.77	gravel	10.67	sandstone	0.00			
G282	495000	2162000	30.49	gravel	0.00		0.00		0.00			
G294	513700	2079500	18.29	clay	15.25	gravel	9.14	gravel	0.00			
G300	505790	2076800	7.62	clay	3.05	sand/gravel	3.05	clay	6.10	gravel	7.62	clay
G313	503763	2069062	1.52	clay	18.30	g	7.62	g/c	1.52	s	16.77	g/c
G327	518600	2143400	19.82	clay	22.86	sandstone	0.00		0.00			
G332	514000	2082800	4.57	siltstone	1.53	c/g	4.57	c	12.20	c	7.62	andesite
G347	515400	2074300	7.62	s	6.10	g	16.77	c	9.14	s	16.77	c
G350	513340	2070640	4.57	c/s	19.82	s	6.10	g/c	19.81	s/g	18.3	c
G351	514650	2070350	1.52	s/c	3.05	c	1.53	c/s	13.72	s/c	24.39	c/s
G354	516250	2069500	3.05	s	6.10	c	12.19	g	13.72	s	3.05	g
G355	518290	2069800	3.05	c	1.52	g	15.25	c	12.19	g		
G356	514700	2071000	3.05	s	7.62	c	9.15	g	1.52	s	6.1	c
G357	509500	2069640	3.05	c	16.77	s	6.09	g	3.05	c		
G360	512000	2069140	3.05	c	1.52	s	1.53	c	7.62	s	6.1	c
G362	513090	2070100	3.05	laterite	4.57	c	3.05	s	94.51	c	6.1	s
G364	509790	2074550	4.57	c	1.53	s	6.10	g	7.62	c	4.57	g
G366	512200	2071690	16.77	c	1.52	s	99.09	c	4.57	s	19.82	s

A.1 (Continued).

Name holes	Easting	Northing	shell1	type	shell2	type1	shell3	type2	shell4	type3	shell5	type4
G368	510000	2078750	7.62	c	4.58	g	4.57	c	3.05	s	25.91	g
G369	510950	2078750	13.72	c	4.57	s	6.10	c	16.77	s	18.29	g
G370	511950	2079690	3.05	s	3.05	c	1.52	g	7.62	c	1.53	s
G371	511350	2080850	10.67	s	6.10	g/c	38.11	s	3.05	g/c	14.73	c
G373	508750	2081850	7.62	c	3.05	g	1.53	s	80.79	g	9.14	g/s
G374	509390	2082250	4.57	c	4.58	s/g	4.57	s	38.11	g	4.57	s
G375	511100	2076690	10.67	c	7.62	g	13.72	c	21.34	g		
G376	510750	2080000	6.10	c	3.05	g	12.19	c	16.77	g	24.39	s
G378	512775	2081375	1.52	g	12.20	c	1.52	s	1.53	g	1.52	c
G379	507890	2080190	1.52	g	6.10	c	1.48	s	4.62	c	12.19	g
G433	496640	2085140	24.39	c/s	25.91	c/s	0.00		0.00			
G443	485250	2108550	1.52	c	36.59	s	0.00		0.00			
G444	485640	2106940	4.57	c	71.65	s	0.00		0.00			
G445	496850	2088600	12.20	c	19.81	s/g	9.15	c	10.67	s	4.57	c
G450	502000	2071140	1.52	c	1.53	s	6.10	c	10.67	s/g	73.17	quartz
G453	493850	2102250	21.34	c/l	22.87	g	0.00		0.00			
G454	495550	2137825	21.34	c	1.53	filled deposit	10.67	c	18.29	filled deposit		
G455	497450	2148200	3.05	c	3.05	s/g	9.14	shale	0.00			
G463	492540	2095440	6.10	c	6.10	filled deposit	3.04	s	1.53	filled deposit	15.24	s
G464	490000	2098800	9.15	c	6.09	siltstone	0.00		0.00			
G480	496790	2083800	7.62	c	3.05	s	3.05	c	62.50	g		
G482	497600	2146400	12.20	c	12.19	shale	0.00		0.00			
G494	497655	2146488	19.82	c	22.86	rock	0.00		0.00			

A.1 (Continued).

Name holes	Easting	Northing	shell1	type	shell2	type1	shell3	type2	shell4	type3	shell5	type4
G495	497150	2144250	1.52	c	4.58	filled deposit	35.06	c	4.57	filled deposit	6.1	c
G496	498575	2147552	22.87	c	12.19	shale	0.00		0.00			
G497	495850	2135800	13.72	c	41.16	s	0.00		0.00			
G498	497500	2138400	4.57	c	1.53	quartz	1.52	c	18.29	filled deposit	3.05	c
G499	494000	2112800	3.05	c	3.05	s	16.77	quartz	9.14	s	15.25	quartz
G500	499000	2151000	3.05	c	32.01	shale	0.00		0.00			
G501	492200	2115550	3.05	quartz	6.10	s	6.09	quartz	4.58	c	3.05	s
G502	491350	2090300	7.62	s	18.29	c	16.77	s	6.10	shale		
G503	516450	2072550	3.05	c	1.52	s	38.11	c	28.97	s		
G504	517900	2073800	1.52	c	16.77	s	12.20	c	1.52	s		
G505	517650	2071800	4.57	quartz	7.63	c	12.19	s	1.52	c	32.02	s
G506	517290	2073350	15.24	quartz	0.67	c	16.10	s	3.05	c	27.44	s
G509	508140	2074600	12.20	c	18.29	s	3.05	c	3.05	s	12.19	c
G510	516150	2071690	9.15	c	4.57	s	35.06	c	27.44	s		
G511	508850	2076750	6.10	c	4.57	s	1.53	c	35.06	s	3.04	c
G512	516950	2070440	6.10	c	4.57	s	4.57	c	30.49	quartz	30.49	s
G514	498040	2086690	22.87	c	3.04	granite washed	56.41	c	47.25	granite washed		
G515	488200	2102100	19.82	c	1.52	granite washed	10.67	c	7.62	granite washed	9.15	c
G516	491890	2093000	12.20	c	13.71	s	1.53	c	10.67	s		
G517	487140	2103250	21.34	c	16.77	s	0.00		0.00			
G518	497350	2124800	4.57	c	4.58	filled deposit	21.34	shale	0.00			
G520	508850	2078850	9.15	c	10.67	s	3.05	c	15.24	c	22.87	s
G521	505600	2082600	6.10	c	3.05	g	7.62	c	4.57	quartz	6.1	c

A.1 (Continued).

Name holes	Easting	Northing	shell1	type	shell2	type1	shell3	type2	shell4	type3	shell5	type4
G522	502100	2090800	25.91	c	15.25	quartz	9.14	c	0.00			
G523	498250	2098190	6.10	filled deposit	7.62	c	79.27	g	0.00			
G530	503850	2112640	24.39	c	33.54	rock	0.00		0.00			
G535	506390	2114600	3.05	l	42.68	shale	0.00		0.00			
G539	486290	2106000	3.05	c	12.19	s	0.00		0.00			
G541	507640	2069440	12.20	c	9.14	g	35.06	c	0.00			
G542	505200	2074000	4.57	c	16.77	quartz	12.20	c	18.29	s/g		
G543	503350	2083640	3.05	c	1.52	g	9.15	c	19.82	quartz		
G544	502450	2083800	4.57	c	3.05	g	1.53	c	18.29	quartz	7.62	c
G545	505100	2083800	6.10	c	27.44	g	12.19	quartz	3.05	c		
G546	502540	2081550	7.62	c	25.92	quartz	0.00		0.00			
G547	502350	2082750	7.62	c	24.39	quartz	1.53	c	0.00			
G548	500140	2091250	7.62	c	32.01	quartz	0.00		0.00			
G549	508040	2085940	6.10	g	4.57	c	18.29	quartz	3.05	c		
G550	498640	2092640	6.10	c	10.67	g	4.57	c	21.34	quartz	6.1	c
G551	493350	2090750	21.34	c	3.05	quartz	22.87	c	4.57	s	4.57	c
G552	490850	2091250	15.24	c	4.58	s	1.52	c	1.53	s		
G553	490640	2092350	10.67	c	13.72	s	0.00		0.00			
G554	492640	2095250	7.62	c	7.62	filled deposit	0.00		0.00			
G555	491500	2097440	9.15	c	6.09	filled deposit	7.63	c	7.62	s		
G556	488950	2099800	4.57	c	13.43	rock	0.00		0.00			
G557	516900	2080100	6.10	c	6.10	filled deposit	82.31	c	6.10	filled deposit		
G565	504200	2115500	12.20	c	10.67	filled deposit	32.01	c	0.00			
G566	501540	2089190	10.67	c	3.05	g	13.72	quartz	1.52	c	25.92	quartz

A.1 (Continued).

Name holes	Easting	Northing	shell1	type	shell2	type1	shell3	type2	shell4	type3	shell5	type4
G567	507140	2089550	15.24	c	19.82	filled deposit	1.53	c	18.29	filled deposit		
G584	507500	2079300	6.10	c	3.05	quartz	1.52	c	1.53	s	1.52	c
G585	502500	2080640	6.10	c	33.53	quartz	0.00		0.00			
G591	492350	2114250	3.05	c	3.05	c	18.29	c	3.05	s	3.05	quartz
G593	500640	2076890	1.52	c	4.58	s/g	4.57	s	10.67	quartz filled	15.25	g/s
G595	494750	2072050	1.52	s/c	1.53	s	1.52	c	4.58	deposit	6.09	c
G596	506540	2078440	7.62	c	7.62	s	4.58	quartz	1.52	g	1.53	s
G598	513540	2081600	3.05	c	1.52	l	7.63	c	9.14	s	7.62	s/c
G599	514950	2077800	3.05	g	10.67	c	1.52	g	18.30	c	3.05	g
G609	510000	2072850	25.91	c	7.63	s	9.14	c	33.54	s		
G610	511290	2071300	19.82	c	7.62	c/g	64.02	c	0.00			
G611	494100	2106550	1.52	c	4.58	quartz	9.14	c	1.53	s	18.29	c
G612	486750	2104300	4.57	c	1.53	s	7.62	c	1.52	s	1.53	c
G627	506790	2076440	15.24	c	4.58	s	1.52	c	3.05	quartz	1.52	c
G629	508750	2079550	18.29	c	4.58	s	4.57	c	3.05	quartz	12.19	c
G630	507950	2081640	12.20	c	6.09	g	7.62	c	4.58	s	14.57	quartz
G631	513500	2083050	15.24	c	4.58	quartz	25.91	c	3.05	g	9.15	c
G632	509290	2077440	16.77	c	9.14	s	18.30	c	32.01	s		
G634	502540	2087640	12.20	s/g	6.09	quartz	7.62	c	50.31	quartz		
G636	511640	2087250	7.62	s	3.05	g	1.53	s	3.04	g	24.39	quartz
G637	509500	2084390	7.62	c	3.05	s	4.57	quartz	1.53	c	6.1	quartz
G638	518150	2069690	3.05	c	6.10	s	3.05	c	3.04	s	4.58	c
G639	514900	2074190	1.52	s	10.68	c	3.04	s	18.30	c	7.62	s
G640	511750	2071890	24.39	c/s	82.33	g/s	0.00		0.00			

A.1 (Continued).

Name holes	Easting	Northing	shell1	type	shell2	type1	shell3	type2	shell4	type3	shell5	type4
G655	493200	2106850	21.34	c	1.53	s	13.72	c	7.62	s/g	3.05	c
G656	493500	2093000	10.67	c	1.53	s	3.04	c	15.25	s	3.05	g
G657	508250	2082050	1.52	top soil	12.20	c	3.05	s	6.10	c	15.24	g
G658	509950	2073140	4.57	c	1.53	s	10.67	c	4.57	s	45.73	c
G659	503850	2081940	3.05	c	3.05	s	13.72	g	28.96	quartz	12.2	s
G660	510390	2085750	1.52	c	4.58	s	6.10	c	3.04	s/g	38.11	quartz
G661	499100	2095600	15.24	c/s	13.72	quartz	4.58	s	27.44	quartz		
G662	500640	2086750	6.10	c	39.63	quartz	0.00		0.00			
G663	503750	2084940	13.72	c	6.10	s	3.05	c	19.81	quartz	33.54	s
G664	499700	2087390	4.57	c	38.11	quartz	0.00		0.00			
G669	502140	2118350	3.05	c	24.39	rock	0.00		0.00			
G689	518400	2078140	27.44	c	18.29	sandstone	0.00		0.00			
G693	496890	2096850	12.20	c/s	9.14	g	0.00		0.00			
G697	510850	2086750	9.15	c	9.14	g	0.00		0.00			
G706	505540	2073390	21.34	c/s	54.88	c/g	0.00		0.00			
G721	492700	2145390	15.24	c/s	25.92	rock	0.00		0.00			
G722	496750	2120390	24.39	c/l	91.46	c/l	36.59	sandstone	0.00			
G724	508250	2074300	15.24	c/s	7.63	c/g	47.25	c/s	0.00			
G725	511640	2085640	10.67	c/s	12.20	c/g	3.04	c/s	0.00			
G726	514840	2085940	3.05	top soil	36.58	c	24.39	shale	0.00			
G732	501750	2117250	15.24	c/s	12.20	rock	0.00		0.00			
G741	513750	2082350	13.72	c	1.52	s	3.05	g	41.16	c	6.1	s/g
G742	514000	2082800	4.57	c	4.58	c/s	6.09	s/g	1.53	c	1.52	c/s
G743	499290	2092600	10.67	c	4.57	s	3.05	g	21.34	s	12.2	s/g
G744	499750	2112250	15.24	c	21.35	g	0.00		0.00			

A.1 (Continued).

Name holes	Easting	Northing	shell1	type	shell2	type1	shell3	type2	shell4	type3	shell5	type4
G745	499790	2111640	10.67	c	10.67	g	0.00		0.00			
G746	501040	2113350	0.00		0.00		0.00		0.00			
G747	505640	2112500	1.52	g	26.30	sandstone	0.00		0.00			
G748	503950	2113390	41.16	c	48.42	s	0.00		0.00			
G749	507600	2113250	4.57	l	14.10	rock	0.00		0.00			
G750	506140	2114640	18.29	shale	36.61	sandstone	0.00		0.00			
G751	502640	2094350	7.62	c	57.93	s/g	0.00		0.00			
G752	502540	2092050	22.87	c	1.52	g	21.34	c	0.00			
G775	514150	2070500	21.34	c/s	67.07	c/s	0.00		0.00			
G776	515590	2070250	21.34	c/s	51.83	c/s	9.15	sandstone	0.00			
					134.1							
G777	510890	2070800	21.34	c/s	5	c/s	0.00		0.00			
G782	513750	2082350	21.34	c	12.20	rock	0.00		0.00			
G783	497000	2088690	13.72	c/l	16.77	g	45.73	c/s	0.00			
G784	494890	2091300	36.59	c/s	15.24	g	0.00		0.00			
G785	497540	2095440	12.20	c/s	15.24	c/g	0.00		0.00			
G786	488290	2102850	10.67	c/s	16.77	sandstone	0.00		0.00			
G787	508350	2074800	21.34	c/s	48.78	c/s	0.00		0.00			
G788	508750	2075500	28.96	c/s	38.11	rock	0.00		0.00			
G789	508350	2074473	21.34	c/s	12.20	c/s	33.53	rock	0.00			
G797	495390	2091500	10.67	c/s	15.24	g	4.58	g/c	0.00			
G799	496890	2088000	38.11	c/s	38.11	s	0.00		0.00			
G800	495250	2076600	27.44	rock	0.00		0.00		0.00			
G801	496040	2091550	6.10	c	4.57	s	27.44	quartz	0.00			
G802	496100	2102100	6.10	s	24.39	sandstone	0.00		0.00			

A.1 (Continued).

Name holes	Easting	Northing	shell1	type	shell2	type1	shell3	type2	shell4	type3	shell5	type4
G805	499850	2091800	3.05	c	19.82	g	0.00		0.00			
G806	507250	2085350	3.05	c	3.05	c/s	28.96	g	0.00			
G807	503850	2081940	3.05	c	7.62	g	3.05	c	1.52	g	1.53	s
G824	497350	2116260	27.44	s/c	9.15	s	85.41	c/s	0.00			
G842	498750	2076750	18.29	c	15.25	g	3.05	c	0.00			
G843	496890	2091000	18.29	s/c	18.30	c	0.00		0.00			
G861	492290	2113390	16.77	c	9.14	rock	16.77	s	0.00			
G862	504890	2072000	3.05	s/c	7.62	c	7.62	s	3.05	c	18.29	sandstone
G872	496140	2106140	6.10	c	9.14	g	0.00		0.00			
G873	504290	2087000	10.67	c	3.05	c/g	16.77	c	24.39	c/g		
G874	507500	2085690	9.15	c/l	10.67	s/c	4.57	c	6.10	s/c	24.39	c/g
G894	494850	2136940	24.39	c/g	3.05	c	12.19	sandstone	0.00			
G896	496890	2141350	16.77	c	10.67	rock	7.62	c	0.00			
G903	505700	2072890	54.88	c	0.00		0.00		0.00			
G905	465890	2092500	48.78	c	0.00		0.00		0.00			
G907	505000	2095100	64.02	c	21.35	c/g	0.00		0.00			
G911	488290	2073000	21.34	c/l	24.39	rock	0.00		0.00			
G914	509390	2073890	60.98	c	0.00		0.00		0.00			
G918	516900	2073500	28.96	c	25.92	sandstone	0.00		0.00			
G919	511200	2069600	7.62	l	7.62	clay/rock	6.10	shale	6.10	rock		
G920	515590	2069500	45.73	c	0.00		0.00		0.00			
G921	516400	2069800	9.15	s/c	9.14	c	6.10	clay/limest one	6.10	clay/rock	6.1	rock
G922	502290	2078300	30.49	c/g	0.00		0.00		0.00			

A.1 (Continued).

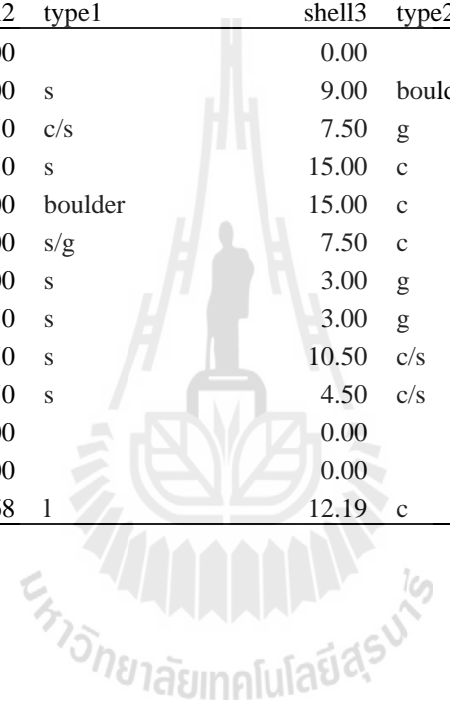
Name holes	Easting	Northing	shell1	type	shell2	type1	shell3	type2	shell4	type3	shell5	type4
G924	509390	2075390	9.15	c/l	6.09	c	6.10	sandstone	9.15	sandstone/1 aterite	9.14	rock/limes tone
G925	498290	2090300	27.44	c	0.00		0.00		0.00			
G926	495500	2098640	48.78	c/g	0.00		0.00		0.00			
G934	497100	2077300	24.39	c/g	24.39	c/s	0.00		0.00			
G936	515400	2087600	38.11	c	16.77	rock	0.00		0.00			
G937	501390	2117800	30.49	c/g	0.00		0.00		0.00			
G938	512590	2069600	54.88	c	0.00		0.00		0.00			
G950	464500	2093000	60.98	c	0.00		0.00		0.00			
G958	508200	2073100	57.93	c	0.00		0.00		0.00			
G959	510290	2075190	6.10	c	3.05	g	1.52	c	3.05	g	1.52	c
G960	511700	2068000	85.37	c/g	0.00		0.00		0.00			
G963	496390	2097250	10.67	c	22.87	g	0.00		0.00			
G964	491850	2092890	45.73	c	0.00		0.00		0.00			
G965	498950	2090850	24.39	c	21.34	c/g	0.00		0.00			
G966	489250	2096500	3.05	silt	12.19	limestone	0.00		0.00			
G967	494640	2100550	21.34	c	21.34	c/g	0.00		0.00			
G975	494290	2106800	24.39	c/l	24.39	c	0.00		0.00			
G983	508890	2073500	4.57	c	6.10	s	10.67	g/s	5.66	c/s		
G984	515590	2084350	16.77	c	1.52	sandstone	9.15	sandstone	0.00			
G987	512290	2074890	39.63	c	0.00		0.00		0.00			
G989	518700	2141900	1.54	c	13.70	sandstone	0.00		0.00			
Q48	497500	2120940	10.67	c	12.20	q/chert	3.04	c	10.68	filled deposit	3.04	c
Q50	494390	2079600	9.15	c	91.46	r	0.00		0.00			

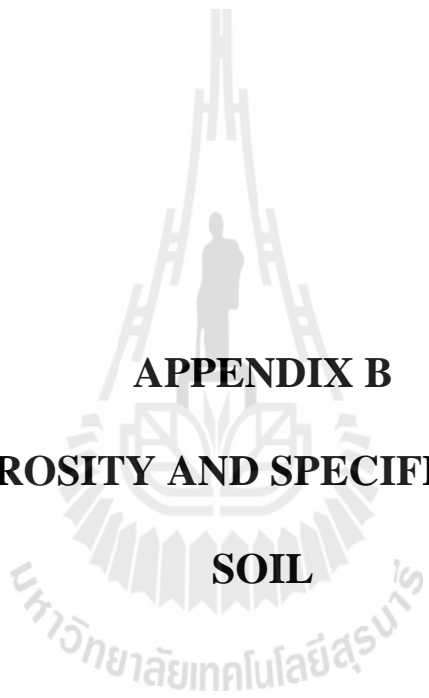
A.1 (Continued).

Name holes	Easting	Northing	shell1	type	shell2	type1	shell3	type2	shell4	type3	shell5	type4
Q52	496950	2077500	1.52	s	1.53	c	3.05	s/g	4.57	c	19.82	s/g
S82	496250	2106000	7.62	c	1.53	s	4.57	g	1.52	q		
S83	508890	2088800	18.29	c	16.77	g	4.57	s/g	0.00			
			246.0									
TG122	512800	2073236	0	c	0.00		0.00		0.00			
			114.0									
TG132	493786	2091157	0	c/g	0.00		0.00		0.00			
TG133	518617	2074934	15.00	c	45.00	r	0.00		0.00			
TG136	516508	2084962	45.00	c	18.00	r	0.00		0.00			
			240.0									
TG140	513500	2071633	0	c	0.00		0.00		0.00			
TG158	509934	2083486	54.00	c/g	0.00		0.00		0.00			
TG159	509465	2081887	60.00	c/g	0.00		0.00		0.00			
TG166	514153	2070644	15.00	c	42.00	c/s	13.50	s/g	13.50	c		
TG167	506238	2074261	9.00	c	10.50	g	21.00	c/s	4.50	s	10.5	c/s
TG168	518500	2078175	22.50	c	3.00	s	3.00	c	6.00	g	69	c
TG170	500102	2067943	13.50	c	1.50	g	7.50	c	22.50	g	3	c
TG181	517129	2073437	3.00	s/c	7.50	c	3.00	s	46.50	c	48	c/g
TG182	518460	2072284	13.50	c	3.00	s	7.50	c	4.50	g	9	c/s
TG185	496629	2084575	9.00	c	1.50	s	21.00	c	3.00	g/c	3	c
TG189	494550	2095000	4.50	c	1.50	s	4.50	c	3.00	s	3	c/s
TG199	517990	2101550	1.50	c	16.50	g	0.00		0.00			
TG20	496332	2104573	24.39	c/g	0.00		0.00		0.00			
TG21	497324	2106124	41.16	c	0.00		0.00		0.00			
TG226	513075	2072250	25.50	c	3.00	s	10.50	c	1.50	s	7.5	c
TG228	498220	2077150	16.50	c	6.00	g	12.00	c	27.00	c/s	9	s

A.1 (Continued).

Name holes	Easting	Northing	shell1	type	shell2	type1	shell3	type2	shell4	type3	shell5	type4
TG23	497868	2100420	40.50	c/g	0.00		0.00		0.00			
TG230	505750	2079000	7.50	c	3.00	s	9.00	boulder	12.00	c	6	s
TG231	518500	2078400	21.00	c	7.50	c/s	7.50	g	6.00	c		
TG232	492770	2114400	25.50	c	4.50	s	15.00	c	3.00	s	10.5	c
TG233	492250	2115550	7.50	c	6.00	boulder	15.00	c	12.00	g	4.5	c
TG240	458600	2070100	10.50	s/c	9.00	s/g	7.50	c	46.50	s		
TG246	499334	2070620	7.50	c	9.00	s	3.00	g	25.50	c	16.5	g
TG248	505233	2070249	9.00	c	7.50	s	3.00	g	9.00	c	3	s
TG313	512437	2074770	7.50	c	4.50	s	10.50	c/s	15.00	c	4.5	s
TG318	506092	2075286	9.00	c	1.50	s	4.50	c/s	3.00	s	10.5	c/s
TG91	491770	2068872	66.00	c/g	0.00		0.00		0.00			
TG92	492310	2070280	90.00	c/g	0.00		0.00		0.00			
W774	518090	2140690	1.52	top soil	10.68	1	12.19	c	9.15	c	9.14	sandstone





APPENDIX B

**EXAMPLE POROSITY AND SPECIFIC YIELD FOR THE
SOIL**

B.1 Example porosity and specific yield for the soil (Tasombat, 1995).

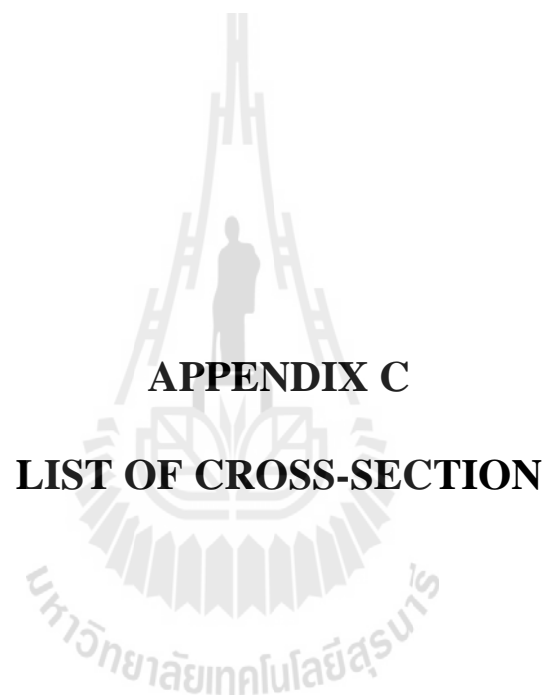
Material	Porosity (%)	Specific yield
Clay	45	3
Sand	35	25
Gravel	25	22
Gravel and Sand	20	16
Sandstone	19	8
Dense Limestone and Shale	5	2
Quartzite, Granite	1	0.5

B.2 Example porosity for the soil (Clapp and Hornberger, 1978).

Soil texture	Porosity (%)
Sand	39.5
Loamy sand	41.0
Sandy loam	43.5
Silty loam	48.5
Loam	45.1
Sandy clay loam	42.0
Silty clay loam	47.7
Clay loam	47.6
Sandy clay	42.6
Silty clay	49.2
Clay	48.2

B.3 Example porosity and specific yield for the soil (Johnson, 1962; 1967).

Material	Porosity (%)	Specific yield
Crushed stone	>30	>20
Coarse gravel	24-36	22
Fine gravel	25-38	22
Coarse sand	31-46	25
Fine sand	25-53	10
Silt	34-61	8
Clay	36-60	3
Sandstone	5-30	5
Limestone	5-50	2
Shale	0-10	3
Basalt	3-35	-
Till	32	16
Peat	92	44



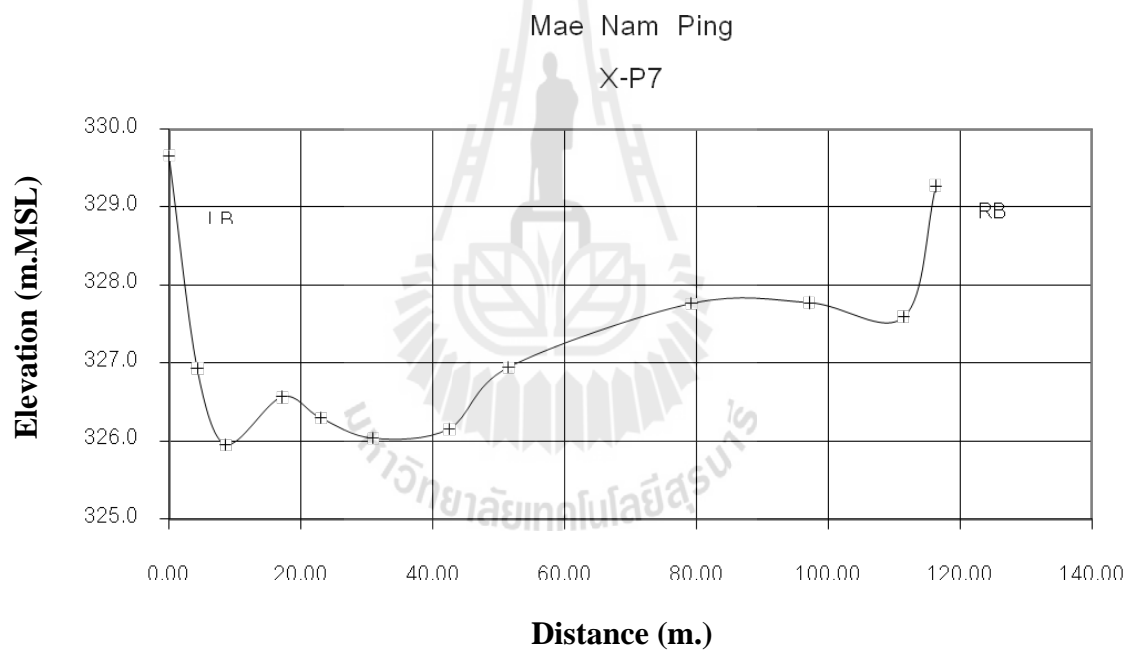
APPENDIX C

LIST OF CROSS-SECTION

C.1 Line X-P7.

MAE NAM PING
Line X-P7

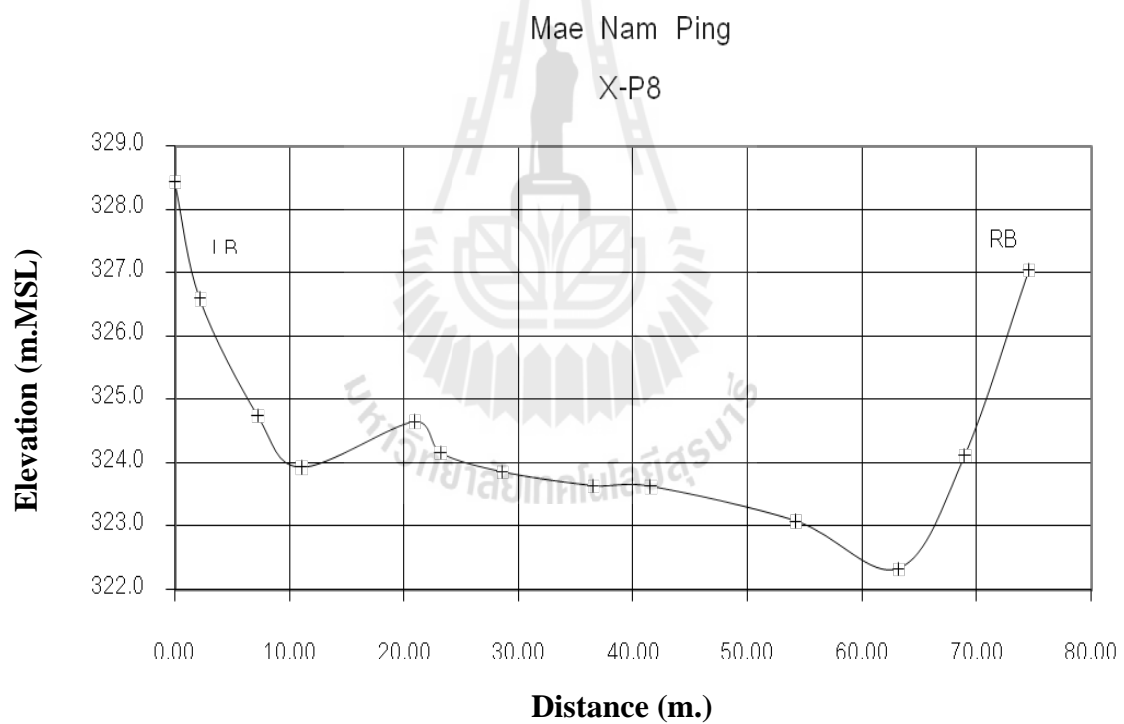
Distance (m)	Elevation (m.AD)	Elevation (m.MSL)	Remark
0.00	0.000	329.656	
4.26	-2.720	326.936	LB
8.56	-3.700	325.956	
17.12	-3.090	326.566	
23.00	-3.360	326.296	
30.92	-3.620	326.036	
42.46	-3.500	326.156	
51.48	-2.710	326.946	RB
79.23	-1.890	327.766	
97.12	-1.880	327.776	
111.47	-2.060	327.596	
116.28	-0.380	329.276	



C.2 Line X-P8.

**MAE NAM PING
Line X-P8**

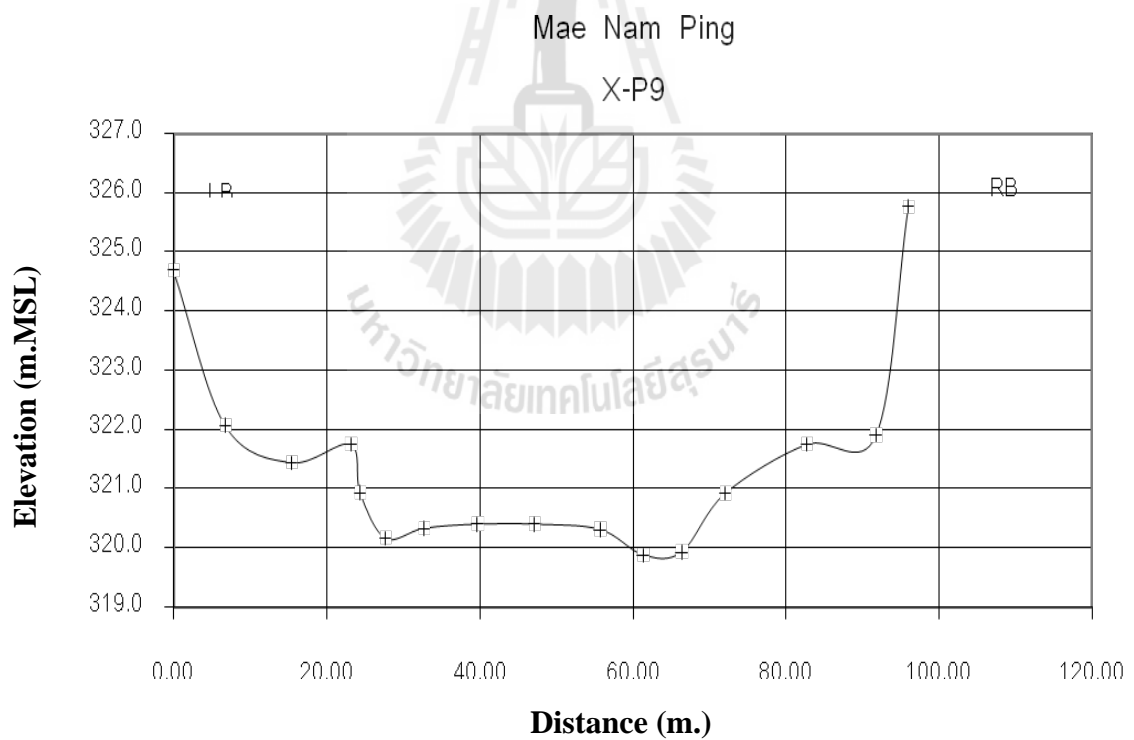
Distance (m)	Elevation (m.AD)	Elevation (m.MSL)	Remark
0.00	0.000	328.429	
2.17	-1.840	326.589	
7.20	-3.680	324.749	
11.03	-4.500	323.929	
20.90	-3.780	324.649	
23.18	-4.270	324.159	LB
28.55	-4.570	323.859	
36.51	-4.790	323.639	
41.51	-4.800	323.629	
54.21	-5.350	323.079	
63.20	-6.100	322.329	
68.96	-4.310	324.119	RB
74.54	-1.390	327.039	



C.3 Line X-P9.

MAE NAM PING
Line X-P9

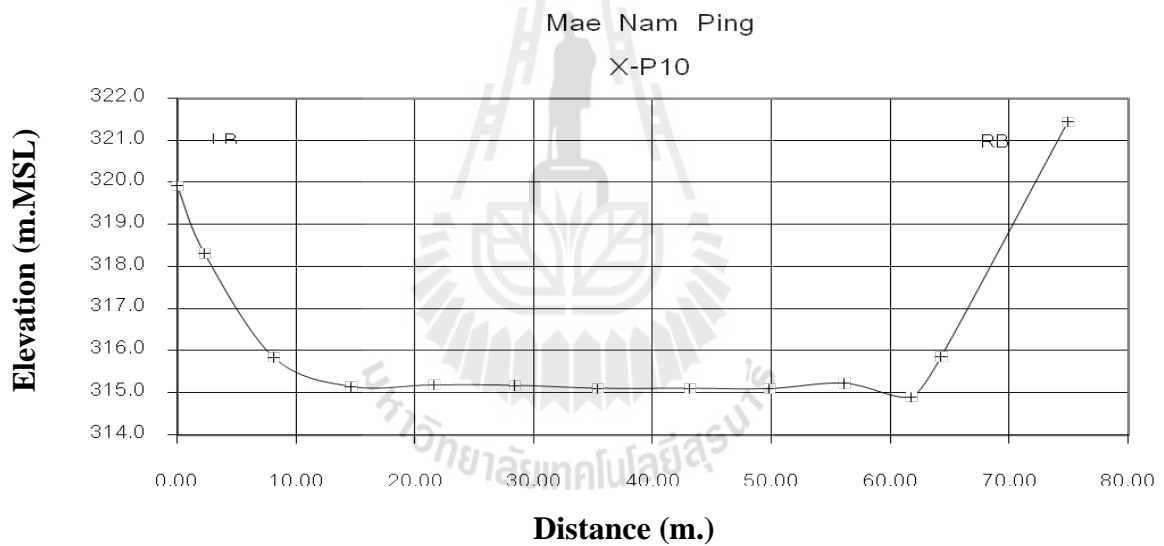
Distance (m)	Elevation (m.AD)	Elevation (m.MSL)	Remark
0.00	-1.070	324.692	
6.71	-3.690	322.072	
15.42	-4.320	321.442	
23.11	-4.010	321.752	
24.35	-4.830	320.932	LB
27.66	-5.600	320.162	
32.71	-5.430	320.332	
39.67	-5.360	320.402	
47.11	-5.360	320.402	
55.70	-5.450	320.312	
61.32	-5.880	319.882	
66.36	-5.830	319.932	
72.03	-4.840	320.922	RB
82.69	-4.010	321.752	
91.73	-3.860	321.902	
95.94	0.000	325.762	



C.4 Line X-P10.

**MAE NAM PING
Line X-P10**

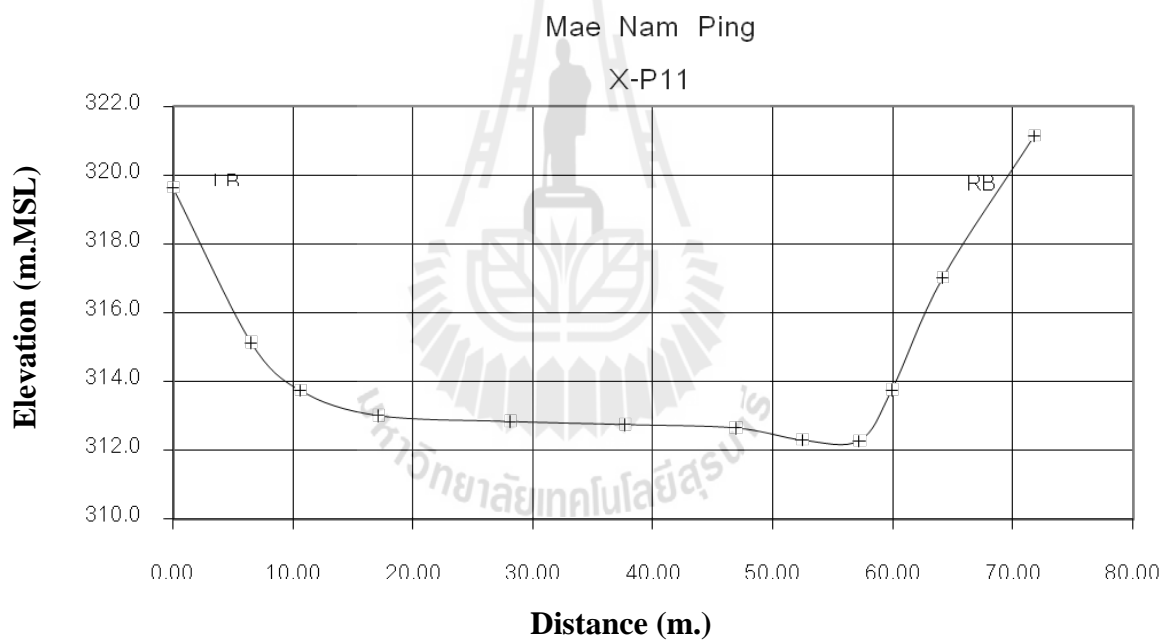
Distance (m)	Elevation (m.AD)	Elevation (m.MSL)	Remark
0.00	0.000	319.922	
2.29	-1.600	318.322	
8.10	-4.070	315.852	LB
14.63	-4.770	315.152	
21.57	-4.730	315.192	
28.36	-4.740	315.182	
35.37	-4.810	315.112	
43.09	-4.810	315.112	
49.79	-4.820	315.102	
56.13	-4.690	315.232	
61.77	-5.010	314.912	
64.27	-4.060	315.862	RB
74.93	1.520	321.442	



C.5 Line X-P11.

**MAE NAM PING
Line X-P11**

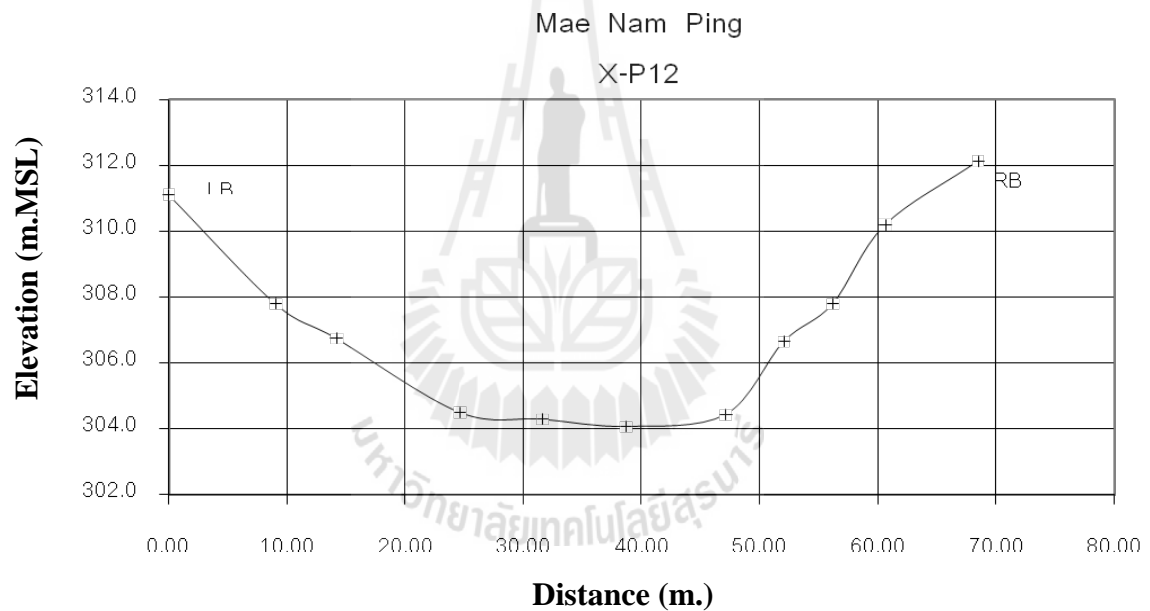
Distance (m)	Elevation (m.AD)	Elevation (m.MSL)	Remark
0.00	0.000	319.629	
6.51	-4.500	315.129	
10.58	-5.890	313.739	LB
17.08	-6.620	313.009	
28.08	-6.790	312.839	
37.64	-6.880	312.749	
46.89	-6.980	312.649	
52.43	-7.330	312.299	
57.20	-7.350	312.279	
59.91	-5.870	313.759	RB
64.14	-2.620	317.009	
71.77	1.500	321.129	



C.6 Line X-P12.

**MAE NAM PING
Line X-P12**

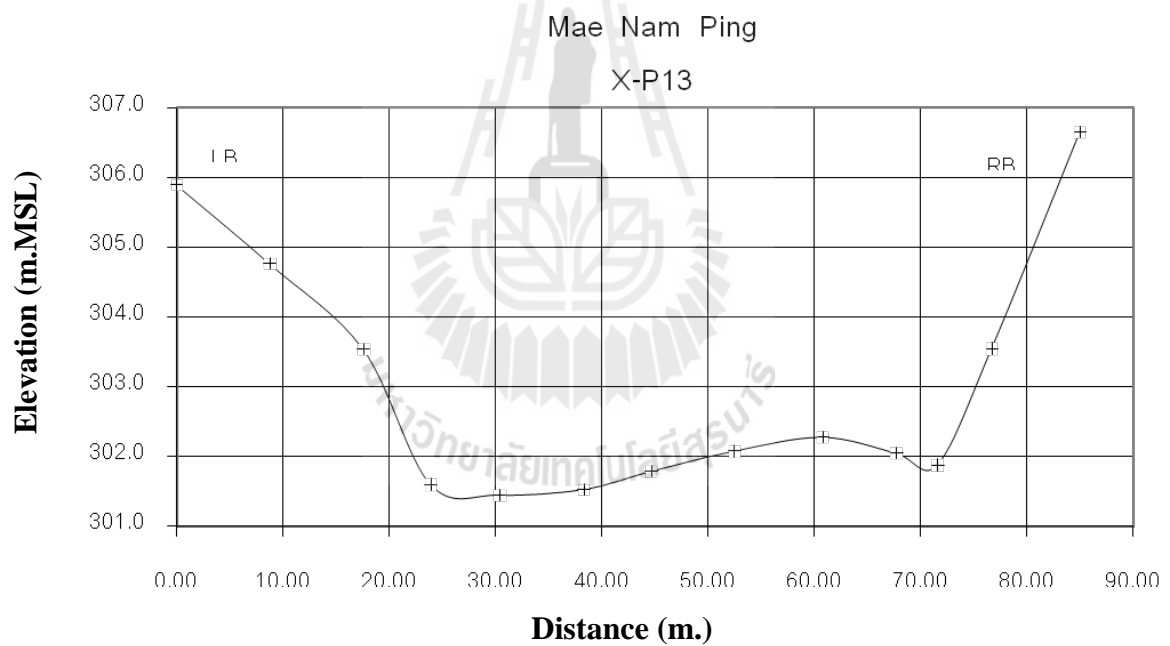
Distance (m)	Elevation (m.AD)	Elevation (m.MSL)	Remark
0.00	0.000	311.109	
9.04	-3.320	307.789	LB
14.17	-4.370	306.739	
24.61	-6.620	304.489	
31.61	-6.830	304.279	
38.68	-7.050	304.059	
47.11	-6.690	304.419	
52.04	-4.470	306.639	
56.18	-3.320	307.789	RB
60.60	-0.920	310.189	
68.46	1.020	312.129	



C.7 Line X-P13.

**MAE NAM PING
Line X-P13**

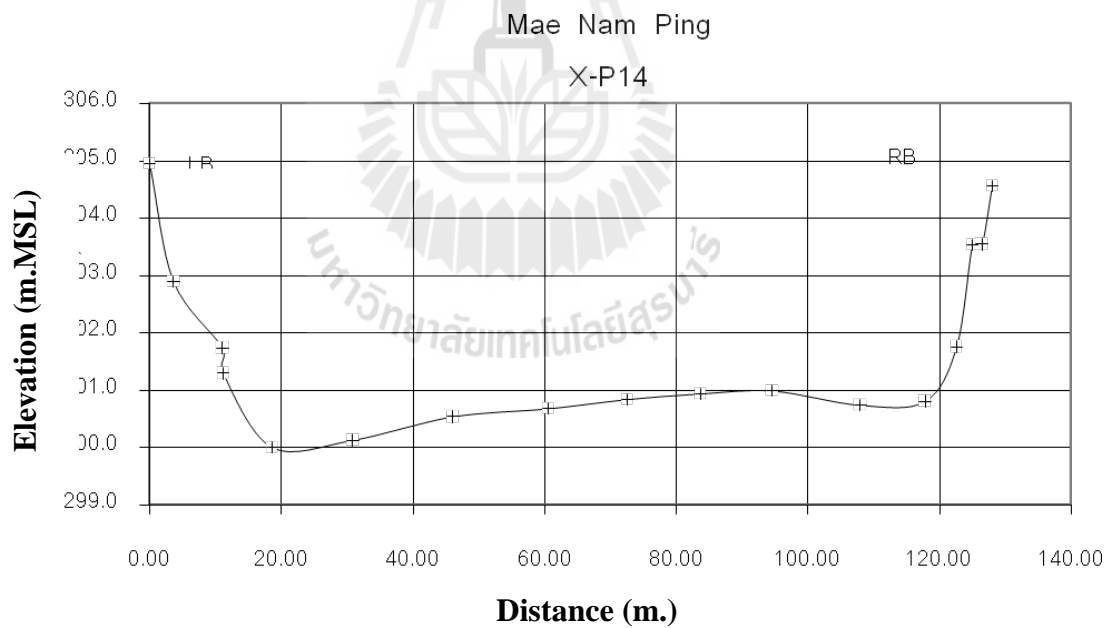
Distance (m)	Elevation (m.AD)	Elevation (m.MSL)	Remark
0.00	0.000	305.888	
8.76	-1.130	304.758	
17.57	-2.360	303.528	LB
23.90	-4.300	301.588	
30.36	-4.450	301.438	
38.30	-4.370	301.518	
44.66	-4.110	301.778	
52.47	-3.820	302.068	
60.80	-3.620	302.268	
67.75	-3.850	302.038	
71.60	-4.020	301.868	
76.71	-2.350	303.538	RB
84.98	0.750	306.638	



C.8 Line X-P14.

**MAE NAM PING
Line X-P14**

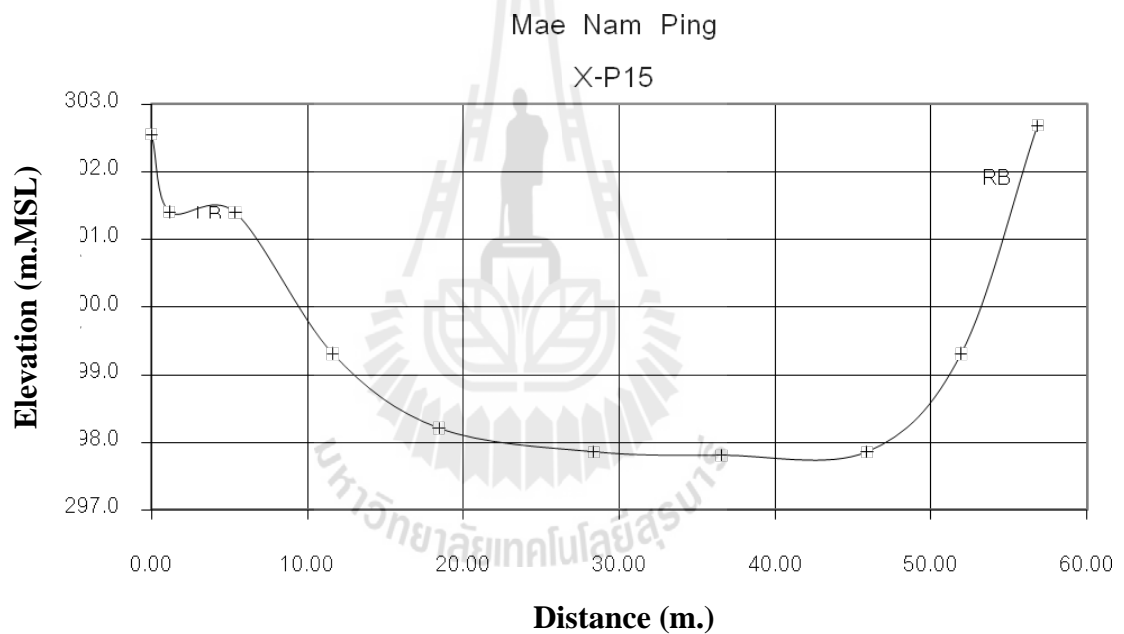
Distance (m)	Elevation (m.AD)	Elevation (m.MSL)	Remark
0.00	0.000	304.950	
3.60	-2.050	302.900	
11.03	-3.210	301.740	LB
11.15	-3.650	301.300	
18.52	-4.940	300.010	
30.82	-4.820	300.130	
46.05	-4.410	300.540	
60.56	-4.270	300.680	
72.49	-4.110	300.840	
83.69	-4.010	300.940	
94.59	-3.960	300.990	
107.94	-4.210	300.740	
117.77	-4.140	300.810	
122.54	-3.190	301.760	RB
124.95	-1.410	303.540	
126.40	-1.400	303.550	
127.96	-0.380	304.570	



C.9 Line X-P15.

**MAE NAM PING
Line X-P15**

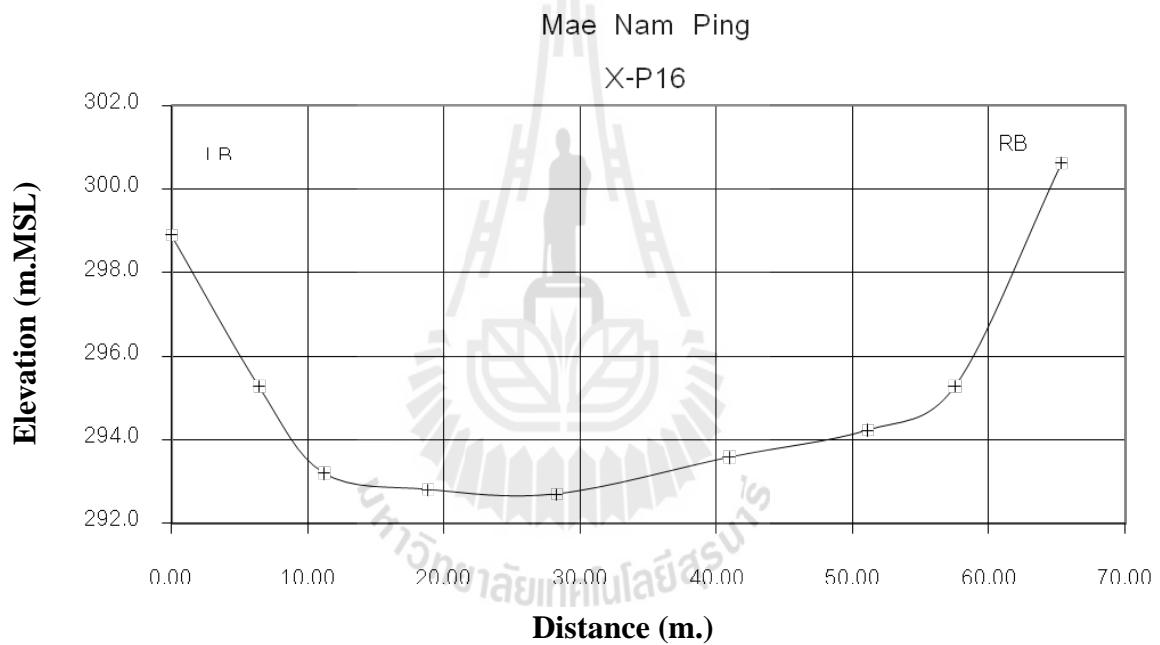
Distance (m)	Elevation (m.AD)	Elevation (m.MSL)	Remark
0.00	-0.130	302.545	
1.13	-1.270	301.405	
5.35	-1.280	301.395	
11.62	-3.370	299.305	LB
18.43	-4.470	298.205	
28.36	-4.820	297.855	
36.56	-4.870	297.805	
45.91	-4.820	297.855	
51.94	-3.370	299.305	RB
56.83	0.000	302.675	

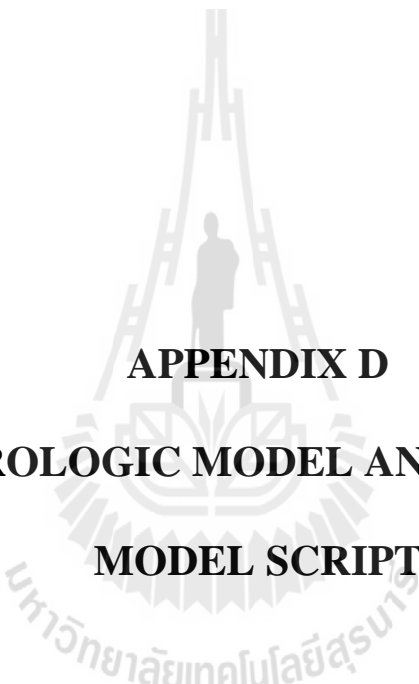


C.10 Line X-P16.

**MAE NAM PING
Line X-P16**

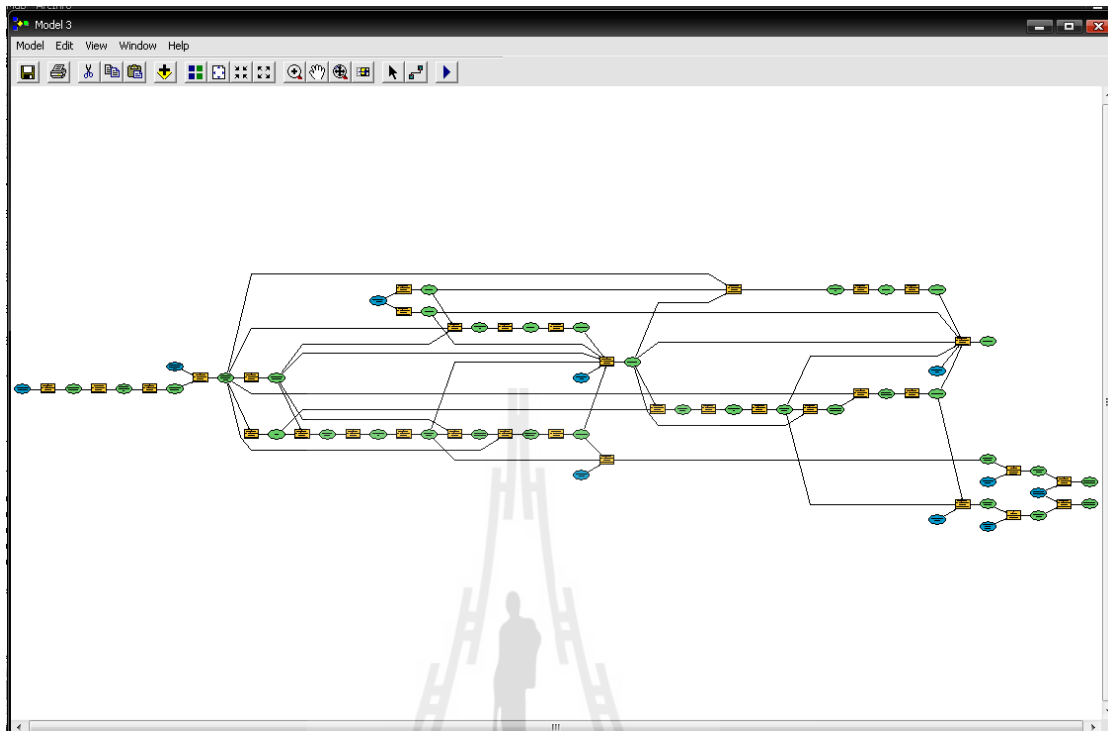
Distance (m)	Elevation (m.AD)	Elevation (m.MSL)	Remark
0.00	0.000	298.899	
6.41	-3.620	295.279	LB
11.20	-5.700	293.199	
18.80	-6.090	292.809	
28.26	-6.200	292.699	
40.95	-5.320	293.579	
51.10	-4.670	294.229	
57.52	-3.620	295.279	RB
65.32	1.710	300.609	





APPENDIX D
DAILY HYDROLOGIC MODEL AND WATER LEVEL
MODEL SCRIPT

D.1 Daily hydrologic model script.



' appendix_D1.vbs

' Created on: อ. น.ย. 26 2012 11:26:05 AM

' (generated by ArcGIS/ModelBuilder)

' Create the Geoprocessor object

```
set gp = WScript.CreateObject("esriGeoprocessing.GPDispatch.1")
```

' Check out any necessary licenses

```
gp.CheckOutExtension "spatial"
```

' Load required toolboxes...

```
gp.AddToolbox "C:/Program Files/ArcGIS/ArcToolbox/Toolboxes/Spatial Analyst Tools.tbx"
```

' Local variables...

```
rain0109 = "C:\floodproject\dailyrain\rain_gid\rain0109"
```

```
up0109mm = "C:\floodproject\dailyrain\Q_upstream\up0109mm"
```

soildeep_use = "C:\floodproject\dailyrain\static\soildeep_use"
soildeep_mm = "C:\floodproject\dailyrain\static\soildeep_mm"
sbidw_poro40_ = "C:\floodproject\dailyrain\static\sbidw_poro40%"
s0109 = "C:\floodproject\dailyrain\Q_waterbalance\s0109"
q_0109 = "C:\floodproject\dailyrain\Q_waterbalance\q_0109"
q0109_qup = "C:\floodproject\dailyrain\Q_waterbalance\q0109_qup"
flow_0109 = "C:\floodproject\dailyrain\Q_flow\flow_0109"
rain0209 = "C:\floodproject\dailyrain\rain_gid\rain0209"
s0209 = "C:\floodproject\dailyrain\Q_waterbalance\s0209"
s0209_sbidw = "C:\floodproject\dailyrain\Q_waterbalance\s0209_sbidw"
up0209mm = "C:\floodproject\dailyrain\Q_upstream\up0209mm"
q0209_qup = "C:\floodproject\dailyrain\Q_waterbalance\q0209_qup"
flowdi111 = "flowdi111"
flow_0209 = "C:\floodproject\dailyrain\Q_flow\flow_0209"
flowdi111__2_ = "flowdi111"
ave_flow0109 = "C:\floodproject\dailyrain\Q_flow\flow_ave\ave_flow0109"
ave_flow0209 = "C:\floodproject\dailyrain\Q_flow\flow_ave\ave_flow0209"
s0109_sbidw = "C:\floodproject\dailyrain\Q_waterbalance\s0109_sbidw"
eva0109 = "C:\floodproject\dailyrain\eva\s_Sb\eva0109"
eva0209 = "C:\floodproject\dailyrain\eva\s_Sb\eva0209"
v0109 = "C:\floodproject\dailyrain\eva\s_sb_use\0109"
v0209 = "C:\floodproject\dailyrain\eva\s_sb_use\0209"
v3e0109 = "C:\floodproject\dailyrain\eva\s_sb_eva3\3e0109"
v3e0209 = "C:\floodproject\dailyrain\eva\s_sb_eva3\3e0209"
Sf = "C:\floodproject\dailyrain\static\sf"
s0109_sf = "C:\floodproject\dailyrain\Q_ss\s0109_sf"
qss0109 = "C:\floodproject\dailyrain\Q_ss\qss0109"
qsst0109 = "C:\floodproject\dailyrain\Q_ss\qsst0109"
s0209_sf = "C:\floodproject\dailyrain\Q_ss\s0209_sf"

```

qss0209 = "C:\floodproject\dailyrain\Q_ss\qss0209"
qsst0209 = "C:\floodproject\dailyrain\Q_ss\qsst0209"
s0109_qsst01 = "C:\floodproject\dailyrain\Q_waterbalance\s0109_qsst01"
s0209_qsst02 = "C:\floodproject\dailyrain\Q_waterbalance\s0209_qsst02"
q_0209 = "C:\floodproject\dailyrain\Q_waterbalance\q_0209"
flowacc_up67 = "C:\floodproject\flowpast\flowacc_up67"
s_begin0109 = "C:\floodproject\dailyrain\static\s_begin0109"
soildeep_idw1 = "C:\floodproject\dailyrain\static\soildeep_idw1"
soildeep_idw = "C:\floodproject\dailyrain\static\soildeep_idw"
lu2005_img = "C:\floodproject\Nuch\lu2005.img"
v2005 = "C:\floodproject\dailyrain\eva\eva_v\2005"
i2005 = "C:\floodproject\dailyrain\intercept\i2005"
porositymask2 = "C:\floodproject\static\porositymask2"

' Process: Single Output Map Algebra (26)...
gp.SingleOutputMapAlgebra_sa "([soildeep_use] * 1000) - 5000", soildeep_mm,
"C:\floodproject\dailyrain\static\soildeep_use"

' Process: Single Output Map Algebra (396)...
gp.SingleOutputMapAlgebra_sa "con ([soildeep_mm] <= 10000 , [soildeep_mm] , [soildeep_mm] >
10000 , [10000])", soildeep_idw1, "C:\floodproject\dailyrain\static\soildeep_mm"

' Process: Single Output Map Algebra...
gp.SingleOutputMapAlgebra_sa "con ([soildeep_idw1] >= 200 , [soildeep_idw1] , [soildeep_idw1] <
200 , [200])", soildeep_idw, "C:\floodproject\dailyrain\static\soildeep_idw1"

' Process: Single Output Map Algebra (27)...
gp.SingleOutputMapAlgebra_sa "[soildeep_idw] * [porositymask2]", sbidw_poro40_,
"C:\floodproject\dailyrain\static\soildeep_idw;C:\floodproject\static\porositymask2"

```

' Process: Single Output Map Algebra (173)...

gp.SingleOutputMapAlgebra_sa "[sbidw_poro40%] * 0.30", s_begin0109,
 "C:\floodproject\dailyrain\static\sbidw_poro40%"

' Process: Single Output Map Algebra (4)...

gp.SingleOutputMapAlgebra_sa "con ([lu2005.img] <= 3 , [0] , [lu2005.img] >= 4 , [1])", v2005,
 "C:\floodproject\Nuch\lu2005.img"

' Process: Single Output Map Algebra (78)...

gp.SingleOutputMapAlgebra_sa "([s_begin0109] / [Sbidw_poro40%]) + [2005]", eva0109,
 "C:\floodproject\dailyrain\static\sbidw_poro40%;C:\floodproject\dailyrain\static\s_begin0109;C:\flood
 project\dailyrain\eva\eva_v\2005"

' Process: Single Output Map Algebra (89)...

gp.SingleOutputMapAlgebra_sa "con ([eva0109] < 1 , [eva0109] , [eva0109] >= 1 , [1])", v0109,
 "C:\floodproject\dailyrain\eva\s_sb\eva0109"

' Process: Single Output Map Algebra (101)...

gp.SingleOutputMapAlgebra_sa "[0109] * 3.7", v3e0109,
 "C:\floodproject\dailyrain\eva\s_sb_use\0109"

' Process: Single Output Map Algebra (14)...

gp.SingleOutputMapAlgebra_sa "[sbidw_poro40%] * 0.4", Sf,
 "C:\floodproject\dailyrain\static\sbidw_poro40%"

' Process: Single Output Map Algebra (113)...

gp.SingleOutputMapAlgebra_sa "[s_begin0109] - [Sf]", s0109_sf,
 "C:\floodproject\dailyrain\static\s_f;C:\floodproject\dailyrain\static\s_begin0109"

' Process: Single Output Map Algebra (114)...

gp.SingleOutputMapAlgebra_sa "con ([S0109_Sf] > 0 , [S0109_Sf] , [S0109_Sf] <= 0 , [0])", qss0109,
"C:\floodproject\dailyrain\Q_ss\s0109_sf"

' Process: Single Output Map Algebra (115)...

gp.SingleOutputMapAlgebra_sa "[qss0109] / 3", qsst0109, "C:\floodproject\dailyrain\Q_ss\qss0109"

' Process: Single Output Map Algebra (149)...

gp.SingleOutputMapAlgebra_sa "[s_begin0109] - [qsst0109]", s0109_qsst01,
"C:\floodproject\dailyrain\Q_ss\qsst0109;C:\floodproject\dailyrain\static\s_begin0109"

' Process: Single Output Map Algebra (77)...

gp.SingleOutputMapAlgebra_sa "[s0109_qsst01] - [sbidw_poro40%]", s0109_sbidw,
"C:\floodproject\dailyrain\static\sbidw_poro40%;C:\floodproject\dailyrain\Q_waterbalance\s0109_qsst
01"

' Process: Single Output Map Algebra (63)...

gp.SingleOutputMapAlgebra_sa "con ([S0109_Sbidw] > 0 , [S0109_Sbidw] , [S0109_Sbidw] <= 0 ,
[0])", q_0109, "C:\floodproject\dailyrain\Q_waterbalance\s0109_sbidw"

' Process: Single Output Map Algebra (9)...

gp.SingleOutputMapAlgebra_sa "con ([lu2005.img] <= 4 , [0] , [lu2005.img] >= 5 , [0.1])", i2005,
"C:\floodproject\Nuch\lu2005.img"

' Process: Single Output Map Algebra (28)...

gp.SingleOutputMapAlgebra_sa "([rain0109] - ([rain0109] * i2005)) + [s_begin0109] - ([3e0109]) -
[qsst0109] - [q_0109]", s0109,
"C:\floodproject\dailyrain\rain_gid\rain0109;C:\floodproject\dailyrain\static\s_begin0109;C:\floodproje"

ct\dailyrain\eva\s_sb_eva3\3e0109;C:\floodproject\dailyrain\Q_waterbalance\q_0109;C:\floodproject\dailyrain\Q_ss\qsst0109;C:\floodproject\dailyrain\intercept\i2005"

' Process: Single Output Map Algebra (76)...

gp.SingleOutputMapAlgebra_sa "([s0109] / [Sbidw_poro40%]) + [2005]", eva0209,

"C:\floodproject\dailyrain\static\sbidw_poro40%;C:\floodproject\dailyrain\Q_waterbalance\s0109;C:\floodproject\dailyrain\eva\eva_v\2005"

' Process: Single Output Map Algebra (90)...

gp.SingleOutputMapAlgebra_sa "con ([eva0209] < 1 , [eva0209] , [eva0209] >= 1 , [1])", v0209,

"C:\floodproject\dailyrain\eva\s_Sb\eva0209"

' Process: Single Output Map Algebra (102)...

gp.SingleOutputMapAlgebra_sa "[0209] * 3.7", v3e0209,

"C:\floodproject\dailyrain\eva\s_sb_use\0209"

' Process: Single Output Map Algebra (116)...

gp.SingleOutputMapAlgebra_sa "[s0109] - [Sf]", s0209_sf,

"C:\floodproject\dailyrain\static\sfc;\floodproject\dailyrain\Q_waterbalance\s0109"

' Process: Single Output Map Algebra (117)...

gp.SingleOutputMapAlgebra_sa "con ([S0209_Sf] > 0 , [S0209_Sf] , [S0209_Sf] <= 0 , [0])", qss0209,

"C:\floodproject\dailyrain\Q_ss\s0209_sf"

' Process: Single Output Map Algebra (118)...

gp.SingleOutputMapAlgebra_sa "[qss0209] / 3", qsst0209, "C:\floodproject\dailyrain\Q_ss\qss0209"

' Process: Single Output Map Algebra (150)...

gp.SingleOutputMapAlgebra_sa "[s0109] - [qsst0209]", s0209_qsst02,

"C:\floodproject\dailyrain\Q_ss\qsst0209;C:\floodproject\dailyrain\Q_waterbalance\s0109"

' Process: Single Output Map Algebra (3)...

gp.SingleOutputMapAlgebra_sa "[s0209_qsst02] - [sbidw_poro40%]", s0209_sbidw,

"C:\floodproject\dailyrain\static\sbidw_poro40%;C:\floodproject\dailyrain\Q_waterbalance\s0209_qsst02"

' Process: Single Output Map Algebra (161)...

gp.SingleOutputMapAlgebra_sa "con ([S0209_Sbidw] > 0 , [S0209_Sbidw] , [S0209_Sbidw] <= 0 , [0])", q_0209, "C:\floodproject\dailyrain\Q_waterbalance\s0209_sbidw"

' Process: Single Output Map Algebra (2)...

gp.SingleOutputMapAlgebra_sa "([rain0209] - ([rain0209] * i2005)) + [s0109] - ([3e0209]) - [qsst0209] - [q_0209]", s0209,

"C:\floodproject\dailyrain\rain_gid\rain0209;C:\floodproject\dailyrain\eva\s_sb_eva3\3e0209;C:\floodproject\dailyrain\Q_waterbalance\s0109;C:\floodproject\dailyrain\Q_ss\qsst0209;C:\floodproject\dailyrain\Q_waterbalance\q_0209;C:\floodproject\dailyrain\intercept\i2005"

' Process: Single Output Map Algebra (65)...

gp.SingleOutputMapAlgebra_sa "[q_0109] + ([up0109mm] * 5962320) + [qsst0109]", q0109_qup,

"C:\floodproject\dailyrain\Q_waterbalance\q_0109;C:\floodproject\dailyrain\Q_upstream\up0109mm;C:\floodproject\dailyrain\Q_ss\qsst0109"

' Process: Flow Accumulation (12)...

gp.FlowAccumulation_sa flowdi111, flow_0109, q0109_qup, "FLOAT"

' Process: Single Output Map Algebra (29)...

```
gp.SingleOutputMapAlgebra_sa "[Flow_0109] / [flowacc_up67]", ave_flow0109,  
"C:\floodproject\dailyrain\Q_flow\flow_0109;C:\floodproject\flowpast\flowacc_up67"
```

' Process: Single Output Map Algebra (6)...

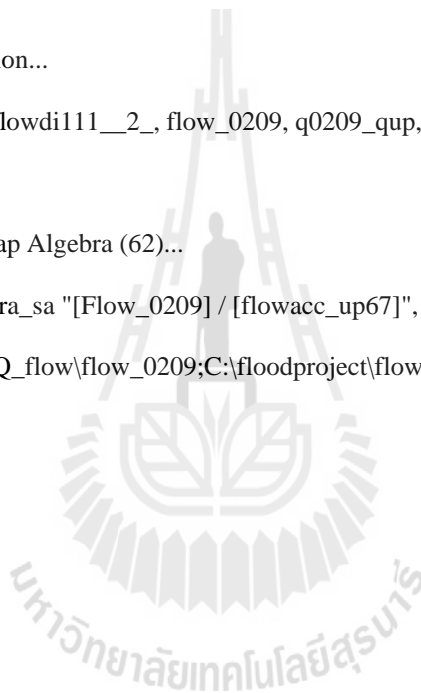
```
gp.SingleOutputMapAlgebra_sa "[q_0209] + ([up0209mm] * 5962320) + [qsst0209]", q0209_qup,  
"C:\floodproject\dailyrain\Q_upstream\up0209mm;C:\floodproject\dailyrain\Q_ss\qsst0209;C:\floodpr  
oject\dailyrain\Q_waterbalance\q_0209"
```

' Process: Flow Accumulation...

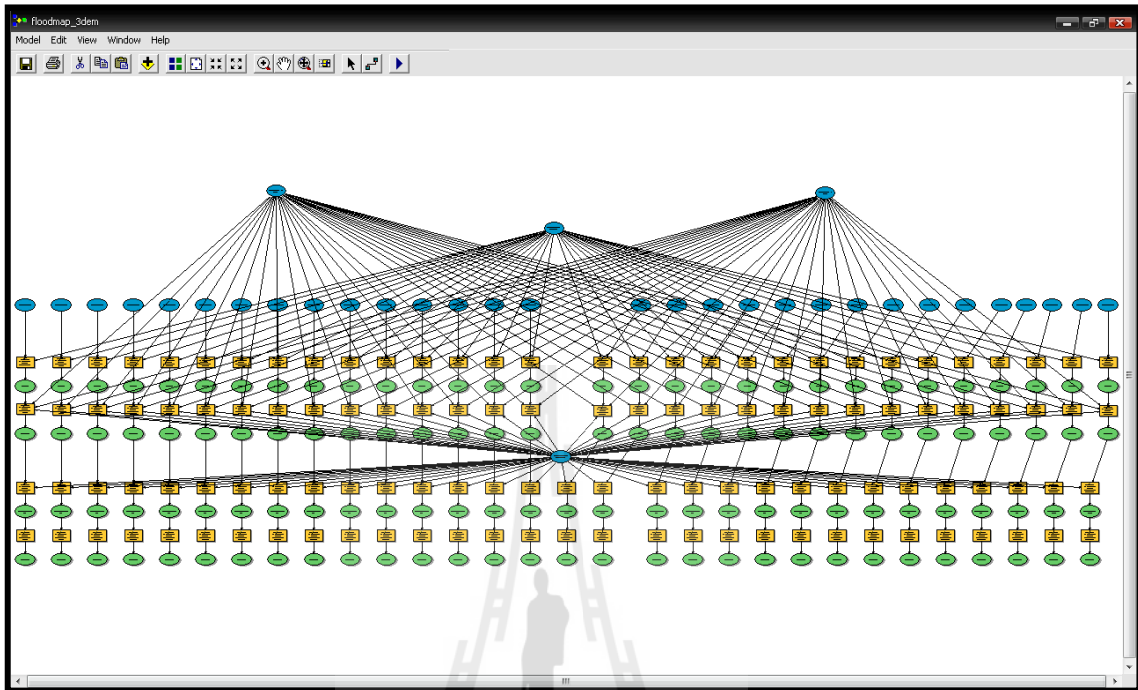
```
gp.FlowAccumulation_sa flowdi111__2_, flow_0209, q0209_qup, "FLOAT"
```

' Process: Single Output Map Algebra (62)...

```
gp.SingleOutputMapAlgebra_sa "[Flow_0209] / [flowacc_up67]", ave_flow0209,  
"C:\floodproject\dailyrain\Q_flow\flow_0209;C:\floodproject\flowpast\flowacc_up67"
```



D.2 Water level model script.



appendix_D2.vbs

' Created on: ๐. ๓.๒. 26 2012 11:36:01 AM

' (generated by ArcGIS/ModelBuilder)

' Create the Geoprocessor object
set gp = WScript.CreateObject("esriGeoprocessing.GPDispatch.1")

' Check out any necessary licenses
gp.CheckOutExtension "spatial"

' Load required toolboxes...
gp.AddToolbox "C:/Program Files/ArcGIS/ArcToolbox/Toolboxes/Spatial Analyst Tools.tbx"

' Local variables...
v0109 = "C:\floodproject\dailyrain\floodmap\Q_m3\0109"
ave0109 = "C:\floodproject\dailyrain\routing\flo_ave\ave0109"
flowaccweight = "C:\floodproject\flowpast\flowaccweight"
z0109 = "C:\floodproject\dailyrain\floodmap\Z_msl\z0109"
z0109_dem = "C:\floodproject\dailyrain\floodmap\area_flood\z0109_dem"
f0109 = "C:\floodproject\dailyrain\floodmap\area_flood\f0109"
zone_a_img = "C:\floodproject\static\zone_a.img"
zone_b_img = "C:\floodproject\static\zone_b.img"
extract_dem_1 = "C:\floodproject\static\extract_dem_1"

' Process: Single Output Map Algebra...

```
gp.SingleOutputMapAlgebra_sa "(([ave0109] / 1000) * ([flowaccweight] * 900)) / 86400", v0109,
"C:\floodproject\dailyrain\routing\flo_ave\ave0109;C:\floodproject\flowpast\flowaccweight"
```

' Process: Single Output Map Algebra (2)...

```
gp.SingleOutputMapAlgebra_sa "([zone_a.img] * (POW ([0109] , 2))) + ([zone_b.img] * [0109]) +
[dem_merge2]", z0109,
"C:\floodproject\dailyrain\floodmap\Q_m3\0109;C:\floodproject\static\zone_a.img;C:\floodproject\static\zone_b.img;C:\floodproject\static\extract_dem_1"
```

' Process: Single Output Map Algebra (3)...

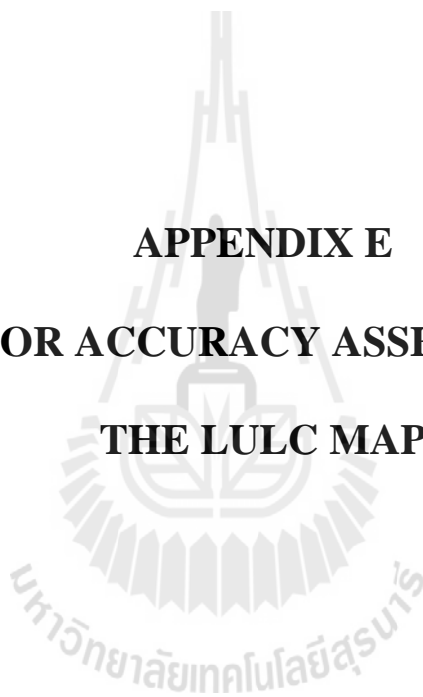
```
gp.SingleOutputMapAlgebra_sa "[z0109] - [dem_merge2]", z0109_dem,
"C:\floodproject\dailyrain\floodmap\Z_msl\z0109;C:\floodproject\static\extract_dem_1"
```

' Process: Single Output Map Algebra (4)...

```
gp.SingleOutputMapAlgebra_sa "con ([z0109_dem] > 0 , [z0109_dem] , [z0109_dem] <= 0 , [0])",
f0109, "C:\floodproject\dailyrain\floodmap\area_flood\z0109_dem"
```



APPENDIX E
DATA FOR ACCURACY ASSESSMENT OF
THE LULC MAP



E.1 Data for accuracy assessment of the 2005 classified LULC map.

Sample_point	Easting	Northting	LULC_classify	LULC_Reference
ID#1	494027	2074806	6	6
ID#2	494927	2093346	2	2
ID#3	497057	2093406	3	0
ID#4	475817	2109696	6	6
ID#5	478157	2107926	6	6
ID#6	486107	2100636	6	6
ID#7	498527	2077626	3	3
ID#8	490157	2094786	6	6
ID#9	474557	2110986	6	6
ID#10	498407	2088966	2	2
ID#11	502007	2096586	1	1
ID#12	494297	2087166	6	6
ID#13	498527	2083026	3	3
ID#14	505727	2085756	2	2
ID#15	478967	2085816	6	6
ID#16	477377	2118126	6	6
ID#17	500567	2089086	3	3
ID#18	499037	2079366	3	3
ID#19	472727	2107416	6	6
ID#20	478667	2114466	6	6
ID#21	475877	2110956	6	6
ID#22	506177	2099616	6	6
ID#23	503957	2089146	3	3
ID#24	481217	2111436	5	6
ID#25	491687	2089236	6	6
ID#26	488087	2099736	6	6
ID#27	477197	2114826	6	6
ID#28	464057	2107686	6	6
ID#29	502067	2084076	3	3
ID#30	480557	2114526	6	6
ID#31	475877	2110326	6	1
ID#32	501887	2077506	3	3
ID#33	471947	2113506	6	6
ID#34	501377	2094816	5	5
ID#35	467417	2108646	6	6
ID#36	495497	2090346	3	3
ID#37	495827	2076786	3	3
ID#38	467837	2108466	6	6
ID#39	494507	2096586	2	2
ID#40	488117	2087916	6	6

E.1 (Continued).

Sample_point	Easting	Northting	LULC_classify	LULC_Reference
ID#41	499907	2080926	3	3
ID#42	495557	2092056	3	3
ID#43	490157	2102556	3	5
ID#44	483857	2087196	6	6
ID#45	468857	2109876	6	1
ID#46	491957	2095746	5	5
ID#47	490367	2098476	5	5
ID#48	493067	2099646	6	5
ID#49	473327	2116476	6	6
ID#50	479117	2095086	6	6
ID#51	481697	2088816	6	2
ID#52	490487	2075256	6	6
ID#53	485537	2095956	6	6
ID#54	492167	2098086	6	1
ID#55	475817	2116596	6	6
ID#56	477887	2096376	6	6
ID#57	480167	2107776	6	6
ID#58	484307	2103636	6	6
ID#59	484877	2092296	6	6
ID#60	478727	2102136	6	6
ID#61	491627	2075496	6	6
ID#62	481367	2107716	6	6
ID#63	507347	2092266	5	5
ID#64	489947	2085696	6	5
ID#65	489467	2097336	5	5
ID#66	498107	2078736	3	3
ID#67	488807	2092086	5	5
ID#68	493397	2091516	3	3
ID#69	494027	2073276	2	0
ID#70	480707	2105586	6	6
ID#71	490517	2092686	5	5
ID#72	507167	2093196	6	6
ID#73	500297	2103576	6	6
ID#74	474437	2115306	6	6
ID#75	493637	2084196	6	6
ID#76	469547	2109666	6	6
ID#77	466367	2111226	6	6
ID#78	484547	2095776	6	6
ID#79	487547	2099616	6	6
ID#80	466397	2110326	6	6

E.1 (Continued).

Sample_point	Easting	Northting	LULC_classify	LULC_Reference
ID#81	505547	2098506	6	6
ID#82	490517	2081526	6	6
ID#83	482717	2111346	6	6
ID#84	503867	2101386	6	6
ID#85	484697	2094306	6	6
ID#86	503417	2101296	6	6
ID#87	501077	2095506	6	6
ID#88	487247	2098476	6	6
ID#89	470417	2107416	6	6
ID#90	480227	2116416	6	5
ID#91	501947	2082336	3	3
ID#92	500567	2076816	3	3
ID#93	466007	2106276	6	6
ID#94	493727	2090436	3	3
ID#95	503987	2102586	6	6
ID#96	507947	2087046	2	2
ID#97	496637	2093256	3	5
ID#98	501407	2079816	3	3
ID#99	487157	2087346	6	6
ID#100	508277	2094426	6	6
ID#101	487247	2084376	6	6
ID#102	485387	2100486	6	6
ID#103	500867	2085276	2	2
ID#104	498737	2080626	3	3
ID#105	504377	2097156	6	6
ID#106	476387	2111106	6	6
ID#107	478817	2106846	6	6
ID#108	477857	2117226	6	6
ID#109	481067	2118246	6	6
ID#110	498437	2075316	3	3
ID#111	488747	2091006	6	6
ID#112	498467	2103726	3	3
ID#113	498647	2097066	3	3
ID#114	483977	2105796	6	6
ID#115	488027	2090466	6	6
ID#116	471617	2109486	6	6
ID#117	487217	2107626	5	6
ID#118	497507	2073966	3	3
ID#119	473957	2104086	6	6
ID#120	489407	2080566	6	6

E.1 (Continued).

Sample_point	Easting	Northting	LULC_classify	LULC_Reference
ID#121	478097	2105496	6	6
ID#122	466307	2107356	6	6
ID#123	469637	2114916	6	6
ID#124	498227	2086236	5	3
ID#125	494297	2082696	6	6
ID#126	499337	2101326	6	5
ID#127	503027	2103096	6	6
ID#128	476057	2116596	6	6
ID#129	481487	2117676	6	6
ID#130	501077	2079936	3	3
ID#131	464747	2107806	6	6
ID#132	480617	2109186	6	6
ID#133	486557	2098686	6	6
ID#134	472067	2106246	6	6
ID#135	498137	2100576	3	3
ID#136	502487	2085456	2	2
ID#137	495167	2105136	3	3
ID#138	498167	2096886	2	2
ID#139	465647	2115546	6	6
ID#140	469757	2106576	6	6
ID#141	504677	2097966	6	6
ID#142	501167	2098176	6	6
ID#143	483557	2112786	6	6
ID#144	475967	2104716	6	6
ID#145	500237	2104236	6	6
ID#146	502877	2099106	6	6
ID#147	500657	2081106	3	3
ID#148	488207	2092236	6	6
ID#149	476747	2113356	6	6
ID#150	495947	2077926	3	3
ID#151	492797	2091306	3	3
ID#152	491417	2088186	6	6
ID#153	474737	2108046	6	6
ID#154	496007	2082546	3	3
ID#155	481337	2118156	6	6
ID#156	478277	2106066	6	6
ID#157	487727	2091456	6	6
ID#158	472577	2117136	6	6
ID#159	496757	2098956	2	2
ID#160	489767	2085786	6	5

E.1 (Continued).

Sample_point	Easting	Northting	LULC_classify	LULC_Reference
ID#161	472997	2106756	6	6
ID#162	503657	2102076	6	6
ID#163	503147	2099136	6	6
ID#164	495557	2096076	2	2
ID#165	492977	2101776	6	6
ID#166	480407	2120346	6	6
ID#167	481487	2102316	6	6
ID#168	485177	2091216	6	6
ID#169	490847	2078886	6	6
ID#170	473447	2107896	6	6
ID#171	470747	2116686	6	6
ID#172	493307	2096676	6	6
ID#173	495137	2072736	3	3
ID#174	475637	2101446	6	6
ID#175	482447	2085876	6	6
ID#176	494987	2090496	2	2
ID#177	477767	2115816	6	6
ID#178	485357	2111286	6	5
ID#179	507107	2091306	5	5
ID#180	498107	2081376	3	3
ID#181	487157	2108136	5	2
ID#182	502907	2096076	5	5
ID#183	474437	2110446	6	6
ID#184	497477	2097126	2	2
ID#185	501197	2097696	6	6
ID#186	486047	2085996	6	6
ID#187	491717	2074986	6	6
ID#188	479597	2088606	6	6
ID#189	463007	2107116	1	1
ID#190	499067	2079726	3	3
ID#191	486887	2109846	5	5
ID#192	500087	2094366	0	5
ID#193	484727	2094726	6	6
ID#194	493427	2102706	6	6
ID#195	490937	2101266	6	5
ID#196	504137	2084676	2	2
ID#197	474197	2115996	6	6
ID#198	503597	2086656	4	4
ID#199	488567	2094876	2	2
ID#200	466907	2115456	6	6

E.1 (Continued).

Sample_point	Easting	Northting	LULC_classify	LULC_Reference
ID#201	495227	2096856	2	2
ID#202	484427	2095566	6	6
ID#203	475427	2111766	6	6
ID#204	500927	2089626	3	3
ID#205	490067	2080626	6	6
ID#206	471497	2105916	6	6
ID#207	492677	2089056	6	6
ID#208	490577	2104536	3	6
ID#209	472727	2117496	6	6
ID#210	469217	2115156	6	6
ID#211	486647	2086536	6	6
ID#212	470387	2116566	6	6
ID#213	482117	2099736	6	6
ID#214	508787	2101506	6	6
ID#215	493847	2095536	1	1
ID#216	500117	2075856	3	3
ID#217	490907	2090496	5	5
ID#218	500747	2094546	5	5
ID#219	496097	2079366	3	3
ID#220	485057	2088336	0	0
ID#221	481007	2120106	6	6
ID#222	502337	2103306	6	6
ID#223	474797	2115576	6	6
ID#224	490697	2079096	6	6
ID#225	481847	2113056	5	5
ID#226	482147	2089086	6	6
ID#227	501887	2085426	2	2
ID#228	486527	2095836	6	6
ID#229	500837	2095056	5	5
ID#230	479297	2098266	6	5
ID#231	487457	2110836	5	5
ID#232	466337	2107326	6	6
ID#233	489377	2105556	6	6
ID#234	494537	2093316	2	2
ID#235	498257	2094546	2	3
ID#236	469037	2111436	6	6
ID#237	481997	2089086	6	6
ID#238	468767	2109966	6	6
ID#239	464147	2111706	6	6
ID#240	493097	2079906	6	6

E.1 (Continued).

Sample_point	Easting	Northting	LULC_classify	LULC_Reference
ID#241	468827	2111916	6	6
ID#242	475667	2114826	6	6
ID#243	478127	2095206	6	6
ID#244	475757	2106426	6	6
ID#245	508817	2089836	5	5
ID#246	464957	2110086	6	6
ID#247	487067	2111496	5	5
ID#248	496097	2093616	2	2
ID#249	484247	2103816	6	6
ID#250	466217	2106696	6	6
ID#251	493637	2093136	3	3
ID#252	468407	2109666	6	6
ID#253	478307	2086356	6	6
ID#254	496487	2079486	3	3
ID#255	489587	2086986	6	6
ID#256	488657	2094306	6	6
ID#257	492047	2106186	1	1
ID#258	498167	2086026	3	3
ID#259	498347	2080776	3	3
ID#260	489527	2100636	5	1
ID#261	469637	2114496	6	6
ID#262	489197	2087796	6	6
ID#263	493307	2101206	3	1
ID#264	485837	2092116	6	6
ID#265	471917	2110086	6	6
ID#266	481097	2109726	6	6
ID#267	503177	2101086	6	6
ID#268	469847	2117286	6	6
ID#269	502307	2093226	5	5
ID#270	501827	2085306	2	2
ID#271	487547	2091036	6	6
ID#272	507737	2102346	6	6
ID#273	479597	2109816	6	6
ID#274	490577	2090226	5	5
ID#275	507407	2101776	6	6
ID#276	491357	2102496	1	6
ID#277	480917	2112816	5	5
ID#278	469967	2112936	6	6
ID#279	482237	2100036	6	6
ID#280	478607	2091036	6	6

E.1 (Continued).

Sample_point	Easting	Northting	LULC_classify	LULC_Reference
ID#281	466487	2106636	6	6
ID#282	495077	2085636	6	6
ID#283	491177	2099466	1	1
ID#284	482117	2098326	6	6
ID#285	479627	2114826	6	6
ID#286	469577	2105346	6	6
ID#287	491027	2093346	5	5
ID#288	482837	2091636	6	6
ID#289	490247	2094456	6	6
ID#290	493187	2104776	6	6
ID#291	504857	2097786	6	6
ID#292	508007	2088126	2	2
ID#293	504527	2097396	6	6
ID#294	495827	2079816	3	3
ID#295	479777	2085606	6	6
ID#296	464867	2107266	6	6
ID#297	469997	2110536	6	6
ID#298	506507	2094936	6	6
ID#299	479237	2100306	6	6
ID#300	479627	2095536	6	5
ID#301	495377	2087556	3	3
ID#302	494267	2076306	6	6
ID#303	502997	2087736	5	2
ID#304	476837	2115546	6	6
ID#305	501077	2102466	6	1
ID#306	484007	2096376	6	6
ID#307	487067	2087226	6	6
ID#308	501287	2083236	2	2
ID#309	489767	2081196	6	6
ID#310	499937	2102946	6	6
ID#311	468857	2107056	6	6
ID#312	479717	2088036	6	6
ID#313	498017	2074716	3	3
ID#314	489437	2089116	6	6
ID#315	493817	2079936	6	6
ID#316	492977	2103936	3	3
ID#317	479747	2084736	6	6
ID#318	491567	2077026	6	6
ID#319	472517	2118096	6	6
ID#320	466067	2113746	6	6

E.1 (Continued).

Sample_point	Easting	Northting	LULC_classify	LULC_Reference
ID#321	488417	2106036	6	6
ID#322	499697	2079066	3	3
ID#323	493457	2081586	6	6
ID#324	499667	2089146	2	2
ID#325	504347	2096826	6	6
ID#326	478547	2087856	6	6
ID#327	476807	2104356	6	6
ID#328	495017	2095656	2	2
ID#329	487757	2101566	2	2
ID#330	488357	2107236	6	6
ID#331	485747	2099346	6	6
ID#332	498437	2101746	5	5
ID#333	471227	2117106	6	6
ID#334	483407	2107296	6	6
ID#335	494477	2081226	6	6
ID#336	506927	2090196	5	5
ID#337	475457	2103906	6	6
ID#338	475727	2104056	6	6
ID#339	496127	2096256	2	2
ID#340	501827	2084256	3	3
ID#341	484847	2105676	6	6
ID#342	500597	2102706	6	6
ID#343	495857	2086146	3	3
ID#344	469547	2110716	6	6
ID#345	498767	2090676	2	2
ID#346	501767	2084106	3	3
ID#347	487487	2107446	5	6
ID#348	498617	2084736	2	5
ID#349	492107	2081916	6	6
ID#350	499457	2092476	5	5
ID#351	502697	2093856	6	5
ID#352	492107	2084466	6	6
ID#353	481577	2116236	6	6
ID#354	505007	2101416	6	6
ID#355	490907	2094306	5	5
ID#356	511937	2092506	6	6
ID#357	483647	2102166	6	6
ID#358	489767	2094546	6	6
ID#359	478067	2103606	6	6
ID#360	479387	2111286	6	6

E.1 (Continued).

Sample_point	Easting	Northting	LULC_classify	LULC_Reference
ID#361	487667	2097516	2	5
ID#362	482267	2107446	6	6
ID#363	486287	2111646	5	5
ID#364	485717	2109336	5	5
ID#365	490907	2105856	5	2
ID#366	495527	2090406	3	3
ID#367	471467	2109846	6	6
ID#368	468917	2105556	6	1
ID#369	485987	2098476	6	6
ID#370	478697	2091396	6	6
ID#371	490127	2100396	6	6
ID#372	502397	2103096	6	6
ID#373	511907	2089626	2	2
ID#374	480137	2097816	6	6
ID#375	492947	2098956	6	6
ID#376	482807	2115096	6	6
ID#377	497057	2092986	2	2
ID#378	498827	2074986	3	3
ID#379	478667	2110926	6	6
ID#380	491507	2094426	3	3
ID#381	498797	2089206	2	2
ID#382	492767	2096046	5	5
ID#383	476777	2111076	6	6
ID#384	483047	2088126	6	6
ID#385	478607	2112246	6	6
ID#386	476267	2102076	6	6
ID#387	496007	2088546	2	2
ID#388	497927	2085276	4	4
ID#389	488267	2109276	5	5
ID#390	486827	2102736	5	4
ID#391	503387	2084286	2	2
ID#392	475577	2118066	6	6
ID#393	485477	2112846	5	5
ID#394	491777	2082246	6	6
ID#395	505517	2090796	5	5
ID#396	500837	2099886	6	6
ID#397	501497	2101296	6	6
ID#398	488807	2099826	5	5
ID#399	489197	2104326	1	1
ID#400	470867	2117046	6	6

E.1 (Continued).

Sample_point	Easting	Northting	LULC_classify	LULC_Reference
ID#401	492137	2099196	6	6
ID#402	486137	2094726	6	6
ID#403	510947	2089776	3	0
ID#404	471527	2106156	6	6
ID#405	486677	2086746	6	6
ID#406	479267	2116086	6	6
ID#407	507347	2102136	6	6
ID#408	492347	2079276	6	6
ID#409	489857	2083326	3	3
ID#410	505877	2102046	6	6
ID#411	501557	2094906	5	5
ID#412	499667	2102226	1	1
ID#413	483437	2109456	6	6
ID#414	474647	2104956	6	6
ID#415	476777	2101986	6	6
ID#416	504017	2092476	2	2
ID#417	483107	2089926	6	6
ID#418	496457	2078226	3	3
ID#419	486857	2085636	6	6
ID#420	480287	2112726	6	6
ID#421	492077	2089926	6	6
ID#422	481277	2101386	6	6
ID#423	492857	2081976	6	6
ID#424	502817	2091156	5	2
ID#425	500657	2094036	5	5
ID#426	477047	2100246	6	6
ID#427	488057	2103396	2	5
ID#428	487547	2109096	5	5
ID#429	483707	2089146	6	6
ID#430	496547	2100906	2	2
ID#431	490547	2086086	6	6
ID#432	500867	2089206	3	3
ID#433	496367	2082216	4	4
ID#434	483257	2114676	6	6
ID#435	473237	2115276	6	6
ID#436	465917	2110656	6	1
ID#437	504107	2084616	2	2
ID#438	488687	2084106	6	6
ID#439	487787	2088486	6	6
ID#440	494567	2077836	6	6

E.1 (Continued).

Sample_point	Easting	Northting	LULC_classify	LULC_Reference
ID#441	480407	2096886	5	6
ID#442	490217	2100816	5	5
ID#443	467777	2109396	6	6
ID#444	496577	2089326	3	6
ID#445	477197	2118006	6	6
ID#446	502727	2098986	6	6
ID#447	492887	2095866	5	5
ID#448	477467	2097546	6	6
ID#449	490337	2084106	6	6
ID#450	494537	2093376	2	2
ID#451	497987	2090556	2	2
ID#452	476117	2113026	6	6
ID#453	483647	2101146	6	6
ID#454	482327	2100546	6	6
ID#455	501377	2084526	2	2
ID#456	507497	2091906	5	4
ID#457	499997	2093436	3	3
ID#458	509927	2090286	5	2
ID#459	496607	2097876	2	5
ID#460	489557	2101476	5	5
ID#461	466637	2114766	6	6
ID#462	498317	2087796	2	2
ID#463	489407	2088576	6	6
ID#464	474557	2114826	6	6
ID#465	503927	2091606	3	3
ID#466	495077	2096556	2	2
ID#467	499727	2088456	2	2
ID#468	490817	2081376	6	6
ID#469	500507	2082786	3	3
ID#470	492047	2077236	6	6
ID#471	486857	2102616	2	5
ID#472	502157	2078106	3	3
ID#473	489797	2084586	6	6
ID#474	465797	2110176	6	6
ID#475	488267	2086926	6	6
ID#476	494207	2102286	3	3
ID#477	499757	2097486	5	5
ID#478	489917	2090826	5	5
ID#479	505067	2097846	6	6
ID#480	484247	2095476	6	6

E.1 (Continued).

Sample_point	Easting	Northting	LULC_classify	LULC_Reference
ID#481	506567	2086356	2	2
ID#482	466217	2115456	6	6
ID#483	508187	2090256	2	1
ID#484	486917	2088606	6	6
ID#485	497657	2078046	3	3
ID#486	488057	2109186	5	5
ID#487	482027	2106486	6	6
ID#488	481217	2098866	6	6
ID#489	496517	2075826	3	3
ID#490	481517	2111706	6	6
ID#491	490937	2075826	6	6
ID#492	469697	2107356	6	6
ID#493	465167	2115066	6	6
ID#494	489557	2106996	6	6
ID#495	471707	2112576	6	6
ID#496	484127	2098536	6	6
ID#497	487457	2086416	6	6
ID#498	499967	2105316	6	6
ID#499	497537	2088456	3	3
ID#500	485627	2091186	6	6
ID#501	481427	2113506	5	5
ID#502	494537	2089176	2	3
ID#503	485627	2091606	6	6
ID#504	466307	2106396	6	6
ID#505	492407	2093016	6	6
ID#506	485777	2085396	6	6
ID#507	485867	2112906	6	6
ID#508	496847	2081316	3	3
ID#509	493097	2077806	6	6
ID#510	475097	2110836	5	6
ID#511	495467	2076276	3	3
ID#512	478997	2117736	6	6
ID#513	488507	2094126	6	6
ID#514	503057	2099406	6	6
ID#515	490097	2087436	6	6
ID#516	481277	2107986	6	6
ID#517	496007	2075166	3	3
ID#518	463937	2114136	6	6
ID#519	474617	2115756	6	6
ID#520	502427	2093136	5	5

E.1 (Continued).

Sample_point	Easting	Northting	LULC_classify	LULC_Reference
ID#521	480947	2110356	6	6
ID#522	502847	2097486	6	6
ID#523	475367	2102106	6	6
ID#524	491237	2087166	6	6
ID#525	501857	2091186	3	3
ID#526	483287	2098866	6	6
ID#527	486317	2090796	6	6
ID#528	478877	2113536	6	6
ID#529	482627	2101446	6	6
ID#530	501767	2088576	3	3
ID#531	498047	2073156	0	0
ID#532	486167	2110356	5	5
ID#533	485387	2102646	5	5
ID#534	489857	2103666	1	1
ID#535	500027	2074446	4	4
ID#536	498767	2104686	1	1
ID#537	497897	2086836	5	2
ID#538	469547	2112726	5	6
ID#539	488087	2096856	5	5
ID#540	486137	2107356	1	1

E.2 Data for accuracy assessment of the 2010 classified LULC map.

Sample_point	Easting	Northting	LULC_classify	LULC_Reference
ID#1	488627	2095866	6	6
ID#2	484247	2086236	6	6
ID#3	494357	2076966	6	6
ID#4	494867	2073816	2	0
ID#5	485777	2107266	2	2
ID#6	487667	2083686	6	6
ID#7	479297	2086956	6	6
ID#8	495947	2071956	3	0
ID#9	499667	2082996	3	3
ID#10	501707	2099226	6	6
ID#11	493667	2103306	6	6
ID#12	492797	2100876	6	6
ID#13	479867	2084166	6	6
ID#14	491447	2084826	6	5
ID#15	478367	2113956	6	6

E.2 (Continued).

Sample_point	Easting	Northting	LULC_classify	LULC_Reference
ID#16	482057	2115726	6	6
ID#17	482087	2102376	6	6
ID#18	472607	2107296	6	6
ID#19	476117	2111256	6	6
ID#20	476567	2109426	5	6
ID#21	479507	2110656	6	6
ID#22	488927	2077866	6	6
ID#23	494207	2088666	3	3
ID#24	487427	2099106	6	6
ID#25	493997	2089326	2	5
ID#26	486977	2110056	5	5
ID#27	482027	2095716	6	6
ID#28	473327	2110896	6	6
ID#29	493307	2092836	5	4
ID#30	464957	2106216	6	6
ID#31	495947	2074686	3	3
ID#32	479627	2101536	6	6
ID#33	497807	2099646	3	4
ID#34	492347	2100636	6	6
ID#35	506297	2099766	6	6
ID#36	500147	2081436	3	3
ID#37	485357	2103966	3	3
ID#38	493547	2073546	1	1
ID#39	495527	2082426	0	3
ID#40	479357	2102436	6	6
ID#41	480347	2115966	6	6
ID#42	503987	2085486	2	2
ID#43	506297	2087826	2	2
ID#44	487007	2093166	6	6
ID#45	497717	2095956	2	2
ID#46	499727	2086776	2	2
ID#47	487007	2100186	6	6
ID#48	483017	2108376	6	6
ID#49	492977	2077506	6	6
ID#50	493937	2084196	6	6
ID#51	501647	2098236	6	6
ID#52	485717	2105676	2	2
ID#53	492557	2105286	6	6
ID#54	486767	2096976	6	6
ID#55	484487	2090436	6	6

E.2 (Continued).

Sample_point	Easting	Northting	LULC_classify	LULC_Reference
ID#56	497027	2098626	2	2
ID#57	474827	2108826	6	6
ID#58	478427	2109606	6	6
ID#59	486587	2090016	6	6
ID#60	499217	2087736	2	2
ID#61	483887	2099496	6	6
ID#62	486467	2098716	6	6
ID#63	485927	2092386	6	6
ID#64	492137	2103576	6	6
ID#65	478877	2094696	6	6
ID#66	495137	2074326	3	3
ID#67	494357	2073756	3	3
ID#68	505937	2087766	2	2
ID#69	486257	2099826	6	6
ID#70	474527	2109756	6	6
ID#71	469667	2115246	6	6
ID#72	498077	2087346	3	3
ID#73	483437	2097366	6	6
ID#74	502517	2084856	2	3
ID#75	464657	2109756	6	6
ID#76	477017	2104896	6	6
ID#77	485507	2097906	6	6
ID#78	497237	2080266	3	3
ID#79	477767	2097516	6	6
ID#80	490907	2086566	6	6
ID#81	472817	2109546	6	6
ID#82	495137	2100336	2	2
ID#83	496757	2086026	3	3
ID#84	491837	2082186	6	6
ID#85	475457	2118036	6	6
ID#86	480287	2094546	6	6
ID#87	475097	2118156	6	6
ID#88	492647	2090616	2	3
ID#89	478277	2106636	6	6
ID#90	506237	2091726	5	5
ID#91	478517	2111856	6	6
ID#92	476057	2112576	6	6
ID#93	491117	2080686	6	6
ID#94	498137	2092206	2	5
ID#95	499397	2089386	2	5

E.2 (Continued).

Sample_point	Easting	Northting	LULC_classify	LULC_Reference
ID#96	479447	2107356	6	6
ID#97	495857	2083926	3	3
ID#98	490757	2104866	5	6
ID#99	494057	2088786	3	3
ID#100	493937	2073126	2	2
ID#101	491837	2085276	6	6
ID#102	503747	2097516	6	6
ID#103	499937	2099766	6	6
ID#104	482027	2108916	6	6
ID#105	511757	2091606	0	0
ID#106	489947	2102106	5	5
ID#107	482237	2113236	5	5
ID#108	494147	2086986	6	6
ID#109	498467	2074356	3	3
ID#110	494087	2089326	2	2
ID#111	492437	2096736	5	5
ID#112	502637	2095806	4	4
ID#113	511997	2091606	2	2
ID#114	502277	2087106	2	2
ID#115	481907	2108496	6	6
ID#116	481997	2086986	6	6
ID#117	489527	2082066	6	6
ID#118	467267	2109336	6	6
ID#119	491927	2094156	2	2
ID#120	495647	2080056	3	3
ID#121	506507	2097066	6	6
ID#122	500717	2084406	3	3
ID#123	496517	2081046	3	3
ID#124	496307	2082216	4	4
ID#125	486827	2086416	6	6
ID#126	511757	2092566	0	0
ID#127	490727	2095446	6	6
ID#128	473177	2117766	6	6
ID#129	491717	2095236	2	2
ID#130	502997	2100336	6	6
ID#131	483377	2089056	6	6
ID#132	485387	2107566	3	3
ID#133	492497	2097756	6	6
ID#134	490217	2093796	6	6
ID#135	468287	2110296	6	6

E.2 (Continued).

Sample_point	Easting	Northting	LULC_classify	LULC_Reference
ID#136	487907	2083026	6	6
ID#137	484367	2095266	6	6
ID#138	479327	2084436	6	6
ID#139	491717	2092626	6	6
ID#140	482327	2104086	6	6
ID#141	500657	2093406	3	4
ID#142	493157	2105706	6	6
ID#143	498557	2099256	5	5
ID#144	498077	2086176	5	5
ID#145	495317	2094036	2	2
ID#146	499217	2088726	2	2
ID#147	479177	2091486	6	6
ID#148	499247	2073726	3	3
ID#149	480737	2084466	6	6
ID#150	498587	2085066	2	5
ID#151	503537	2094036	1	5
ID#152	467117	2105706	6	6
ID#153	492917	2083476	6	6
ID#154	490517	2080596	6	6
ID#155	496907	2079756	3	3
ID#156	505757	2086146	2	3
ID#157	478787	2100156	6	6
ID#158	478817	2116206	6	6
ID#159	468197	2112456	6	6
ID#160	488057	2096376	5	5
ID#161	479357	2107056	6	6
ID#162	474917	2116986	6	6
ID#163	504797	2102406	6	6
ID#164	464147	2112006	6	6
ID#165	478367	2103966	6	6
ID#166	499037	2077206	3	3
ID#167	499037	2070636	3	3
ID#168	496427	2074896	3	3
ID#169	481007	2100336	6	6
ID#170	474347	2111826	6	6
ID#171	492827	2094876	6	6
ID#172	505907	2102196	6	6
ID#173	479897	2100966	6	6
ID#174	477257	2115096	6	6
ID#175	464897	2111856	6	6

E.2 (Continued).

Sample_point	Easting	Northting	LULC_classify	LULC_Reference
ID#176	494777	2080506	3	3
ID#177	506807	2088426	2	2
ID#178	476327	2107056	6	6
ID#179	490517	2084736	6	6
ID#180	479897	2084346	6	6
ID#181	501887	2080716	3	3
ID#182	472847	2113806	6	6
ID#183	474197	2112696	6	6
ID#184	493787	2087436	6	6
ID#185	483677	2099586	6	6
ID#186	506597	2088516	5	5
ID#187	481457	2116326	6	6
ID#188	495557	2080296	3	3
ID#189	499337	2073186	3	3
ID#190	500087	2092356	3	3
ID#191	468647	2113896	6	6
ID#192	502907	2098956	6	6
ID#193	473657	2106486	6	6
ID#194	499877	2097906	5	5
ID#195	505517	2097966	6	6
ID#196	482327	2084796	5	5
ID#197	483437	2086506	6	6
ID#198	498647	2080776	3	3
ID#199	471707	2112066	6	6
ID#200	482837	2095116	6	6
ID#201	501317	2084616	3	3
ID#202	470177	2113416	6	6
ID#203	496067	2080536	3	3
ID#204	491087	2095836	5	5
ID#205	487637	2109366	5	5
ID#206	499007	2088966	2	2
ID#207	501767	2082816	3	3
ID#208	500117	2086566	3	3
ID#209	506507	2088096	5	5
ID#210	479327	2112516	2	2
ID#211	489377	2102976	5	5
ID#212	489167	2091936	5	6
ID#213	490067	2098296	6	5
ID#214	483437	2097546	6	6
ID#215	482957	2103786	6	6

E.2 (Continued).

Sample_point	Easting	Northting	LULC_classify	LULC_Reference
ID#216	486347	2097996	6	6
ID#217	491447	2083506	6	6
ID#218	481427	2119386	6	6
ID#219	478127	2087316	6	6
ID#220	501107	2100456	6	6
ID#221	489437	2077266	6	6
ID#222	492437	2095806	5	5
ID#223	479687	2100036	6	6
ID#224	493367	2085876	6	6
ID#225	490607	2096946	6	6
ID#226	494147	2092986	3	3
ID#227	487397	2090586	6	6
ID#228	508787	2087616	5	5
ID#229	487637	2101116	6	2
ID#230	488687	2097276	5	5
ID#231	487367	2108886	5	5
ID#232	478067	2103876	6	6
ID#233	469787	2107506	6	6
ID#234	494387	2093286	2	2
ID#235	493937	2102466	6	5
ID#236	492887	2095056	6	6
ID#237	502307	2087496	2	3
ID#238	479687	2107446	6	6
ID#239	486377	2112216	5	5
ID#240	477557	2096016	6	6
ID#241	474107	2111526	6	6
ID#242	506027	2095086	6	6
ID#243	478097	2115846	6	6
ID#244	501947	2082696	3	3
ID#245	510347	2092026	6	6
ID#246	510977	2091186	1	1
ID#247	475757	2110806	6	6
ID#248	473777	2118216	6	6
ID#249	489677	2085306	6	6
ID#250	482987	2115786	6	6
ID#251	473447	2112186	6	6
ID#252	491987	2087136	6	6
ID#253	480827	2086326	6	6
ID#254	483917	2091456	6	6
ID#255	505487	2098266	6	6

E.2 (Continued).

Sample_point	Easting	Northting	LULC_classify	LULC_Reference
ID#256	510347	2091786	6	6
ID#257	499397	2094246	5	2
ID#258	477977	2115096	6	6
ID#259	479267	2105886	6	6
ID#260	498707	2095296	5	2
ID#261	475667	2115546	6	6
ID#262	505907	2091306	5	5
ID#263	482147	2097006	6	6
ID#264	484397	2108826	2	2
ID#265	465497	2106696	6	6
ID#266	476207	2102586	6	6
ID#267	496367	2100396	3	0
ID#268	497627	2080446	3	3
ID#269	484367	2113536	6	6
ID#270	490247	2101056	5	5
ID#271	485597	2100726	6	6
ID#272	495887	2086386	3	3
ID#273	471107	2107206	6	6
ID#274	501647	2101296	6	6
ID#275	474587	2108856	6	6
ID#276	492767	2075016	6	6
ID#277	487217	2087736	6	6
ID#278	489557	2097216	3	5
ID#279	489257	2097966	6	5
ID#280	500897	2103246	6	6
ID#281	507347	2089116	5	5
ID#282	471857	2115996	6	6
ID#283	482387	2098866	6	6
ID#284	498377	2086446	3	3
ID#285	502367	2095326	5	5
ID#286	466277	2114016	6	6
ID#287	481667	2107836	6	6
ID#288	480047	2098296	6	6
ID#289	487007	2086416	6	6
ID#290	476777	2098116	6	6
ID#291	505727	2094906	6	6
ID#292	479807	2116536	6	6
ID#293	497507	2082636	3	3
ID#294	480587	2097606	6	6
ID#295	484817	2111406	5	5

E.2 (Continued).

Sample_point	Easting	Northting	LULC_classify	LULC_Reference
ID#296	494957	2104296	3	2
ID#297	487817	2105136	6	6
ID#298	499547	2085516	2	2
ID#299	498677	2095176	5	2
ID#300	502397	2085846	2	3
ID#301	487967	2093496	6	6
ID#302	497267	2076096	3	3
ID#303	495047	2081226	3	3
ID#304	499997	2104716	6	6
ID#305	469967	2104956	6	6
ID#306	498047	2088786	5	2
ID#307	499157	2083866	3	3
ID#308	502937	2081466	3	3
ID#309	503987	2099766	6	6
ID#310	499007	2099826	5	5
ID#311	490697	2101176	3	1
ID#312	491477	2079006	3	3
ID#313	480617	2087496	6	3
ID#314	491417	2098596	5	5
ID#315	489617	2085096	6	6
ID#316	479387	2088246	6	6
ID#317	493157	2080776	6	6
ID#318	466397	2111646	6	6
ID#319	465047	2115486	6	6
ID#320	484637	2096946	6	6
ID#321	479747	2104746	6	6
ID#322	486257	2108166	1	1
ID#323	492587	2088456	6	6
ID#324	478847	2096706	6	6
ID#325	503927	2094396	6	6
ID#326	495167	2097216	2	2
ID#327	477467	2088216	6	3
ID#328	473117	2109396	6	6
ID#329	465017	2110176	6	6
ID#330	473987	2115156	6	6
ID#331	504107	2093136	5	5
ID#332	498947	2085636	2	2
ID#333	475487	2105856	6	6
ID#334	478367	2084196	6	6
ID#335	489467	2081646	6	6

E.2 (Continued).

Sample_point	Easting	Northting	LULC_classify	LULC_Reference
ID#336	496607	2097636	5	5
ID#337	475097	2108886	6	6
ID#338	502097	2093406	5	5
ID#339	483707	2111496	2	2
ID#340	468467	2109066	6	6
ID#341	470777	2114196	6	6
ID#342	486257	2093166	6	6
ID#343	506027	2085906	2	2
ID#344	499577	2086356	2	2
ID#345	487907	2103156	2	5
ID#346	486257	2108976	5	6
ID#347	501647	2083146	3	0
ID#348	478757	2095956	6	6
ID#349	484997	2089626	6	6
ID#350	509327	2091516	5	5
ID#351	493457	2099136	3	1
ID#352	501917	2083266	3	3
ID#353	503807	2088786	2	3
ID#354	483527	2100306	6	6
ID#355	503057	2084136	3	3
ID#356	498167	2085096	2	3
ID#357	507047	2095866	6	6
ID#358	495317	2089356	3	3
ID#359	475847	2114496	6	6
ID#360	494147	2100276	3	1
ID#361	471467	2116146	6	6
ID#362	494987	2099496	2	2
ID#363	498827	2072766	3	3
ID#364	495437	2090946	2	3
ID#365	498497	2085696	2	2
ID#366	496817	2078226	3	3
ID#367	482057	2087976	6	3
ID#368	493247	2075676	6	6
ID#369	476267	2103726	6	6
ID#370	505757	2095296	6	6
ID#371	499007	2102466	5	5
ID#372	485267	2088426	6	6
ID#373	475187	2109126	6	6
ID#374	483017	2112876	5	5
ID#375	465287	2112936	6	6

E.2 (Continued).

Sample_point	Easting	Northting	LULC_classify	LULC_Reference
ID#376	465077	2115096	6	6
ID#377	466367	2108496	6	6
ID#378	490697	2082906	6	6
ID#379	496907	2073996	5	3
ID#380	494177	2093196	2	2
ID#381	504527	2094156	6	6
ID#382	493577	2073126	3	3
ID#383	469637	2113866	1	6
ID#384	497087	2088276	5	3
ID#385	475667	2110926	6	6
ID#386	500507	2090106	3	3
ID#387	494417	2096076	2	2
ID#388	511967	2091246	2	2
ID#389	495317	2075076	3	3
ID#390	487877	2093136	6	6
ID#391	477317	2115216	6	6
ID#392	464057	2111226	6	6
ID#393	480227	2116146	6	6
ID#394	484847	2103786	2	2
ID#395	490787	2083686	6	6
ID#396	483647	2102676	6	6
ID#397	479777	2112966	6	6
ID#398	468947	2108916	6	6
ID#399	488207	2108136	5	5
ID#400	492797	2092176	3	6
ID#401	495467	2074866	3	3
ID#402	493667	2072706	3	3
ID#403	495827	2083776	3	3
ID#404	468377	2106396	6	6
ID#405	469937	2114856	6	6
ID#406	465227	2109186	6	6
ID#407	470957	2111256	6	6
ID#408	474707	2102886	6	6
ID#409	478427	2085786	6	6
ID#410	482897	2111316	6	6
ID#411	486287	2100876	6	6
ID#412	498617	2092146	3	3
ID#413	476957	2102796	6	6
ID#414	479777	2086296	6	6
ID#415	486587	2107716	5	5

E.2 (Continued).

Sample_point	Easting	Northting	LULC_classify	LULC_Reference
ID#416	482927	2103636	6	6
ID#417	487667	2098206	6	6
ID#418	474947	2116326	6	6
ID#419	482537	2097576	6	1
ID#420	479447	2092326	6	6
ID#421	467267	2112276	6	6
ID#422	487697	2098866	6	6
ID#423	479327	2087436	6	1
ID#424	481067	2084556	6	6
ID#425	489617	2104836	6	6
ID#426	489407	2098266	6	6
ID#427	489227	2102766	5	5
ID#428	485117	2096436	6	6
ID#429	483677	2086896	5	1
ID#430	505997	2101656	6	6
ID#431	503357	2085246	3	3
ID#432	490547	2078286	6	6
ID#433	479387	2091996	6	6
ID#434	486587	2109696	5	5
ID#435	476927	2118126	6	6
ID#436	490007	2092356	6	6
ID#437	498617	2104086	3	3
ID#438	471077	2114406	6	6
ID#439	496727	2078976	3	3
ID#440	486707	2088666	6	6
ID#441	493667	2087406	6	6
ID#442	475487	2118966	6	6
ID#443	493607	2104026	3	5
ID#444	497507	2080146	3	3
ID#445	479057	2106666	6	6
ID#446	483257	2109606	6	6
ID#447	498617	2102976	5	5
ID#448	501527	2079006	3	3
ID#449	480347	2094756	6	6
ID#450	480797	2116746	6	5
ID#451	475817	2115816	6	6
ID#452	472877	2115996	6	6
ID#453	500837	2091516	3	3
ID#454	484847	2106186	6	6
ID#455	462737	2108376	6	6

E.2 (Continued).

Sample_point	Easting	Northting	LULC_classify	LULC_Reference
ID#456	491027	2092326	6	6
ID#457	501647	2099496	6	6
ID#458	505097	2093946	6	6
ID#459	491057	2077956	6	6
ID#460	498437	2082396	3	3
ID#461	479117	2092596	6	6
ID#462	484337	2106606	6	6
ID#463	487187	2092446	6	6
ID#464	488297	2103156	5	5
ID#465	488507	2102106	5	5
ID#466	489617	2099166	5	6
ID#467	469427	2116506	6	6
ID#468	484607	2113386	6	5
ID#469	480407	2119806	6	5
ID#470	498797	2093406	5	3
ID#471	495197	2080176	3	3
ID#472	478967	2087496	6	6
ID#473	482927	2085036	6	6
ID#474	483737	2092776	6	1
ID#475	476477	2117016	6	6
ID#476	494297	2079186	6	3
ID#477	480137	2120076	6	6
ID#478	468767	2110086	6	6
ID#479	500747	2090436	5	2
ID#480	500837	2099946	6	6
ID#481	491327	2082186	6	6
ID#482	465377	2113086	6	6
ID#483	493067	2074626	4	4
ID#484	502637	2098806	6	6
ID#485	470177	2105886	6	6
ID#486	489857	2077926	6	6
ID#487	473087	2117256	6	6
ID#488	500957	2080476	5	5
ID#489	468857	2112546	6	6
ID#490	464867	2116206	6	6
ID#491	493937	2079726	6	6
ID#492	503717	2093826	5	1
ID#493	485477	2107266	5	5
ID#494	482177	2089566	6	6
ID#495	484427	2100426	6	6

E.2 (Continued).

Sample_point	Easting	Northting	LULC_classify	LULC_Reference
ID#496	465797	2115036	6	6
ID#497	487757	2109426	5	1
ID#498	467177	2113476	6	6
ID#499	489287	2073456	6	6
ID#500	493307	2084766	6	6
ID#501	478757	2119326	6	6
ID#502	484037	2086956	6	6
ID#503	481127	2112366	5	1
ID#504	499757	2100816	5	1
ID#505	470777	2112246	6	6
ID#506	483197	2106936	6	6
ID#507	488507	2101836	6	6
ID#508	492257	2103906	6	6
ID#509	478847	2095626	6	1
ID#510	490067	2101986	5	5
ID#511	489557	2102796	5	5
ID#512	475397	2111586	6	6
ID#513	505157	2094666	6	6
ID#514	493247	2081826	6	6
ID#515	470957	2110986	6	6
ID#516	481487	2090496	6	6
ID#517	484817	2113206	6	6
ID#518	487937	2088666	6	6
ID#519	470447	2104776	6	6
ID#520	492827	2097126	6	6
ID#521	475337	2115576	6	6
ID#522	475697	2107626	6	6
ID#523	474857	2109246	6	6
ID#524	477437	2107776	6	6
ID#525	466217	2112126	6	6
ID#526	506057	2096616	6	6
ID#527	479387	2119866	6	6
ID#528	481517	2104416	6	6
ID#529	489677	2085216	6	6
ID#530	479387	2094666	6	5
ID#531	483467	2110416	6	5
ID#532	487247	2090916	6	6
ID#533	509777	2091156	1	5
ID#534	490547	2080056	6	6
ID#535	478337	2111826	1	6

E.2 (Continued).

Sample_point	Easting	Northting	LULC_classify	LULC_Reference
ID#536	479867	2094576	1	1
ID#537	481187	2093856	1	1
ID#538	480557	2093436	1	1
ID#539	501137	2091336	1	0
ID#540	493607	2087706	4	4

Note: LULC class 0 = Miscellaneous land

1 = Field crop

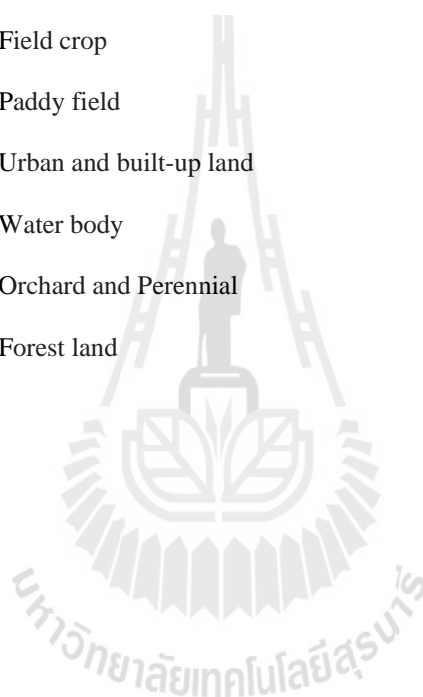
2 = Paddy field

3 = Urban and built-up land

4 = Water body

5 = Orchard and Perennial

6 = Forest land



CURRICULUM VITAE

Name Mr. Wichan Phandee

Date of Birth October 28, 1978

Place of Birth Nakhon Ratchasima Province, Thailand.

Education Bachelor of Science (Environmental Science Resource management): March, 2001. Faculty of Science and Technology, Nakhon Ratchasima Rajabhat University, Thailand.

Master of Science (Geographic Information System): August, 2004. Faculty of Science and Technology, Nakhon Ratchasima Rajabhat University, Thailand.

Grants and Fellowships Scholarship, Nakhon Ratchasima Rajabhat University.